UNIVERSIDAD COMPLUTENSE DE MADRID

FACULTAD DE CIENCIAS QUÍMICAS
Departamento de Bioquímica y Biología Molecular I

TESIS DOCTORAL

Hidroxiapatitas y nanopartículas de óxido de grafeno: respuesta celular y aplicación biomédica

MEMORIA PARA OPTAR AL GRADO DE DOCTOR

PRESENTADA POR

María de la Concepción Matesanz Sancho

Directores

María Teresa Portolés Pérez
María José Feito Castellano

Madrid, 2015

UNIVERSIDAD COMPLUTENSE DE MADRID
Departamento de Bioquímica y Biología Molecular I

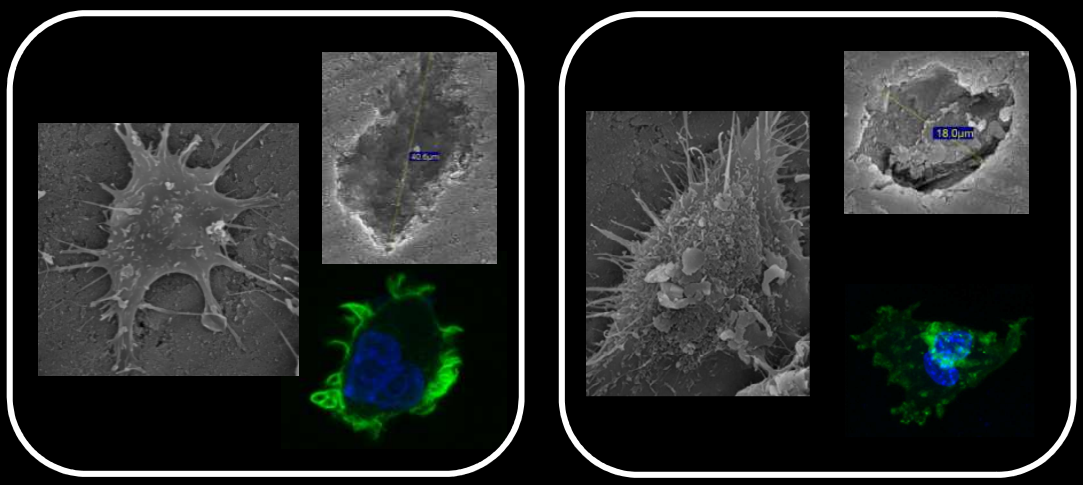

HIDROXIAPATITAS Y NANOPARTÍCULAS DE ÓXIDO DE GRAFENO: Respuesta celular y aplicación biomédica

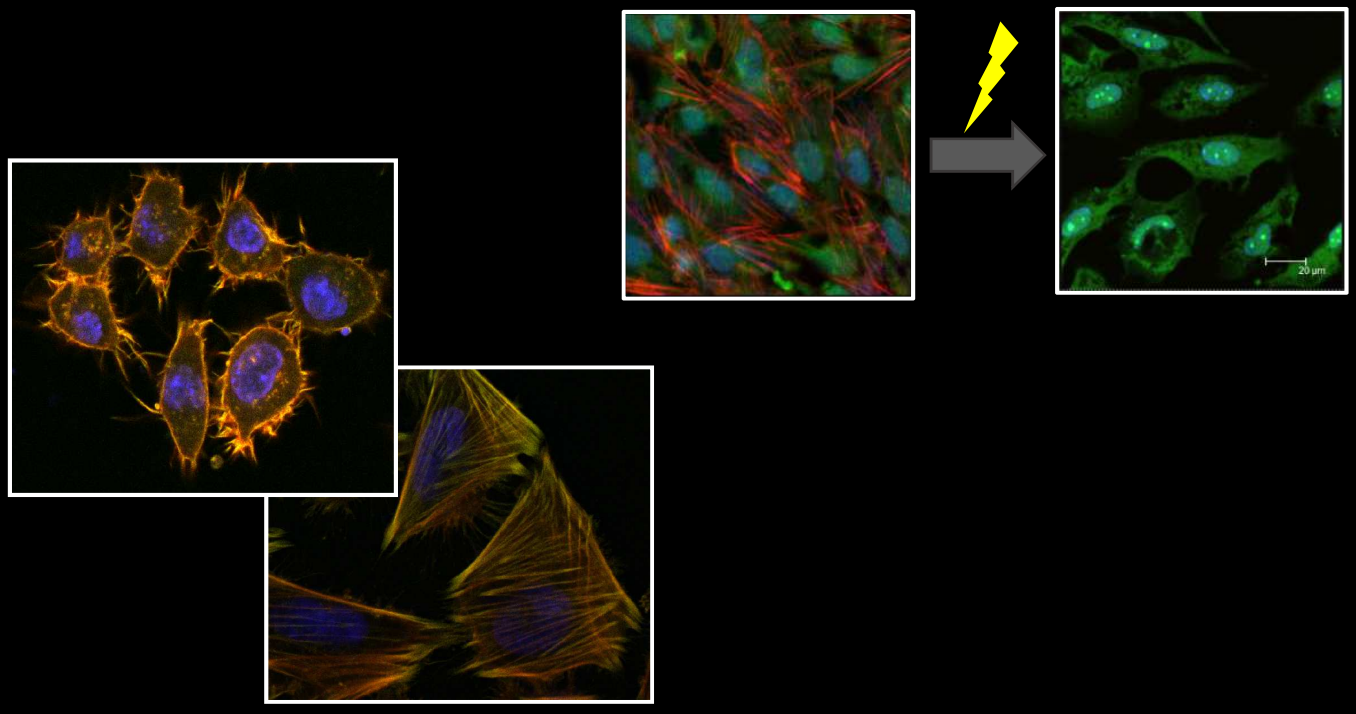

María de la Concepción Matesanz Sancho

TESIS DOCTORAL Mención DOCTOR EUROPEO

Madrid, 2015

UNIVERSIDAD COMPLUTENSE DE MADRID

FACULTAD DE CIENCIAS QUÍMICAS

Departamento de Bioquímica y Biología Molecular I

HIDROXIAPATITAS Y NANOPARTÍCULAS DE ÓXIDO DE GRAFENO: RESPUESTA CELULAR Y APLICACIÓN BIOMÉDICA

María de la Concepción Matesanz Sancho

Memoria para optar al Grado de Doctor - Mención Doctor Europeo - por la Universidad Complutense de Madrid

DIRECTORAS

Prof. Dra. María Teresa Portolés Pérez

Dra. María José Feito Castellano

Madrid, 2015

Prof. Dra. María Teresa Portolés Pérez, Catedrática del Departamento de Bioquímica y Biología Molecular I de la Facultad de Ciencias Químicas de la Universidad Complutense de Madrid

Dra. María José Feito Castellano, Profesora Titular del Departamento de Bioquímica y Biología Molecular I de la Facultad de Ciencias Biológicas de la Universidad Complutense de Madrid

CERTIFICAN:

Que la presente Memoria titulada **"Hidroxiapatitas y nanopartículas de óxido de grafeno: Respuesta celular y aplicación biomédica"** ha sido realizada por la Doctoranda María de la Concepción Matesanz Sancho en el Departamento de Bioquímica y Biología Molecular I de la Facultad de Ciencias Químicas de la Universidad Complutense de Madrid, bajo nuestra dirección y autorizamos su presentación para que sea calificada como Tesis Doctoral dado que reúne las condiciones necesarias para su defensa.

Este estudio ha sido posible gracias a la Ayuda Predoctoral de Formación de Profesorado Universitario (FPU, referencia AP2010-0110) y a los Proyectos de Investigación S-0505/ MAT/0324 y S2009/MAT-1472 financiados por la Comunidad de Madrid y MAT2013-43299-R financiado por el Ministerio de Economía y Competitividad.

En Madrid, a 25 de mayo de 2015

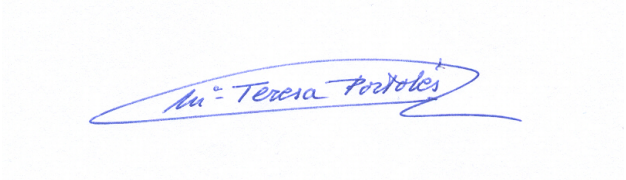

Fdo.: Prof. Dra. María Teresa Portolés Pérez

Fdo.: Dra. María José Feito Castellano

AGRADECIMIENTOS

Todo dio comienzo en el último curso de carrera, cuando empezábamos a inquietarnos por la siguiente etapa de nuestra vida. Buscando laboratorios donde poder iniciarme en la vida investigadora mediante una Beca de Colaboración, encontré un laboratorio donde trabajaban con materiales para su aplicación en patologías óseas. Y yo, que por aquel entonces ya andaba bastante fastidiadilla con mi espalda, sentí mucho interés por esta investigación y no pude evitar ponerme en contacto con el grupo. Aún recuerdo el día que, llena de nervios, entré en el despacho número 8, donde Teresa y Rafaella estaban esperándome con una sonrisa (algo que no siempre se encuentra). Luego conocí a María José y a mi querida Ceci y, poco a poco, así sin darme cuenta, el tiempo comenzó a pasar y decidí que si hacía una Tesis Doctoral, sin duda sería con ellas.

Les estoy profundamente agradecidas a mis directoras de Tesis, Teresa y María José, por su inconmensurable flexibilidad y paciencia. También estoy profundamente agradecida a todos aquellos con los que en estos seis años me he cruzado por el laboratorio, en especial a Ceci, Javier, Carmen, Isabel, Ana y Mónica. Han sido muchas horas de trabajo, pero también de grandes charlas y confidencias.

Quiero expresar también mi gratitud al grupo de la Profesora María Vallet-Regí, sin cuya colaboración, este trabajo no se habría podido llevar a cabo. Muchas gracias a Daniel Arcos por su asesoramiento para la comprensión de las propiedades de las hidroxiapatitas.

También deseo expresar mi agradecimiento a Mercedes, por brindarme la oportunidad de pasar tres meses inolvidables en la Universidad de Aveiro gracias a los cuales he podido aprender gran cantidad de cosas sobre grafeno. Sin duda, esta ha sido una experiencia que siempre guardaré en mi mente y que ha contribuido enormemente a mi formación laboral y personal. Gracias por tu manera de trabajar, por tu ayuda y por tus valiosos consejos. *Eu também estou muito agradecida a todas as pessoas que conhecí em Portugal. Eu tenho saudades de muitas coisas do meu estágio lá*.

Por otro lado, quiero expresar mi gratitud al grupo CIBER-BBN, por otorgarme la beca de iniciación a la investigación que me permitió comenzar mi carrera investigadora, y al Ministerio de Educación y Ciencia, cuya financiación mediante una beca de Formación de Profesorado Universitario ha sido la base para que pudiera realizar la presente Tesis Doctoral.

A continuación, quisiera expresar mi agradecimiento a todos los amigos y compañeros que a lo largo, no solo de los años de desarrollo de la Tesis, sino también durante la carrera de Biología me han apoyado en momentos tremendamente difíciles. Gracias especialmente a Emma y Estefanía, con las que he compartido muchas horas de "*tupper*", muchas alegrías y

penurias y, en definitiva, donde he encontrado el apoyo que necesitaba. Tampoco me quiero olvidar del resto de mis biólogos: Belén, Jota, Carlos y Alicia. Ya va una década desde que nos conocemos, gracias por todos estos años de amistad.

No me olvido tampoco de mi amiga Cris, ejemplo de una amistad inquebrantable, a pesar de los años y la distancia. Siempre te he considerado como una hermana por todos los momentos que hemos pasado juntas y, en este cambio de etapa tan importante, también quiero compartirlo contigo. Te estoy profundamente agradecida por tu amistad y tu apoyo incondicional.

Y por último, aunque sin duda lo más importante, estoy tremendamente agradecida a mi familia: Currinchi, este año nos has dejado, pero siempre recordaré la gran cantidad de horas que pasé estudiando a tu lado, y como siempre te subías a mis apuntes para captar mi atención y reclamar unas cuantas carantoñas. Teníamos un vínculo muy especial, y compartimos momentos que solo nosotros dos presenciamos. No existirá nunca nadie tan noble ni cariñoso como tú lo fuiste. Víctor, qué puedo decirte que no te haya dicho o demostrado ya. Eres la razón por la que me levanto por las mañanas y por la que estoy deseando llegar a casa para volver a tu lado: el mejor momento del día. Has tenido una enorme paciencia con mis interminables horas de estudio, con mis momentos de estrés y con mis inseguridades. Eres un pilar fundamental en mi vida y sin ti no podría haber llegado hasta aquí.

Y para finalizar, quiero expresar mi agradecimiento a las personas a las que esta Tesis Doctoral está especialmente dedicada: mis padres. Papi, eres el responsable de esta mente tan científica y pragmática. Desde pequeñita me has inculcado la pasión por la ciencia y has vivido con orgullo todas las etapas que me han llevado hasta aquí. Mamá, siempre recordaré esos momentos, que aunque no han podido ser muchos, he podido compartir contigo. Me siento orgullosa de poseer tanto tus defectos como tus virtudes. Solo espero que estés donde estés, tú también te sientas orgullosa de mí, y de los triunfos, como éste, que con gran esfuerzo he logrado alcanzar.

A todos, gracias.

María de la Concepción Matesanz Sancho

Madrid, 2015

A mis padres

ABREVIATURAS

- AFM: Microscopía de Fuerza Atómica
- ALP: Fosfatasa alcalina
- BCP: Fosfato cálcico bifásico
- BMP: Proteína morfogenética ósea
- BSA: Albúmina de suero bovino
- CDHA: Hidroxiapatita deficientes en calcio
- CFU-GM: Unidades formadoras de colonias de granulocitos y macrófagos
- CHA: Hidroxiapatita carbonatada
- CTR: Receptor de calcitonina
- CVD: Deposición química de vapor
- DAG: Diacilglicerol
- DKK: Dickkopf
- DLS: Dispersión dinámica de luz
- DMO: Densidad mineral ósea
- EDAC: 1-etil-3-(3-dimetilaminopropil)carbodiimida)
- EPCs: Células progenitoras de endotelio
- ERK: Quinasa regulada por señales extracelulares
- FBS: Suero fetal bovino
- FDA: *Food and Drug Administration*
- FGF: Factor de crecimiento fibroblástico
- FGFR: Receptor del factor de crecimiento fibroblástico
- FITC: Isotiocianato de fluoresceína
- FTIR: Espectrofotometría Infrarroja por Transformada de Fourier
- GFP: Proteína verde fluorescente
- HA: Hidroxiapatita
- Hh: Hedgehog
- HSC: Célula madre hematopoyética
- IGF-1: Factor de crecimiento similar insulínico-1
- Ihh: Indian Hedgehog
- IL-6: Interleuquina 6
- IP3: Inositol 1,4,5-trisfosfato
- LDH: Lactato deshidrogenasa
- LRP5/6: Receptor de lipoproteínas de baja densidad

- MAPK: Proteína quinasas activadas por mitógenos
- M-CSF: Factor estimulador de colonias de macrófagos
- MEK: MAP quinasa/ERK quinasa
- MMP: Metaloproteinasas de matriz
- MSC: Célula madre mesenquimática
- MWCNT: Nanotubos de carbono de pared múltiple
- nano-GO: Nanopartículas de óxido de grafeno
- nano-HA: Hidroxiapatita nanocristalina
- nano-SiHA: Hidroxiapatita sustituída con silicio nanocristalina
- NFAT: Factor nuclear de células T activadas
- NF-κB: Factor nuclear kappaB
- OPG: Osteoprotegerina
- OST: Osteostatina
- Osx: Factor de transcripción Osterix
- PEI: Polietilenimina
- PEG: Polietilenglicol
- PGE2: Prostaglandina E2
- PKC: Proteína quinasa C
- PLCɣ: Fosfolipasa C ɣ
- PLD: Deposición de láser pulsada
- PMMA: Polimetilmetacrilato
- PTH: Hormona paratiroidea
- PTHrP: Proteína relacionada con la hormona paratiroidea
- PVA: Polivinil alcohol
- PVD: Deposición física de vapor
- RANKL: Ligando del receptor activador de NF-κB
- RGD: Arg-Gly-Asp
- ROS: Especies reactivas de oxígeno
- Runx2/Cbfa1: Factor de transcripción 2 relacionado con Runt
- SBF: Fluido corporal simulado
- SEM: Microscopía Electrónica de Barrido
- SiHA: Hidroxiapatita sustituída con silicio
- SiHA/FGF-2: Hidroxiapatita sustituída con silicio unida a factor de crecimiento fibroblástico 2
- SR.D10: Clon D10 de linfocitos T singenéicos reactivos
- SWCNT: Nanotubos de carbono de pared sencilla

- TCP: Fosfato tricálcico
- TGF-β: Factor de crecimiento transformante β
- TNF-α: Factor de necrosis tumoral α
- TRAF: Factor asociado al receptor de TNF
- TRAIL: Ligando relacionado con TNF inductor de apoptosis
- TRAP: Fosfatasa ácida resistente a tartrato
- VBM: Vidrios bioactivos mesoporosos
- VEGF: Factor de crecimiento de endotelio vascular
- VEGFR: Receptor de factor de crecimiento de endotelio vascular
- Wnt: Wingless e Int

ÍNDICE

RESUMEN 17

SUMMARY 21

INTRODUCCIÓN

1. CONCEPTO DE BIOMATERIAL Y APROXIMACIÓN HISTÓRICA 27

2. TIPOS DE BIOMATERIALES Y PRINCIPALES APLICACIONES BIOMÉDICAS

2.1 Metales 31

2.2 Cerámicas 32

2.3 Polímeros sintéticos 39

2.4 Materiales de origen biológico 40

2.5 Materiales basados en estructuras de carbono 41

2.6 Materiales compuestos 47

3. TEJIDO ÓSEO

3.1 Tipos de hueso 48

3.2 Componentes del tejido óseo 50

REFERENCIAS DE LA INTRODUCCIÓN 63

CAPÍTULO I *Hidroxiapatitas para regeneración ósea y tratamiento de osteoporosis*

1. HIDROXIAPATITA SUSTITUIDA CON SILICIO E HIDROXIAPATITAS NANOCRISTALINAS 77

2. UNIÓN DE FACTORES DE CRECIMIENTO A HIDROXIAPATITAS 81

3. OSTEOPOROSIS 83

OBJETIVOS 89

RESULTADOS

- **Matesanz MC**, Feito MJ, Ramírez-Santillán C, Lozano RM, Sánchez-Salcedo S, Arcos D, Vallet-Regí M, Portolés MT. Signaling pathways of immobilized fgf-2 on silicon substituted hydroxyapatite. **Macromolecular Bioscience 12: 446-453, 2012** 91

- Lozano D, Feito MJ, Portal-Nuñez S, Lozano RM, **Matesanz MC**, Serrano MC, Vallet-Regí M, Portolés MT, Esbrit P. Osteostatin improves the osteogenic activity of fibroblast growth factor-2 immobilized on Si-doped hydroxyapatite in osteoblastic cells. **Acta Biomaterialia 8:2770-2777, 2012.** 103

- **Matesanz MC**, Feito MJ, Oñaderra M, Ramírez-Santillán C, daCasa C, Arcos D, Vallet-Regí M, Rojo JM, Portolés MT. Early *in vitro* response of macrophages and T lymphocytes to nanocrystalline hydroxyapaties. **Journal of Colloid and Interface Science 416: 59–66, 2014**..... 115

-**Matesanz MC**, Linares J, Lilue I, Sánchez-Salcedo S, Feito MJ, Arcos D, Vallet-Regí M, Portolés MT.Nanocrystalline silicon substituted hydroxyapatite effects on osteoclast differentiation and resorptive activity. **Journal of Materials Chemistry B, 2:2910-2919, 2014.**..... 127

REFERENCIAS DEL CAPÍTULO I 139

CAPÍTULO II *Nanopartículas de óxido de grafeno para tratamiento antitumoral por hipertermia*

1. **PROPIEDADES Y APLICACIONES BIOMÉDICAS DEL ÓXIDO DE GRAFENO**..... 147
2. **TUMORES ÓSEOS** 153

OBJETIVOS..... 157

RESULTADOS

- Síntesis y caracterización de nano-GO/PEG/FITC 159

- Vila M, Portolés MT, Marques PAAP, Feito MJ, **Matesanz MC**, Ramírez-Santillán C, Gonçalves G, Cruz SMA, Nieto-Peña A, Vallet-Regi M. Cell uptake survey of pegylated nano graphene oxide. **Nanotechnology, 23: 465103(9pp), 2012**. 163

- **Matesanz MC**, Vila M, Feito MJ, Linares J, Gonçalves G, Vallet-Regi M, Marques PAAP, Portolés MT. The effects of graphene oxide nanosheets localized on F-actin filaments on cell cycle alterations. **Biomaterials, 34:1562-1569, 2013.**..... 177

- Vila M, **Matesanz MC**, Gonçalves G, Feito MJ, Linares J, Marques PAAP, Portolés MT, Vallet-Regí M. Triggering cell death by nanographene oxide mediated hyperthermia. **Nanotechnology 25: 035101 (7pp); Global Medical Discovery, Key Nanotechnology Articles, June 27, 2014**..... 187

REFERENCIAS DEL CAPÍTULO II 201

CONCLUSIONES..... 209

CONCLUSIONS 211

ANEXO. Otras publicaciones de la Doctoranda relacionadas con esta Tesis Doctoral.....213

Resumen / Summary

RESUMEN

La Ciencia de los Biomateriales comprende el estudio de aquellos materiales diseñados para interactuar con sistemas biológicos y resolver problemas muy diversos en el área de Biomedicina.

En la presente Tesis Doctoral titulada **"Hidroxiapatitas y nanopartículas de óxido de grafeno: Respuesta celular y aplicación biomédica"**, se analizan a nivel celular los efectos de dos tipos de materiales con fines biomédicos muy diferentes: a) hidroxiapatitas para regeneración ósea y tratamiento de osteoporosis y b) nanopartículas de óxido de grafeno para tratamiento antitumoral por hipertermia.

CAPÍTULO I

El aumento de la esperanza de vida ha provocado una mayor incidencia de patologías asociadas a la edad como la osteoporosis, producida por un desequilibrio en el remodelado óseo que induce perdida de masa ósea y degeneración de la microestructura del hueso, con mayor riesgo de fracturas que afectan de forma significativa a la calidad de vida. Debido a esta situación, existe una gran demanda de biomateriales para la prevención y el tratamiento local de fracturas osteoporóticas.

La hidroxiapatita sustituida con silicio (SiHA) despierta un gran interés por el papel que desempeña este elemento en el proceso de calcificación ósea y por el mejor comportamiento bioactivo de este material. Las hidroxiapatitas nanocristalinas (nano-HA), debido a su similitud con el componente mineral del hueso y a sus propiedades osteoconductivas, ocupan una posición clave con respecto a otras biocerámicas. Como alternativa prometedora para la restauración de defectos óseos, en la presente Tesis Doctoral se ha evaluado el efecto del factor de crecimiento fibroblástico básico (FGF-2) unido a SiHA como inductor de los procesos de osteogénesis y angiogénesis. Asimismo, se han investigado los efectos de nano-HA y nano-SiHA sobre los macrófagos y los linfocitos T, implicados en la respuesta inmune, y sobre la diferenciación y actividad de los osteoclastos, responsables de la resorción ósea, analizando los posibles beneficios de estos materiales para el tratamiento de la osteoporosis. Los resultados obtenidos se recogen en el **Capítulo I** y han dado lugar a las siguientes publicaciones:

- **Matesanz MC**, Feito MJ, Ramírez-Santillán C, Lozano RM, Sánchez-Salcedo S, Arcos D, Vallet-Regí M, Portolés MT. Signaling pathways of immobilized fgf-2 on silicon substituted hydroxyapatite. ***Macromolecular Bioscience 12: 446-453, 2012.***

- Lozano D, Feito MJ, Portal-Nuñez S, Lozano RM, **Matesanz MC**, Serrano MC, Vallet-Regí M, Portolés MT, Esbrit P. Osteostatin improves the osteogenic activity of fibroblast growth factor-

2 immobilized on Si-doped hydroxyapatite in osteoblastic cells. ***Acta Biomaterialia 8: 2770-2777, 2012.***

- **Matesanz MC**, Feito MJ, Oñaderra M, Ramírez-Santillán C, daCasa C, Arcos D, Vallet-Regí M, Rojo JM, Portolés MT. Early *in vitro* response of macrophages and T lymphocytes to nanocrystalline hydroxyapatites. ***Journal of Colloid and Interface Science 416: 59–66, 2014.***

- **Matesanz MC**, Linares J, Lilue I, Sánchez-Salcedo S, Feito MJ, Arcos D, Vallet-Regí M, Portolés MT. Nanocrystalline silicon substituted hydroxyapatite effects on osteoclast differentiation and resorptive activity. ***Journal of Materials Chemistry B, 2: 2910-2919, 2014.***

Todos estos estudios indican el elevado potencial de nano-SiHA como biomaterial biocompatible para la combinación con factores de crecimiento así como para la modulación del remodelado óseo, previniendo la resorción y estimulando la formación de hueso, lo que le convierte en candidato ideal para tratamiento de procesos osteoporóticos y de regeneración ósea.

CAPÍTULO II

El osteosarcoma es una patología ósea que, a pesar de no presentar una alta prevalencia en la población, es de gran importancia al afectar mayoritariamente a adolescentes. La inducción de hipertemia local mediante nanopartículas está siendo estudiada actualmente como terapia antitumoral alternativa a la quimioterapia y la radioterapia para el tratamiento de este tipo de tumores. Las nanopartículas de óxido de grafeno (nano-GO) presentan un gran potencial para su aplicación biomédica en este campo debido a las propiedades únicas de su estructura y a su capacidad para inducir hipertermia cuando se exponen a radiación infrarroja cercana (NIR), no invasiva, inocua, y que penetra la piel. Este hecho permitiría, una vez internado el nano-GO en las células tumorales, inducir el incremento de temperatura local sobre el material y provocar la muerte celular. En la presente Tesis Doctoral se ha llevado a cabo el estudio de la cinética de incorporación de nano-GO en diferentes tipos celulares, la evaluación de la biocompatibilidad de este nanomaterial y su localización intracelular, así como los efectos que distintos tratamientos de fototermia diseñados con nano-GO producen sobre osteoblastos humanos Saos-2 derivados de osteosarcoma. Los resultados obtenidos se recogen en el **Capítulo II** y han dado lugar a las siguientes publicaciones:

- Vila M, Portolés MT, Marques PAAP, Feito MJ, **Matesanz MC**, Ramírez-Santillán C, Gonçalves G, Cruz SMA, Nieto-Peña A, Vallet-Regi M. Cell uptake survey of pegylated nano graphene oxide. ***Nanotechnology, 23: 465103(9pp), 2012.***

- **Matesanz MC**, Vila M, Feito MJ, Linares J, Gonçalves G, Vallet-Regi M, Marques PAAP, Portolés MT. The effects of graphene oxide nanosheets localized on F-actin filaments on cell cycle alterations. ***Biomaterials, 34: 1562-1569, 2013.***

- Vila M, **Matesanz MC**, Gonçalves G, Feito MJ, Linares J, Marques PAAP, Portolés MT, Vallet-Regí M. Triggering cell death by nanographene oxide mediated hyperthermia. ***Nanotechnology 25: 035101 (7pp); Global Medical Discovery, Key Nanotechnology Articles, June 27, 2014.***

Estos estudios revelan los efectos que nano-GO produce sobre diferentes tipos celulares tras su incorporación, su localización intracelular, así como la importancia de la elección de las condiciones adecuadas de tiempo y potencia de exposición a luz NIR para controlar el tipo de muerte celular, reduciendo los efectos secundarios para su posible utilización en el tratamiento local del osteosarcoma.

Los resultados de la presente Tesis Doctoral permiten conocer las respuestas celulares especificas a nano-SiHA y nano-GO que son fundamentales para la possible aplicación biomédica de estos materiales en patologías óseas como osteoporosis y osteosarcoma, respectivamente.

SUMMARY

Biomaterials Science is focused on the study of those materials designed to interact with living sistems and to solve different problems in Biomedicine.

In this PhD Thesis entitled **"Hydroxyapatites and graphene oxide nanoparticles: Cell response and biomedical application"**, the effects of two materials with very different biomedical application are studied at the cellular level: a) hydroxyapatites for bone tissue regeneration and osteoporosis treatment and b) graphene oxide nanosheets for osteosarcoma treatment by hyperthermia.

CHAPTER I

The increase in life expectancy results in a higher prevalence of age-related bone diseases, such as osteoporosis, caused by the imbalance in tissue remodelling which induces bone mass loss and bone microsestructure degeneration, with higher fracture risk that greatly drecreases the life quality. For this reason, there is a great demand of biomaterials for prevention and local treatment of osteoporotic fractures.

Silicon-substituted hydroxyapatite (SiHA) arouses a great interest because of the role this element carries out in bone calcification and the bioactive behaviour of this material. Nanocrystalline hydroxyapatites (nano-HA) have a crucial position with respect to other bioceramics, due to their similarities with the mineral phase of bone and their osteoconductive properties.

As a promising alternative for bone defect repair, the effect of fibroblast growth factor 2 (FGF-2) adsorbed on SiHA, as both osteogenic and angiogenic inductor, has been studied in the current PhD Thesis. On the other hand, the effects of nanocrystalline hydroxyapatite (nano-HA) and nanocrystalline silicon-substituted hydroxyapatite (nano-SiHA) on macrophages and T lymphocytes, cells involved in immune response, as well as on the differentiation and activity of osteoclasts, cells responsible for bone resorption, have been studied analysing the possible benefits of these biomaterials for osteoporosis treatment. The obtained results are described in **Chapter I** and they have led to the following publications:

- **Matesanz MC**, Feito MJ, Ramírez-Santillán C, Lozano RM, Sánchez-Salcedo S, Arcos D, Vallet-Regí M, Portolés MT. Signaling pathways of immobilized fgf-2 on silicon substituted hydroxyapatite. ***Macromolecular Bioscience 12: 446-453, 2012.***

- Lozano D, Feito MJ, Portal-Nuñez S, Lozano RM, **Matesanz MC**, Serrano MC, Vallet-Regí M, Portolés MT, Esbrit P. Osteostatin improves the osteogenic activity of fibroblast growth factor-

2 immobilized on Si-doped hydroxyapatite in osteoblastic cells. ***Acta Biomaterialia 8:2770-2777, 2012.***

- **Matesanz MC**, Feito MJ, Oñaderra M, Ramírez-Santillán C, daCasa C, Arcos D, Vallet-Regí M, Rojo JM, Portolés MT. Early *in vitro* response of macrophages and T lymphocytes to nanocrystalline hydroxyapatites. ***Journal of Colloid and Interface Science 416: 59–66, 2014***.

- **Matesanz MC**, Linares J, Lilue I, Sánchez-Salcedo S, Feito MJ, Arcos D, Vallet-Regí M, Portolés MT. Nanocrystalline silicon substituted hydroxyapatite effects on osteoclast differentiation and resorptive activity. ***Journal of Materials Chemistry B, 2:2910-2919, 2014.***

All these studies show the great potential of nano-SiHA as a biocompatible material for its combination with growth factors, as well as for bone tissue remodelling modulation, which prevents bone resorption and stimulates bone formation, making it an ideal candidate for bone regeneration and osteoporosis treatment.

CHAPTER II

Osteosarcoma is a pathology that, in spite of not exhibiting a high prevalence in population, is of great interest because it is suffered mainly by teenagers. The use of nanoparticles to induce hyperthermy as an alternative to chemotherapy and radiotherapy, is recently being widely studied for the treatment of this tumor. More specifically, graphene oxide nanoparticles (nano-GO) show a great potential for their biomedical application in this area, because of their unique structure properties, specially their ability to induce hyperthermia when they are exposed to near infrared irradiation (NIR), which is not invasive, innocuous and that penetrates the skin. This fact could induce the local increase of temperature on the material and subsequently, cell death, once nano-GO is internalized by tumoral cells. In the current PhD Thesis, the study of the nano-GO incorporation kinetics in different cell types, the bicompatibility evaluation of this material and its intracellular localization, as well as the effect of different fotothermia treatments designed with this nano-GO on human Saos-2 osteoblasts derived from osteosarcoma have been carried out.

The obtained results are described in **Chapter II** and they have led to the following publications:

- Vila M, Portolés MT, Marques PAAP, Feito MJ, **Matesanz MC**, Ramírez-Santillán C, Gonçalves G, Cruz SMA, Nieto-Peña A, Vallet-Regi M. Cell uptake survey of pegylated nano graphene oxide. ***Nanotechnology, 23: 465103(9pp), 2012***.

- **Matesanz MC**, Vila M, Feito MJ, Linares J, Gonçalves G, Vallet-Regi M, Marques PAAP, Portolés MT. The effects of graphene oxide nanosheets localized on F-actin filaments on cell cycle alterations. ***Biomaterials, 34: 1562-1569, 2013***.
- Vila M, **Matesanz MC**, Gonçalves G, Feito MJ, Linares J, Marques PAAP, Portolés MT, Vallet-Regí M. Triggering cell death by nanographene oxide mediated hyperthermia. ***Nanotechnology 25: 035101 (7pp); Global Medical Discovery, Key Nanotechnology Articles, June 27, 2014.***

These studies reveal the effects of nano-GO on different cell types after its uptake, its intracellular localization, as well as the importance of choosing suitable NIR exposure time and laser power conditions in order to control cell death, reducing the secondary effects for its potential use in local osteosarcoma treatment.

The results of the current PhD Thesis allow us to know the specific cell responses to nano-SiHA and nano-GO which are fundamental for the possible biomedical application of these materials in bone diseases, such as osteoporosis and osteosarcoma, respectively.

Introducción

1. CONCEPTO DE BIOMATERIAL Y APROXIMACIÓN HISTÓRICA

La Ciencia de los Biomateriales comprende el estudio de aquellos materiales diseñados para interactuar con sistemas biológicos y resolver problemas muy diversos en el área de Biomedicina. Esta ciencia, por su carácter multidisciplinar, requiere actualmente la participación de investigadores especializados en los campos de Medicina, Biología, Química, Ingeniería Tisular y Ciencia de Materiales.

El uso de materiales con fines clínicos se remonta a casi 10000 años y es tan antiguo como la Medicina. En el 3000 a.C. los egipcios ya usaban materiales como implantes. Las civilizaciones griega y romana (600 a.C. - 300 d.C.) hicieron uso de materiales no biológicos, mayoritariamente metales y materiales naturales como la madera para tratar diferentes heridas y patologías. Es conocido el uso de oro en la cirugía dental en las poblaciones etruscas (300 a.C.), fenicias (400-600 a.C.), chinas y aztecas, encontrándose también implantes dentales con nácar en restos de poblaciones mayas (600 a.C.) [*Bobbio 1972, Bull Hist Dent*].

A lo largo de la historia se han utilizado materiales metálicos clásicamente con fines ortopédicos. En el siglo XVI se empleaba oro y plata para reparaciones dentales en Europa, y más tarde hilos de hierro para la inmovilización de fracturas óseas. En 1829 HS Jervert realizó los primeros estudios de biocompatibilidad de metales en perros. El cirujano J Lister introdujo entonces la técnica quirúrgica aséptica, reduciendo los procesos de infección. En 1886, el cirujano alemán H Hansmann empleó por primera vez placas de acero para la reparación de fracturas óseas. En 1893, WA Lane desarrolló un sistema de tornillos de carbón para placas de fijación de fractura de huesos. Dos años más tarde, W Roentgen descubrió los rayos X, facilitando el proceso de diagnóstico en ortopedia y traumatología.

Ya en el siglo XX se comenzó a trabajar con acero inoxidable por ser más resistente a la corrosión y presentar mejores propiedades mecánicas que los metales. En 1928, A Fleming descubrió la penicilina, esencial para evitar los procesos infecciosos postoperatorios y mejorar el éxito de cualquier implante. Tras la I Guerra Mundial comenzaron a desarrollarse nuevos materiales metálicos, cerámicos y poliméricos. Estos materiales inertes, que clásicamente se habían utilizado para la industria del automóvil y aplicaciones electrónicas, empezaron a emplearse con fines médicos como injertos y sustitutos óseos. En 1931, M Smith-Petersen desarrolló un dispositivo de vidrio para prótesis parciales de cadera y clavos para la fijación de huesos. En 1938, se llevó a cabo el primer reemplazo total de cadera.

Los materiales no metálicos también han tenido relevancia histórica. Comenzaron a ser utilizados en la Edad Media para la obtención de ligaduras destinadas a detener hemorragias y

para algunos de los procedimientos quirúrgicos. Su desarrollo se aceleró a principios del siglo XX con el descubrimiento de materiales para fabricar hilos de sutura capaces de ser degradados y absorbidos por el organismo. Pero es tras la II Guerra Mundial cuando comenzó la investigación sistemática y planificada de los materiales útiles para la fabricación de prótesis e implantes, como consecuencia principalmente del enorme aumento de su demanda producida por la necesidad de rehabilitar a los inválidos de guerra. Este acontecimiento histórico trajo consigo el desarrollo de esta área de investigación. Por ejemplo, se observó que los soldados heridos toleraban las partículas metálicas incluidas en su cuerpo, justificando el uso de implantes metálicos para traumatismos craneales o para la fijación interna de fracturas. También pudo observarse en pilotos de guerra con inclusiones oculares de astillas de poli(metilmetacrilato), material utilizado en las ventanillas de los aviones, que no perdían la funcionalidad del ojo afectado, llevando al desarrollo de lentes intraoculares fabricadas con este material. Hoy en día, estos dos tipos de implantes siguen en uso y cuentan con un mayor porcentaje de éxito.

En paralelo a estos avances tuvo lugar el descubrimiento de nuevos antibióticos y el mejor conocimiento de los procesos biológicos desencadenados como consecuencia del contacto con estos materiales. Estos hechos crearon condiciones favorables para obtener soluciones eficaces basadas en el desarrollo de nuevos materiales biocompatibles, denominados biomateriales.

El Primer Simposio de Biomateriales se celebró en la Universidad de Clemson (SC, EEUU) en 1969, marcando el punto de partida de la necesaria integración de disciplinas complementarias a la Ingeniería y a la Medicina para el desarrollo de materiales biomédicos. Hasta ese momento el papel principal en el empleo de biomateriales lo habían desempeñado los cirujanos, pero en esa década cobró cada vez más importancia la participación de los ingenieros. Esto permitió el desarrollo de técnicas para caracterizar la estructura y la superficie de los materiales, con la finalidad de correlacionarlas con las respuestas biológicas observadas. También se incorporó el uso de materiales cerámicos para el reemplazo de tejido óseo y se desarrolló el estudio de materiales compuestos.

La comunidad científica relacionada con este campo se agrupó en diversas sociedades, tales como la Sociedad de Biomateriales (EEUU) fundada en 1974 y la Sociedad Europea de Biomateriales en 1976.

El término **biomaterial** se introdujo en 1976 para hacer referencia a la capacidad de este tipo de materiales para interaccionar con sistemas biológicos. Sin embargo, esta definición ha ido evolucionando en paralelo con el desarrollo de nuevos biomateriales diseñados con aplicaciones muy diversas. En 1999 la Sociedad Europea de Biomateriales los define como materiales preparados con el objetivo de evaluar, tratar, aumentar o reemplazar cualquier

tejido, órgano o función del cuerpo. DF Williams, en 2009, establece una definición mucho más actual: *"Un biomaterial es una sustancia diseñada para tomar una forma que, ya sea sola o como parte de un sistema complejo, pueda dirigir, mediante el control de las interacciones de los sistemas vivos, el curso de cualquier procedimiento terapéutico o diagnóstico, tanto en Medicina como en Veterinaria"* [*Williams DF 2009, Biomaterials*].

Biocompatibilidad es la característica que distingue a los biomateriales de cualquier otro tipo de materiales y, aunque inicialmente se refería a la ausencia de toxicidad de un material, este término se ha ido modificando en paralelo con el desarrollo de nuevas aplicaciones terapéuticas y diagnósticas. Así, un biomaterial no solo no tiene que ser citotóxico, sino que debe producir la respuesta celular adecuada, de acuerdo con la aplicación biomédica para la que ha sido diseñado [*Williams DF 2008, Biomaterials*].

Atendiendo a la finalidad de los biomateriales y desde un punto de vista conceptual, se distinguen tres generaciones que pueden coexistir en el tiempo. La denominada primera generación de biomateriales comprende materiales inertes, preparados con el fin de reducir su corrosión y la liberación de iones o partículas tras la implantación. Los biomateriales de segunda generación se caracterizan por ser bioactivos y biodegradables. Los biomateriales de tercera generación despiertan actualmente un gran interés al ser materiales bioactivos y biofuncionales, cuyo objetivo es la regeneración tisular. Con esta finalidad resulta necesario en muchos casos combinar estos biomateriales con células y moléculas bioactivas que permitan mejorar y reemplazar las diversas funciones biológicas del tejido afectado.

La **Ingeniería de Tejidos** es un área multidisciplinar que combina los principios de la Ingeniería, la Física y las Ciencias de la vida con el fin de desarrollar sustitutos biológicos de tejidos u órganos dañados que reparen, reemplacen o mejoren la función biológica perdida debido a anomalías congénitas, lesiones traumáticas, enfermedades o envejecimiento [*Langer R 1993, Science*]. El diseño de biomateriales para Ingeniería de Tejidos debe tener en cuenta los conocimientos actuales acerca de aspectos biológicos fundamentales como las interacciones célula-matriz extracelular, las funciones de los distintos factores de crecimiento y las rutas de señalización celular implicadas en respuestas específicas.

El gran desarrollo de la investigación en biomateriales está directamente relacionado con el aumento de la esperanza de vida, ya que este hecho ha provocado el incremento de la incidencia de patologías asociadas a la edad, como la osteoporosis. Debido a esta situación, existe una gran demanda de biomateriales para reemplazamiento de tejido óseo que, sumado a la alta tasa actual de fallo de estos implantes a nivel clínico, hace que esta área de estudio esté cobrando actualmente mayor importancia [*Pietak AM 2007, Biomaterials*]. Estos materiales son

utilizados hoy en día como sustitutos óseos para todo tipo de cirugías ortopédicas, dentales y maxilofaciales [*Balamurugan A et al. 2008, Dent Mater*].

En los últimos años han despertado gran interés los materiales de dimensiones nanométricas. En el caso de los de aplicación ósea, los fosfatos cálcicos que componen dientes y huesos son nanodimensionales y nanocristalinos, por lo que el uso de este tipo de materiales puede ser óptimo para mimetizar las condiciones del hueso *in vivo* [*Dorozhkin SV 2009, Materials*].

Aunque en un sentido estricto el concepto "nano" hace referencia a órdenes de magnitud de 10^{-9}, se ha llegado al consenso de considerar la nanoescala desde los 100 nm hasta valores inferiores. De esta manera, se define nanomaterial como "*cualquier tipo de material compuesto por partes funcionales discretas, que en su mayoría tienen una o más dimensiones en el orden de los 100 nm o por debajo de este valor*" (*European Commission, Scientific Committee on Emerging and Newly Identified Health Risks, SCENIHR, 2007*). En este contexto, se define un material nanocristalino como aquel que está compuesto por cristales que en su mayoría tienen dimensiones de 100 nm o inferiores. Con este mismo criterio se han definido los conceptos de *nanocomposite*, material nanoestructurado, nanorecubrimiento (*nanocoating*) y nanopulverizado (*nanopowder*) [*Dorozhkin SV 2009, Materials*].

La primera vez que se comprobaron las ventajas del uso de los nanomateriales fue en la industria electrónica, para los procesos de deposición en lámina. A partir de ahí, se empezaron a desarrollar este tipo de materiales en otras áreas. En el caso de las biocerámicas se comprobó la mejora frente a los procesos de fricción y desgaste asociados al reemplazamiento de articulaciones, al ser más fuertes las nanobiocerámicas que las biocerámicas de mayor tamaño [*Catledge SA et al. 2002, J Nanosci and Nanotechno*].

La gran importancia de los nanomateriales se debe a las propiedades únicas que les confiere su tamaño. Al disminuir las dimensiones aumenta en gran medida la relación superficie/volumen, proporcionando a los nanomateriales un mayor número de defectos en su superficie, una estructura electrónica alterada y una enorme área de superficie [*Williams DF 2008, Biomaterials; Traykova T et al. 2006, Nanomedicine*]. Estas características van asociadas a un alto poder de difusión, especialmente a temperaturas altas, una agregación de las nanopartículas para formar partículas más grandes y una mayor solubilidad [*Dorozhkin SV 2009, Materials*]. Los nanomateriales poseen también propiedades ópticas, mecánicas, eléctricas y magnéticas diferentes de los materiales de la misma composición pero de mayor tamaño [*Rempel AA 2007, Russ Chem Re*v]. Por otra parte, los nanomateriales utilizados en aplicaciones ortopédicas presentan ciertas características de superficie como un mayor número de

nanoporos que influyen en la capacidad de adsorción de ciertas proteínas que puede potenciar la adhesión de osteoblastos [*Sato M et al 2004, Expert Rev Med Devic]*.

Uno de los materiales de dimensiones nanométricas que ha cobrado gran importancia en los últimos años es el grafeno, cuya estructura presenta un solo atomo de carbono de grosor, lo que le confiere propiedades únicas y excelentes para numerosas aplicaciones. Las características y aplicaciones de este material serán desarrolladas en el apartado 2.5 y en el Capítulo II de la presente Tesis Doctoral.

2. TIPOS DE BIOMATERIALES Y PRINCIPALES APLICACIONES BIOMÉDICAS

Atendiendo a su composición, los biomateriales se dividen clásicamente en cuatro grupos: metales, cerámicas, polímeros y materiales compuestos o *composites*. Otro grupo lo constituyen los materiales de origen biológico y un grupo aparte, que algunos autores clasifican como cerámicas, son los carbones, que presentan ventajas como elasticidad similar al tejido óseo y que no experimentan fatiga, a diferencia de los metales y los polímeros sintéticos [*Lizarbe MA 2007, Rev R Acad Cienc Exact Fis Nat*].

2.1 Metales

Los metales han sido utilizados desde tiempos antiguos ya sea para la fabricación de prótesis para reemplazar diferentes partes del cuerpo, como placas craneales y prótesis de cadera, o bien para contribuir a la reparación de un tejido dañado, como en las fracturas óseas. Los más utilizados actualmente son los aceros inoxidables, aleaciones del tipo Co-Cr, Co-Cr-Mo o Co-Cr-Ni, titanio y sus distintas aleaciones (con aluminio y vanadio).

Para el diseño de un implante metálico se debe tener en cuenta la magnitud y la dirección de las fuerzas que sobre él actuarán, las limitaciones del diseño anatómico, el entorno del tejido donde se va a implantar y la respuesta del tejido al material [*Kokubo T et al. 2004, J Mater Sci Mater Med*].

Uno de los problemas a los que se enfrentan los implantes metálicos es la corrosión que conlleva la liberación de productos al medio y como consecuencia, cambios electroquímicos que pueden alterar el comportamiento celular y la liberación de iones metálicos que actúen sobre el metabolismo o produzcan inflamación crónica. Para solucionar este problema se recurre a las aleaciones a partir de óxidos o películas de hidróxidos sobre la superficie del material [*Singh R et al. 2007, J Mater Sci Mater Med*].

El acero inoxidable supuso un cambio drástico en la utilización de estos materiales por ser resistente a la oxidación y a la corrosión. Estas propiedades se consiguen gracias a la adición de cromo sobre el acero común que forma una película de óxido de cromo en la superficie, evitando la corrosión del hierro.

Aunque poco frecuente, los implantes metálicos también pueden sufrir fractura por un mal diseño del mismo o por determinadas condiciones durante su utilización (exceso de peso del paciente o de movimiento) que pueden producir fracturas por fatiga al existir una carga superior a la permitida por el implante.

Tras la implantación se pueden producir una serie de respuestas tisulares adversas, como la formación de una cápsula fibrosa alrededor del implante o el reemplazo de tejido muscular por tejido graso o fibroso.

2.2 **Cerámicas**

Se consideran cerámicas todos aquellos materiales inorgánicos estables químicamente frente al oxígeno, los medios ácidos, alcalinos o salinos, y los disolventes orgánicos. Sin embargo presentan la desventaja de tener menor resistencia mecánica que otros materiales [*Lizarbe MA 2007, Rev R Acad Cienc Exact Fis Nat*].

La clasificación de las cerámicas puede realizarse atendiendo a su composición, estructura o aplicación. Desde un punto de vista químico, estos materiales incluyen la alúmina (óxido de aluminio), la zirconia, fosfatos de calcio, como las hidroxiapatitas, y los denominados vidrios bioactivos, cuya composición se basa en SiO_2 - CaO - Na_2O - P_2O_5, conteniendo en algunos casos MgO y K_2O [*Vallet-Regí M et al. 2011, Advanced Materials*].

En función de las características de su interacción con el tejido óseo, las cerámicas pueden dividirse en **bioinertes** (no reaccionan con el hueso), **bioactivas** (se unen fuertemente al hueso) y **reabsorbibles** (son solubles y acaban siendo sustituídas por nuevo tejido óseo).

2.2.1 Cerámicas bioinertes

Las cerámicas bioinertes son aquellas que no reaccionan con el hueso y se utilizan como meros sustitutos del tejido dañado. En este grupo se encuentran las denominadas biocerámicas de primera generación como la **alúmina** y la **zirconia**, empleadas para fabricar cabezas femorales de prótesis de cadera [*Arcos D 2013, Acta Materialia*]. Estos materiales presentan buenas propiedades mecánicas y resistencia a la corrosión. Por su buena biocompatibilidad son muy utilizados en implantes dentales [*Lizarbe MA 2007, Rev R Acad Cienc Exact Fis Nat*].

2.2.2 Cerámicas bioactivas

Debido a las limitaciones de las cerámicas bioinertes, se desarrollaron en los años 80 una serie de cerámicas denominadas bioactivas, capaces de reaccionar con el hueso para formar nuevo tejido óseo. De acuerdo con la definición der SF Hulbert et al, "*un **material bioactivo** es aquel que induce una respuesta biológica específica en la interfaz del material que conduce a la formación de uniones entre el tejido y el material*" [*Hulbert SF et al. 1982, Ceram Int*]. Este tipo de materiales no provocan la formación de una cápsula fibrosa alrededor, ni respuesta inflamatoria o toxicidad [*Hench LL 1991, J Am Ceram Soc; Castner RG et al. 2002, Surface Science*]. Su alta reactividad da lugar a productos de reacción que cristalizan en una fase similar a la apatita, análoga al componente mineral del hueso, que a su vez permite la unión de proteínas que favorecen la adhesión y proliferación celular (**osteoconducción**), dando lugar a una unión fuerte entre el implante y el hueso (**osteointegración**) con formación de nuevo tejido óseo [*Anselme K 2000, Biomaterials*] Esta característica hace que se empleen en procesos de reparación periodontal y formación ósea [*Arcos D et al.2013, Acta Materialia*].

Dentro de las cerámicas bioactivas se encuentran las hidroxiapatitas y los vidrios bioactivos basados en sílice. Aunque ambos tipos se consideran cerámicas bioactivas, se debe tener en cuenta que el grado de bioactividad no es el mismo, ya que éste depende de su composición y estructura, resultando la reactividad de la hidroxiapatita mucho menor que la que presentan los vidrios bioactivos.

- Hidroxiapatitas

La hidroxiapatita (**HA**), $Ca_{10}(PO_4)_6(OH)_2$, es el fosfato de calcio más utilizado para implantes dentales y óseos debido a su similitud con la fase mineral del hueso, como se describe en el apartado 3.2.1 de la Introducción y en el Capítulo I. Sin embargo, las apatitas biológicas de mamíferos son deficientes en calcio, carbonatadas, iónicamente sustituidas y, por lo tanto, no se corresponden con dicha fórmula estequiométrica [*Arcos D 2014, Bioceramics with clinical applications, Chapter 3*]. Además, estos materiales presentan estructura nanocristalina. Con el objetivo de mimetizar estas apatitas biológicas, se han diseñado hidroxiapatitas deficientes en calcio (**CDHA**), hidroxiapatitas carbonatadas (**CHA**) e hidroxiapatitas nanocristalinas (**nano-HA**).

En las **CDHA**, las deficiencias de calcio son compensadas con la sustitución de PO_4^{3-} por HPO_4^{2-} o CO_3^{2-} o con la creación de vacantes adicionales en los grupos hidroxilo. Estos defectos en la estructura cristalina conllevan generalmente una mejor respuesta biológica a causa de una

mayor reactividad. En los organismos vivos, las CDHA siempre presentan sustituciones catiónicas de calcio por iones de sodio o magnesio. Además de las deficiencias en calcio, estas apatitas presentan un bajo nivel de grupos carbonato y pequeños cambios en la estructura cristalina en comparación con HA. La síntesis de CDHA es realizada a temperaturas entre 25 y 100˚C y a pH inferior a 12, para que se generen suficientes aniones HPO_4^{2-} que compensen las deficiencias de calcio. La aplicación clínica de CDHA está indicada en los casos de cirugía poco invasiva, siendo principalmente utilizado este material como componentes de cementos de fosfatos de calcio.

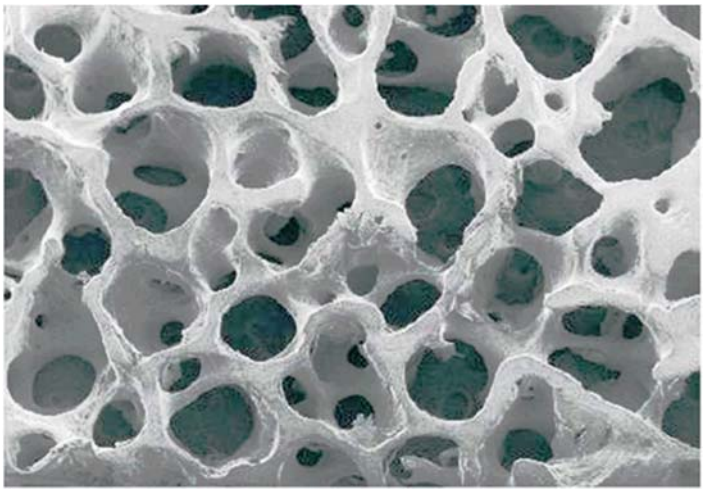

Figura 1. Fase mineral de hueso de mamífero. Imagen tomada de [*Alonso S 2012, Seminario Internacional CFATA-UNAM*]. http://www.fata.unam.mx/difusion/actividades/eventos/evento_20121129.html

Las **CHA** pueden ser clasificadas en tipo-A o tipo-B en función del lugar donde se posicione el anión carbonato. Estas apatitas presentan menor tamaño de cristal y mayor área de superficie comparado con la HA estequiométrica. La incorporación de CO_3^{2-} da lugar a distorsiones en la estructura produciendo microtensiones en el cristal. Este hecho junto con el menor tamaño de cristal determinan la mayor solubilidad de las CHA. La aplicación biomédica de CHA está orientada hacia la fabricación de implantes para sustitución y reconstrucción ósea [*Doi Y et al. 1998, J Biomed Mater Res*]. En los años 80, Impladent Ltd comercializó OsteoGen, implante basado en CHA destinado a elevaciones de seno maxilar, huecos dentales tras la extracción y reparación de defectos periodontales. Estas apatitas comerciales son sintetizadas a bajas temperaturas, lo que aumenta la porosidad y solubilidad del biomaterial, haciéndolo más reabosobible y capaz de ser colonizado por células formadoras de hueso [*Valen M et al. 2002, J Oral Implantol*].

Las **nano-HA** presentan una mayor rugosidad de superficie y poros individuales de menor tamaño que la HA [*Webster TJ et al. 2000, J Biomed Mater Res*], lo que estimula la función osteoblástica y mejora la osteoinducción [*Sato M et al. 2004, Expert Rev Med Devic*].

Por otra parte, la hidroxiapatita sustituida con silicio (**SiHA**) ha sido recientemente utilizada por el papel que desempeña este elemento en el proceso de calcificación ósea [*Carlisle E 1972, Science*] y por el mejor comportamiento bioactivo de este material.

En la presente Tesis Doctoral se han evaluado los efectos que producen la sustitución con silicio y la nanocristalinidad en el comportamiento de las células óseas *in vitro* frente a la hidroxiapatita, por lo que las propiedades y aplicaciones de la hidroxiapatita sustituida con silicio y de las hidroxiapatitas nanocristalinas se desarrollan con detalle en el Capítulo I.

Las hidroxiapatitas poseen pobres propiedades mecánicas, al presentar fragilidad y poca resistencia a la fatiga. Este problema se ve incrementado cuando se utilizan en andamios y en estructuras de alta porosidad. Por este motivo, su aplicación principal son los recubrimientos y la reparación de pequeños defectos óseos [*Dorozhkin SV 2010, Biomaterials; Salinas A et al. 2007, Z Anorg Allg Chem*]. Las hidroxiapatitas se utilizan frecuentemente como recubrimiento de prótesis metálicas preparadas a partir de aleaciones de titanio o de titanio puro, utilizado por su baja densidad, fuerza mecánica y resistencia a ciclos de carga [*Vallet-Regí M et al. 2011, Advanced Materials*]. Se han desarrollado implantes metálicos recubiertos con hidroxiapatita con uso comerial producidos por spray de plasma [*Sun L et al. 2001, J Biomed Mater Res; Yan L et al. 2003, Biomaterials*]. La principal ventaja que presenta esta técnica es la rápida tasa de deposición y la producción a bajo coste. Sin embargo, existen ciertos problemas que deben ser mejorados como la producción de una fase amorfa de fosfato cálcico en los recubrimientos que dificulta su resorción, la inestabilidad de la HA a altas temperaturas y la fase de transición del titanio a 1163˚K. Existen otras maneras de obtener recubrimientos de materiales metálicos como la deposición física de vapor (PVD), deposición química de vapor (CVD), deposición electroforética o deposición de láser pulsada (PLD). Según el método utilizado se puede controlar en menor o mayor grado el grosor del recubrimiento y la cristalinidad de las fases [*Vallet-Regí M et al. 2011, Advanced Materials*].

Otra de las aplicaciones de las hidroxiapatitas es su utilización como componente de cementos óseos de sales de calcio [*Cabañas MV et al. 2002, Chem Mater*] o poliméricos [*Cisneros-Pineda OG et al. 2014, Mat Sci Eng C*]. Estos cementos presentan la ventaja de no necesitar estar conformados de una manera determinada y poseen la capacidad de endurecerse *in situ*. Los cementos de fosfato de calcio son lentamente reemplazados por hueso nuevo [*Vallet-Regí M et al. 2011, Advanced Materials*]. Las propiedades físicoquímicas de estos materiales como el tiempo de fraguado, la porosidad y el comportamiento mecánico dependen de la

formulación del cemento y de la presencia de aditivos [*Ginebra MP et al. 2004, Biomaterials; Real RP et al. 2002, Biomaterials ; Real RP et al. 2003, J Biomed Mater Res A ; 57-60 Vallet-Regí M et al. 2011, Advanced Materials*].

La HA ha sido recientemente utilizada para reforzar andamios preparados con hidrogeles como agarosa o gelano, empleados por su capacidad para cargar y liberar diferentes moléculas, conservando estos andamios las propiedades microestructurales y texturales de la HA y su funcionalidad [*Cabañas MV et al. 2014, Mat Chem Phys*, ANEXO]. Los cristales de apatita, del mismo orden de magnitud que los del hueso, quedan embebidos en una matriz tridimensional polisacarídica que recuerda a la matriz extracelular y protege a las moléculas de la degradación enzimática *in vivo.* En este estudio el método de conformado permite monitorizar el tamaño de poro del andamio con el objetivo de mimetizar la estructura jerárquica del hueso, lo que facilita la colonización celular, vascularización e intercambio de nutrientes. La **Figura 2** muestra la capacidad de osteoblastos humanos Saos-2 para adherirse y proliferar, colonizando dichos soportes.

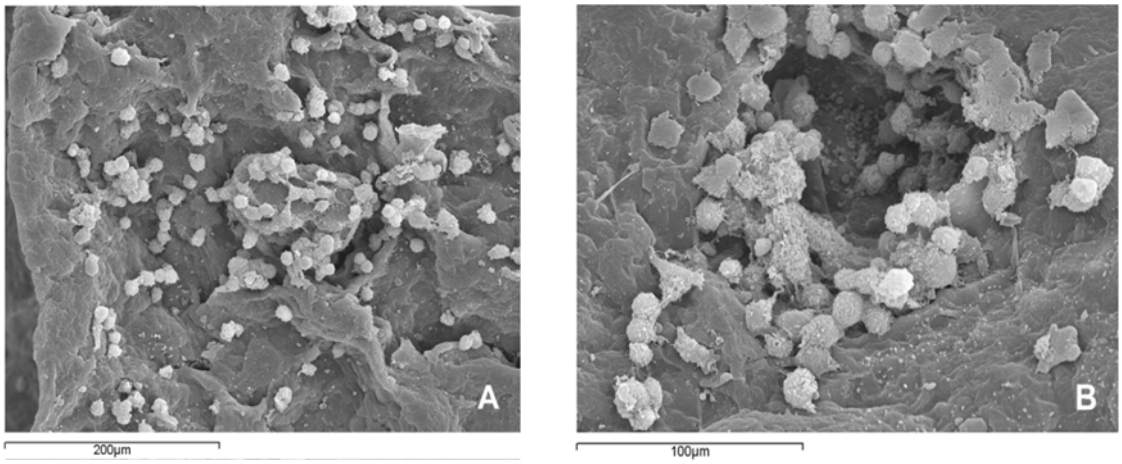

Figura 2. Imágenes de Microscopía Electrónica de Barrido (SEM) de osteoblastos Saos-2 cultivados sobre andamios de HA/gelanos. Imagen tomada de [*Cabañas MV et al. 2014, Mat Chem Phys*, ANEXO].

Por otra parte, se evaluó en estos andamios el efecto del método de carga de albúmina de suero bovino (BSA) en el hidrogel sobre la cinética de liberación de esta proteína, comprobándose que la liberación de BSA es más controlada cuando ésta es incorporada durante el proceso de síntesis [*Cabañas MV et al. 2014, Mat Chem Phys*, ANEXO].

- *Vidrios bioactivos*

Los vidrios bioactivos están compuestos por una red de sílice modificada por la adición de una cierta proporción de elementos como calcio, sodio y fósforo que se unen al entramado de dicha red [*Vallet-Regí M et al. 2011, Advanced Materials*].

Hench desarrolló en 1969 la primera generación de materiales 45S5, pertenecientes a este grupo de biocerámicas, que se utilizan desde 1985 a nivel clínico [*Hench LL 1989, J Biomed Mater Res; Hench LL 2006, J Mater Sci Mater Med*]. Su aplicación en la odontología dio lugar al desarrollo de numerosos vidrios bioactivos. El éxito de estos biomateriales se debe a su alta biocompatibilidad y a los efectos biológicos positivos observados tras la implantación [*Vallet-Regí M et al. 2003, Eur J Inorg Chem; Verrier S et al. 2004, Biomaterials*].

Los vidrios bioactivos han sido ampliamente estudiados para procesos de regeneración tisular ósea [*Hench LL et al. 1998, Handbook of Biomaterial Properties*]. La técnica sol-gel permite fabricar vidrios bioactivos a baja temperatura, con mejores propiedades de superficie y porosidad, siendo posible la unión de moléculas activas y células durante el proceso de síntesis. Estos vidrios favorecen el crecimiento óseo desde la periferia hacia el implante. El nuevo hueso penetra en el implante, mientras que el vidrio es lentamente reabsorbido [*Vallet-Regí M et al. 2011, Advanced Materials*].

Las pobres propiedades mecánicas que presentan estas biocerámicas han limitado su utilización en aplicaciones biomédicas [*Vallet-Regí M et al. 2006, J Mater Sci: Mater Med; Chen QZ et al. 2006, Biomaterials*]. En la actualidad su estudio está centrado en la unión de agentes osteogénicos a estos materiales para la preparación de andamios tridimensionales para Ingeniería Tisular [*Vallet-Regí M et al. 2011, Advanced Materials*].

La incorporación de la química supramolecular a la técnica sol-gel ha dado lugar recientemente a una nueva generación de vidrios bioactivos mesoporosos (**VBM**) con mejores características texturales y bioactivas. Estos materiales presentan poros altamente ordenados y magnitudes de superficie y porosidad muy superiores a las obtenidas mediante el método sol-gel convencional, dando lugar a la mayor cinética de bioactividad encontrada *in vitro* [*Arcos D 2012, Anales de RANF*]. Su estructura mesoporosa permite la carga y liberación controlada de fármacos y diferentes moléculas con actividad biológica [*Wang S 2009, Micropor Mesopor Mat*].

2.2.3 <u>Cerámicas reabsorbibles</u>

Este tipo de biomateriales son solubles tras la implantación, permitiendo el crecimiento de nuevo tejido óseo en las irregularidades del mismo. Debido a su elevada reactividad, el principal problema que presentan estas cerámicas es el mantenimiento de la estabilidad en la interfaz tejido-implante durante la resorción del biomaterial, así como alcanzar el equilibrio

entre las velocidades de resorción del material y de formación de nuevo tejido óseo [*Arcos D 2014, Bioceramics with clinical applications, Chapter 3*].

Dentro de las cerámicas reabsorbibles el fosfato tricálcico o TCP es el material más representativo, y más concretamente el **β-TCP**. Este material se emplea en clínica cuando se desea una reabsorción del mismo en un periodo de 4-6 meses, como en casos de reparación de defectos periodontales, extirpación de quistes o en injertos de defectos alveolares. A altas temperaturas este material se transforma en la fase **α-TCP**, con la misma composición química pero diferente estructura cristalina que hace que el α-TCP sea menos estable [*Arcos D 2014, Bioceramics with clinical applications, Chapter 3*]. En estudios realizados con minicerdos a los que se les colocaban implantes de α-TCP o β-TCP en defectos óseos producidos en la tibia, se observó una completa degradación de ambos materiales a las 86 semanas [*Wiltfang J et al. 2002, J Biomed Mater Res*].

Otro biomaterial comprendido en este grupo es el fosfato cálcico bifásico (**BCP**), compuesto por una mezcla de dos fases con diferente solubilidad: la fase más estable de HA y la fase más soluble de β-TCP [*Daculsi G 1998, Biomaterials*]. El correcto balance entre ambos componentes convierte al BCP en una biocerámica más eficiente que la HA sola para diferentes aplicaciones [*Sánchez-Salcedo S et al. 206, Tissue Eng*]. Cuando CDHA es tratada a temperaturas superiores a 700˚C se transforma en β-TCP, convirtiéndose en el material bifásico de β-TCP/HA o BCP, donde a medida que aumenta la fase β-TCP disminuye el promedio Ca/P. Este es el método de obtención de BCP más común en la actualidad [*Arcos D 2014, Bioceramics with clinical applications, Chapter 3*]. Estudios *in vitro* muestran la capacidad de fibroblastos murinos L929 y osteoblastos humanos Saos-2 para adherirse y proliferar sobre discos de HA/β-TCP/agarosa sin que se produzca estrés oxidativo ni alteraciones en la membrana plasmática, demostrando la biocompatibilidad de este material [*Alcaide M et al. 2009, J Biomed Mat Res A*].

La velocidad de degradación de una biocerámica de fosfato de calcio depende de varios factores. La estructura cristalina y composición química de la misma determinan la solubilidad del material a un determinado pH. Cuanto menor es la proporción Ca/P, mayor es la tasa de solubilidad de estas cerámicas. Por este motivo, el TCP (ratio 1,5) puede reabsorberse *in vivo* en pocas semanas, mientras que la HA estequiométrica (ratio 1,67) puede permanecer en el organismo durante varios años. Valores de Ca/P inferiores a 1 son considerados demasiado solubles y ácidos como para ser implantados. La microestructura es otro factor determinante, ya que son los defectos microestructurales los lugares en los que comienza el proceso de degradación. De este modo, materiales con defectos en la superficie, grandes poros o pequeño límite de grano se degradarán a mayor velocidad que piezas densas cristalinas. Este hecho hace que, dependiendo del diseño, un mismo tipo de biocerámica pueda tener mayor o menor

reactividad. Por este motivo, ciertas cerámicas bioactivas pueden incluirse entre las cerámicas reabsorbibles y viceversa. Por otro lado, tras la implantación de estos materiales se genera siempre un proceso inflamatorio en el que los macrófagos acuden para ejercer su función fagocítica. Para ello, liberan una serie de enzimas que acidifican el medio incrementando también la velocidad de degradación de las biocerámicas de fosfato cálcico en las primeras fases de la implantación [*Arcos D 2014, Bioceramics with clinical applications, Chapter 3*].

2.3 **Polímeros sintéticos**

La utilización de estos materiales en clínica se debe a la observación de que los pilotos de guerra a los que se les incrustaban astillas de polimetacrilato (PMMA), material de las ventanas de los aviones, no veían alterada su funcionalidad ocular. Gracias a este descubrimiento, se diseñaron lentes intraoculares con este tipo de polímeros. Posteriormente comenzaron a emplearse como cemento de fijación de prótesis, tanto en odontología como en cirugía ortopédica para estabilización de vértebras en pacientes osteoporóticos y reparación de defectos en cavidades óseas y craneales [*Frazer RQ et al. 2005, J Long Term Eff Med Implants*]. Con el tiempo, se incorporaron otros polímeros, como el acetato de celulosa, componente de los tubos de diálisis desde 1940, el dacron para injertos vasculares, y el polieteruretano para prótesis cardíacas.

Dependiendo de la composición química y su grado de entrecruzamiento, el polímero presentará unas determinadas propiedades físicas y estabilidad. La unión de otros aditivos químicos, macromoléculas o segundas fases permite obtener diferentes morfologías, estructuras, texturas, rigidez o flexibilidad, según el objetivo específico de cada material.

Se pueden establecer dos clases de polímeros sintéticos:

- **Elastómeros**, aquellos que pueden ser sometidos a grandes deformaciones sin perder la capacidad de volver a adquirir sus dimensiones y formas originales.
- **Plásticos**, son materiales de estructura más rígida y que se subdividen en función de su comportamiento térmico. Los termoplásticos son aquellos a los que se les puede dar una forma determinada tras ser sometidos a tratamiento térmico.

Entre los polímeros sintéticos también se consideran los hidrogeles, cuyo nombre se debe a su gran afinidad por el agua y a la incorporación de la misma en su estructura. Estos pueden ser tanto elastómeros como plásticos. La composición de los hidrogeles es muy variada existiendo diversos polímeros naturales que comprenden polímeros aniónicos (ácido hialurónico, pectina, condroitín sulfato o ácido algínico), polímeros catiónicos (polilisina o quitosán), polímeros anfipáticos (colágeno, fibrina) o polímeros neutros (dextrano o agarosa).

Por otro lado, existen un gran número de polímeros sintéticos y diferentes mezclas de los mismos [*Hoffman AS 2002, Adv Drug Deliver Rev*].

A la hora de evaluar la respuesta tisular al implante polimérico se deben tener en cuenta propiedades del material como la hidrofobicidad y la carga iónica de la superficie del implante. La presencia de monómero libre es probablemente la principal causa de toxicidad de este tipo de implantes, pudiendo deberse a una polimerización incompleta o a la degradación del polímero.

Entre las aplicaciones biomédicas de los polímeros sintéticos destaca su utilización en suturas preparadas con materiales como el nylon, el polipropileno, el dacron, los poliésteres y el ácido poliglicólico. Asimismo, se han utilizado polímeros adhesivos biodegradables y agentes hemostáticos como adhesivos tisulares, para promover la unión de los tejidos. Los materiales poliméricos también se han empleado como vehículos para liberación de fármacos, membranas de diálisis, sistemas de oxigenación sanguínea o lentes de contacto.

2.4 **Materiales de origen biológico**

Existe una amplia variedad de materiales naturales, en su mayoría derivados del tejido conjuntivo, que pueden ser utilizados como biomateriales. Deben ser tratados previamente para evitar posibles respuestas inmunológicas que den lugar al rechazo del implante.

- *Colágeno*: es el más utilizado como biomaterial gracias a sus características mecánicas (elevada fuerza tensil, extensibilidad, retención de agua y posibilidad de formación de geles), químicas (capacidad para formar enlaces de entrecruzamiento, degradación por colagenasas, reabsorción tisular, semipermeabilidad y capacidad para interaccionar con diversas moléculas) y biológicas (antigenicidad reducida, adhesión celular, interacción con plaquetas y activación de componentes del sistema de coagulación sanguínea). Por otra parte, se puede modular la biocompatibilidad del mismo mediante agentes de entrecruzamiento como el formaldehído [*Lee CH et al. 2001, Int J Pharm*].

Las formas de aplicación del colágeno son muy diversas, utilizándose para la preparación de membranas (sustitutivo de córnea, hemodiálisis, piel artificial o reparación de hernias), esponjas (tratamiento de lesiones en la piel, sustitución de hueso y cartílago, tampones quirúrgicos y contraceptivos vaginales), geles (sistemas liberadores de fármacos, inyectable en cirugía plástica) o en forma de fibras (material de sutura, componente de vasos y válvulas cardíacas). [*Lee CH et al. 2001, Int J Pharm / Patino MG et al. 2002, J Oral Implant*].

- *Fibronectina*: aunque en mucha menor medida que el colágeno, se utiliza para recubrimiento de prótesis mejorando la adhesión celular debido a la secuencia RGD (Arg-Gly-Asp) [*Rammelt S et al. 2006, Biomaterials; Honduvilla NG et al. 1995, Artif Organs*].

- *Cerámicas de origen natural*: utilizadas para la regeneración de defectos óseos, como las derivadas de corales químicamente tratados y de carácter reabsorbible. La estructura del coral le confiere una arquitectura similar al hueso y la capa de hidroxiapatita con la que se fabrica el implante controla la reabsorción del mismo [*Chapman-Sheath P et al. 2003, J Bone Joint Surg*]. Estos materiales permiten el crecimiento vascular, la diferenciación de células osteoprogenitoras y la remodelación ósea.

- *Polisacáridos naturales*: como la celulosa para suturas, membranas y sistemas de liberación de fármacos. Otros polisacáridos como la heparina se utilizan para la preparación de biomateriales tromborresistentes. Los alginatos se emplean para la cura de quemaduras o liberación de fármacos y el ácido hialurónico como relleno facial con fines estéticos. Otros materiales como la quitina se utilizan en la industria farmacéutica, cosmética y de alimentos. Derivado de la quitina, se obtiene el quitosano, empleado para suturas biodegradables, membranas de hemodiálisis y como sustituto artificial de la piel, agente cicatrizante de quemaduras y sistema de liberación de fármacos [*Coviello T et al. 2007, J Control Release*].

2.5 Materiales basados en estructuras de carbono

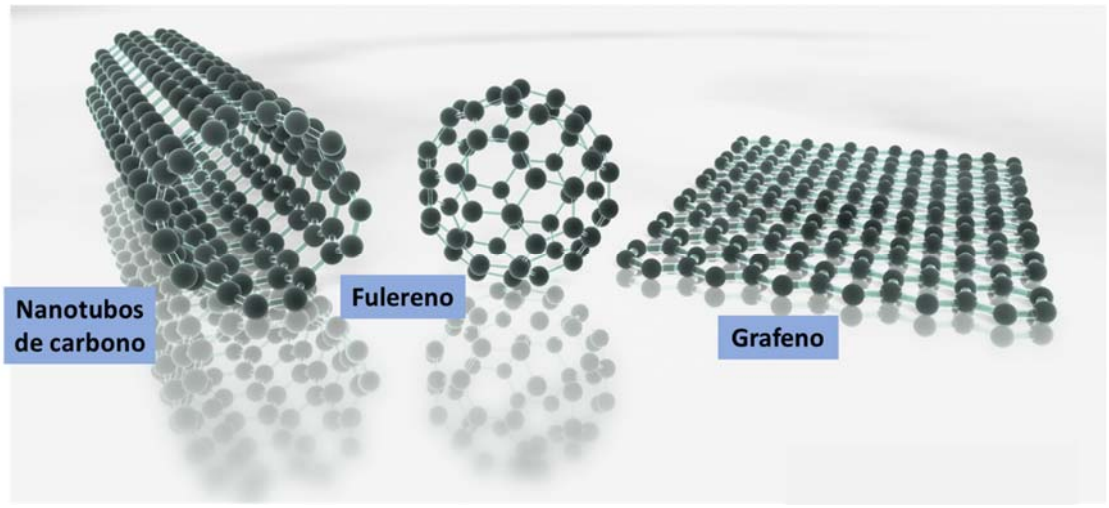

Figura 3. Estructuras de carbono: a) Nanotubos de carbono, b) Fulerenos y c) Grafeno. Imagen modificada a partir de https://flagellum.wordpress.com/tag/grafeno/

Estos materiales son ampliamente utilizados en gran cantidad de aplicaciones tecnológicas gracias a sus propiedades y a su diversidad estructural, presentando características físicas y químicas muy variadas. Mediante distintas metodologías se puede sintetizar una amplia gama de alotropos de carbono, es decir, diferentes estructuras basadas en este elemento químico con un mismo estado físico [*Guldi DM et al. 2011, Chem Commun*].

Clásicamente se conocían dos formas alotrópicas del carbono: el diamante (con los átomos dispuestos en una red tetraédrica) y el grafito (consistente en una red hexagonal plana). Recientemente, se han descubierto otras formas alotrópicas que han dado lugar a varios grupos de materiales basados en diferentes nanoestructuras de carbono: los fulerenos, los nanotubos de carbono y el grafeno (por orden cronológico).
[*www.cdlmadrid.org/cdl/archivospdf/ciencias/estructuras-carbono.pdf*]

- *Fulerenos*: estructuras huecas formadas por átomos de carbono dispuestos en forma esférica. Cada átomo de carbono presenta hibridación sp^2, estando unido a otros tres átomos originando una estructura aromática que recuerda a la del grafito. Sin embargo, a diferencia de éste último, la molécula no es plana debido a que los tres enlaces se desvían hacía un mismo lado, generando una tensión en la estructura, compensada por la gran simetría de la misma. Esta estructura cerrada solo es compatible con doce pentágonos y un número variable de hexágonos. Cuando la estructura es muy grande, podemos encontrar fulerenos de varias capas, donde cada estructura queda encerrada dentro de una mayor.
[*www.cdlmadrid.org/cdl/archivospdf/ciencias/estructuras-carbono.pdf*].

Su descubrimiento se atribuye oficialmente a HW Kroto et al. [*Kroto HW et al. 1985, Nature*]. Fueron producidos artificialmente por primera vez en 1990, a partir de la evaporación y reconstitución del grafito [*Krätschmer W et al. 1990, Nature*]. Sin embargo, ya en 1970 E Osawa propuso su existencia. Su nombre se debe al arquitecto R Buckminster Fuller que, entre otras aportaciones, es conocido por la cúpula geodésica, diseñada en la década de los 60 y de morfología muy similar a estas nanoestructuras de carbono.

Gracias a esta estructura cerrada y simétrica el material presenta gran resistencia. A grandes presiones puede deformarse, recuperando la forma inicial. Los fulerenos son solubles en solventes orgánicos como el benceno o el cloroformo. Aunque el tamaño de su estructura es de orden nanométrico, las partículas se asocian de forma espontánea formando agregados que puede alcanzar el orden de micras.

Su aplicación es más limitada que otras nanoestructuras de carbono. Se ha propuesto su utilización como catalizadores y células fotovoltaicas.

Desde un punto de vista biomédico, son pocos los estudios realizados actualmente para su posible aplicación. Aunque el fulereno puro es prácticamente insoluble en agua, se puede modificar químicamente con derivados polihidroxilados que pueden ser aceptados por sistemas biológicos [*Da Ros T et al. 1999, Chem Commun*]. Varios estudios han comprobado el carácter antioxidante de estos materiales [*Grebowski J et al. 2013, Biomed Res Int*]. T Çavas et al. observaron la ausencia de toxicidad de las nanopartículas de fulereno soluble en agua (fulerenol) sobre células humanas de pulmón IMR-90 y su papel protector frente a acetamiprida, insecticida que causa citotoxicidad por la producción de especies reactivas de oxígeno [*Çavaş T et al. 2014, Pestic Biochem Physiol*]. J Mrdanović et al. comprobaron un descenso en la producción de aberraciones cromosómicas y micronúcleos en células de ovario de hámster CHO-K1 que habían sido tratadas con mitomicina C, agente que produce reacciones de entrecruzamiento en el ADN [*Mrdanović J et al. 2009, Mutat Res*]. Sin embargo, existen estudios con fulerenol contradictorios en los que se ha observado la disrupción del citoesqueleto, acumulación de vacuolas autofágicas y pérdida del potencial de membrana mitocondrial en células del túbulo proximal renal LLC-PK1 [*Johnson-Lyles DN et al. 2010, Toxicol Appl Pharmacol*]. Esta toxicidad parece ser dependiente del tipo celular a la vista de los resultados de Y Su et al., cuyo estudio muestra citotoxicidad en células de hámster de ovario y de pulmón pero no en fibroblastos murinos L929 [*Su Y et al. 2010, Toxicology*].

- <u>*Nanotubos de carbono*</u>: estructuras formadas por una lámina de átomos de carbono enrollada sobre sí misma, de manera que sus bordes quedan unidos formando un cilindro. Los extremos también pueden estar cerrados formando una semiesfera (hemifulereno). Su nombre se debe a que el diámetro de los mismos es de escala nanométrica pero la longitud puede llegar a ser macroscópica.

Aunque ya se conocían los nanotubos de carbono obtenidos de forma catalítica, no llamaron la atención, por la imperfección de su estructura, hasta 1991 cuando S Iijima, mediante un sistema de evaporación por arco eléctrico, observó el crecimiento de agujas de hasta 1 mm sobre el cátodo de grafito, identificadas después como láminas concéntricas de átomos de carbono dispuestas en forma cilíndrica, conocidas actualmente como nanotubos de carbono de pared múltiple (**MWCNTs**). Mediante la adición de metales como el cobalto sobre el ánodo, se obtuvieron los primeros nanotubos de carbono de pared sencilla (**SWCNTs**). Los SWCNTs tienen un diámetro de 1-2 nm, mientras que los MWCNTs de unas 20 capas pueden tener hasta 30 nm. Los nanotubos tienden a agruparse entre sí y formar varias capas de forma espontánea. Por lo general, se obtienen mezclas heterogéneas de diferente diámetro y longitud. Dependiendo del proceso de cierre de la lámina, se pueden obtener diferentes estructuras veinte veces más resistentes que el acero, con una densidad seis veces menor. También presentan gran rigidez y,

en general, son muy buenos conductores eléctricos. La conductividad depende de la forma en que se produce el cierre de la lámina de átomos de carbono, pudiendo ser desde superconductores hasta aislantes. Son solubles en disolventes polares como la dimetilformamida, pudiendo aumentar su solubilidad mediante la adición de grupos funcionales en su estructura.

Gracias a sus propiedades tienen aplicaciones muy variadas en el campo de la electrónica, óptica, ciencia de materiales y nanotecnología. Se valora especialmente su papel como semiconductores y su utilización en materiales compuestos, como refuerzo de otros polímeros como las resinas epoxi.

Desde un punto de vista biomédico, los nanotubos de carbono carecen de solubilidad en medio acuoso, por lo que requieren una funcionalización previa para su aplicación. Actualmente, estos materiales son estudiados como posibles potenciadores de funciones celulares, para la formación de apatita sobre su superficie, para la síntesis de andamios para Ingeniería de Tejidos, para la liberación de fármacos y genes o como biosensores [*Li X et al. 2010, Biomed Mater*].

Varios autores muestran la capacidad de los nanotubos de carbono (CNT) para afectar al comportamiento celular. En estudios con células mioblásticas de ratón C2C12 se observó la adhesión, proliferación y diferenciación de las mismas sobre MWCNTs compactos [*Li X et al. 2009, J Biomed Mater Res A*]. El cultivo de osteoblastos humanos Saos-2 sobre MWCNTs induce también una mayor expresión de marcadores de diferenciación como osteonectina, osteocalcina u osteopontina [*Li X et al. 2009, Biomed Mater*].

Por otra parte se ha observado la formación de una capa de apatita sobre la superficie de MWCNTs cuando se mantienen en soluciones de fosfato cálcico [*Akasaka T et al. 2006, Mater Sci Eng*]. Esto ha dado lugar a la fabricación de materiales compuestos por MWCNTs y nano-HA que podrían emplearse para Ingeniería de Tejido óseo [*Liao S et al. 2007, Acta Biomaterialia*]. Estudios *in vitro* con células mioblásticas de ratón C2C12 cultivadas sobre andamios de MWCNTs-quitosano mostraron buenos resultados de adhesión, proliferación y viabilidad celular. La implantación de estos materiales con la proteína morfogenética de hueso 2 humana (rhBMP2) en músculo de ratón indujeron la formación de hueso ectópico [*Abarrategi A et al. 2008, Biomaterials*].

La funcionalización de CNTs para volverlos hidrofílicos y con superficie catiónica también permite utilizar este tipo de materiales como sistema de liberación de genes y fármacos. Esta funcionalización no solo vuelve al material más soluble sino que reduce notablemente la toxicidad *in vitro*.

Por último, se ha estudiado el papel de los nanotubos de carbono como biosensores y, más concretamente, como sensores electroquímicos para su uso en patologías como la diabetes mediante la detección de los niveles de glucosa [*Wang J et al. 2003, J Am Chem Soc*].

- *Grafeno*: material bidimensional de tan solo un átomo de grosor, compuesto por carbonos dispuestos en forma hexagonal. El método de aislamiento y caracterización a partir de grafito cristalino fue desarrollado en 2004 por Konstantin Novoselov y Andrey Guéim [*Novoselov KS et al. 2004, Science*], obteniendo por este trabajo el Premio Nobel de Física en 2010.

Desde su descubrimiento, el grafeno atrajo la atención de numerosos investigadores, llegándose a publicar en 2010 más de 3000 trabajos debido a las características únicas que este material posee [*Sánchez VC et al 2012, Chem Res Toxicol*]. Entre las propiedades más sobresalientes se encuentran su transparencia, flexibilidad, resistencia extraordinaria, impermeabilidad y óptima conducción eléctrica. Todos estos factores tienen como consecuencia un amplio potencial del grafeno para su utilización en numerosos campos de investigación. La principal ventaja del grafeno sobre el resto de materiales de carbono es su gran área de superficie, gracias a su estructura bidimensional. Esto le confiere una alta capacidad de funcionalización y de interacción con los sistemas biológicos [*Gonçalves G et al. 2013, Adv Healthc Mater*].

Se han descrito diferentes métodos de obtención del grafeno, siendo la exfoliación química del grafito la más utilizada por la posibilidad de producirlo a gran escala de manera sencilla y a bajo coste. La exfoliación del grafito en solución requiere la oxidación de la estructura aromática para debilitar las interacciones de Van der Waals entre las diferentes capas. El grafito puede ser exfoliado completamente mediante sonicación o agitación magnética en medio oxidante hasta producir una suspensión coloidal de partículas con pocas láminas de carbono [*Gonçalves G et al. 2013, Adv Healthc Mater*]. Dependiendo de las etapas seguidas durante el proceso de exfoliación del grafito se pueden obtener diferentes **tipos de partículas de grafeno**:

- Grafeno en monocapa, obtenido directamente a partir de la exfoliación repetida del grafito [*Novoselov KS et al. 2004, Science*], por deposición de vapor sobre sustratos para aplicaciones electrónicas o por descomposición de fases de carburo [*Sprinkle M et al. 2010, Nat Nanotechnol*]. Este material presenta unas propiedades electrónicas excelentes.

- Grafeno de pocas capas (2 a 10 capas), precursor del grafeno en monocapa. Se obtiene mediante la introducción de grupos sulfato y nitrato entre las capas de grafito y su posterior calentamiento, que provoca la expansión de toda la estructura.

- Óxido de grafeno (GO), producido a partir de la oxidación fuerte del grafito y su posterior dispersión por métodos como la sonicación, pudiendo llegar a obtenerse GO

en monocapa, generalmente en suspensión acuosa. Presenta la estructura del grafeno con grupos carboxilato en la periferia, responsables de la carga de superficie negativa dependiente de pH y de la estabilidad coloidal [*Park S et al. 2009, Nano Lett*]. En la superficie basal contiene grupos hidroxilo y epóxido (no cargados pero polares) y dominios hidrofóbicos capaces de establecer interacciones π-π relevantes para la adsorción de sondas y de ciertas drogas. Por tanto, es una molécula anfifílica, capaz de actuar como surfactante y estabilizar moléculas hidrofóbicas en solución [*Sánchez VC et al. 2012, Chem Res Toxicol].*

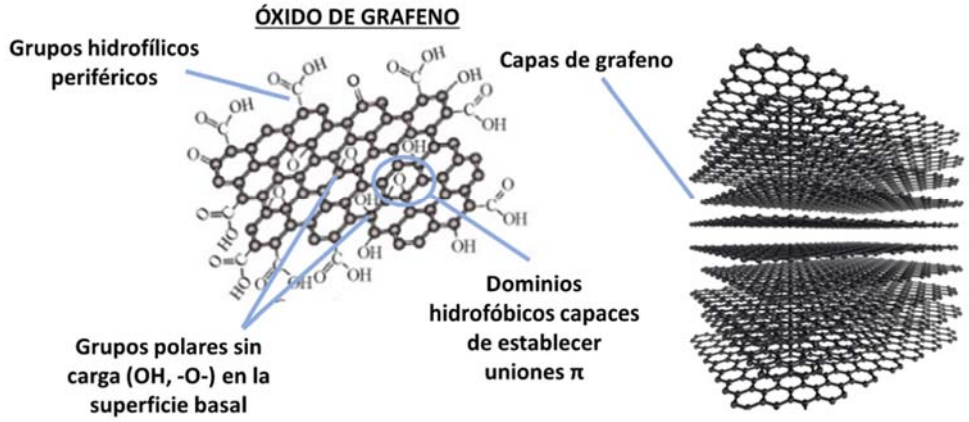

Figura 4. Detalle de la estructura molecular del óxido de grafeno. Imágenes procedentes de http://research.pbsci.ucsc.edu/chemistry/li/research.html y http://www.nanotechbio.com/applications/

- Óxido de grafeno reducido (rGO), obtenido mediante condiciones reductoras como altas temperaturas o tratamiento con hidracina [*Park S et al. 2009, Nano Lett*]. Estas condiciones se utilizan con el objetivo de restaurar la conductividad eléctrica y otras propiedades [*Bagri A et al. 2010, Nat Chem*].

- Nanopartículas de óxido de grafeno (nano-GO), GO de dimensión lateral inferior a los 20 nm. Su interés radica en su pequeño tamaño ya que esto les facilita la entrada en las células y les da estabilidad en solución, aumentando la dispersión [*Sánchez VC et al. 2012, Chem Res Toxicol*]. Se obtienen a partir de GO mediante energía ultrasónica. Dependiendo del grado de oxidación del GO, o lo que es lo mismo, del grado de defectos en la estructura, se puede controlar la dimensión lateral del material ya que estos defectos determinarán el número de puntos de rotura durante el proceso de sonicación [*Pan S et al. 2011, ACS Nano*].

Dentro de los diferentes tipos de grafeno, el nano-GO presenta las mejores características para su aplicación biomédica, ya que posee en su superficie grupos

capaces de establecer interacciones para la unión de diferentes moléculas. Por este motivo este nanomaterial ha sido objeto de estudio en la presente Tesis Doctoral. Las principales aplicaciones biomédicas del GO son desarrolladas en el Capítulo II.

2.6 **Materiales compuestos**

No existe consenso en la definición de este tipo de materiales ya que, dependiendo del criterio de clasificación, ciertos materiales pueden ser catalogados o no como compuestos o *composites*. En términos generales, éstos se pueden definir como "*dos o más materiales física y/o químicamente distintos que se encuentran organizados con una interfaz entre ellos, mostrando propiedades que no están presentes en los materiales que lo componen por separado y que son el objetivo por el cual el material composite es sintetizado*" [*Iftekhar A 2004, Standard Handbook of Biomedical Engineering and Design, McGrawHill*].

Los *composites* tienen una fase continua (matriz) y una o varias fases discontínuas (de refuerzo) con propiedades mecánicas y térmicas generalmente superiores a las de la matriz. La fase continua acepta la carga gracias a su gran área de superficie y se la transfiere a la fase de refuerzo, modificándose propiedades del *composite* como fuerza, dureza o resistencia mecánica a la fatiga [*Iftekhar A 2004, Standard Handbook of Biomedical Engineering and Design, McGrawHill*]. Muchos de estos materiales también suelen presentar resistencia a la corrosión y oxidación a altas temperaturas y al desgaste.

Materiales como las cerámicas ven mejorada su resistencia mecánica al formar parte de *composites* y pueden tener aplicaciones biomédicas para las que el material en solitario no es adecuado [*Zweben C 2006, Mechanical Engineers Handbook: Materials and Mechanical Design, John Wiley & Sons*].

Debido a que la fase de refuerzo es la que determina las propiedades del *composite*, la clasificación de este tipo de materiales suele hacerse atendiendo a las características de esta fase como forma, tamaño, distribución, orientación, composición o modo de incorporación de dicha fase. Sin embargo, también se pueden clasificar según el material empleado en la matriz: *composites* de matriz polimérica (PMC), cerámica (CMC) o metálica (MMC) [*Iftekhar A 2004, Standard Handbook of Biomedical Engineering and Design, McGrawHill*].

Las propiedades de este tipo de materiales hacen que tengan aplicación en numerosos campos de investigación como en la Biomedicina. Existen numerosos ejemplos de *composites* diseñados para regeneración ósea como las mezclas colágeno-hidroxiapatita o biovidrio-polietileno de alta densidad [*Lizarbe MA 2007, Rev R Acad Cienc Exact Fis Nat*]. En estudios *in vitro* con fibroblastos L929 y osteoblastos Saos-2 cultivados sobre *nanocomposites* compuestos

por partículas de apatita nanocristalina embebidas uniformemente en un vidrio mesoporoso, se obtuvo una mejor biocompatibilidad que la encontrada con vidrios mesoporosos sin apatita [*Cicuéndez M et al. 2012, Chem Mater*].

3. TEJIDO ÓSEO

El hueso es un tipo especializado de tejido conectivo y forma con el cartílago el sistema esquelético que, junto con el sistema nervioso, articular y muscular, constituye el aparato locomotor. Además de las funciones mecánicas, el hueso desempeña un papel protector de órganos vitales y de la médula ósea, así como una importante función metabólica actuando de reservorio de calcio, fosfato y otros iones.

3.1 Tipos de hueso

Atendiendo a su estructura macroscópica, se identifican dos tipos de tejido óseo: **hueso cortical o compacto**, más denso localizado en la zona externa del hueso, y **hueso trabecular o esponjoso**, formado por una malla esponjosa compuesta por espículas anastomosadas en la zona más interna, limitando el espacio ocupado por la médula ósea.

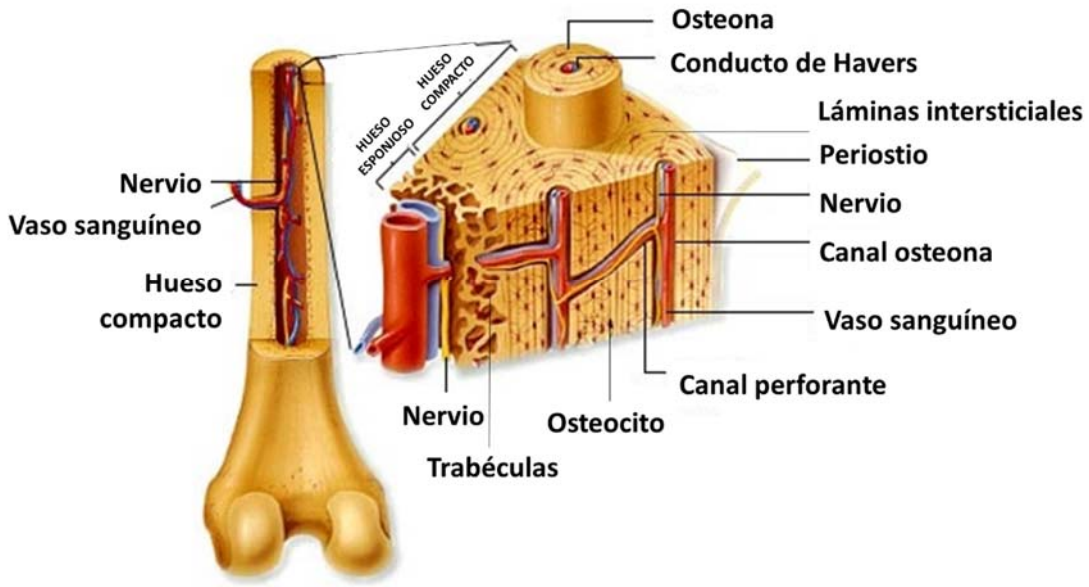

Figura 5. Detalle de la estructura del hueso compacto y el hueso esponjoso. Imagen procedente de http://www.anatomiahumana.ucv.cl/kine1/top2.html

Cuando el hueso está maduro está compuesto de unidades estructurales llamadas **osteonas o sistemas de Havers**. Tal como se aprecia en la **Figura 3**, las osteonas se componen a su vez de laminillas concéntricas de matriz ósea alrededor de un conducto central (conducto de

Havers) por donde pasan vasos y nervios. Las fibras colágenas de las laminillas son paralelas entre sí pero presentan una orientación diferente a las de las laminillas contiguas, confiriendo una mayor resistencia a esta estructura. Los canales perforantes o conductos de Volkmann se encargan de unir los conductos de Havers entre sí y con el endostio y el periostio. Entre los sistemas de Havers se encuentran laminillas intersticiales que consisten en restos de otras osteonas más antiguas.

Atendiendo a la forma y a su ubicación específica en el cuerpo, se diferencian cuatro tipos de hueso [*Ross MH et al. 2010, Editorial Médica Panamericana*]:

- **Huesos largos**, como el fémur o la tibia, llamados así por su mayor longitud respecto a las otras dos dimensiones. Se componen de una diáfisis (parte central del hueso) y dos epífisis (extremo dilatado) recubiertas de cartílago hialino. Entre ambas partes se encuentra la metáfisis. La parte interna del hueso la forma la cavidad medular, que en la diáfisis está rodeada de una pequeña capa de tejido óseo esponjoso. El resto de la diáfisis lo forma el tejido óseo compacto. Sin embargo, en las epífisis ocurre lo contrario, siendo mayoritario el tejido óseo esponjoso.
- **Huesos cortos**, como los huesos del carpo, con tres dimensiones casi iguales, formados por una fina corteza de hueso compacto y un interior de hueso esponjoso. Suelen encontrarse en articulaciones móviles por lo que están rodeados por cartílago hialino en la superficie articular. El resto de la superficie está recubierta por una cápsula de tejido conjuntivo denominada periostio.
- **Huesos planos***,* como el esternón, son delgados y anchos. Están formados por dos capas de hueso compacto gruesas con una capa interpuesta de tejido óseo esponjoso.
- **Huesos irregulares**, como las vértebras, son aquellos que por su forma no se pueden clasificar dentro de los grupos anteriores.

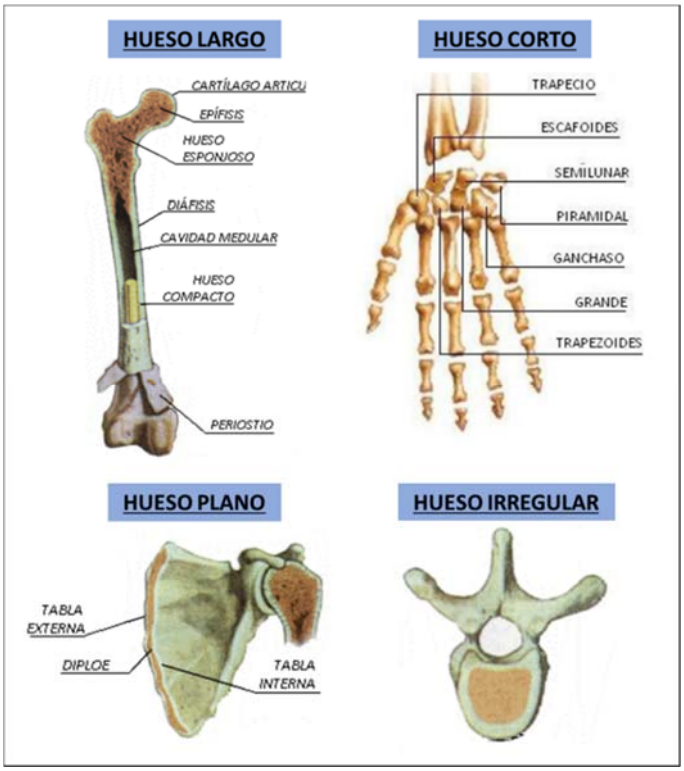

Figura 6. **Detalle de los tipos de hueso que componen el esqueleto humano.** Imagen procedente de http://biologiaconlastics.blogspot.com.es/2014/10/tejido-oseo-esqueleto.html

3.2 Componentes del tejido óseo

El tejido óseo es un tipo de tejido conjuntivo que tiene la particularidad de tener su matriz mineralizada, causa por la cual presenta la dureza necesaria para ejercer una función de sostén y protección. Inmersos en dicha matriz se encuentran diferentes tipos celulares encargados del mantenimiento de la estructura y de las funciones óseas, tal como se describe a continuación.

3.2.1 Matriz ósea

La matriz ósea está formada por una fase mineral (65%) y una fase orgánica (35%), responsable de las propiedades biomecánicas del hueso.

La **fase mineral** se compone mayoritariamente de hidroxiapatita [$Ca_{10}(PO_4)_6(OH)_2$] que le da rigidez al tejido. Esta fase presenta también una serie de sustituciones aniónicas y catiónicas que constituyen una fuente de nutrientes inorgánicos importante. Estas sustituciones pueden representar hasta el 8 % de carbonato, 0,5 % de magnesio, 0,8 % de sodio y una serie de elementos ultra-traza como zinc, estroncio, potasio y silicio [*Yamada MO et al. 2003, Biol Trace Elem Res*].

La **fase orgánica** está constituida principalmente por fibras de colágeno de tipo I y V, aunque se pueden encontrar otros tipos minoritarios. El colágeno constituye el 90% de las proteínas de la matriz ósea, confiriéndole flexibilidad al hueso. Los cristales de hidroxiapatita se encuentran embebidos en las fibras de colágeno. Esta unión no es directa sino a través de otras proteínas que además permiten el anclaje de células. El 10% restante lo constituyen proteínas no estructurales encargadas del desarrollo, crecimiento, remodelado y reparación del hueso. Estas proteínas no colágenas se clasifican en macromoléculas de proteoglicanos (otorgan la resistencia a la compresión), glicoproteínas multiadhesivas (mediadoras de la adhesión de las células óseas con las proteínas de la fase orgánica), proteínas dependientes de vitamina K osteoespecíficas y factores de crecimiento y citoquinas con funciones diversas. Entre las glicoproteínas multiadhesivas destaca la osteonectina, con un papel adhesivo entre el colágeno y los cristales de hidroxiapatita, y las sialoproteínas como la osteopontina, que media la adhesión de las células a la matriz ósea. La osteocalcina es una proteína dependiente de vitamina K encargada de captar el calcio desde la circulación y atraer a los osteoclastos para estimular el remodelado óseo. Por su parte, las proteínas morfogenéticas (BMPs) óseas son péptidos producidos por los osteoblastos que participan en la regulación de procesos de proliferación y diferenciación celular implicados en la formación de tejido óseo [*Ross MH et al. 2010, Editorial Médica Panamericana*].

3.2.2 Células óseas

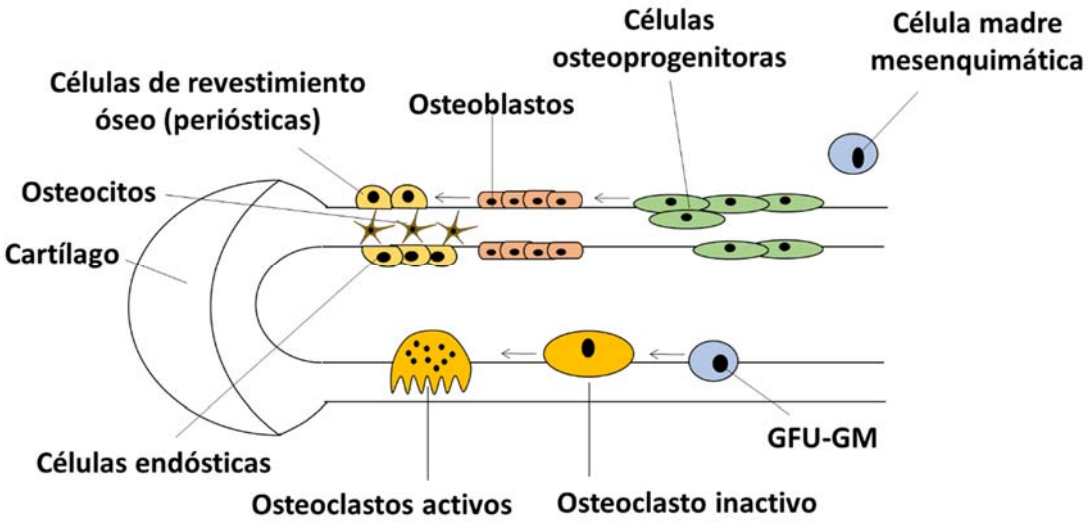

Figura 7. Detalle de las células que componen el tejido óseo. Imagen modificada procedente de [Ross MH et al. 2010, Editorial Médica Panamericana].

En el tejido óseo se encuentran diferentes tipos celulares: osteoblastos (encargados de la osteogénesis), osteoclastos (encargadas de la resorción ósea), osteocitos (células maduras del hueso con un papel regulador), células osteoprogenitoras (precursoras) y células de revestimiento (encargadas de la transferencia de nutrientes y la respuesta hormonal) [*Skalak R et al. 1987, McGrawHill*]. Todas ellas proceden de un mismo tipo de células progenitoras de origen mesenquimal, a excepción de los osteoclastos, que proceden de células progenitoras hematopoyéticas.

- Células osteoprogenitoras

Son derivadas de células madre mesenquimales de médula ósea y son, a su vez, precursoras de los osteoblastos, principales encargados de la formación de hueso. Estas células se encuentran en la superficie externa e interna del hueso y posiblemente en la microvasculatura que irriga el tejido óseo.

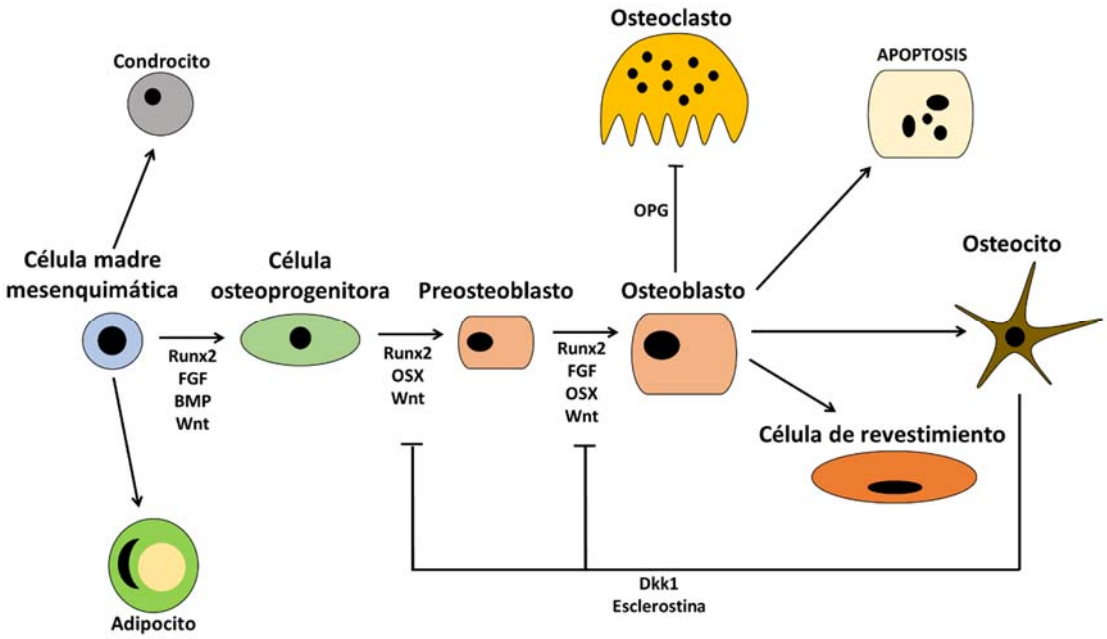

Figura 8. **Proceso de diferenciación de osteoblastos a partir de células madre mesenquimáticas.** Imagen modificada a partir de figuras de los trabajos [*Escobar-Gómez F et al. 2009, REEMO; Arboleya L et al. 2013, Reumatología Clínica*].

Como queda detallado en la **Figura 8**, el proceso de diferenciación de osteoblastos comienza a partir de las células mesenquimales que dan lugar a dos grandes poblaciones: condrocitos formadores de cartílago y células pericondriales. Una subpoblación de estas células pericondriales es diferenciada a osteoblastos gracias al papel esencial que juegan el factor de

transcripción 2 relacionado con Runt (Runx2/Cbfa1) y el factor de transcripción osterix (Osx) [*Otto F et al. 1997, Cell / Nakashima K et al. 2002, Cell*]. El proceso de diferenciación completo tiene lugar mediante la formación de diferentes precursores asociada a la activación secuencial de determinados factores de transcripción. En primer lugar, se forman células mesenquimales osteocondroprogenitoras, seguidas de precursores de osteoblastos Runx2-positivos. A continuación, estas células se diferencian a precursores de osteoblastos Osx-positivos que finalmente se diferencian a osteoblastos formadores de hueso [*Akiyama H et al. 2005, PNAS USA*]. Runx2 es el factor más relevante durante la diferenciación, aunque no es suficiente para llevar a cabo todo el proceso. Runx2/Cbfa1 activa directamente la expresión de muchos marcadores de osteoblastos y osteocitos como el colágeno tipo I, osteopontina, sialoproteína y osteocalcina [*Inohaya K et al. 2000, Dev Genes Evol*] Ambos factores Osx y Runx2 parecen ser puntos integradores de otras señales, a través de diferentes rutas, regulando así la actividad y la diferenciación osteoblástica [*Chau JF et al. 2009, Histol Histopathol*].

Como se observa en la **Figura 9**, en el proceso de diferenciación también intervienen otras moléculas a través de diferentes rutas de señalización, como la hormona paratiroidea (PTH), la proteína relacionada con la misma (PTHrP), hedgehog (Hh), Wnt (Wingless e Int), la proteína morfogenética ósea (BMP) y Notch (Delta) [*Arboleya L et al. 2013, Reumatol Clín*]. Se desconoce el orden exacto de activación de cada vía durante el proceso, sin embargo, todos los estudios parecen indicar que se inicia por el ligando Hh, el cual solo parece participar en las etapas iniciales de la diferenciación [*Hojo H et al. 2014, Regen Med*]. Más concretamente, uno de los homólogos de Hh que se encuentran en mamíferos, Ihh (Indian Hedgehog), es esencial en el proceso de osificación endocondral al ser expresado y secretado por precondrocitos para forzar la diferenciación a osteoblastos de una subpoblación de células del pericondrio [*Long F et al. 2004, Development*] en el paso en el que las células se convierten en Runx2-postivas.

En el caso de la vía Wnt, tanto la vía canónica como la no canónica parecen estar implicadas en el proceso de osificación [*Andrade AC et al. 2007, Bone*]. La vía canónica es la dominante, en la que Wnts se une a los receptores Frizzled desencadenando la estabilización de la β-catenina por parte de la proteína 5/6 relacionada con el receptor de baja densidad de lipoproteínas (LRP5/6), y con ello, dando lugar a la activación de ciertos factores de transcripción que a su vez activan determinados genes como Runx2 y Sox9 [*Kobayashi Y et al. 2008, Jpn Dent Sci Rev*]. La vía no canónica de Wnt incluye una ruta de señalización Ca^{2+}/proteína quinasa A, una ruta de polaridad celular y una ruta dependiente de proteína quinasa C [*Johnson ML et al. 2006, Rev Endocr Metab Dis*]. Estudios genéticos muestran que la actividad de la vía Wnt es esencial en varios puntos del proceso de diferenciación de osteoblastos y, más concretamente, cuando las células se convierten en Osx-positivas [*Rodda SJ et al. 2006, Development*]. La vía

Wnt no solo ejerce un efecto potenciador sobre la diferenciación de las células mesenquimales a osteoblastos, sino que también inhibe la diferenciación de estas células hacia otros tipos celulares como adipocitos o condrocitos, y está implicada en la producción de osteoprotegerina, reduciendo la actividad osteoclástica y la resorción ósea [*Escobar-Gómez F et al. 2009, REEMO*].

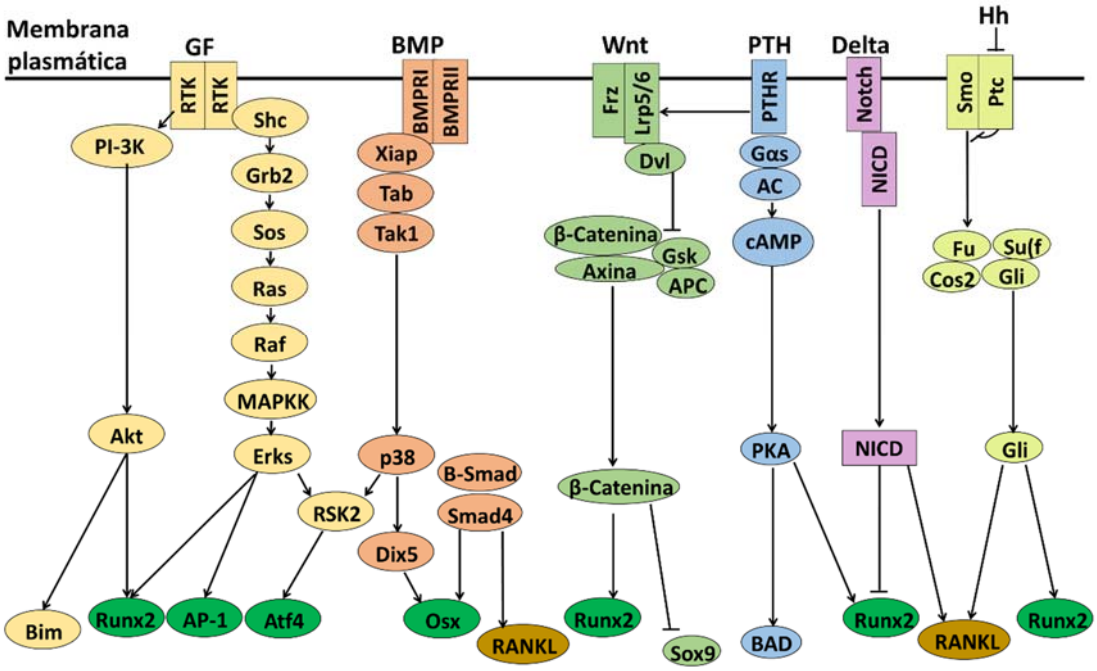

Figura 9. **Rutas de señalización implicadas en el proceso de diferenciación de los osteoblastos.** Imagen modificada a partir [*Chau JF et al. 2009, Histol Histopathol*].

Los ligandos Notch como Jagged o similares a Delta (Delta-like) se unen a los receptores Notch ocasionando su autoprocesamiento proteolítico. Esto da lugar a la liberación del dominio intracelular, el cual se transloca al núcleo [*Schroeter EH et al. 1998, Nature*] e interacciona con el factor de transcripción de la familia CSL dando lugar en última instancia a la transcripción de genes implicados en el proceso de diferenciación osteoblástica. Concretamente, estos genes parecen implicados en el mantenimiento de un *pool* de células progenitoras mesenquimales. El proceso de homeostasis y formación ósea controlada por Notch posiblemente sea modulado por otros factores de señalización como son BMP, Wnt, Runx2 y Osx [*Hojo H et al. 2014, Regen Med*].

Por último, el factor de crecimiento transformante β (TGF-β) y la proteína morfogenética de hueso o BMP, actúan a través de receptores heterotetraméricos serina-treonina quinasas tipo I y II. Una vez unido el ligando el receptor de tipo II, fosforila al receptor de tipo I en un dominio rico en serina y glicocola dando lugar a la activación del receptor Smad. A su vez, Smad se une a Co-Smad y juntos se translocan al núcleo activando factores de transcripción implicados

en el proceso de diferenciación [*Derynck R et al. 2003, Nature*]. Aunque BMP tiene un papel potenciador de la diferenciación de osteoblastos [*Gazzerro E et al. 2006, Rev Endocr Metab Dis*], no parece estar directamente implicada en el proceso de especificación de linaje osteoblástico sino en el mantenimiento de la homeostasis ósea tras el nacimiento [*Hojo H et al. 2014, Regen Med*]. En cuanto TGF-β, es liberado durante el proceso de resorción ósea induciendo la migración de células mesenquimales a la médula ósea [*Tang Y et al. 2009, Nat Med*]. Ciertos estudios muestran una acción recíproca entre los miembros de la superfamilia TGF-β y las proteínas Wnt, Hh y Notch, por lo que podrían actuar de forma conjunta en diferentes estadíos del proceso de diferenciación [*Guo X et al. 2009, Cell Res*].

Los osteocitos son capaces de secretar Dkk1 y esclerostina (ésta última sintetizada a partir de la expresión del gen SOST), encargados de producir una retroalimentación negativa, inhibiendo el proceso de diferenciación de osteoblastos (**Figura 6**) [*Escobar-Gómez F et al. 2009, REEMO].*

- *Osteoblastos*

Este tipo celular está formado por células diferenciadas que aún poseen capacidad proliferativa y secretora. Son las encargadas de secretar colágeno tipo I así como proteínas de la matriz que constituyen el osteoide (matriz ósea no mineralizada inicial). Estas proteínas incluyen proteínas fijadoras de calcio como la osteonectina, osteocalcina, sialoproteínas, osteopontina, proteoglicanos y fosfatasa alcalina. Esta última está implicada en la iniciación del proceso de mineralización por parte de los osteoblastos y es secretada en gran cantidad por este tipo celular [*Ross MH et al. 2010, Editorial Médica Panamericana*].

Desde un punto de vista morfológico, los osteoblastos secretores de matriz en mamíferos presentan una forma característica cuboidal, con un gran núcleo excéntrico y prominente retículo endoplasmático rugoso y áreas de Golgi. Emiten protrusiones y pseudópodos hacia el osteoide y expresan ciertos marcadores como sialoproteína, osteocalcina, E11, vitronectina o colágeno de tipo I. Sin embargo, los preosteoblastos presentan una morfología menos cuboidal y se localizan a mayor distancia de la superficie ósea. Además de producir colágeno tipo I también poseen marcadores específicos como osteonectina, fosfatasa alcalina, IL6, receptor de PTH/PTHrP o algunas integrinas [*Franz-Odendaal TA et al. 2006, Dev Dynam*].

Los osteoblastos intervienen en el crecimiento y en el **remodelado óseo**. Una vez los osteoclastos han resorbido una determinada zona del hueso, el osteoblasto recibe señales para migrar a la zona de remodelado (ya sea de la propia matriz reabsorbida o procedentes de osteoclastos activos) para iniciar la formación de nuevo hueso. Con la constitución del osteoide, los osteoblastos se ven rodeados por la matriz que van produciendo y quedan incluidos

totalmente en él (**Figura 10**). Según se van rodeando de la matriz, los osteoblastos se van transformando en osteocitos de forma progresiva pasando por etapas intermedias que algunos autores definen como osteocitos grandes, osteocitos jóvenes u osteocitos osteoides, caracterizados por el mayor tamaño en comparación con los osteocitos maduros y por presentar un aparato de Golgi muy desarrollado para el almacenamiento de colágeno [*Franz-Odendaal TA et al. 2006, Dev Dynam*].

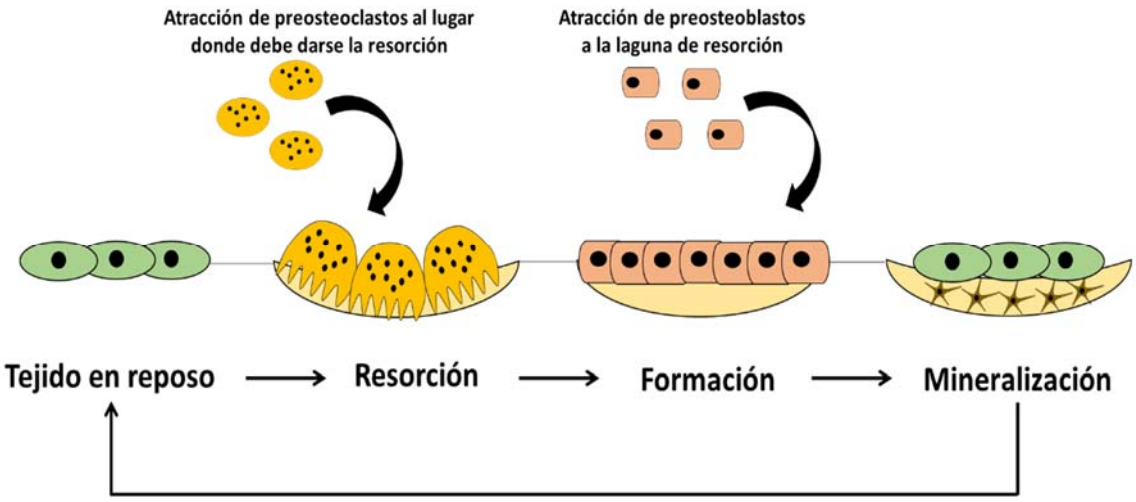

Figura 10. Proceso de remodelado óseo. Imagen modificada a partir [*Reyes-García R et al. 2011, Endocrinología y nutrición*].

Ciertos autores defienden que durante la transformación a osteocitos, los osteoblastos pueden quedar embedidos por la matriz de células adyacentes que continúan con el proceso de secreción [*Franz-Odendaal TA et al. 2006, Dev Dynam / Palumbo C et al. 1990, Acta Anat]*. Por otro lado, los osteoblastos también pueden entrar en apoptosis o quedar inactivos como células de revestimiento [*Arboleya L et al. 2013, Reumatol Clín*].

- Osteocitos

Este tipo celular es el más abundante del tejido óseo (90-95%) y también el más longevo, pudiendo alcanzar 25 años de vida [*Franz-Odendaal TA et al. 2006, Dev* Dynam]. Su función consiste en el mantenimiento de la matriz ósea en la que se encuentra inmerso. El espacio que ocupan los osteocitos se adapta a la morfología celular y se denomina laguna u osteoplasto. A través de una serie de canalículos, estas células entran en contacto con osteocitos vecinos y otras células como osteoblastos, células endoteliales y osteoclastos superficiales, mediante la emisión de prolongaciones citoplasmáticas compuestas por estructuras nodales especializadas [*Batra N et al. 2012, Biochim Biophys Acta*]. A través de estos canalículos, los osteocitos secretan

una gran cantidad de moléculas de señalización como RANKL y OPG (para estimular el proceso de remodelado), PGE2 (estimulador de la formación ósea), óxido nítrico (estimulador de osteoformación e inhibidor de resorción), Dkk y esclerostina (antagonistas de la vía Wnt canónica) [*Lerner UH 2012, Seminars in Orthodontics*]. También establecen contacto indirecto con osteoblastos y otras células lejanas mediante la expresión de diferentes moléculas de señalización [*Franz-Odendaal TA et al. 2006, Dev* Dynam].

Los osteocitos maduros presentan una morfología estelar y un tamaño menor que sus precursores así como un retículo endoplasmático y aparato de Golgi mucho más reducidos debido la menor síntesis de proteínas de secreción [*Dudley HR et al. 1961, J Biophys Biochem Cytol*].

Una de sus funciones es la mecano-transducción, es decir, la respuesta a fuerzas mecánicas sobre el hueso como por ejemplo el aumento de carga mecánica y la falta de gravedad. Para ello, el osteocito cuenta con la capacidad de sintetizar matriz nueva y resorberla, aunque en un grado limitado. Este hecho hace que también tengan un papel importante en la calcemia. Sin embargo, estas células no poseen capacidad proliferativa [*Ross MH et al. 2010, Editorial Médica Panamericana*]. Cuando éstas mueren por apoptosis, por ejemplo tras la producción de microfracturas óseas, secretan RANKL dando lugar a la resorción de la zona por parte de los osteoclastos, seguida del proceso de de formación de nuevo hueso por los osteoblastos [*Martin TJ et al. 2008, Best Pract Res Clin Endocrinol Metab*].

- *Osteoclastos*

Son células multinucleadas de gran tamaño encargadas de la resorción ósea que incluye la degradación de la fase mineral del hueso y de la matriz ósea. Este proceso es esencial para la reparación y el remodelado óseo.

A diferencia del resto de tipos celulares que componen el hueso, los osteoclastos proceden de células madre hematopoyéticas medulares denominadas "Unidades Formadoras de Colonias de Granulocitos y Macrófagos" (CFU-GM), pertenecientes al linaje monocito/macrófago [*Burger et al. 1982, J Exp Med*].

A partir de precursores mieloides la célula lleva a cabo su diferenciación cuando recibe el estímulo de diferentes factores de crecimiento y citoquinas entre los cuales son esenciales el ligando del receptor activador del factor nuclear kappa B (RANKL) y el factor estimulador de colonias macrofágico (M-CSF) (**Figura 11**) [*Väänänen HK et al. 2008 Arch Biochem Biophys*].
M-CSF estimula la proliferación de CFU-GM para mantener el *pool* de células mononucleares. En esta fase de diferenciación los precursores se caracterizan por la falta de dos marcadores: la fosfatasa ácida resistente a tartrato (TRAP) y el receptor de calcitonina (CTR). Cuando reciben

señales de tipo quimiotáctico se induce su migración desde el torrente sanguíneo al lugar de resorción y la unión a la matriz ósea. Ante la estimulación por M-CSF y RANKL las células se prefusionan dando lugar a células TRAP+ y CTR+, que finalmente se convierten en células multinucleadas por fusión [*Feng X 2005, Gene*]. En este estadio aún no son funcionales ya que debe darse el proceso de polarización celular, para lo que es esencial el estímulo de RANKL [*Suda et al. 1999, Endocr Rev*]. RANKL es una molécula de superficie implicada en el mantenimiento de la homeostasis del hueso, la función inmune, el desarrollo de glándulas mamarias y el proceso de diferenciación de osteoclastos. Esta molécula es esencial también para la supervivencia de este tipo celular. Otros miembros de la familia TNF, a la que pertenece RANKL, tales como TNF-α, FasL y TRAIL, parecen implicados en los procesos de diferenciación, actividad, supervivencia y apoptosis de los osteoclastos [*Feng X 2005, Gene*].

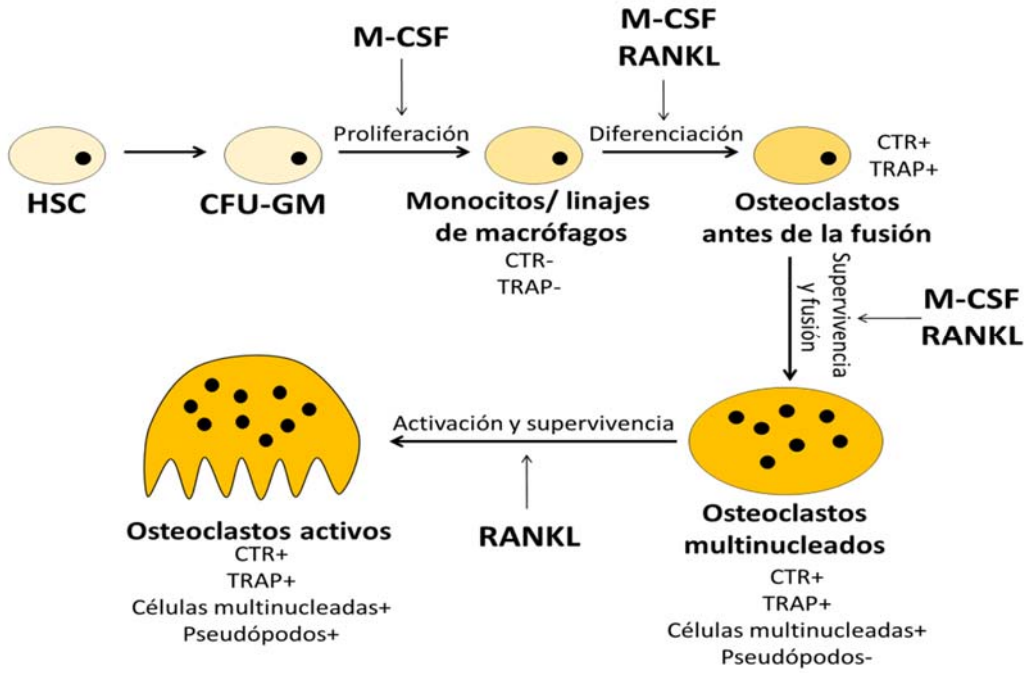

Figura 11. Proceso de diferenciación de osteoclastos. Esquema procedente de [*Feng X 2005, Gene*].

Tanto M-CSF como RANKL (soluble y unido a la membrana) son expresados por los osteoblastos y células mesenquimales estromales (MSC). Estas moléculas se unen a c-fms [*Sherr CJ et al. 1988, J Cell Biochem*] y RANK respectivamente, expresadas por los precursores de osteoclastos, lo que demuestra que la interacción entre osteoblastos y osteoclastos es esencial para que cada tipo celular pueda ejercer su función y tenga lugar el acoplamiento necesario entre osteoblastos y osteoclastos para el remodelado óseo. [*Spence et al. 2008, J Biomed Mater Res A*]. Se ha podido observar *in vitro* que solo M-CSF y RANKL son esenciales para la osteoclastogénesis [*Quinn et al. 1998 Endocrinology*]. Los osteoblastos también producen moléculas inhibitorias del proceso de diferenciación de osteoclastos como la osteoprotegerina

(OPG) que se une a RANKL y compite con RANK, impidiendo la unión RANK-RANKL [*Suda et al. 1999, Endocr Rev / Teitelbaum SL 2000 Science*].

Muchas sustancias osteotrópicas como dexametasona, vitamina D3 $1\alpha25(OH)_2$ [*Kitazawa et al. 1999, Biochim Biophys Acta*] y citoquinas como IL-1 y TNF-α [*Yasuda et al. 1998, Proc Natl Acad Sci USA*] regulan la osteoclastogénesis de forma indirecta, al modular la expresión de RANKL en osteoblastos. Sin embargo TGF-β tiene el efecto contrario ya que suprime la expresión de este ligando [*Takai et al. 1998, J Biol Chem*].

En experimentos *in vivo*, ratones carentes del gen de RANK o RANKL presentaron osteopetrosis, demostrando que ambas moléculas son esenciales para la función osteoclástica [*Dougall WC et al. 1999, Genes Dev*]. Por otra parte, ratones con deficiencia en OPG desarrollaron osteoporosis [*Bucay N et al. 1998, Genes Dev*] mientras que aquellos con sobreexpresión de esta proteína padecieron osteopetrosis [*Simonet WS et al. 1997, Cell*]. Todo ello demuestra la gran importancia de todas estas moléculas en la regulación de los procesos implicados en el correcto mantenimiento del hueso.

Una vez que RANKL interacciona con RANK se activa una cascada de señalización intracelular que comienza por la activación de proteínas TRAF que a su vez activan el complejo NF-κB y JNK que estimulan la expresión de genes implicados en la diferenciación.

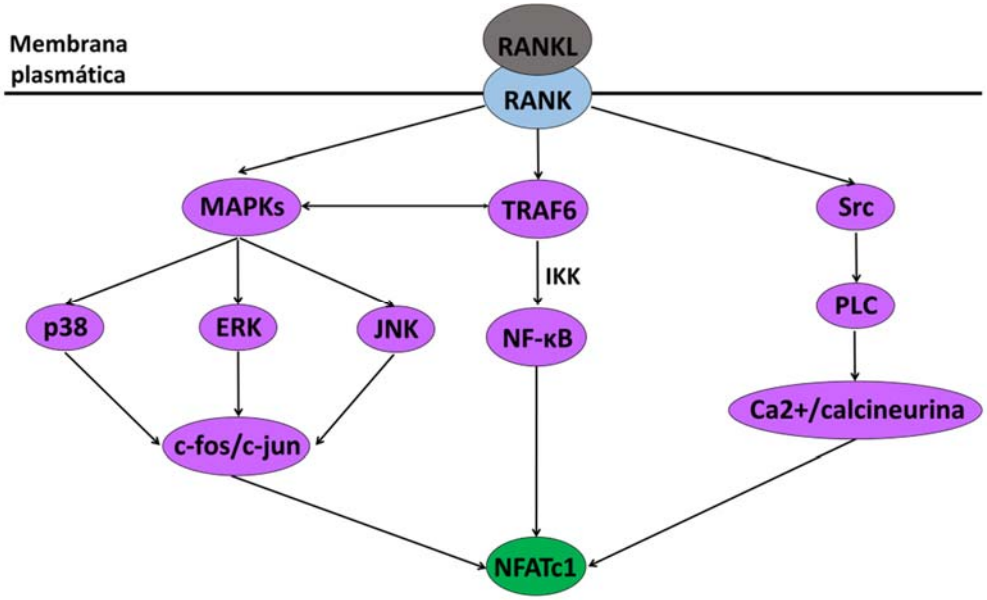

Figura 12. **Rutas de señalización implicadas en el proceso de diferenciación de los osteoclastos.** Imagen modificada a partir [*Riancho JA et al. 2011, Reumatol Clin*].

Cuando el osteoclasto está totalmente diferenciado posee entre cinco y ocho núcleos y la disposición de los filamentos de actina en forma de anillo, ambos parámetros visibles por microscopía confocal. Sin embargo, experimentos *in vitro* muestran que osteoclastos

mononucleares pueden poseer capacidad resortiva, aunque las células multinucleares son necesarias en procesos de resorción rápida. A pesar de desconocerse la edad media de un osteoclasto, hay muchas evidencias que apoyan que una vez que comienzan su función resortiva tienen un tiempo limitado de vida y terminan por entrar en apoptosis [*Väänänen HK et al. 2008 Arch Biochem Biophys*].

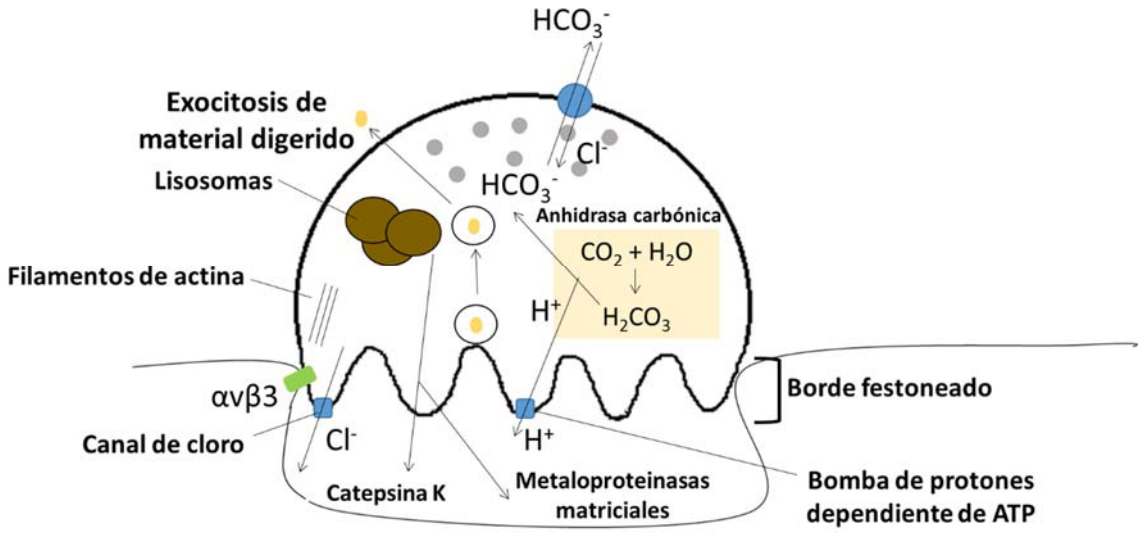

Figura 13. Detalle de la actividad del octeoclasto. Imagen modificada [*Ross MH et al. 2010, Editorial Médica Panamericana*].

El osteoclasto funcional posee al menos cuatro dominios de membrana claramente diferenciados: zona de sellado, borde festoneado, región basolateral y dominio secretor [*Väänänen HK et al. 1998, Mater Sci Eng*].

- Zona de sellado: Cuando la célula monocítica llega al hueso se une a la matriz ósea íntimamente creando una laguna de resorción aislada del fluido extracelular. Es en esta laguna donde se produce el proceso de resorción siendo visible por microscopía confocal un anillo de actina claramente definido, compuesto por microfilamentos de actina y rodeado por proteínas como vinculina y talina. La fuerte interacción con la matriz ósea se debe a diferentes moléculas de adhesión como la integrina $\alpha_v\beta_3$.

- Borde festoneado: Es la porción de la célula en contacto directo con el tejido óseo y encargado directamente de la resorción. Su nombre se debe a la gran cantidad de repliegues de la membrana plasmática de este dominio, en forma de microvellosidades, destinados a aumentar la superficie para la exocitosis de enzimas hidrolíticas y protones a la zona de sellado. Una serie de bombas dependientes de ATP (ATPasa de tipo V) se encargan de la liberación de protones (que acidifican la zona de sellado) y son necesarias para la endocitosis de los productos de degradación y detritos óseos.

- Región secretora: Zona apical de la célula donde concretamente se liberan las sustancias contenidas en vesículas destinadas al proceso de resorción ósea.

- Región basolateral: Una vez producida la resorción, el material disuelto es endocitado y transportado mediante vesículas de transporte con material óseo por un proceso de transcitosis hasta la región basolateral donde se libera al medio extracelular.

Cuando el osteoclasto está totalmente diferenciado puede llevar a cabo el proceso de resorción que comienza con la disolución de la hidroxiapatita, para lo cual es esencial el pH ácido promovido por los protones secretados a la laguna de resorción. Estos protones son producidos por la anhidrasa carbónica citoplásmica que realiza un intercambio entre protones y aniones bicarbonato que son expulsados al medio a través de un intercambiador Cl^-/HCO_3 localizado en la región basolateral. A su vez hay un gran número de canales de cloro en el borde festoneado para poner mantener la electroneutralidad (**Figura 13**) [*Väänänen HK et al. 1998, Mater Sci Eng*]. Tras la disolución de la fase mineral del hueso, quedan en forma soluble iones calcio y fosfato que deben ser liberados al medio extracelular. El mecanismo por el que esto ocurre no se conoce con claridad aunque se presume que puede llevarse a cabo mediante transcitosis, la unión de estos iones a proteínas o liberación de los iones por debajo del borde festoneado.

Una vez disuelta la fase mineral, queda expuesta la matriz ósea a enzimas proteolíticas entre las cuales destacan dos grandes grupos: las metaloproteinasas (MMPs) y las catepsinas lisosomales. La catepsina K es expresada por los osteoclastos en grandes cantidades y secretada a la laguna de resorción pudiendo hidrolizar el colágeno de tipo I a pH ácido. [*Väänänen HK et al. 2008 Arch Biochem Biophys*]. Modelos tanto *in vitro* como *in vivo* han mostrado que la inhibición de este enzima suprime la degradación de la matriz orgánica [*Bossard MJ et al. 1996, J Biol Chem / Votta BJ et al. 1997, J Bone Miner Res*] y que la deleción del gen para esta proteína causa osteopetrosis en ratones (*Saftig P et al. 1998, PNAS / Gowen M et al. 1999, J Bone Miner Res*]. Por otra parte, también se ha observado que casi todos los tipos de catepsina K son producidos por macrófagos RAW 264.7 que han sido diferenciados a osteoclastos [*Czupalla C et al. 2006, Mol Cell Proteomics*].

La catepsina K activa por procesamiento proteolítico otra de los enzimas características de osteoclastos, la fosfatasa ácida resistente a tartrato (TRAP) que, a su vez, estimula la producción de especies reactivas de oxígeno. Esto último facilita la degradación de colágeno [*Halleen JM et al. 2003, J Bone Miner Res*].

Respecto a las metaloproteinasas, los osteoclastos producen principalmente MMP9 y MMP14 [*Andersen TI et al. 2004, Bone*]. Al inhibir estos enzimas no se altera de forma significativa el proceso de degradación de la matriz mostrando un papel menos importante en

el proceso de resorción. Los últimos estudios parecen indicar que MMP, como MMP13, inician el proceso de degradación, que continúan las catepsinas. [*Behonick DJ et al. 2007, PLoS ONE*].

- Células de revestimiento óseo

Son células derivadas de osteoblastos que tapizan el tejido óseo que no está en proceso de remodelación. Según su localización en el hueso pueden ser perióstica (superficies externas) o endósticas (superficies internas). Presentan una serie de prolongaciones con las que contactan con los osteocitos por lo que se las cree implicadas en el mantenimiento y nutrición de osteocitos así como en el transporte de calcio y fosfato entre hueso y sangre. Entre ellas se establecen uniones intercelulares en hendidura [*Ross MH et al. 2010, Editorial Médica Panamericana*]. Estas células están implicadas en la delimitación de la zona multicelular de remodelado, creando un microentorno para el acoplamiento de osteoclastos y osteoblastos [*Hauge EM et al. 2001, J Bone Miner Res*].

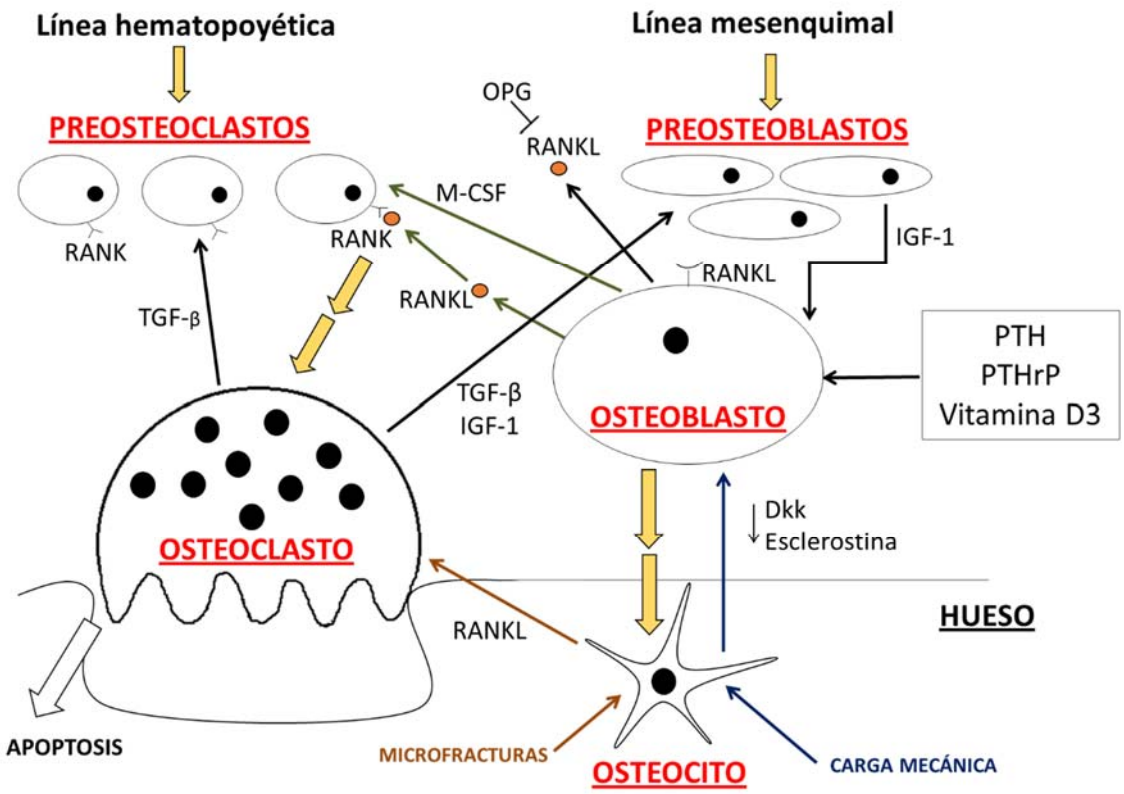

Figura 14. Detalle de las principales interacciones entre las diferentes células que componen el tejido óseo. Imagen modificada a partir de la ilustración de [Lerner UH 2012, Seminars in Orthodontics; Garzón-Alvarado DA 2010, Revista Cubana de Investigación Biomédica 29(1):17-50, 2010].

REFERENCIAS DE LA INTRODUCCIÓN

1. Abarrategi A, Gutiérrez MC, Moreno-Vicente C, Hortigüela MJ, Ramos V, López-Lacomba JL, Ferrer ML, del Monte F. Multiwall carbon nanotube scaffolds for tissue engineering purposes. Biomaterials, 29(1):94-102, 2008.
2. Akasaka T, Watari F, Sato Y, Tohiji K. Apatite formation on carbon nanotubes. Materials Science and Engineering: C, 26(4):675-678, 2006.
3. Akiyama H, Kim JE, Nakashima K, Balmes G, Iwai N, Deng JM, Zhang Z, Martin JF, Behringer RR, Nakamura T, de Crombrugghe B. Osteo-chondroprogenitor cells are derived from Sox9 expressing precursors. Proc Natl Acad Sci U S A, PNAS USA;102(41):14665-70, 2005.
4. Alcaide M, Serrano MC, Pagani R, Sánchez-Salcedo S, Nieto A, Vallet-Regí M, Portolés MT. L929 fibroblast and Saos-2 osteoblast response to hydroxyapatite-betaTCP/agarose biomaterial. Journal of Biomedical Materials Research Part A, 89(2):539-549, 2009.
5. Alonso S. Control de la macroporosidad de un material compuesto orgánico-inorgánico a base e Hidroxiapatita. Seminario Internacional. Centro de Física Aplicada y Tecnología Avanzada. Universidad Nacional Autónoma de México, 2012.
6. Andersen TL, del Carmen Ovejero M, Kirkegaard T, Lenhard T, Foged NT, Delaissé JM. A scrutiny of matrix metalloproteinases in osteoclasts: evidence for heterogeneity and for the presence of MMPs synthesized by other cells. Bone, 35(5):1107-1119, 2004.
7. Andrade AC, Nilsson O, Barnes KM, Baron J. Wnt gene expression in the post-natal growth plate: regulation with chondrocyte differentiation. Bone, 40(5):1361-1369, 2007.
8. Anselme K. Osteoblast adhesion on biomaterials. Biomaterials, 21(7):667-681, 2000.
9. Arboleya L, Castañeda S. Osteoimmunology: The Study of the Relationship Between the Immune System and Bone Tissue. Reumatología Clínica, 9(5):303–315, 2013.
10. Arcos D. Vidrios mesoporosos bioactivos: implantes y sistemas de liberación de fármacos al servicio de las terapias regenerativas óseas. Anales de la Real Academia Nacional de Farmacia, 2:192-211, 2012.
11. Arcos D, Vallet-Regí M. Bioceramics for drug delivery. Acta Materialia, 61:890-911, 2013.
12. Arcos D. Chapter 3: Calcium Phosphate Bioceramics. Bioceramics with clinical applications. First Edition. Editado por María Vallet, John Wiley & Sons, Ltd, 25-72, 2014.

13. Bagri A, Mattevi C, Acik M, Chabal YJ, Chhowalla M, Shenoy VB. Structural evolution during the reduction of chemically derived graphene oxide. Nature Chemistry. 2(7):581-7, 2010.

14. Balamurugan A, Rebelo AHS, Lemos AF, Rocha JHG, Ventura JMG, Ferreira JMF. Suitability evaluation of sol-gel derived Si-substituted hydroxyapatite for dental and maxillofacial applications through *in vitro* osteoblasts response. Dental Materials, 24:1374-1380, 2008.

15. Batra N, Kar R, Jiang JX. Gap junctions and hemichannels in signal transmission, function and development of bone. Biochimica et Biophysica Acta – Biomembranes, 1818(8):1909-1918, 2012.

16. Behonick DJ, Xing Z, Lieu S, Buckley JM, Lotz JC, Marcucio RS, Werb Z, Miclau T, Colnot C. Role of matrix metalloproteinase 13 in both endochondral and intramembranous ossification during skeletal regeneration. PLoS One, 2(11):e1150, 2007.

17. Best SM, Porter AE, Thian ES, Huang J. Bioceramics: Past, present and for the future. Journal of the European Ceramic Society 28:1319–1327, 2008.

18. Bobbio A. The first endosseus alloplastic implant in the history of man. Bull Hist Dent, 20: 1-6, 1972.

19. Bossard MJ, Tomaszek TA, Thompson SK, Amegadzie BY, Hanning CR, Jones C, Kurdyla JT, McNulty DE, Drake FH, Gowen M, Levy MA. Proteolytic activity of human osteoclast cathepsin K. Expression, purification, activation, and substrate identification. The Journal of Biological Chemistry, 271(21):12517-12524, 1996.

20. Bucay N, Sarosi I, Dunstan CR, Morony S, Tarpley J, Capparelli C, Scully S, Tan HL, Xu W, Lacey DL, Boyle WJ, Simonet WS.. Osteoprotegerin-deficient mice develop early onset osteoporosis and arterial calcification. Genes & Development. 12(9):1260-1268, 1998.

21. Burger EH, van der Meer JW, van de Gevel JS, Gribnau JC, Thesingh GW, van Furth R. *In vitro* formation of osteoclasts from long-term cultures of bone marrow mononuclear phagocytes. The Journal of the Experimental Medicine, 156:1604-1614, 1982.

22. Cabañas MV, Rodríguez-Lorenzo LM, Vallet-Regí M. Setting Behavior and *in Vitro* Bioactivity of Hydroxyapatite/Calcium Sulfate Cements. Chemistry of Materials, 14:3550-3555, 2002.

23. Cabañas MV, Peña J, Román J, Ramírez-Santillán C, Matesanz MC, Feito MJ, Portolés MT, Vallet-Regí M. Design of tunable protein-releasing nanoapatite/hydrogel scaffolds for hard tissue engineering. Materials Chemistry and Physics, 144(3):409-417, 2014.

24. Carlisle E. Si: an essential element for the chick. Science, 178:619-621, 1972.

25. Castner DG, Ratner BD. Biomedical surface science: Foundations to frontiers. Surface Science, 500(1):28-60, 2002.

26. Catledge SA, Fries MD, Vohra YK, Lacefield WR, Lemons JE, Woodard S, Venugopalan R. Nanostructured ceramics for biomedical implants. Journal of Nanoscience and Nanotechnology, 2(3-4):293-312, 2002.

27. Chapman-Sheath P, Cain S, Debes J, Svehla M, Bruce W, Yu Y and Walsh WR. *In vivo* response of coral biomaterials, Journal of Bone and Joint Surgery 85-B:1-2, 2003.

28. Chau JF, Leong WF, Li B. Signaling pathways governing osteoblast proliferation, differentiation and function. Histology & Histopathology, 24(12):1593-1606, 2009.

29. Chen QZ, Thompson ID, Boccaccini AR. 45S5 Bioglass-derived glass-ceramic scaffolds for bone tissue engineering. Biomaterials, 27(11):2414-2425, 2006.

30. Cicuéndez M, Portolés MT, Izquierdo-Barba I, Vallet-Regí M. New Nanocomposite System with Nanocrystalline Apatite Embedded into Mesoporous Bioactive Glass. Chemistry of Materials, 24(6):1100–1106, 2012.

31. Cisneros-Pineda OG, Herrera Kao W, Loría-Bastarrachea MI, Veranes-Pantoja Y, Cauich-Rodríguez JV, Cervantes-Uc JM. Towards optimization of the silanization process of hydroxyapatite for its use in bone cement formulations. Materials Science and Engineering: C, 40:157-163, 2014.

32. Coviello T, Matricardi P, Marianecci C, Alhaique F. Polysaccharide hydrogels for modified release formulations. Journal of Controlled Release 14;119(1):5-24, 2007.

33. Cui W, Cuartas E, Ke J, Zhang Q, Einarsson HB, Sedgwick JD, Li J, Vignery A. CD200 and its receptor, CD200R, modulate bone mass via the differentiation of osteoclasts. Proceedings of the National Academy of Sciences USA. 104(36):14436-41, 2007.

34. Czupalla C, Mansukoski H, Riedl T, Thiel D, Krause E, Hoflack B. Proteomic analysis of lysosomal acid hydrolases secreted by osteoclasts: implications for lytic enzyme transport and bone metabolism. Molecular and Cellular Proteomics, 5(1):134-143, 2006.

35. Çavaş T, Çinkılıç N, Vatan Ö, Yılmaz D. Effects of fullerenol nanoparticles on acetamiprid induced cytoxicity and genotoxicity in cultured human lung fibroblasts. Pesticide Biochemistry and Physiology, 114:1-7, 2014.

36. Da Ros T, Prato M. Medicinal chemistry with fullerenes and fullerene derivatives. Chemical Communications, 663-669, 1999.

37. Daculsi G. Biphasic calcium phosphate concept applied to artificial bone, implant coating and injectable bone substitute. Biomaterials, 19(16):1473-1478, 1998.

38. Derynck R, Zhang YE. Smad-dependent and Smad-independent pathways in TGF-beta family signalling. Nature, 425(6958):577-584, 2003.

39. Doi Y, Shibutani T, Moriwaki Y, Kajimoto T, Iwayama Y. Sintered carbonate apatites as bioresorbable bone substitutes. Journal of Biomedical Materials Research, 39(4):603-610, 1998.

40. Dorozhkin SV. Nanodimensional and Nanocrystalline Apatites and Other Calcium Orthophosphates in Biomedical Engineering, Biology and Medicine. Materials, 2(4), 1975-2045, 2009.

41. Dougall WC, Glaccum M, Charrier K, Rohrbach K, Brasel K, De Smedt T, Daro E, Smith J, Tometsko ME, Maliszewski CR, Armstrong A, Shen V, Bain S, Cosman D, Anderson D, Morrissey PJ, Peschon JJ, Schuh J. RANK is essential for osteoclast and lymph node development. Genes Development 13(18):2412-2424, 1999.

42. Dudley HR, Spiro D. THE FINE STRUCTURE OF BONE CELLS. The Journal of Biophysical and Biochemical Biology. 11(3):627-649, 1961.

43. Escobar-Gómez F, Jódar E, Hawkins F. Receptor Wnt: Fisiología, fisiopatología y potenciales nuevas dianas terapéuticas. Revista Española de Enfermedades Metabólicas Óseas (REEMO), 18(2):39-44, 2009.

44. Feng X. Regulatory roles and molecular signaling of TNF family members in osteoclasts. Gene, 350(1):1-13, 2005.

45. Franz S, Rammelt S, Scharnweber D, Simon JC. Immune responses to implants – A review of the implications for the design of imunomodulatory biomaterials. Biomaterials, 32:6692-6709, 2011.

46. Franz-Odendaal TA, Hall BK, Witten PE. Buried alive: how osteoblasts become osteocytes. Developmental Dynamics, 235(1):176-190, 2006.

47. Frazer RQ, Byron RT, Osborne PB, West KP. PMMA: an essential material in medicine and dentistry. Journal of Long-Term Effects of Medical Implants 15(6):629-39, 2005.

48. Garzón-Alvarado DA, Ramírez-Martínez AM, Silva O. Descripción de la metástasis del cáncer en el tejido óseo a través de un modelo matemático. Revista Cubana de Investigación Biomédica, 29(1):17-50, 2010.

49. Gazzerro E, Canalis E. Bone morphogenetic proteins and their antagonists. Reviews in Endocrine and Metabolic Disorders, 7(1-2):51-65, 2006.

50. Ginebra MP, Driessens FC, Planell JA. Effect of the particle size on the micro and nanostructural features of a calcium phosphate cement: a kinetic analysis. Biomaterials, 25(17):3453-3462, 2004.

51. Gonçalves G, Vila M, Portolés MT, Vallet-Regí M, Gracio J, Marques PA. Nano-Graphene oxide: A potential multifunctional platfor for cancer therapy. Advanced Healthcare Materials 2(8):1072-90, 2013.

52. Gowen M, Lazner F, Dodds R, Kapadia R, Feild J, Tavaria M, Bertoncello I, Drake F, Zavarselk S, Tellis I, Hertzog P, Debouck C, Kola I. Cathepsin K knockout mice develop osteopetrosis due to a deficit in matrix degradation but not demineralization. Journal of Bone and Mineral Research, 14(10):1654-1663, 1999.

53. Grebowski J, Kazmierska P, Krokosz A. Fullerenols as a new therapeutic approach in nanomedicine. Biomed Research International, 2013:751913, 2013.

54. Guldi DM, Sgobba V. Carbon nanostructures for solar energy conversion schemes. Chem Commun 47: 606-610, 2011.

55. Guo X, Wang XF. Signaling cross-talk between TGF-beta/BMP and other pathways. Cell Research,19(1):71-88, 2009.

56. Halleen JM, Räisänen SR, Alatalo SL, Väänänen HK. Potential function for the ROS-generating activity of TRACP. Journal of Bone and Mineral Research, 18(10):1908-1911, 2003.

57. Hauge EM, Qvesel D, Eriksen EF, Mosekilde L, Melsen F. Cancellous bone remodeling occurs in specialized compartments lined by cells expressing osteoblastic markers. Journal of Bone and Mineral Research, 16(9):1575-1582, 2001.

58. Hench LL. Bioceramics and the origin of life. Journal Biomedical Material Research, 23:685-703, 1989.

59. Hench LL. Bioceramics: From Concept to Clinic. Journal of the American Ceramic Society, 74(7), 1487-1510, 1991.

60. Hench LL, Kokubo T. Properties of bioactive glasses and glass-ceramics. Handbook of Biomaterial Properties, 355-363, 1998.

61. Hench LL. The story of Bioglass. Journal of Materals Science: Materials in Medicine, 17:967-978, 2006.

62. Hoffman AS. Hydrogels for biomedical applications. Advanced Drug Delivery Reviews 17;54(1):3-12, 2002.

63. Hojo H, Ohba S, Chung U. Signaling pathways regulating the specification and differentiation of the osteoblast lineage. Regenerative Medicine, 1:57-62, 2015.

64. Honduvilla NG, Bujan J, Lizarbe MA, Bellon JM, Olmo N, Hernando A. Adhesion and stability of fibronectin on PTFE before and after seeding with normal and synchronized endothelial cells: *in vitro* study. Artif Organs, 19:144-153, 1995.

65. Hulbert SF, Hench LL, Forbers D, Bowman LS. History of bioceramics. Ceramics International, 8:131-140, 1982.

66. Iftekhar A. Standard Handbook of Biomedical Engineering and Design. Chapter 12: Biomedical Composites, McGrawHill, 2004.

67. Inohaya K, Kudo A. Temporal and spatial patterns of cbfal expression during embryonic development in the teleost, Oryzias latipes. Development Genes and Evolution, 210(11):570-574, 2000.

68. Johnson ML, Rajamannan N. Diseases of Wnt signaling. Reviews in Endocrine and Metabolic Disorders, 7(1-2):41-49, 2006.

69. Johnson-Lyles DN, Peifley K, Lockett S, Neun BW, Hansen M, Clogston J, Stern ST, McNeil SE. Fullerenol cytotoxicity in kidney cells is associated with cytoskeleton disruption, autophagic vacuole accumulation, and mitochondrial dysfunction. Toxicology and Applied Pharmacology, 248(3):249-258, 2010.

70. Kitazawa R, Kitazawa S, Maeda S. Promoter structure of mouse RANKL/TRANCE/OPGL/ODF gene. Biochim. Biophys. Acta 1445,134-141, 1999.

71. Kobayashi Y, Maeda K, Takahashi N. Roles of Wnt signaling in bone formation and resorption. Japanese Dental Science Review, 44:76-82, 2008.

72. Kokubo T, Kim HM, Kawashita M, Nakamura T. Bioactive metals: preparation and properties. Journal of Materials Science: Materials in Medicine, 15(2):99-107, 2004.

73. Krätschmer W, Lamb LD, Fostiropoulos K, Huffman DH. Solid C60: A new form of carbon. Nature 347: 354-358, 1990.

74. Kroto HW, Heath JR, O´Brien SC, Curl RF, Smalley RE. C60: Buckminsterfullerene. Nature 318: 162-163, 1985.

75. Kular J, Tickner J, Chim SM, Xu J. An overview of the regulation of bone remodelling at the cellular level. Clinical Biochemistry, 45(12):863-873, 2012.

76. Langer R, Vacanti JP. Tissue engineering. Science, 14:260(5110):920-926, 1993.

77. Lanza R, Langer R, Vacanti JP. Principles of Tissue Engineering. Academic Press, 2011. Lee CH, Singla A, Lee Y. Biomedical applications of collagen. International Journal of Pharmaceutics 19;221(1-2):1-22, 2001.

78. Lerner UH. Osteoblasts, osteoclasts and osteocytes: unveiling their intimate-associated responses to applied orthodontic forces. Seminars in Orthodontics, 18(4):237-248, 2012.

79. Li X, Gao H, Uo M, Sato Y, Akasaka T, Feng Q, Cui F, Liu X, Watari F. Effect of carbon nanotubes on cellular functions *in vitro*. Journal of Biomedical Materials Research Part A, 91(1):132-139, 2009.

80. Li X, Gao H, Uo M, Sato Y, Akasaka T, Abe S, Feng Q, Cui F, Watari F. Maturation of osteoblast-like SaoS2 induced by carbon nanotubes. Biomedical Materials 4(1):015005, 2009.

81. Li X, Fan Y, Watari F. Current investigations into carbon nanotubes for biomedical application. Biomedical Materials, 5(2):22001, 2010.

82. Liao S, Xu G, Wang W, Watari F, Cui F, Ramakrishna S, Chan CK. Self-assembly of nano-hydroxyapatite on multi-walled carbon nanotubes. Acta Biomaterialia, 3(5):669-75, 2007.

83. Lizarbe MA. Sustitutivos de tejidos: de los biomaterials a la Ingeniería Tisular. Revisión de la Real Academia de Ciencias Exactas, Físicas y Naturales (VII Programa de Promoción de la Cultura Científica y Tecnológica), 101(1):227-249, 2007.

84. Long F, Chung UI, Ohba S, McMahon J, Kronenberg HM, McMahon AP. Ihh signaling is directly required for the osteoblast lineage in the endochondral skeleton. Development, 131(6):1309-1318, 2004.

85. Martin TJ, Seeman E. Bone remodelling: its local regulation and the emergence of bone fragility. Best Practice & Research Clinical Endocrinology & Metabolism, 22(5):701-722, 2008.

86. Mrdanović J, Solajić S, Bogdanović V, Stankov K, Bogdanović G, Djordjevic A. Effects of fullerenol C60(OH)24 on the frequency of micronuclei and chromosome aberrations in CHO-K1 cells. Mutation Research, 680(1-2):25-30, 2009.

87. Nakashima K, Zhou X, Kunkel G, Zhang Z, Deng JM, Behringer RR, de Crombrugghe B. The novel zinc finger-containing transcription factor osterix is required for osteoblast differentiation and bone formation. Cell, 108(1):17-29, 2002.

88. Novoselov KS, Geim AK, Morozov SV, Jiang D, Zhang Y, Dubonos SV, Grigorieva IV, Firsov AA. Electric field effect in atomically thin carbon films. Science. 306: 666-669, 2004.

89. Otto F, Thornell AP, Crompton T, Denzel A, Gilmour KC, Rosewell IR, Stamp GW, Beddington RS, Mundlos S, Olsen BR, Selby PB, Owen MJ. Cbfa1, a Candidate Gene for Cleidocranial Dysplasia Syndrome, Is Essential for Osteoblast Differentiation and Bone Development. Cell, 89(5):765-771, 1997.

90. Palumbo C, Palazzini S, Zaffe D, Marotti G. Osteocyte differentiation in the tibia of newborn rabbit: an ultrastructural study of the formation of cytoplasmic processes. Acta Anatomica, 137(4):350-358, 1990.

91. Pan S, Aksay A. Factors controlling the size of graphene oxide sheets produced via the graphite oxide route. ACS Nano 5(5):4073-83, 2011.

92. Park S, An J, Jung I, Piner RD, An SJ, Li X, Velamakanni A, Ruoff RS. Colloidal suspensions of highly reduced graphene oxide in a wide variety of organic solvents. Nano Letters. 9(4):1593-1597, 2009.

93. Patino MG, Neiders ME, Andreana S, Noble B, Cohen RE. Collagen as an implantable material in medicine and dentistry. Journal of Oral Implantology 28(5):220-5, 2002.

94. Pietak AM, Reid JW, Stott MJ, Sayer M. Silicon substitution in the calcium phosphate bioceramics. Biomaterials, 28:4023-4032, 2007.

95. Quinn JM, Elliott J, Gillespie MT, Martin TJ. A combination of osteoclast differentiation factor and macrophage colony stimulating factor is sufficient for both human and mouse osteoclast formation *in vitro*. Endocrinology 139, 4424-4427, 1998.

96. Ramakrishna S, Ramalingam M, Sampath Kumar TS, Soboyejo WO. Biomaterials: A Nano Approach, CRC Press, 2010.

97. Rammelt S, Illert T, Bierbaum S, Scharnweber D, Zwipp H, Schneiders W. Coating of titanium implants with collagen, RGD peptide and chondroitin sulfate. Biomaterials. 27(32):5561-71, 2006.

98. Ratner BD. A history of biomaterials. Biomaterials Science (Third Edition)xli-liii, 2013.

99. Real RP, Wolke JG, Vallet-Regí M, Jansen JA. A new method to produce macropores in calcium phosphate cements. Biomaterials, 23(17):3673-3680, 2002.

100. Real RP, Ooms E, Wolke JG, Vallet-Regí M, Jansen JA. *In vivo* bone response to porous calcium phosphate cement. Journal of Biomedical Materials Research Part A, 1;65(1):30-36, 2003.

101. Rempel AA. Nanotechnologies. Properties and applications of nanostructured materials. Russian Chemical Reviews, 76(5):435-461, 2007.

102. Reyes-García R, Rozas-Moreno P, Muñoz-Torres M. Enfermedad cardiovascular y metabolism óseo. Endocrinología y nutrición, 58(7):353-359, 2011.

103. Riancho JA, Delgado-Calle J. Mecanismos de interacción osteoblasto-osteoclasto. Reumatología Clínica, 7(S2):S1-S4, 2011.

104. Rodda SJ, McMahon AP. Distinct roles for Hedgehog and canonical Wnt signaling in specification, differentiation and maintenance of osteoblast progenitors. Development, 133(16):3231-3244, 2006.

105. Saftig P, Hunziker E, Wehmeyer O, Jones S, Boyde A, Rommerskirch W, Moritz JD, Schu P, von Figura K. Impaired osteoclastic bone resorption leads to osteopetrosis in cathepsin-K-deficient mice. Proceeding of the National Academy of Sciences of the United States of America, 95(23):13453-13458, 1998.

106. Sánchez VC, Jachak A, Hurt RH, Kane AB. Biological interactions of graphene-family nanomaterials: an interdisciplinary review. Chemical Research in Toxicology. 25(1):15-34, 2012.

107. Sánchez-Salcedo S, Izquierdo-Barba I, Arcos D, Vallet-Regí M. *In vitro* evaluation of potential calcium phosphate scaffolds for tissue engineering. Tissue Engineering, 12(2):279-290, 2006.

108. Sato M, Webster TJ. Nanobiotechnology: implications for the future of nanotechnology in orthopedic applications. Expert Review of Medical Devices, 1(1):105-14, 2004.

109. Schroeter EH, Kisslinger JA, Kopan R. Notch-1 signalling requires ligand-induced proteolytic release of intracellular domain. Nature, 393(6683):382-386, 1998.

110. Sherr CJ, Roussel MF, Rettenmier CW. Colony-stimulating factor-1 receptor (c-fms). Journal of Cellular Biochemistry, 38(3):179-187, 1988.

111. Simonet WS, Lacey DL, Dunstan CR, Kelley M, Chang MS, Lüthy R, Nguyen HQ, Wooden S, Bennett L, Boone T, Shimamoto G, DeRose M, Elliott R, Colombero A, Tan HL, Trail G, Sullivan J, Davy E, Bucay N, Renshaw-Gegg L, Hughes TM, Hill D, Pattison W, Campbell P, Sander S, Van G, Tarpley J, Derby P, Lee R, Boyle WJ. Osteoprotegerin: a novel secreted protein involved in the regulation of bone density. Cell, 89(2):309-319, 1997.

112. Singh R, Dahotre NB. Corrosion degradation and prevention by surface modification of biometallic materials. Journal of Materials Science: Materials in Medicine, 18(5):725-751, 2007.

113. Skalak R, Chien S. Handbook of Bioengineering, McGraw-Hill, 1987.

114. Spence G, Patel N, Brooks R, Rushton N. Carbonate substitute hydroxiapatite: Resorption by osteoclasts modifies the osteoblastic response. Journal of Biomedical Research Part A, 90(1):217-24, 2009.

115. Sprinkle M, Ruan M, Hu Y, Hankinson J, Rubio-Roy M, Zhang B, Wu X, Berger C, de Heer WA. Scalable templated growth of graphene nanoribbons on SiC. Nature Nanotechnology. 5(10):727-31, 2010.

116. Su Y, Xu JY, Shen P, Li J, Wang L, Li Q, Li W, Xu GT, Fan C, Huang Q. Cellular uptake and cytotoxic evaluation of fullerenol in different cell lines. Toxicology, 269(2-3):155-159, 2010.

117. Suda T, Takahashi N, Udagawa N, Jimi E, Gillespie MT, Martin TJ. Modulation of osteoclast differentiation and function by the new members of the tumor necrosis factor receptor and ligand families. Endocrine Reviews, 20:345-57,1999.

118. Sun L, Berndt CC, Gross KA, Kucuk A. Material fundamentals and clinical performance of plasma-sprayed hydroxyapatite coatings: a review. Journal of Biomedical Materials Research, 58(5):570-592, 2001.

119. Takai H, Kanematsu M, Yano K, Tsuda E, Higashio K, Ikeda K, Watanabe K, Yamada Y. Transforming growth factor-beta stimulates the production of

osteoprotegerin/osteoclastogenesis inhibitory factor by bone marrow stromal cells. The Journal of the Biological Chemistry, 273, 27091-27096, 1998.

120. Tang Q, Brooks R, Rushton N, Best S. Production and characterization of HA and SiHA coatings. Journal of Materials Science: Materials in Medicine, 21:173-181, 2010.

121. Tang Y, Wu X, Lei W, Pang L, Wan C, Shi Z, Zhao L, Nagy TR, Peng X, Hu J, Feng X, Van Hul W, Wan M, Cao X. TGF-beta1-induced migration of bone mesenchymal stem cells couples bone resorption with formation. Nature Medicine, 15(7):757-765, 2009.

122. Teitelbaum SL. Bone resorption by osteoclasts. Science 289,1504-1508, 2000.

123. Traykova T, Aparicio C, Ginebra MP, Planell JA. Bioceramics as nanomaterials. Nanomedicine London, 1(1):91-106, 2006.

124. Väänänen HK, Liu YK, Lehenkari, P, Uemara T. How do osteoclasts resorb bone? Materials Science and Engineering C 6:205-9, 1998.

125. Väänänen HK, Laitala-Leinonen T. Osteoclast lineage and function. Archives of Biochemistry and Biophysics 473:132-138, 2008.

126. Valen M, Ganz SD. A synthetic bioactive resorbable graft for predictable implant reconstruction: part one. Journal of Oral Implantology, 28(4):167-177, 2002.

127. Välimäki VV, Aro HT. Molecular basis for action of bioactive glasses as bone graft substitute. Scand J Surg 95(2):95-102, 2006.

128. Vallet-Regí M, Ragel CV, Salinas AJ. Glasses with Medical Applications. European Journal of Inorganic Chemistry, 2003(6):1029-1042, 2003.

129. Vallet-Regí M, Salinas AJ, Arcos D. From the bioactive glasses to the star gels. Journal of Materials Science: Materials in Medicine, 17(11):1011-1017, 2006.

130. Vallet-Regí M, Ruíz-Hernández E. Bioceramics: from bone regeneration to cancer nanomedicine. Advanced Materials, 23(44):5177-5218, 2011.

131. Verrier S, Blaker JJ, Maquet V, Hench LL, Boccaccini AR. PDLLA/Bioglass composites for soft-tissue and hard-tissue engineering: an *in vitro* cell biology assessment. Biomaterials, 25(15):3013-3021, 2004.

132. Votta BJ, Levy MA, Badger A, Bradbeer J, Dodds RA, James IE, Thompson S, Bossard MJ, Carr T, Connor JR, Tomaszek TA, Szewczuk L, Drake FH, Veber DF, Gowen M. Peptide aldehyde inhibitors of cathepsin K inhibit bone resorption both *in vitro* and *in vivo*. Journal of Bone and Mineral Research, 12(9):1396-1406, 1997.

133. Yamada MO, Tohno Y, Tohno S, Utsumi M, Moriwake Y, Yamada G. Silicon compatible with the height of human vertebral column. Biological Trace Element Research, 95:113–121, 2003.

134. Yan L, Leng Y, Weng LT. Characterization of chemical inhomogeneity in plasma-sprayed hydroxyapatite coatings. Biomaterials, 24(15):2585-2592, 2003.

135. Yasuda H et al. Osteoclast differentiation factor is a ligand for osteoprotegerin/osteoclastogenesis-inhibitory factor and is identical to TRANCE/RANKL. Proceedings of the National Academy of Sciences. 95, 3597-3602, 1998.

136. Wang J, Musameh M, Lin Y. Solubilization of carbon nanotubes by Nafion toward the preparation of amperometric biosensors. Journal of the American Chemical Society, 125(9):2408-2409, 2003.

137. Wang S. Ordered mesoporous materials for drug delivery. Microporous and Mesoporous Materials, 117(1-2):1-9, 2009.

138. Webster TJ, Ergun C, Doremus RH, Siegel RW, Bizios R. Specific proteins mediate enhanced osteoblast adhesion on nanophase ceramics. Journal of Biomedical Materials Research, 51(3):475-483, 2000.

139. Williams DF. The relationship between biomaterials and nanotechnology. Biomaterials, 29(12):1737-1738, 2008.

140. Williams DF. On the mechanism of biocompatibility. Biomaterials, 29: 2941:2953, 2008.

141. Williams DF. On the nature of biomaterials. Biomaterials, 30(30):5897-5909, 2009.

142. Wiltfang J, Merten HA, Schlegel KA, Schultze-Mosgau S, Kloss FR, Rupprecht S, Kessler P. Degradation characteristics of alpha and beta tri-calcium-phosphate (TCP) in minipigs. Journal of Biomedical Materials Research, 63(2):115-121, 2002.

143. Zweben C. Mechanical Engineers Handbook: Materials and Mechanical Design. Volumen 1, Tercera Edición. Chapter 10: Composite materials. Editado por Myer Kutz. John Wiley & Sons, Inc, 2006.

Páginas web citadas en la Introducción:

http://www.fata.unam.mx/difusion/actividades/eventos/evento_20121129.html

https://flagellum.wordpress.com/tag/grafeno/

https://www.cdlmadrid.org/cdl/archivospdf/ciencias/estructuras-carbono.pdf

http://research.pbsci.ucsc.edu/chemistry/li/research.html

http://www.nanotechbio.com/applications/

http://biologiaconlastics.blogspot.com.es/2014/10/tejido-oseo-esqueleto.html

http://www.anatomiahumana.ucv.cl/kine1/top2.html

Capítulo I

Hidroxiapatitas para regeneración ósea y tratamiento de osteoporosis

Como alternativa prometedora para la restauración de defectos óseos, en la presente Tesis se ha evaluado el efecto de la unión del factor de crecimiento fibroblástico básico (FGF-2) a hidroxiapatita sustituida con silicio (SiHA) como inductor de los procesos de osteogénesis y angiogénesis. Asimismo, se han investigado los efectos de hidroxiapatita nanocristalina (nano-HA) e hidroxiapatita nanocristalina sustituida con silicio (nano-SiHA) sobre los tipos celulares implicados en el proceso de remodelado óseo, analizando los posibles beneficios para el tratamiento de la osteoporosis. Los materiales han sido preparados y caracterizados por el grupo de la Profesora María Vallet-Regí (Dpto. Química Inorganica y Bioinorgánica, Facultad de Farmacia, Universidad Complutense de Madrid).

1. HIDROXIAPATITA SUSTITUIDA CON SILICIO E HIDROXIAPATITAS NANOCRISTALINAS

Como se detalla en la Introducción (apartado 3.2.2), el tejido óseo está formado por diferentes tipos celulares inmersos en una matriz orgánica mineralizada constituida principalmente por fosfato cálcico análogo a la hidroxiapatita (HA) sintética. Por esta razón, este material bioactivo es el más utilizado en cirugía ortopédica y odontología [*Balamurugan A et al. 2008, Dent Mater*]. Su bioactividad se debe a un **mecanismo de disolución-precipitación** que tiene lugar en la superficie del material (**Figura 15**). Al disolverse genera una concentración elevada de calcio y fosfato inorgánico en el espacio entre el hueso y el implante de modo que, al alcanzar una determinada concentración, precipita en forma de HA creando una nueva capa que sirve de anclaje para los osteoblastos, que comienzan a proliferar y diferenciarse sobre ella [*Porter AE et al. 2003, Biomaterials*].

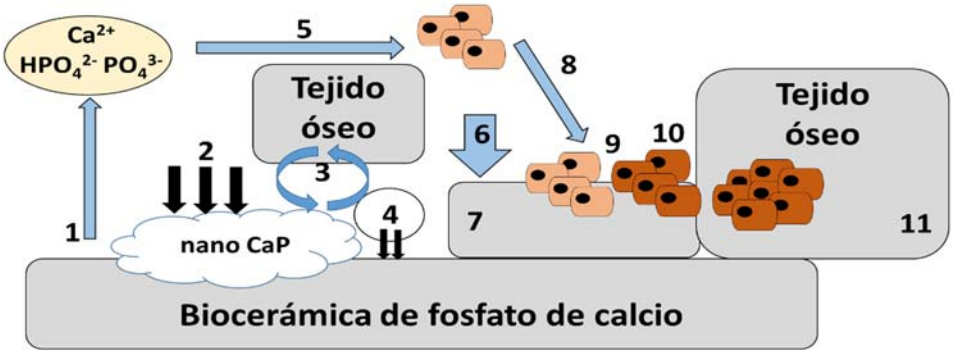

Figura 15. Mecanismo de disolución-precipitación de los fosfatos de calcio como la hidroxiapatita. Esquema procedente de [*Arcos D 2014, Bioceramics with clinical applications, Chapter 3*]. 1) Disolución de la cerámica; 2) Precipitación de iones calcio y fosfato sobre la cerámica; 3) Intercambio de iones y reorganización estructural en la interfaz tejido/implante; 4) Interdifusión desde la superficie a la cerámica; 5) efectos mediados por la solución sobre la actividad celular; 6) Deposición de la fase mineral u orgánica, sin integración en la cerámica; 7) Deposición con integración en la cerámica; 8) Quimiotaxis hacia la superficie de la cerámica; 9) Adhesión y proliferación; 10) Diferenciación celular; 11) Síntesis de matriz extracelular.

Otra característica importante de la hidroxiapatita es la osteoconductividad, permitiendo la adhesión, proliferación y diferenciación de los osteoblastos en su superficie (*Thian ES et al. 2006, Biomaterials; Balamurugan A et al. 2008, Dent Mater*]. Sin embargo, este material presenta ciertas limitaciones debido a la baja velocidad de formación de la nueva capa de apatita y a su lenta degradación, pudiendo ocasionar retrasos en los procesos de rehabilitación y fallos a largo plazo [*Vallet-Regí M et al. 2005, J Mater Chem*; *Mastrogiacomo M et al. 2005, Orthod Craniofacial Res*]. Con el fin de aumentar su reactividad, se realizan en la estructura de HA sustituciones catiónicas (Ca^{2+} sustituido por Sr^{2+}, Pb^{2+}, Mg^{2+}) o aniónicas (grupos OH^- sustituidos por F^-, Cl^-). También son comunes diferentes sustituciones iónicas que afectan a las propiedades químicas, estructurales y microestructurales. Una de estas sustituciones es la de silicio en forma de silicato (SiO_4^{4-}), que es introducido en el lugar de un grupo fosfato (PO_4^{3-}), incrementando la carga negativa a nivel de superficie del material y rompiendo el equilibrio de fuerzas presente en la estructura cristalina. Para compensar la carga se pierden grupos OH^- que dejan huecos o vacantes, incrementando la reactividad del material [*Vallet-Regí M et al. 2005, J Mater Chem*; *Pietak AM 2007, Biomaterials*].

La SiHA utilizada en la presente Tesis Doctoral responde a la fórmula:

$$\mathbf{Ca_{10}(PO_4)_{5.7}(SiO_4)_{0.3}(OH)_{1.7}\,\square_{0.3}}$$ donde □ son vacantes

Los grupos silicato son de mayor tamaño que los grupos fosfato por lo que su introducción presenta mayor dificultad, quedando en superficie y generando una distorsión tetraédrica. La estructura deja de ser estequiométrica y se producen tensiones dentro de la misma. La **Figura 16** muestra la estructura cristalina de este material en el que la celda unidad es de forma hexagonal. Dentro de ella se encuentran los grupos fosfato con forma tetraédrica y con una disposición concreta. Alrededor de estos fosfatos hay grupos de calcio que se encuentran en columnas. Los grupos OH^- se disponen también en columnas dentro del denominado parámetro c, que corresponde a la altura del hexágono. Alrededor de cada OH^- hay tres grupos Ca^{2+} que compensan la carga. Son necesarias unas distancias concretas entre estos grupos para que la energía sea mínima y la estructura sea estable, dando lugar a esta disposición tan definida. Tal como se indica en la figura, al sustituir un fosfato por un grupo silicato de mayor tamaño y diferente carga, toda la estructura se desestabiliza. De este modo, el OH^- abandona la estructura para compensar el desequilibrio, dejando tres cargas positivas juntas que se repelen entre sí. Como consecuencia, se genera una tensión que desestabiliza la estructura y produce su mayor reactividad.

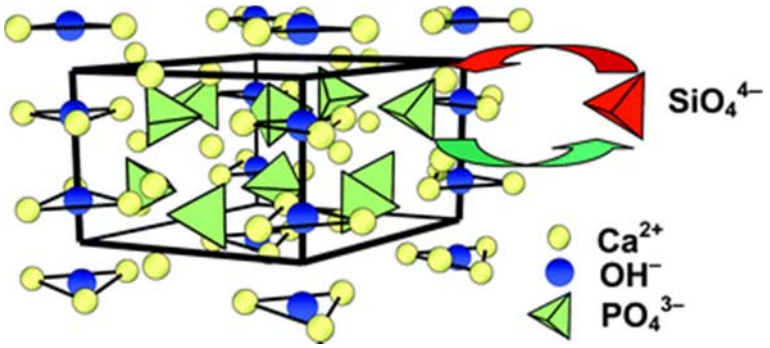

Figura 16. Estructura de la hidroxiapatita dopada con silicio. Esquema procedente de [*Vallet-Regí M et al. 2005, J Mater Chem*].

Los grupos silicato forman una estructura en red sobre la superficie del material que permite la adsorción de proteínas, incrementando el número de motivos biológicos que actúan como puntos de anclaje para las células por medio de moléculas de adhesión, como las integrinas, que a su vez desencadenan cascadas de señalización intracelular específicas [*Thian ES et al. 2006, Biomaterials; Pietak AM 2007, Biomaterials*]. La introducción de grupos silicato favorece estos procesos debido a la generación de defectos en la superficie y a un menor tamaño de grano que facilita la disolución, aumentando la solubilidad del material [*Pietak AM 2007, Biomaterials*]. El concepto de tamaño de grano y tamaño de cristal es diferente. El tamaño de grano no tiene por qué ser más pequeño en la SiHA pero sí el tamaño de cristal, dado que al ser una estructura menos estable los cristales que se forman son más numerosos y de menor tamaño. Sin embargo, los cristales estequiométricos, mucho más estables, de la hidroxiapatita sin sustituir tienden a agregarse entre sí para formar cristales de mayor tamaño.

El incremento de la solubilidad producido por la sustitución con silicio supone una mayor liberación de iones calcio, fosfato y silicio al medio, que contribuye a la formación de la nueva capa de apatita [*Balamurugan A et al. 2008, Dent Mater*]. Esta mayor solubilidad incrementa la reactividad del material y potencia la osteointegración. Sin embargo, niveles excesivos de silicio producen una excesiva solubilidad del material así como un tamaño de cristal mucho menor que puede llegar a dificultar la adhesión de las células en etapas tempranas del proceso [*Thian ES et al. 2006, Biomaterials*]. Se debe llegar a un equilibrio entre estas dos situaciones para conseguir los efectos deseados. En la bibliografía se puede observar que la incorporación de silicio al material oscila entre 0,1 y 5% del peso, aunque pequeñas cantidades (0,5-1%) parecen ser suficientes para mejorar notablemente la bioactividad del material [*Vallet-Regí M et al. 2005, J Mater Chem*].

Estudios de bioactividad *in vitro* con SBF (*simulated body fluid*), de composición similar al plasma, muestran que la SiHA es más reactiva que la HA sola, desarrollándose sobre su

superficie una nueva capa de apatita con morfología acicular y plana que permite las uniones hueso-implante posteriores, lo que presupone un mejor comportamiento *in vivo*. Esta nueva capa permite que las fibras de colágeno se adhieran, siendo una superficie excelente para la incorporación de osteoblastos.

El silicio es esencial para el desarrollo del tejido óseo y del cartílago, comprobándose en numerosos estudios con modelos animales alimentados con dietas deficientes en este elemento, que su carencia conduce a pérdida de peso y diversas malformaciones óseas. Los niveles en suero de silicio son de 1 ppm. Sin embargo, en hueso y ligamentos se pueden encontrar niveles de hasta 100 ppm y en cartílago y otros tejidos conectivos hasta 200-600 ppm. [*Carlisle E 1972, Science*].

El silicio desempeña un papel importante a nivel metabólico como elemento esencial para la síntesis del colágeno, y un papel estructural mediante la unión química a glicosaminoglicanos [*Porter AE et al. 2004, Biomaterials*]. En estudios *in vitro* se ha observado que la presencia de silicio induce una mayor producción de colágeno y un incremento en la expresión de fosfatasa alcalina y osteocalcina, marcadores temprano y tardío de diferenciación de osteoblastos, respectivamente [*Thian ES et al. 2010, Acta Biomaterialia*]. Por otro lado, el silicio ejerce un efecto dosis-dependiente sobre osteoclastos, provocando la inhibición de la diferenciación y la actividad resortiva de este tipo celular con dosis superiores a 30 ppm [*Pietak AM 2007, Biomaterials*].

La SiHA utilizada en la clínica es sintetizada a altas temperaturas (comúnmente a unos 1200°C) para aumentar la densidad y mejorar las propiedades mecánicas. Mediante estos tratamientos se consiguen grandes cristales con dimensiones del orden de micras dependiendo de la dirección del cristal considerada y una menor porosidad y área de superficie. La síntesis a bajas temperaturas mejora las propiedades mecánicas del material, produciendo mayor dureza, a medida que el tamaño de grano se reduce, y mayor bioactividad [*Wang J et al. 2009, Biomaterials*].

En los últimos años, con el amplio desarrollo de la nanotecnología, se ha propuesto la síntesis de SiHA a temperaturas inferiores, lo que permite obtener materiales nanocristalinos (**nano-SiHA**) con mayor área de superficie y menor tamaño del cristal. Estas características inducen mejores respuestas biológicas, dado que el efecto osteogénico del silicio se explica por su localización en los límites del cristal [*Dorozhkin SV 2009 Materials*]. La hidroxiapatita nanocristalina (**nano-HA**) presenta una mayor rugosidad de superficie y poros individuales de menor tamaño que la HA con cristales de tamaño micrométrico [*Webster TJ et al. 2000, J Biomed Mater Res*], lo que incrementa la función osteoblástica y mejora la osteoinducción, respectivamente [*Sato M et al. 2004, Expert Rev Med Devic*]. Por otra parte, la adsorción de

proteínas de suero fetal bovino se ve incrementada en la nano-HA [*Chan CK et al. 2006, Nanomedicine*].

Estudios con biocomposites de nano-HA y gelatina muestran una mayor adhesión de osteoblastos MG-63 sobre estos materiales que sobre los de tamaño micrométrico [*Kim HW et al. 2005, Biomaterials*]. En recubrimientos de titanio con nano-HA y nano-SiHA se obtiene también una mayor adhesión de osteoblastos pero menor adhesión de fibroblastos [*Sato M et al. 2006, Biomaterials; Thian ES et al. 2006, Biomaterials; Palin E et al. 2005, Nanotechnology*]. Otros estudios demuestran una mayor función osteoclástica en presencia de nanocerámicas de HA y alúmina [*Webster TJ et al. 2001, Biomaterials*]. El análisis histológico de defectos en tibia de rata a las tres semanas de implantar un sustituto óseo de biocomposites con nano-HA muestra una mayor biocompatibilidad y osteointegración [*Lewandrowski KU et al. 2003, Biomed Mater Eng*]. Andamios de nano-HA/colágeno/ácido poliláctico con células madre mesenquimales implantados en defectos radiales de conejo inducen también una mayor regeneración ósea [*Zhou DS et al. 2006, J Bioact Compat Pol*].

2. UNIÓN DE FACTORES DE CRECIMIENTO A HIDROXIAPATITAS

Los biomateriales de tercera generación se combinan en muchas ocasiones con agentes bioactivos que permiten la mejora o el reemplazo de las funciones biológicas del tejido dañado. En este sentido, se ha estudiado la unión de diversos factores de crecimiento para potenciar el proceso de regeneración tisular. Un grupo de factores utilizados para este fin es la familia de factores de crecimiento fibroblástico (**FGFs**), polipétidos relacionados con el desarrollo, crecimiento y reparación del tejido óseo [*Ornitz DM et al. 2002, Gene Dev*]. Estos factores controlan procesos de proliferación y diferenciación de varios tipos celulares como son los osteoblastos [*Jaye M et al. 1992, Biochim Biophys Acta / Marie PJ 2012, Gene*], pero además son fuertes inductores de la angiogénesis [*Jonca F et al. 1997, J Biol Chem*], necesaria para el éxito de la regeneración tisular. De las 24 proteínas que componen esta familia, los factores FGF-1 (ácido, FGFa) y FGF-2 (básico, FGFb) son los más representativos. Estudios de inmovilización de ambos factores sobre andamios de SiHA realizados en nuestro grupo de investigación, mostraron una mejora en la adhesión y proliferación de osteoblastos Saos-2 sobre el material, comprobando que el factor inmovilizado mantenía su actividad sobre las células [*Feito MJ et al. 2011, J Mater Sci: Mater Med*]. La inmovilización del factor permite la utilización de dosis menores que en la administración exógena *in vivo* ya que disminuye la dispersión en el organismo [*Nakamura T et al. 1998, J Bone Miner Res*]. Dosis muy elevadas del factor pueden

provocar efectos deletéreos como estimulación del crecimiento tumoral, función vascular anormal, hipotensión e hipervascularidad [*Brey EM et al. 2005, Tissue Eng*]. Otros estudios basados en hidroxiapatita recubierta con FGF-2 muestran una mayor formación ósea en los animales tratados con este material [*Tsurushima H et al. 2010, Acta Biomater; Schnettler R et al. 2003, Biomaterials*].

Layman et al. estudiaron el efecto de la liberación controlada de FGF-2 unido a hidrogeles de gelatina sobre la angiogénesis, en un modelo isquémico murino, observando una mayor estimulación de este proceso que con la administración intravenosa directa del factor [*Layman H et al. 2007, Biomaterials*]. Mabilleau et al. encontraron una mayor masa ósea en conejos de Nueva Zelanda a los que se les implantó FGF-2 inmovilizado sobre cilindros de poli(2-hidroxyethilmethacrilato) copolimerizado con vinilpirrolidona [*Mabilleau G et al. 2008, Biomaterials*].

Los factores de la superfamilia TGF y, más concretamente, las proteínas morfogenéticas óseas (**BMPs**) son también muy utilizados para potenciar la regeneración ósea ya que estas moléculas están estrechamente relacionadas con el proceso de osteogénesis (apartado 3.2.2 de la Introducción). Sachse et al., en un modelo experimental de oveja osteoporótica senil con implantes cilíndricos de titanio e hidroxiapatita recubiertos de BMP-2, demostraron un aumento significativo de la formación ósea a las veinte semanas [*Sachse A et al. 2005, Bone*]. Otros estudios con hidroxiapatita y fosfato tricálcico (HA/TCP) tratados con BMP e implantados en el canal medular femoral de ratas, mostraron la formación de callos óseos a las ocho semanas y una gran cantidad de material fibrocartilaginoso a las cuatro semanas [*Yang JH et al. 2012, Cytotherapy*]. Estudios de liberación controlada de factor de crecimiento transformante beta 2 (TGF-β2), a partir de materiales porosos formados por HA/TCP implantados en perros en el húmero proximal, mostraron a las cuatros semanas una clara estimulación de la formación ósea tanto a nivel local como en áreas óseas remotas [*Sumner DR et al. 2001, J Orthopaed Res*].

La correcta estimulación de la angiogénesis es esencial para el proceso de regeneración ósea debido a la necesidad del transporte de nutrientes y oxígeno a través de los vasos sanguíneos hasta el lugar donde se ha producido la lesión o fractura. Por este motivo, el factor de endotelio vascular (**VEGF**) también es objeto de estudio en los procesos de liberación controlada de factores a partir de biomateriales. Estudios *in vitro* con células endoteliales humanas aórticas y VEGF unido a HA mostraron un aumento de su actividad metabólica a los 28 días y una producción significativa de angiopoyetina-2 como marcador angiogénico [*Solomon K et al. 2013, Thin Solid Films*].

La hormona paratiroidea o parathormona (**PTH**) está estrechamente relacionada con el proceso de remodelado óseo debido a su papel regulador de los niveles de calcio en sangre

(calcemia). En situación de hipocalcemia, PTH estimula el número y la función de los osteoclastos y con ello la liberación de calcio al medio para recuperar los niveles fisiológicos. La calcitonina por el contrario inhibe la actividad osteoclástica cuando los niveles de calcio en sangre son elevados [*Vallet-Regí M 2011, Anales de la Real Sociedad Española de Química*].

La proteína relacionada con la parathormona (**PTHrP**) es otro factor importante en la regeneración ósea, influyendo en los procesos de proliferación y diferenciación de los osteoblastos (apartado 3.2.2. de la Introducción). Como consecuencia del procesamiento post-trasduccional, la PTHrP puede generar distintos fragmentos bioactivos: un fragmento N-terminal 1-36; uno o varios fragmentos en la región media; y un fragmento C-terminal que contiene la secuencia 107-111 conocida como **osteostatina**. Se ha demostrado que esta región C-terminal de la PTHrP señaliza en parte a través de la transactivación del receptor 2 del factor de crecimiento del endotelio vascular (VEGF) asociada a sus acciones en los osteoblastos. Por este motivo, se han llevado a cabo diversos estudios con HA unida a osteostatina. Preosteoblastos MC3T3-E1 cultivados sobre andamios de SiHA a los que se les unió osteostatina por adsorción o por inmovilización covalente, mostraron en ambos casos una mayor proliferación y mineralización [*Manzano M et al. 2011, Acta Biomater*]. La implantación de andamios de HA recubiertos con un polímero de glutaraldehido y osteostatina unida en la metáfisis de la tibia distal de ratas adultas, dio lugar a un incremento de la masa ósea y del grosor del hueso trabecular, así como una mayor expresión de osteocalcina y de la molécula de adhesión vascular 1 [*Lozano D et al. 2014, Acta Biomater*].

3. OSTEOPOROSIS

La **osteoporosis** es una enfermedad esquelética sistémica en la que se produce una desmineralización con pérdida generalizada de la masa ósea y un deterioro de la microarquitectura del hueso, dando lugar a una mayor fragilidad ósea y, por tanto, mayor susceptibilidad a fracturas [*Eastell R 2013 Medicine; Hsu WL et al. 2014, J Formos Med Assoc*]. Estas fracturas tienen lugar principalmente en vértebras, muñeca y cuello del fémur [*Nanes MS et al. 2014, Semin Nucl Med*], estando asociadas a un significativo aumento de la mortalidad, morbilidad y menor calidad de vida [*Hsu WL et al. 2014, J Formos Med Assoc; Pasco JA et al. 2009, Osteoporosis Int*].

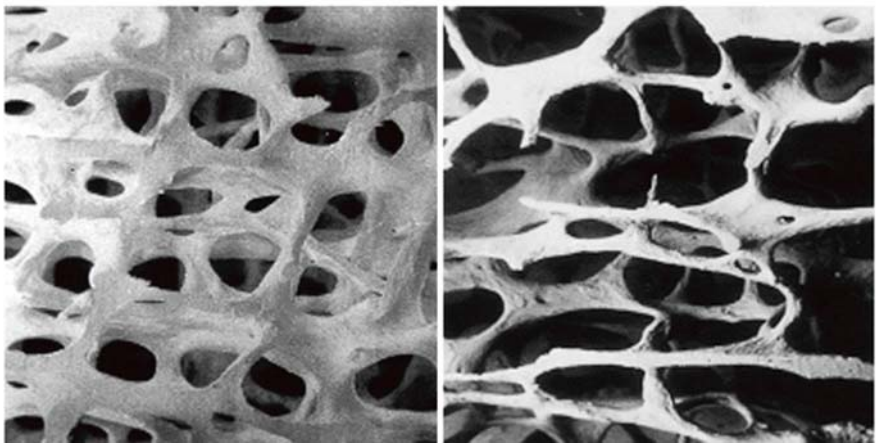

Figura 17. Diferencias estructurales entre un hueso sano (izquierda) y un hueso osteoporótico (derecha). Fotos tomadas de [*Mellibovsky L et al.2006, Seminarios de la Fundación Nacional de Reumatología*].

Se estima que anualmente se producen a nivel mundial más de 9 millones de fracturas, que sufren una de cada tres mujeres y uno de cada cinco hombres mayores de 50 años de edad [*Richards JB et al. 2012, Nat Rev Genet*], aumentando la prevalencia de esta patología al incrementarse la esperanza de vida. Por otra parte, se trata de la enfermedad metabólica más frecuente entre la población occidental, siendo padecida en España por más 3 millones de personas [*Guerra-García MM et al. 2008, Atención Primaria*]. En la Unión Europea, 22 millones de mujeres y 5,5 millones de hombres mayores de 50 años están diagnosticados con osteoporosis, siendo la prevalencia de la enfermedad del 21% y 6%, respectivamente [*Hernlund E et al. 2013, Arch Osteoporos*].

Esta enfermedad está producida por un desequilibrio entre la actividad opuesta de osteoblastos y osteoclastos, encargados de la formación y degradación de hueso, respectivamente, procesos necesarios para el remodelado óseo. A partir de los 50 años comienza a darse una mayor actividad osteoclástica que osteoblástica, originándose la pérdida de la masa ósea [*Malkin et al. 2002, Ann Hum Biol*].

Para el diagnóstico de la osteoporosis se utiliza como parámetro la medida de la densidad mineral ósea (DMO), empleando como valor de referencia la DMO de individuos sanos del mismo sexo a los 30 años de edad en dos zonas estándar: cuello del fémur y columna lumbar (**Figura 18**). Un valor bajo de DMO está asociado a un mayor riesgo de padecer fracturas óseas. Los factores de riesgo que influyen en la producción de una futura fractura son la edad, el sexo femenino, el estado postmenopáusico, la raza caucásica, la historia familiar y las fracturas previas [*Estrugo-Devesa A et al. 2013, Med Clín-Barcelona]*. Otros factores de riesgo dependientes de los hábitos del individuo son el tabaco, el consumo de alcohol y la dieta [*Cech D 2012, Hong Kong Physiotherapy Journal*]. Por otro lado, una alimentación rica en vitamina D y

en calcio parece tener un efecto protector frente a esta patología (*Chan R et al. 2011, J Nutr Health Aging*]. La realización de ejercicio regular a lo largo de las diferentes etapas de la vida, incluido el ejercicio de alto impacto, potencia la adquisición de una mayor densidad mineral ósea durante las fases de crecimiento, minimiza la pérdida ósea en la edad adulta y fortalece la musculatura reduciendo el riesgo de caídas y fracturas en edades avanzadas (*Beck BR et al. 2003, Exerc Sport Sci Rev; DeBar LL et al. 2006, Arch Pediatr Adolesc Med*].

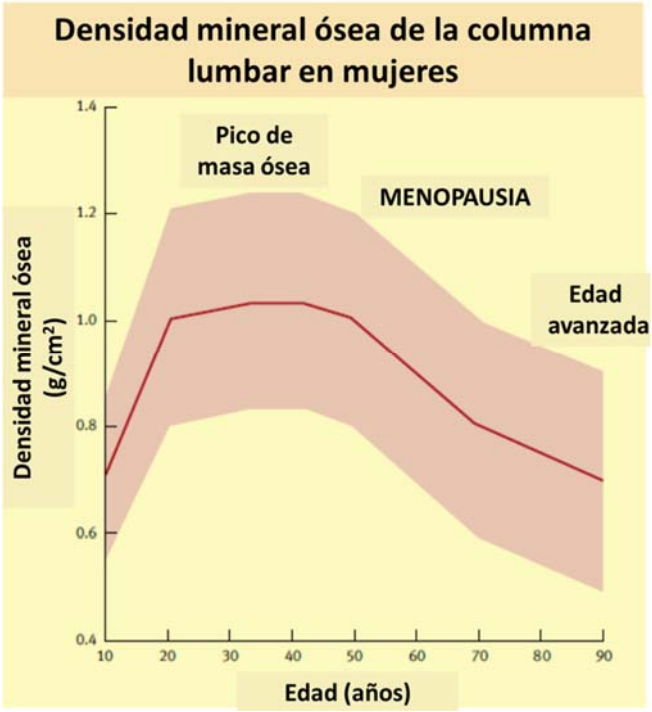

Figura 18. Densidad mineral ósea de la columna lumbar en mujeres. Esquema procedente de [*Eastell R 2013, Medicine*].

Aunque ambos sexos se ven afectados por esta patología, las mujeres presentan mayor prevalencia de osteoporosis una vez alcanzada la menopausia, debido a la disminución de los niveles de estrógenos, implicadas en la absorción intestinal del calcio, esencial para desarrollar una estructura ósea adecuada. La testosterona también tiene un papel en la absorción del calcio, por lo que los hombres de edad avanzada también pueden presentar pérdidas de masa ósea. Sin embargo, los niveles disminuidos de estrógenos también están relacionados con una mayor sensibilidad del hueso a la PTH, que potencia el proceso de resorción ósea [*Cech D 2012, Hong Kong Physiotherapy Journal*]. En los primeros años tras la menopausia las mujeres pierden grandes cantidades de hueso esponjoso que contribuye a la mayor frecuencia de fracturas en comparación con los hombres, que sufren una disminución de masa ósea más gradual [*Khosla S et al. 2005, Endocrin Metab Clin; Riggs BL et al. 2004, J Bone Miner Res*] (**Figura 19**).

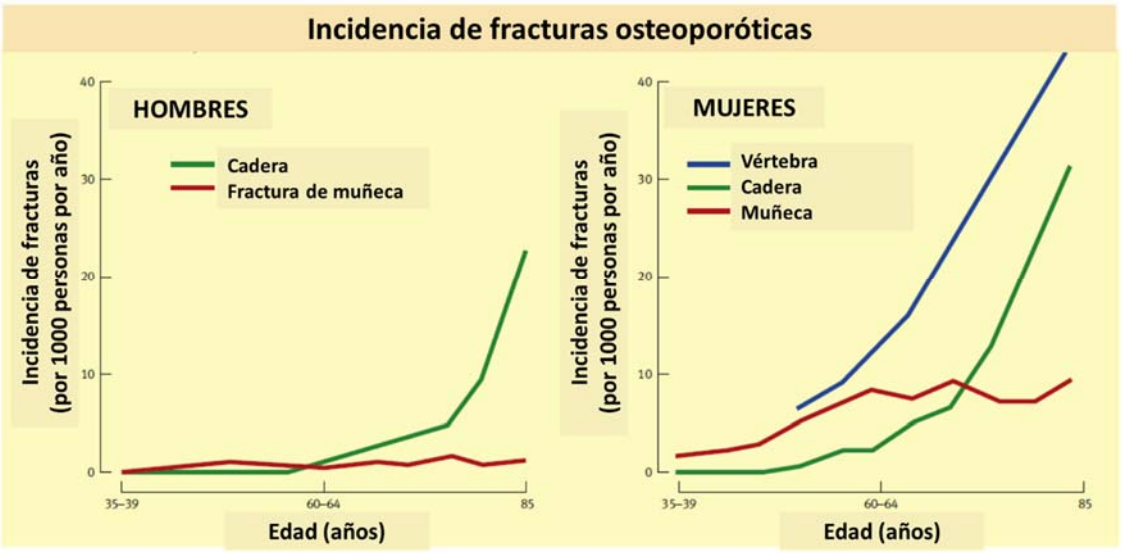

Figura 19. Incidencia de fracturas osteoporóticas en hombres y mujeres a lo largo de diferentes años de vida. Esquema procedente de [*Eastell R 2013, Medicine*].

El tratamiento de esta enfermedad consiste en aliviar los síntomas y en reducir el riesgo de fracturas. En fases tempranas se puede recurrir a una vertebroplastia (inyección de cemento óseo en una fractura dañada), o una cifoplastia con balón (inserción de un balón en la vértebra colapsada antes de la adición de cemento óseo). Por otro lado, se recurre a fármacos que reducen la resorción ósea y/o estimulan la producción de hueso, permitiendo un incremento de DMO. En la actualidad, los fármacos empleados reducen en más del 50% el riesgo de padecer nuevas fracturas [*Eastell R 2013, Medicine*]. Todos ellos suelen ir acompañados con suplementos de calcio y vitamina D en la dieta [*Marini F et al. 2014, Best Pract Res Clin Endocrinol Metab*]. Los fármacos antirresortivos más utilizados en el tratamiento de la osteoporosis son **bifosfonatos** como el etidronato disódico, el risedronato sódico, el ácido ibandrónico o el ácido zoledrónico. Estos compuestos son análogos de pirofosfatos con una gran afinidad por la hidroxiapatita y con una acción inhibitoria específica sobre osteoclastos [*Lehenkari PP et al. 2002, Mol Pharmacol; Rogers MJ 2003, Curr Pharm Des*]. Todos los bifosfonatos aprobados son potentes moléculas antirresortivas que reducen el número de fracturas a la mitad [*Tella SH et al. 2014, J Steroid Biochem Mol Biol*]. Sin embargo, estos fármacos presentan diversos efectos secundarios dependiendo de la vía de administración. En el caso de una administración intravenosa se desarrolla hasta en un 4% de los casos osteonecrosis de la mandíbula y fracturas femorales del subtrocánter (una de cada mil personas tratadas) [*Marini F et al. 2014, Best Pract Res Clin Endocrinol Metab*]. Por el contrario, mediante la administración oral los pacientes pueden presentar otro tipo de efectos secundarios relacionados con el sistema digestivo debido a la lenta absorción del medicamento [*Marini F et al. 2014, Best Pract Res Clin Endocrinol*

Metab]. Ciertos estudios muestran una serie de fracturas femorales atípicas pasados 3-5 años del tratamiento con estos fármacos [*Lenart BA et al. 2009, Osteoporos Int; Ing-Lorenzini K et al. 2009, Drug Safety*]. Por este motivo, solo está recomendado el tratamiento con bifosfonatos durante los primeros 3-5 años [*Marini F et al. 2014, Best Pract Res Clin Endocrinol Metab*]. Por todos estos efectos secundarios, se hace necesario el uso de otros fármacos antirresortivos como el anticuerpo monoclonal anti-RANKL humano (Denosumab) [*Eastell R 2013 Medicine; Marini F et al. 2014, Best Pract Res Clin Endocrinol Metab*], los moduladores de los receptores de estrógenos (raloxifeno) [*Cranney A et al. 2002, Endocr Rev*], la PTH y su péptido recombinante (teriparatide) [*Gates BJ et al. 2009, Am J Geriatr Pharmacother*] y la calcitonina [*Chesnut CH et al. 2000, Am J Med*]. Sin embargo, un pequeño porcentaje de pacientes no responde a estos fármacos, ya sea porque no ven mejorada su DMO o bien por los efectos secundarios que les provocan. Por este motivo, ciertos estudios recientes defienden el uso de la farmacogenómica para configurar tratamientos específicos para cada paciente [*Marini F et al. 2014, Best Pract Res Clin Endocrinol Metab*].

Otros estudios están encaminados a la utilización de **biomateriales** diseñados para el tratamiento y prevención de fracturas de hueso osteoporótico. Actualmente, están en desarrollo diversos materiales que pueden ser cargados con fármacos o células para el tratamiento de la osteoporosis, aunque muy pocos están en fase clínica. Recientemente se ha creado para este fin la Red Española y Europea de Excelencia para la Prevención y Tratamiento de las Fracturas Osteoporóticas (Ageing) [*Arcos D et al. 2014, Acta Biomater*]. Estas fracturas provocan una gran disminución de la estabilidad y dificultan la reconstrucción quirúrgica. Al producirse una fractura en un hueso sano, se liberan numerosas citoquinas al torrente sanguíneo que reclutan células madre mesenquimales al lugar de la fractura para comenzar la reparación del tejido. Sin embargo, en el hueso osteoporótico estas células presentan una menor capacidad para diferenciarse a osteoblastos, posiblemente debido a la menor cantidad de señales osteoinductivas y/o a la menor expresión de la proteína morfogenética ósea-2 (BMP-2). Todo esto se ve agravado por una menor capacidad angiogénica en el lugar donde se produce la fractura [*Kwong FN et al. 2008, J Am Acad Orthop Surg*].

Otra dificultad añadida es la gran variabilidad de carga a la que se someten los huesos y articulaciones en función del lugar donde se ha producido la fractura, lo que determina el diseño de implantes con diferentes propiedades mecánicas. El reto actual en el diseño de biomateriales para el tratamiento de fracturas osteoporóticas consiste en combinar en éstos la orientación de carga, la porosidad interconectada y la capacidad para ser cargados con factores biológicos que induzcan la cicatrización de la fractura [*Arcos D et al. 2014, Acta Biomater*].

Los biomateriales para reducir las fracturas osteoporóticas en la actualidad son básicamente de dos tipos: implantes metálicos y cementos. Los primeros son usados con el objetivo primario de fijación, mientras que los segundos son utilizados principalmente como refuerzo de los implantes metálicos [*Arcos D et al. 2014, Acta Biomater*]. También se puede utilizar este tipo de cementos para su inyección en el hueso osteoporótico [*Heini PF et al. 2001, Eur Spine J*]. Estudios recientes están enfocados al uso de cementos de fosfato cálcico inyectables a los que se les une elementos bioactivos como vidrios bioactivos [*Yu L et al. 2013, PLoS One*] o polímeros biodegradables [*Chen W et al. 2013, Tissue Eng Pt A*]. Mientras que en los implantes metálicos la importancia radica en modificar la forma del implante para adaptarlo a los requerimientos del hueso osteoporótico, la importancia del estudio de los cementos radica en la composición del mismo para conseguir la viscosidad constante y una alta radiopacidad [*Arcos D et al. 2014, Acta Biomater*].

Diferentes materiales han sido diseñados como sistemas de carga y liberación de fármacos antiosteoporóticos [*Arcos D et al. 2013, Acta Mater*] y como soportes que permitan la colonización por células para terapia celular [*Manzano M et al. 2012, Prog Solid State Ch; Trejo CG et al. 2010, Biomaterials*]. Sin embargo, el uso de biomateriales con células implica una serie de limitaciones como la viabilidad celular o la integridad biológica en la zona específica en que se implanta el biomaterial, que hacen necesarios estudios previos *in vitro* e *in vivo* que permitan esclarecer el tipo de biomaterial adecuado para el tratamiento de esta patología [*Arcos D et al. 2014, Acta Biomater*].

OBJETIVOS

1. Estudio de la biocompatibilidad de la hidroxiapatita sustituída con silicio (SiHA) y evaluación de la biofuncionalidad del factor de crecimiento fibroblástico 2 (FGF-2) unido a dicho material mediante el análisis de las rutas de señalización que este factor activa en osteoblastos.
2. Evaluación del efecto beneficioso de osteostatina sobre la actividad del FGF-2 unido a SiHA en células óseas y angiogénicas.
3. Efectos de hidroxiapatitas nanocristalinas nano-HA y nano-SiHA sobre células inmunes implicadas en la inmunidad innata (macrófagos) y adquirida (linfocitos T).
4. Efectos de hidroxiapatitas nanocristalinas nano-HA y nano-SiHA sobre el proceso de diferenciación de osteoclastos y su actividad resortiva.

OBJECTIVES

1. Biocompatibility study of silicon-substituted hydroxiapatite (SiHA) and biofunctionality evaluation of fibroblast growth factor 2 (FGF-2) adsorbed on this material through the analysis of its signaling pathways in osteoblasts.
2. Evaluation of osteostatin beneficial effect on the activity of FGF-2 adsorbed on SiHA on bone and angiogenic cells.
3. Effects of nanocristalline hydroxiapatites, nano-HA and nano-SiHA, on immune cells involved in innate (macrophages) and adquired (T lymphocytes) immunity.
4. Effects of nano-HA and nano-SiHA on osteoclast differentiation and resorptive activity.

RESULTADOS

Las estrategias terapéuticas para regeneración ósea implican la selección de biomateriales, factores de crecimiento y tipos celulares adecuados que mimeticen el microambiente presente *in vivo*, donde las señales mecánicas y moleculares controlan el proceso de reconstrucción del tejido óseo.

En la presente Tesis Doctoral se aborda el estudio de la biocompatibilidad de la hidroxiapatita sustituída con silicio (SiHA) sobre diferentes tipos celulares, analizando sus efectos en comparación con la hidroxiapatita (HA), ya que las características químicas y estructurales de SiHA incrementan su solubilidad y reactividad respecto a HA. Como alternativa prometedora para la restauración de defectos óseos, se ha utilizado el factor de crecimiento fibroblástico básico FGF-2 unido a SiHA, evaluando su biofuncionalidad a través de rutas de señalización que este factor activa en osteoblastos.

Los resultados obtenidos se resumen a continuación y han dado lugar a la siguiente publicación:

- Matesanz MC, Feito MJ, Ramírez-Santillán C, Lozano RM, Sánchez-Salcedo S, Arcos D, Vallet-Regí M, Portolés MT. Signaling pathways of immobilized fgf-2 on silicon substituted hydroxyapatite. Macromolecular Bioscience 12: 446-453, 2012.

En el presente estudio se ha comparado el efecto que SiHA y HA ejercen sobre fibroblastos murinos L929, osteoblastos humanos Saos-2 y preosteoblastos murinos MC3T3-E1, analizando diferentes parámetros de biocompatibilidad: morfología celular, proliferación, viabilidad, apoptosis, fases del ciclo celular, liberación de lactato deshidrogenasa (LDH) y contenido en especies reactivas de oxígeno (ROS) como indicador de estrés oxidativo.

Las células conservaron su capacidad proliferativa en contacto con ambos materiales aunque con cierto retraso respecto al control. Los osteoblastos Saos-2 proliferaron mejor en contacto con 1 mg/ml de SiHA pulverizada que con la misma dosis de HA a los 4 días de cultivo. Este resultado concuerda con las imágenes observadas por Microscopía Electrónica de Barrido (SEM) en las que las células Saos-2 se adhirieron y proliferaron más fácilmente sobre discos de SiHA que sobre HA (**Figura 20**).

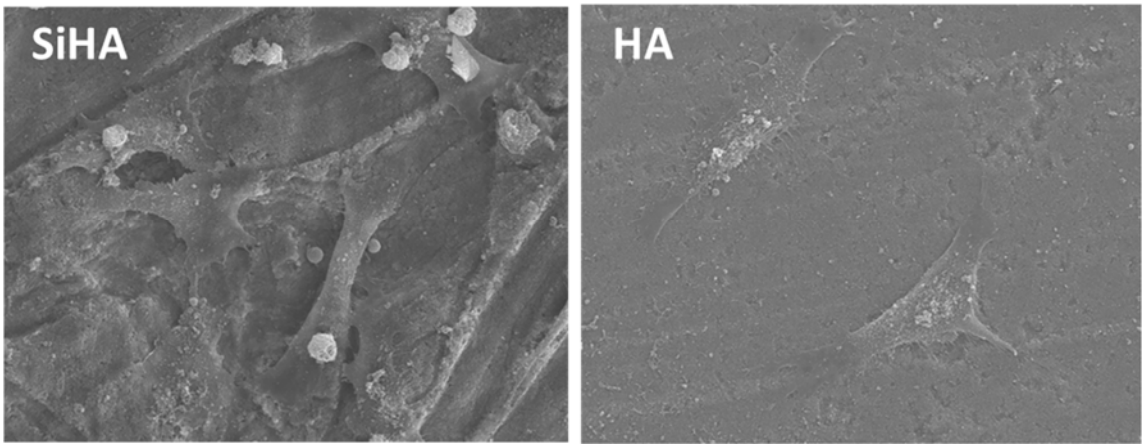

Figura 20. Imágenes de Microscopía Electrónica de Barrido (SEM) de osteoblastos Saos-2 cultivados sobre discos de SiHA y HA. Imagen procedente de [*Matesanz MC et al. 2012, Macromol Biosci*].

El estudio del ciclo celular demostró un incremento en la fase de síntesis (fase S) de preosteoblastos y osteoblastos cultivados en contacto con SiHA pulverizada en comparación con HA. Dado que la fase S es aquella en la que el ADN celular se duplica, este resultado indica un proceso de replicación activa del ADN sin que se altere la transición G1/S, conocido punto de control del ciclo celular.

El resto de parámetros de biocompatibilidad analizados demuestró el correcto estado de los tres tipos celulares ensayados en contacto con ambos materiales, mostrando altos valores de viabilidad, bajos niveles de apoptosis, así como una correcta morfología celular observada por microscopía confocal y SEM. Sin embargo, se obtuvieron mejores resultados de biocompatibilidad con SiHA que con HA.

Dado el papel de FGF-2 como inductor de la osteogénesis y angiogénesis (apartado 2 del Capítulo I), la unión de dicho factor a SiHA representa una alternativa muy prometedora para la restauración de defectos óseos [*Feito MJ et al. 2011, J Mat Sci: Mat Med*].

En el presente trabajo se ha evaluado la biofuncionalidad de FGF-2 unido a SiHA a través de las rutas de señalización que este factor activa en osteoblastos.

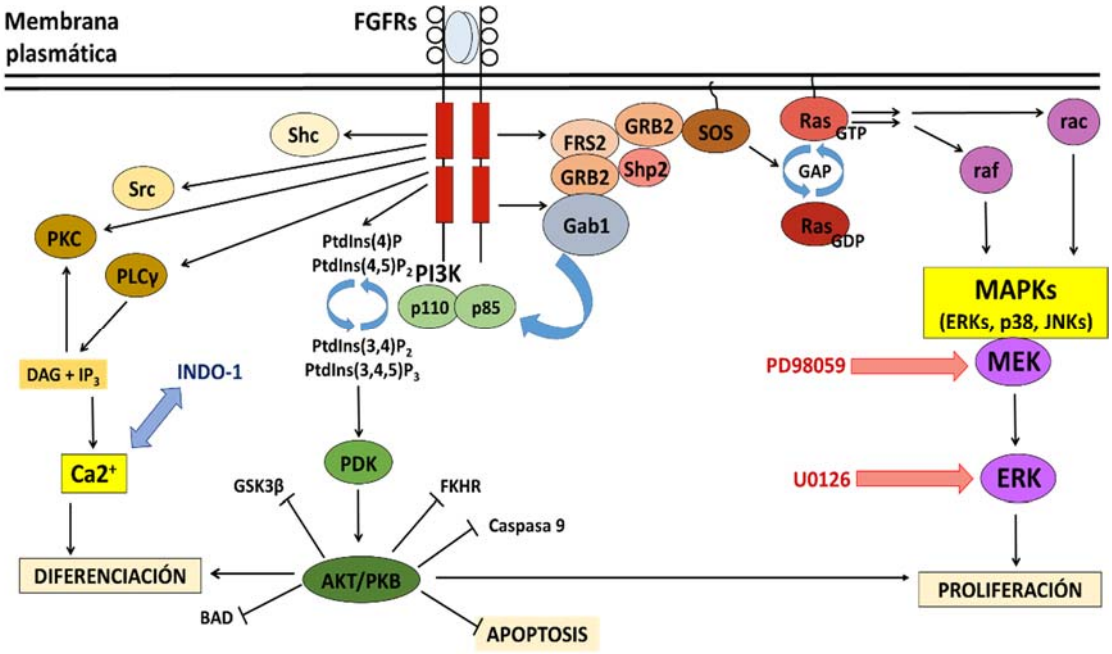

Figura 21. Vías de señalización activadas por FGF. Esquema procedente de [*Dayley L et al. 2005, Cytokine and Growth Factor Reviews*].

Una vez que FGF se une a su receptor, se produce la activación de la fosfolipasa C ɣ (PLCɣ) que produce la liberación de diacilglicerol (DAG) e inositol 1,4,5-trisfosfato (IP_3) y estos conducen a la activación de la proteína quinasa C (PKC) y a la liberación de calcio al citoplasma procedente de reservorios intracelulares, respectivamente (**Figura 21**). Los niveles citosólicos de Ca^{2+}, esencial para los procesos de proliferación, diferenciación y formación ósea, se han evaluado mediante citometría de flujo y microscopía confocal con la sonda Indo-1.

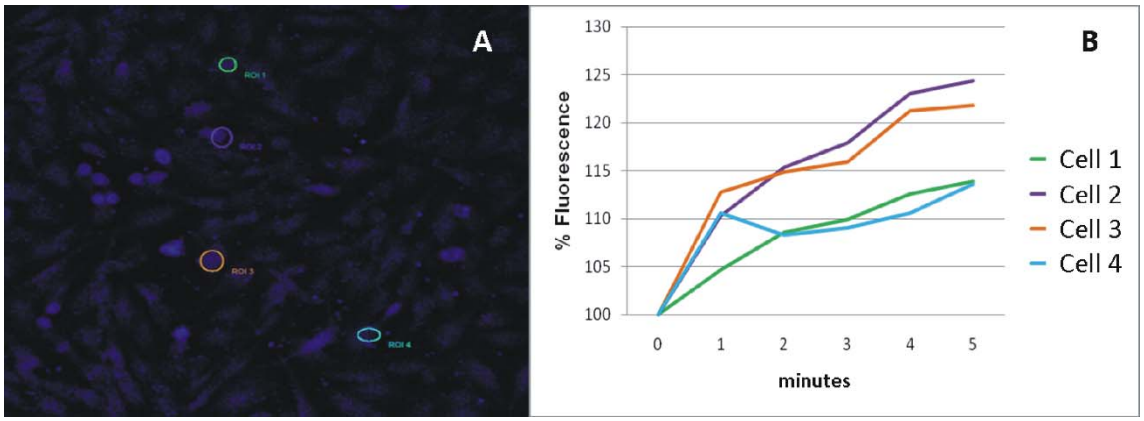

Figura 22. Estudio de los cambios de los niveles de Ca^{2+} en osteoblastos Saos-2 escogidos aleatoriamente tras la adición de SiHA/FGF-2 sobre el cultivo. Imagen procedente de [*Matesanz MC et al. 2012, Macromol Biosci*].

Mediante un estudio de célula única se comprobó por Microscopía Confocal el incremento del calcio citosólico en osteoblastos Saos-2 al añadir el FGF-2/SiHA sobre el cultivo, demostrando la funcionalidad del factor (**Figura 22**). Resultados similares se obtuvieron con células en suspensión mediante citometría de flujo.

Por otra parte, la vía de las MAP quinasas también es estimulada por FGF entre otros factores de crecimiento, con importantes efectos en los procesos de proliferación y diferenciación. Una de las moléculas de la cascada de señalización, generalmente considerada responsable de la respuesta mitogénica, es ERK quinasa, activada por MAP quinasa quinasa (MEK). La actividad biológica de FGF-2/SiHA sobre preosteoblastos MC3T3-E1 fue evaluada a través de la ruta de señalización de MAPK, mediante la utilización de los inhibidores PD98059 y U0126 específicos de las quinasas MEK y ERK respectivamente. Los resultados mostraron que los inhibidores producen una disminución en la proliferación en presencia de FGF-2/SiHA, más pronunciado en el caso de PD98059, justificado por la posición que ocupa MEK en la cascada de señalización intracelular (**Figura 23**).

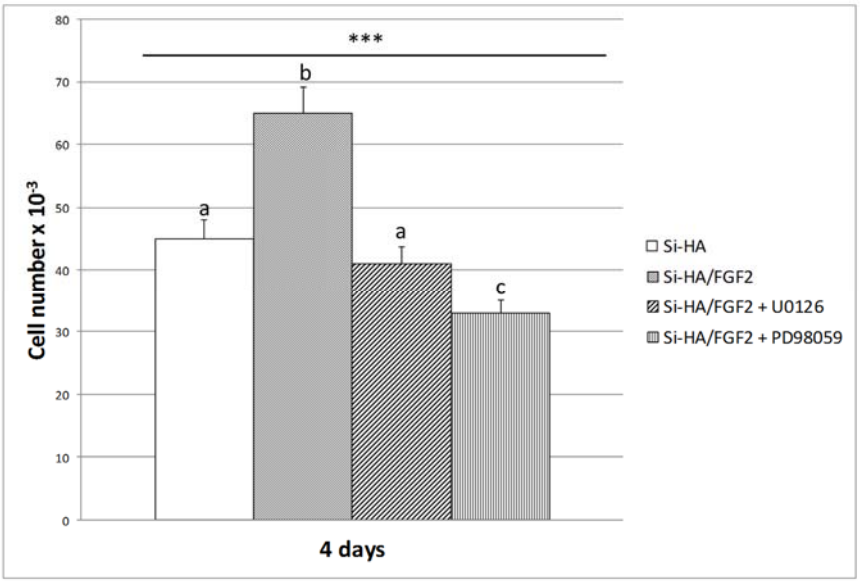

Figura 23. Proliferación de preosteoblastos MC3T3-E1 cultivados en presencia de SiHA, SiHA unido a FGF-2 (SiHA/FGF-2) en ausencia o en presencia de los inhibidores de MAP quinasas U0126 y PD98059. Gráfica procedente de [*Matesanz MC et al. 2012, Macromol Biosci*].

Estos estudios han demostrado que FGF-2 mantiene su actividad una vez unido a SiHA y confiere a las células las señales adecuadas para estimular los mecanismos intracelulares implicados en la proliferación y diferenciación osteoblástica.

Signaling Pathways of Immobilized FGF-2 on Silicon-Substituted Hydroxyapatite

María de la Concepción Matesanz, María José Feito, Cecilia Ramírez-Santillán, Rosa María Lozano, Sandra Sánchez-Salcedo, Daniel Arcos, María Vallet-Regí, María-Teresa Portolés*

Therapeutic strategies for bone regeneration involve the selection of suitable biomaterials, growth factors, and cell types to mimic the cellular microenvironment where molecular and mechanical signals control the reconstruction of bone tissue. The immobilization of basic fibroblast growth factor (FGF-2) on powdered silicon-substituted hydroxyapatite (Si-HA) allows to prepare a biofunctional biomaterial able to interact with bone cells in a very specific way. The biological activity of FGF-2/Si-HA, evaluated in Saos-2 osteoblasts and MC3T3-E1 preosteoblasts through the PLCγ and MAPK/ERK signal transduction pathways, shows that FGF-2 immobilized on Si-HA provides the right signals to cells stimulating crucial intracellular mechanisms of osteoblast proliferation and differentiation.

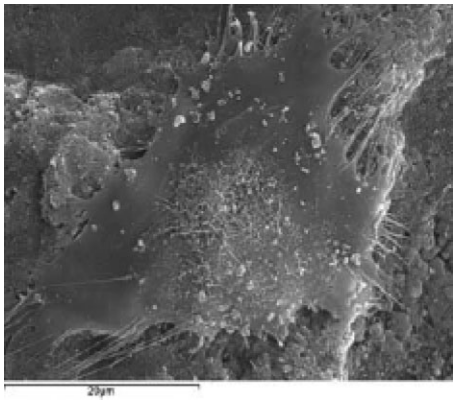

1. Introduction

Synthetic hydroxyapatite (HA) is successfully used in the field of dentistry and orthopedic surgery due to its crystallographic structural similarity to bone mineral.[1,2] However, the bone inorganic component presents calcium, phosphate, and hydroxyl deficiency, internal crystal disorder and different substituents as carbonate (up to 8 wt%), sodium (up to 0.8 wt%), magnesium (up to 0.5 wt%), and potential trace level substituents as silicon (Si).[1,3] Si is an essential trace element required for healthy bone and connective tissues which influences the biological activity of calcium phosphate biomaterials by modifying their properties and by direct effects on the physiological processes in skeletal tissue.[4,5] The observed beneficial actions of Si-substituted calcium phosphates (bioactivity increase, higher osteoclastic resortion activity, increase of bone ingrowth, and bone-implant coverage) have been critically revised by Bohner.[6] Several passive and active mechanisms have been proposed to explain the Si substitution effects: the material solubility increase, topographical changes, the reduction of the grain size, and the ionic release of Si and Ca, which can directly act on bone cells, in particular osteoblasts.[4,6–9]

On the other hand, recent therapeutic tissue regeneration strategies are based on the combination of cells, biomaterials, and growth factors.[10–13] Basic fibroblast

M. de la Concepción Matesanz, Dr. M. J. Feito, C. Ramírez-Santillán, Prof. M.-T. Portolés
Department of Biochemistry and Molecular Biology I, Faculty of Chemistry, Universidad Complutense, 28040 Madrid, Spain
E-mail: portoles@quim.ucm.es
Dr. R. M. Lozano
Department of Physical and Chemical Biology, Centro de Investigaciones Biológicas, Consejo Superior de Investigaciones Científicas, 28040 Madrid, Spain
Dr. S. Sánchez-Salcedo, Dr. D. Arcos, Prof. M. Vallet-Regí
Department of Inorganic and Bioinorganic Chemistry, Faculty of Pharmacy, Universidad Complutense, 28040 Madrid, Spain
Dr. S. Sánchez-Salcedo, Dr. D. Arcos, Prof. M. Vallet-Regí
Networking Research Center on Bioengineering, Biomaterials and Nanomedicine, Madrid, Spain

DOI: 10.1002/mabi.201100456

growth factor (FGF-2) plays an important role in osteogenesis and is also a strong inducer of angiogenesis which allows the supply of oxygen and nutrients for cells during tissue repair.[14] The immobilization of FGF-2 on biomaterials and the local delivery of this protein represent promising alternatives treatment for restoring bone defects.[15–21] The FGF binding to specific cell receptors activates multiple signal transduction pathways that are often inter-dependent.[22] The best understood of these mechanisms are the Ras/mitogen-activated protein kinase (RAS-MAP kinase) pathway which include extracellular signal-regulated kinases (ERK 1/2), p38 kinase, and c-Jun N-terminal kinase (JNK); the P-I-3 kinase-AKT pathway and the phospholipase Cγ (PLCγ) pathway. The FGFs effect on signaling events leads to osteoblast proliferation/differentiation and stimulates gene expression of procollagen, osteopontin, osteocalcin, and VEGF.[23] The activation of PLCγ results in phosphatidyl inositol hydrolysis, stimulation of protein kinase C (PKC), and intracellular calcium mobilization which triggers kinases dependent on calcium/calmodulin, promoting finally the expression of cbfa1/Runx2 genes.[24] In addition, the signaling pathway FGF cooperates with bone morphogenetic proteins (BMPs).[25]

In the present study, the comparative response of L929 fibroblasts, Saos-2 osteoblasts, and MC3T3-E1 preosteoblasts to both silicon-substituted HA (Si-HA) and HA have been evaluated in vitro analyzing different biocompatibility parameters. Then, in order to obtain a biofunctional material able to participate in specific biological reactions, FGF-2 was immobilized on powdered Si-HA and the analysis of specific FGF-2 signal transduction pathways was carried out on both osteoblasts and preosteoblasts. This study includes the evaluation of intracellular calcium mobilization in single cells for the first time by confocal microscopy and the use of MAPK (ERK 1/2) inhibitor U0126 and MAP kinase kinase (MEK) inhibitor PD98059 to specifically detect these FGF pathways.

2. Experimental Section

2.1. Synthesis of Silicon-Substituted HA

Si-HA with nominal formula $Ca_{10}(PO_4)_{5.7}(SiO_4)_{0.3}(OH)_{1.7}\square_{0.3}$, where □ denoted vacancies at the hydroxyl position, was prepared by aqueous precipitation reaction of $Ca(NO_3)_2 \cdot 4H_2O$, $(NH_4)_2HPO_4$, and $Si(CH_3CH_2O)_4$ solutions, as described elsewhere.[26] Briefly, a 1 M solution of $Ca(NO_3)_2 \cdot 4H_2O$ was added to $(NH_4)_2HPO_4$ and $Si(CH_3CH_2O)_4$ solutions of stoichiometric concentration to obtain the composition described above. The mixture was stirred for 12 h at 80 °C. The pH was kept at 9.5 by NH_3 solution addition. During the reaction the pH was continuously adjusted to 9.5 to ensure constant conditions during the synthesis. The precipitated Si-HA powder was treated at 700 °C to remove nitrates without introducing important changes in the structure and microstructure of the materials.[26] Elemental chemical analysis was carried out by fluorescence X-ray spectrometry. Twelve different batches were tested to ensure the chemical homogeneity of the synthesized powders. Particle size distribution of Si-HA powder material was determined with a Sedigraph 5100 after aqueous suspension. Non-doped HA was obtained under analogous conditions in order to carry out a comparative study.

2.2. Preparation of Silicon-Doped HA Disks

Fractions of 300 mg of both HA and Si-HA materials were pressed into disk-shape (11 mm diameter, 2 mm height) by means of 3 tons of uniaxial pressing.

2.3. Cell Culture for in vitro Biocompatibility Studies

Murine L929 fibroblasts, human Saos-2 osteoblasts, and murine MC3T3-E1 preosteoblasts were seeded on 6 well culture plates (Cultek S.L.U., Madrid, Spain), at a density of 10^5 cells · mL^{-1} in Dulbecco's modified Eagle medium (DMEM) supplemented with 10% fetal bovine serum (FBS, Gibco, BRL), 10^{-3} M L-glutamine (BioWhittaker Europe, Belgium), penicillin (200 μg · mL^{-1}, BioWhittaker Europe, Belgium), and streptomycin (200 μg · mL^{-1}, BioWhittaker Europe, Belgium), under a CO_2 (5%) atmosphere and at 37 °C for 24 h. To evaluate the effects of both HA and silicon-doped HA on different cell parameters, cells were cultured for 4 d in the presence of 1 mg · mL^{-1} of either HA or Si-HA synthesized under the same experimental conditions. Controls without material were always carried out.

After 4 d culture, the attached cells were washed with phosphate buffer saline (PBS) and harvested using 0.25% trypsin/ethylenediamine tetraacetic acid (EDTA) solution for 5 min. The reaction was stopped with culture medium and cells were counted with a Neubauer hemocytometer for the analysis of cell proliferation, centrifuged at 310*g* for 10 min and resuspended in fresh medium for the analysis of viability, cell cycle, apoptosis, and reactive oxygen species (ROS) content by flow cytometry.

2.4. Morphological Studies by Scanning Electron Microscopy (SEM)

Morphological studies were carried out by SEM with human Saos-2 osteoblasts cultured for 4 d on the surface of both HA and Si-HA disks prepared in the same experimental conditions. For SEM studies, the attached cells on the biomaterial were fixed with glutaraldehyde [2.5% in phosphate-buffered saline (PBS)] for 45 min. Sample dehydration was performed by slow water replacement using series of ethanol solutions (30, 50, 70, 90%) for 15 min with a final dehydration in absolute ethanol for 30 min, allowing samples to dry at room temperature and under vacuum. Afterwards, the pieces were mounted on stubs and coated in vacuum with gold-palladium. Cells were examined with a JEOL JSM-6400 scanning electron microscope.

2.5. Morphological Studies by Confocal Microscopy

For confocal microscopy studies, murine L929 fibroblasts, human Saos-2 osteoblasts and murine MC3T3-E1 preosteoblasts were cultured for 4 d on glass coverslips in the presence of 1 mg · mL^{-1} of

either HA or Si-HA synthesized in the same experimental conditions. Controls without material were always carried out. After fixation with 3.7% paraformaldehyde in PBS for 10 min, samples were washed with PBS and permeabilizated with 0.1% Triton X-100 for 3–5 min. The samples were then washed with PBS and preincubated with PBS containing 1% BSA for 20–30 min. Then cells were incubated for 20 min with Alexa-488 phalloidin (Dilution 1:40, Molecular Probes) which stains F-actin filaments. Samples were then washed with PBS and the cell nuclei were stained with 4'-6-diamidino-2'-phenylindole (DAPI), 3×10^{-6} M in PBS, Molecular Probes). After staining and washing with PBS, cells were examined using a Leica SP2 Confocal Laser Scanning Microscope. The fluorescence of Alexa-488 was excited at 488 nm and the emitted fluorescence was measured at 530/30 nm. The fluorescence of DAPI was excited at 405 nm and measured at 420–480 nm.

2.6. Lactate Dehydrogenase (LDH) Measurement

LDH activity was measured in the culture medium by an enzymatic method at 340 nm (Bio-Analítica, S.L.) using a Beckman DU 640 UV-Vis spectrophotometer. The medium was collected after every culture time and centrifuged at 12 000*g* at 4 °C. The enzymatic assay was performed in the supernatant.

2.7. Flow Cytometry Studies

Cells cultured for 4 days in the absence or the presence of 1 mg · mL^{-1} of either HA or Si-HA were washed twice with PBS and incubated at 37 °C with trypsin-EDTA solution for cell detachment. After 5 min, the reaction was stopped with culture medium; cells were centrifuged at 310*g* for 10 min and resuspended in fresh medium.

After the incubation with the different probes, as it is described below, the conditions for the data acquisition and analysis were established using negative and positive controls with the CellQuest Program of Becton Dickinson and these conditions were maintained during all the experiments. Each experiment was carried out three times and single representative experiments are displayed. For statistical significance, at least 10 000 cells were analyzed in each sample and the mean of the fluorescences emitted by these single cells was used.

2.7.1. Cell Cycle Analysis and Apoptosis Detection

Cell suspensions were incubated with Hoechst 33258 (Poly-Sciences, Inc., Warrington, PA) [Hoechst 5 μg · mL^{-1}, ethanol 30%, and bovine serum albumin (BSA) 1% in PBS], used as a nucleic acid stain, for 30 min at room temperature in darkness. The fluorescence of Hoechst was excited at 350 nm and the emitted fluorescence was measured at 450 nm in an LSR Becton Dickinson Flow Cytometer. The cell percentage in each cycle phase, G_0/G_1, S, and G_2/M was calculated with the CellQuest Program of Becton Dickinson and the $SubG_1$ fraction was used as indicative of apoptosis.

2.7.2. Intracellular ROS Content and Cell Viability

Cells were incubated at 37 °C for 30 min with 10^{-4} M 2′,7′-dichlorofluorescein diacetate (DCFH/DA, Serva, Heidelberg, Germany). To measure the intracellular ROS, the fluorescence of dichlorofluorescein was excited by a 15 mW laser tuning to 488 nm and the emitted fluorescence was measured with a 530/30 band pass filter in a FACScalibur Becton Dickinson flow cytometer. Cell viability was determined by addition of propidium iodide (PI; 0.005% in PBS, Sigma-Aldrich Corporation, St. Louis, MO, USA) to stain the DNA of dead cells.

2.8. FGF-2 Immobilization on Powdered Si-HA

The immobilization of FGF-2 on powdered Si-HA was carried out through non-covalent binding by mixing 1 g of this biomaterial with 200 μg of soluble FGF-2 in 10^{-2} M sodium phosphate (pH = 7.2) in a final volume of 6 mL as it is described previously.[18] The final concentration of NaCl was 5×10^{-2} M in the samples. After 2 h of slight rotation at 4 °C, 3 mL of the mix was lyophilized and maintained at −20 °C for subsequent biofunctionality assays.

2.9. Biofunctionality Studies

The specific analysis of FGF-2 signal transduction pathways was carried out as a biofunctionality measure of FGF/Si-HA on both osteoblasts and preosteoblasts.

2.9.1. Intracellular Calcium Transients in Single Cells by Confocal Microscopy and Flow Cytometry

Cultured Saos-2 osteoblasts were incubated with the probe Indo-1 AM (Enzo Life Sciences) at a concentration of 10^{-5} M under a CO_2 (5%) atmosphere and darkness at 37 °C for 30 min. Then, to evaluate the effect on PLCγ pathway of FGF-2 immobilized on powered Si-HA, 10 ng · mL^{-1} of FGF-2/Si-HA (1 ng FGF-2 immobilized on 5 μg Si-HA) were added to the culture medium and intracellular calcium transients were just detected by confocal microscopy. The fluorescence of Indo-1 was excited at 405 nm and the emitted fluorescence was measured in single cells with 410–509 nm band pass filter in an LEICA SP2 confocal laser scanning microscope. After all the measurements, 10^{-5} M A-23187 ionophore (Enzo Life Sciences) was added in order to prove the sensitivity of the assay.

On the other hand, the effect of FGF-2/Si-HA on intracellular calcium was also evaluated by flow cytometry with Saos-2 osteoblasts in suspension. In these experiments, cells were incubated with the probe Indo-1 AM (Enzo Life Sciences) at a concentration of 10^{-5} M for 30 min at room temperature, darkness, and shaking. Then, FGF-2/Si-HA (10 ng · mL^{-1}) was added to the cell suspension, the fluorescence of Indo-1 was excited at 325 nm and the emitted fluorescence was measured at 380 nm in an LSR Becton Dickinson Flow Cytometer.

2.9.2. Treatments with MAPK (ERK 1/2) Inhibitor U0126 and MAP Kinase Kinase (MEK) Inhibitor PD98059

Murine MC3T3-E1 preosteoblasts were seeded on 24 well culture plates (Cultek S.L.U., Madrid, Spain), at a density of 2×10^4 cells · mL^{-1} in DMEM supplemented with 10% FBS (Gibco, BRL), 10^{-3} M L-glutamine (BioWhittaker Europe, Belgium), penicillin (200 μg · mL^{-1}, BioWhittaker Europe, Belgium), and streptomycin (200 μg · mL^{-1}, BioWhittaker Europe, Belgium), under a CO_2 (5%) atmosphere and at 37 °C. After 4 d culture, either MAPK (ERK 1/2) inhibitor U0126 or MAP kinase kinase (MEK) inhibitor PD98059 were added at a concentration of 10^{-5} M to the culture medium and incubated for 1 h. Then, 10 ng · mL^{-1} of FGF-2/Si-HA (1 ng FGF-2 immobilized on 5 μg Si-HA) were added and the cultures were maintained for 4 d. Controls without inhibitors were always carried out. After 4 d culture, the attached cells were washed with PBS and

harvested using 0.25% trypsin/EDTA solution for 5 min. The reaction was stopped with culture medium and cells were counted with a Neubauer hemocytometer for the analysis of cell proliferation.

2.9.3. Statistics

Data are expressed as means + standard deviations of a representative of three experiments carried out in triplicate. Statistical analysis was performed using the Statistical Package for the Social Sciences (SPSS) version 19 software. Statistical comparisons were made by analysis of variance (ANOVA). Scheffé test was used for post hoc evaluations of differences among groups. In all statistical evaluations, $p < 0.05$ was considered as statistically significant.

3. Results and Discussion

In order to stimulate bone regeneration, the selection of suitable biomaterials, growth factors, and cell types is necessary to mimic the cellular microenvironment where molecular and mechanical signals control the reconstruction of this specific tissue.[1,10,27]

Si-HAs are among the most interesting calcium phosphates for bone repair because present comparable biocompatibility and mechanical properties to HA but improved bioactivity which enhances bone tissue growth rate.[1–5] Although the use of Si-HA has been proposed for different biomedical applications, only few studies have been carried out to know the specific cellular responses to these materials.[5,18,28] In the present study, the comparative response of L929 fibroblasts, Saos-2 osteoblasts, and MC3T3-E1 preosteoblasts to both HA and Si-HA have been evaluated in vitro analyzing different biocompatibility cell parameters: cell morphology, proliferation, viability, apoptosis, ROS content, LDH release, and cell cycle phases.

Figure 1 shows cell proliferation values after 4 d culture in the presence of either HA or Si-HA (1 mg · mL^{-1} in powder form). Controls without material were also carried out. As it can be observed, L929 fibroblasts, Saos-2 osteoblasts, and MC3T3-E1 preosteoblasts proliferate in contact with HA and Si-HA, but the cell number was significantly lower in the presence of these materials than in controls. This effect has been previously observed.[18] Recently, the intracellular signal transduction pathway involved in the slow cell proliferation in osteoblasts grown on the calcium phosphate surface has been investigated and the inhibition of RhoA/ROCK/PTEN pathway has been proposed to increase the osteoblast proliferation on apatite surfaces.[28] It must be underlined that L929 fibroblasts present higher proliferation rates than Saos-2 osteoblasts and MC3T3-E1 cells in all cases and lower sensitivity to the presence of both HA and Si-HA materials (Figure 1). The number of Saos-2 cells after 4 d culture in contact with Si-HA was significantly higher than with HA, indicating that this cell type grows better in the presence of Si-HA. This result has been also observed by SEM when Saos-2 osteoblasts were cultured for 4 d on surface of both HA and Si-HA disks. SEM images demonstrate that Saos-2 cells adhere to the Si-HA disk, proliferate and colonize its surface (Figure 2B–D) better than on HA disk (Figure 2A). Osteo-

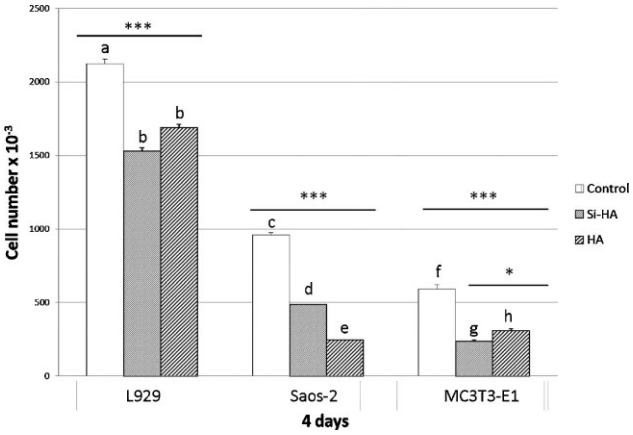

Figure 1. Proliferation assays of L929 fibroblasts, Saos-2 osteoblasts, and MC3T3-E1 preosteoblasts cultured in the presence of 1 mg · mL^{-1} of either powered Si-HA or powdered HA. Controls without material were always carried out. Columns with the same letter are statistically equivalent. Columns with different letters are statistically different. Statistical significance: * $p < 0.05$, *** $p < 0.005$, $n = 6$.

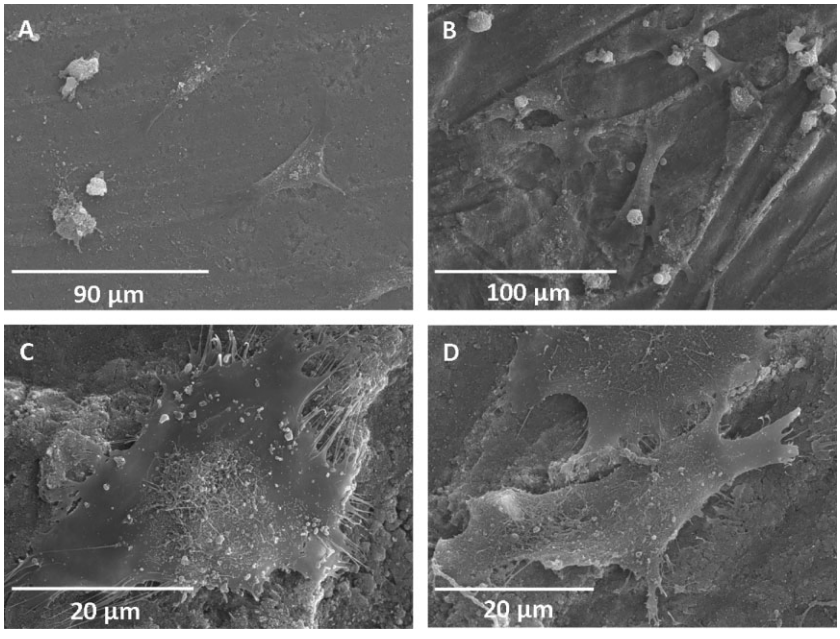

Figure 2. Morphology evaluation of Saos-2 osteoblasts cultured on either HA (A) or Si-HA (B, C, D) disks by SEM.

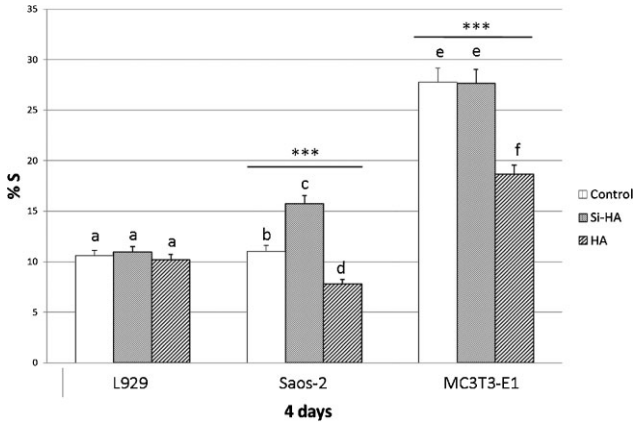

Figure 3. Cell cycle S phase analysis of L929 fibroblasts, Saos-2 osteoblasts, and MC3T3-E1 preosteoblasts cultured in the presence of 1 mg · mL^{-1} of either powered Si-HA or powdered HA. Controls without material were always carried out. Columns with the same letter are statistically equivalent. Columns with different letters are statistically different. Statistical significance: *** $p < 0.005$, $n = 6$.

blasts cultured on Si-HA surface show the typical bone cell morphology, cube-shape, and big sized (Figure 2C), joining other cells to construct a net through strong cellular unions (Figure 2B and D). Adhesion and proliferation processes are good indicators of the cell response that could be expected when a biomaterial is used in vivo.

Proliferation is dependent on the cell cycle progression, in which cells pass through the G_0/G_1 phase (Quiescence/Gap 1) to the S phase (Synthesis) and finally to the G_2/M phase (Gap 2 and Mitosis). The analysis of cell cycle phases of both Saos-2 osteoblasts and MC3T3-E1 preosteoblasts shows a slight but significant increase of the cell percentage in S phase in the presence of powdered Si-HA in comparison with HA (Figure 3). This fact reveals an active DNA replication (the major event in S-phase) without alteration in the G_1/S transition which is a principal checkpoint in the regulation of the cell cycle.

High levels of cell viability (95–87%) evaluated by PI exclusion and low percentages of apoptosis (0.3–1.8%) detected by $SubG_1$ fraction, were obtained after culture of L929 and MC3T3-E1 cells in the presence of 1 mg · mL^{-1} powdered HA and Si-HA (Table 1). Although low levels of apoptosis were also obtained in Saos-2 osteoblasts, this cell type showed a slight decrease of cell viability obtaining values of 65.9 and 69.0% in the presence of HA and Si-HA, respectively. Since no significant changes of LDH levels in the culture medium were detected, the integrity of the cell plasma membrane was proved in all cases (data not shown, Table 1). Thus, the viability decrease observed in Saos-2 cells by PI exclusion test can be due to a higher sensitivity of this cell type to the detachment with trypsin/EDTA (necessary for the flow cytometric analysis) after culture in the presence of powdered materials. Previous studies have shown that Saos-2 osteoblasts are more sensitive than fibroblasts to HA-βTCP/agarose disks which induced apoptosis (11%) in osteoblasts cultured 4 d on its surface but not in fibroblasts (0.5%).[29]

It is remarkable that better biocompatibility results of Si-HA in comparison with HA were obtained with Saos-2 osteoblasts in the present study (Figure 2, Table 1). Intracellular ROS content did not show alteration thus indicating no oxidative stress in all the cases (data not shown).

Figure 4 shows the correct morphology of L929 fibroblasts (Figure 4A and B), Saos-2 osteoblasts (Figure 4C and D), and MC3T3-E1 preosteoblasts (Figure 4E and F) in the presence of powdered HA (Figure 4A, C, and E) and Si-HA (Figure 4B, D, and F). Cells are well spread, with a distinctive

Table 1. Biocompatibility parameters of L929 fibroblasts, Saos-2 osteoblasts, and MC3-T3 preosteoblasts cultured for 4 d in the presence of 1 mg · mL^{-1} of either powdered HA or powered Si-HA. Controls without material were carried out; in all cases $n = 4$.

		Viability	Apoptosis	ROS	LDH
L929	Control	98.0 ± 1.2	0.5 ± 0.1	No oxidative stress	No changes
	HA	93.0 ± 0.1[a)]	0.3 ± 0.1		
	Si-HA	95.4 ± 0.4	1.8 ± 1.8		
Saos-2	Control	95.0 ± 1.2	0.6 ± 0.3	No oxidative stress	No changes
	HA	65.9 ± 5.5[b)]	2.1 ± 1.7[b)]		
	Si-HA	69.0 ± 13.8[c)]	0.4 ± 0.7		
MC3T3-E1	Control	96.5 ± 0.2	0.8 ± 0.4	No oxidative stress	No changes
	HA	87.5 ± 1.5[a)]	1.3 ± 0.2		
	Si-HA	92.1 ± 0.3[a)]	1.8 ± 0.2		

[a)] $p < 0.05$; [b)] $p < 0.005$; [c)] $p < 0.01$.

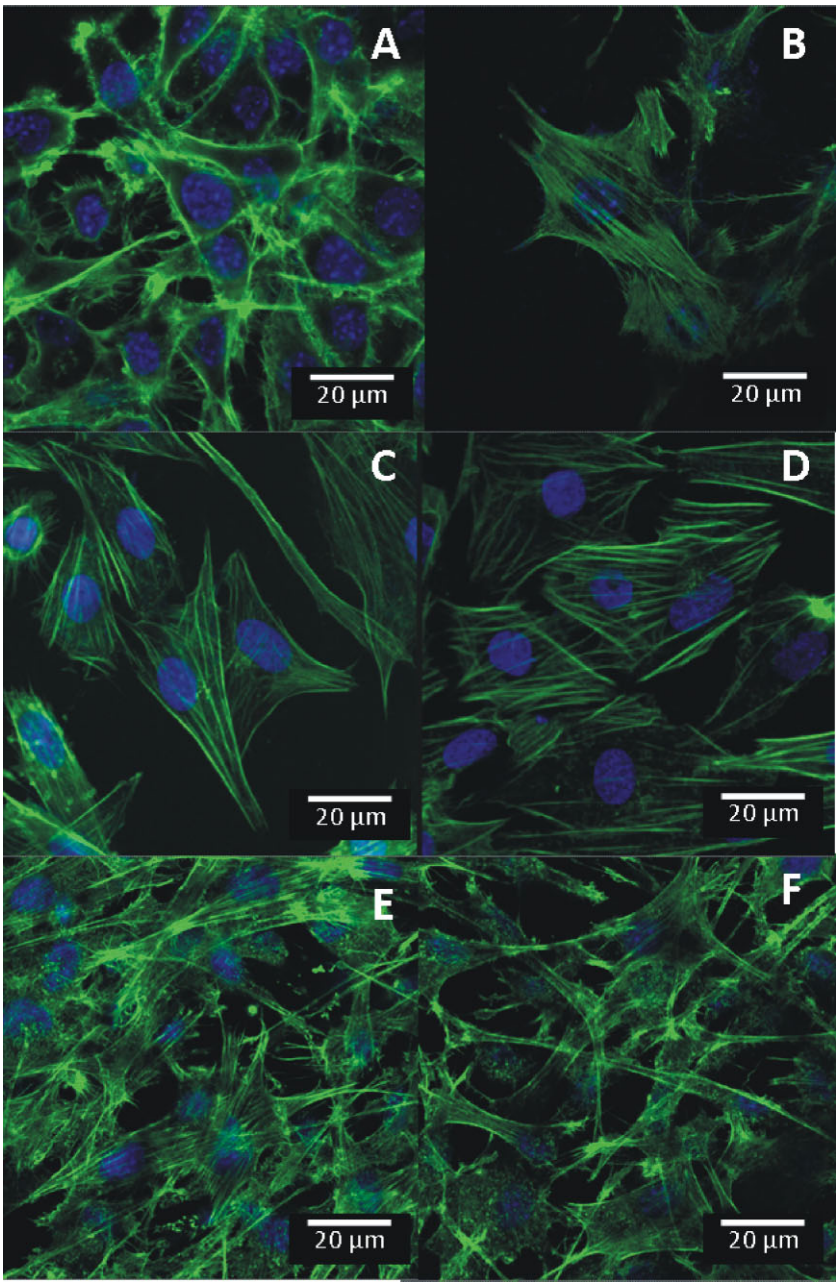

Figure 4. Morphology evaluation by confocal microscopy of L929 fibroblasts (A, B), Saos-2 osteoblasts (C, D), and MC3T3-E1 preosteoblasts (E, F) cultured in the presence of 1 mg · mL^{-1} of either powered HA (A, C, E) or powdered Si-HA (B, D, F). Cells were stained with DAPI (for the visualization of the cell nuclei) and Alexa-488 phalloidin (for the visualization of cytoplasmic F-actin filaments).

actin network and no apoptotic nuclei are detected by DAPI staining in the presence of these materials.

The incorporation of biological agents in biomaterials improves their integration rate because it stimulates endogenous repair mechanisms by providing the right signals to cells and thereby accelerating the functional restoration of damaged tissues. The advantages and disadvantages of different systems for controlled release of these agents have been recently reviewed in the literature.[10,17] The immobilization of growth factors is a strategy that allows to obtain the desirable local concentration of these molecules involved in cell proliferation and differentiation.[15–21] The basic FGF (bFGF or FGF-2) plays important roles in osteogenesis and also in angiogenesis, necessary to obtain oxygen and nutrients during tissue repair.[27]

In the present study, the immobilization of FGF-2 on powdered Si-HA was performed as previously described to obtain a biofunctional biomaterial able to interact with cells in a very specific way.[18] With this objective, the analysis of the biological activity of immobilized FGF-2 on Si-HA was evaluated through specific signal transduction pathways in cultured Saos-2 osteoblasts and MC3T3-E1 preosteoblasts.

The biological action of FGF-2 involves the binding to specific receptors on cell surface and the activation of multiple signaling pathways that are often interdependent.[22] Among FGF signals, the activation of PLCγ produces the phosphatidyl inositol hydrolysis releasing diacylglycerol and inositol-1,4,5-trisphosphate. These molecules stimulate, respectively, the protein kinase C and the Ca^{2+} release from intracellular stores to cytosol.[22] Since calcium signaling is essential for the osteoblast proliferation, differentiation, and bone formation, the evaluation of intracellular calcium transients in response to FGF-2/Si-HA was carried out for the first time in the present study with single cells by confocal microscopy as measure of PLCγ activation pathway.[30]

Figure 5B shows the time courses of changes in cytosolic Ca^{2+} in randomly selected single cells (Figure 5A), monitored with the fluorescent probe Indo-1 and measured by confocal microscopy just after the addition of 10 ng · mL^{-1} of FGF-2/Si-HA (1 ng FGF-2 immobilized on 5 μg Si-HA) to cultured Saos-2 osteoblasts. As it can be observed, FGF-2/SiHA triggers a cytosolic Ca^{2+} increase in osteoblasts demonstrating that FGF-2 maintains its biological activity after its immobilization on powdered Si-HA. This immobilized factor is able to bind

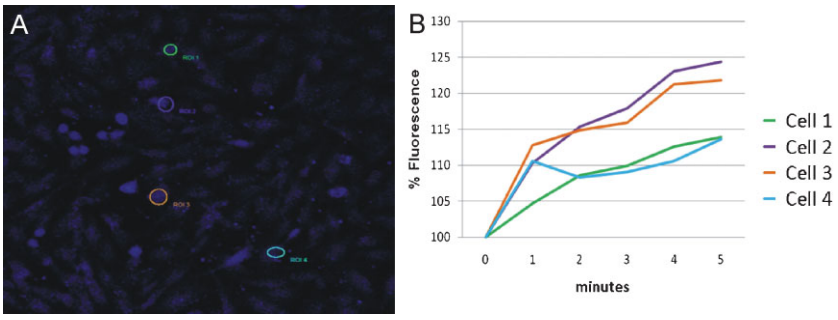

Figure 5. Times courses of changes in cytosolic Ca^{2+} (5B) in randomly selected single cells (5A), monitored with the fluorescent probe Indo-1 and measured by confocal microscopy just after the addition of 10 ng · mL^{-1} of FGF-2/Si-HA (1 ng FGF-2 immobilized on 5 μg Si-HA) to cultured Saos-2 osteoblasts.

extracellular receptors on human osteoblasts and to activate the PLCγ pathway which involves phosphatidyl inositol hydrolysis and release of calcium from intracellular stores to cytosol.[22] These effects were also observed by flow cytometry in Saos-2 suspensions after FGF-2/Si-HA addition (Figure 6). Controls without FGF were always carried out and no changes in cytosolic Ca^{2+} were obtained (data not shown).

The MAP kinases are a family of proteins that regulate the activity of downstream kinases or transcription factors and are also activated by FGF signals.[31] ERK1/2 kinases are generally considered responsible for the mitogenic response and MAP kinase kinase (MEK) is the kinase upstream of ERK1/2.[32] This intracellular signaling pathway of FGF-2 plays a crucial role in osteoblast proliferation and differentiation and it is well studied in MC3T3-E1 preosteoblasts.[23,33,34] The proliferative effect of FGF-2 on this cell type has been recently related with down regulation of TAZ protein.[34] In order to evaluate the effects of immobilized FGF-2/Si-HA on MC3T3-E1 preosteoblast proliferation through the activation of MEK and ERK 1/2 kinases, their respective inhibitors U0126 and PD98059 were added at a concentration of 10^{-5} M to the culture medium of these cells 1 h before the addition of 10 ng · mL^{-1} FGF-2/Si-HA (1 ng FGF-2 immobilized on 5 μg Si-HA). After FGF-2/Si-HA addition, MC3T3-E1 cultures were maintained for 4 d and the cell number was evaluated after detachment with trypsin-EDTA. As it can be observed in Figure 7, FGF-2/Si-HA produces a significant increase of MC3T3-E1 proliferation which is specifically inhibited by U0126 and PD98059. The PD98059 inhibition is significantly more pronounced than U0126 inhibition in agreement with the MEK upstream position with respect to ERK 1/2. All these results demonstrate the biological activity of immobilized FGF-2 on Si-HA through specific signaling pathways detection suggesting the potential utility of FGF-2/Si-HA as a biofunctional material for bone repair.

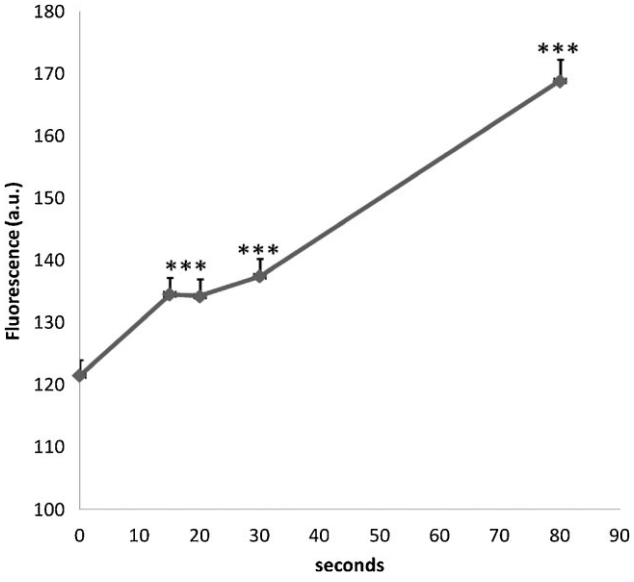

Figure 6. Time course of changes in cytosolic Ca^{2+} (5B) in Saos-2 osteoblast monitored with the fluorescent probe Indo-1 and measured by flow cytometry just after the addition of 10 ng · mL^{-1} of FGF-2/Si-HA (1 ng FGF-2 immobilized on 5 μg Si-HA). Statistical significance: *** $p < 0.005$, $n = 4$.

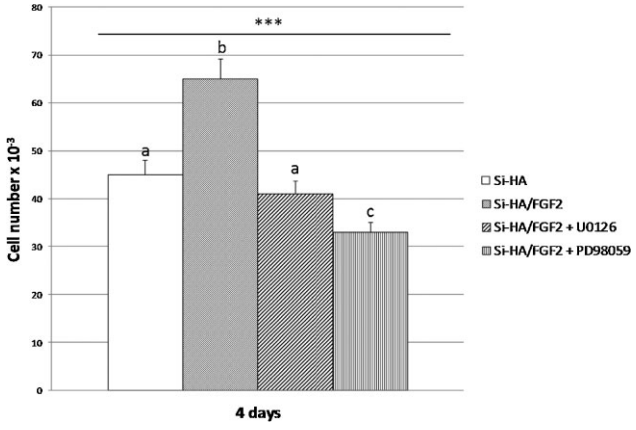

Figure 7. Effects of immobilized FGF-2/Si-HA on MC3T3-E1 preosteoblast proliferation through the activation of MEK and ERK 1/2 kinases. U0126 and PD98059 inhibitors were added at a concentration of 10^{-5} M to the culture medium 1 h before the addition of 10 ng · mL^{-1} FGF-2/Si-HA (1 ng FGF-2 immobilized on 5 μg Si-HA). MC3T3-E1 cultures were then maintained for 4 d and the cell number was evaluated after detachment with trypsin/EDTA. Columns with the same letter are statistically equivalent. Columns with different letters are statistically different. Statistical significance: *** $p < 0.005$, $n = 6$.

4. Conclusion

Immobilized FGF-2 on Si-HA maintains its biological activity stimulating crucial intracellular signaling mechanisms as PLCγ and MAPK/ERK pathways in Saos-2 osteoblasts and MC3T3-E1 preosteoblasts.

Acknowledgements: This study was supported by research grants from Comunidad de Madrid (S2009/MAT-1472) and Ministerio de Ciencia e Innovacion through the projects MAT2008-06719-C03-02, MAT2008-00736 and CS2010-11384-E. M. C. Matesanz is greatly indebted to Networking Research Center on Bioengineering, Biomaterials, and Nanomedicine for a fellowship. The authors wish to thank also to the staff of the Microscopy and Cytometry Center of the Universidad Complutense de Madrid (Spain) for the assistance in the SEM, flow cytometry, and confocal microscopy studies.

Received: November 11, 2011; Revised: December 21, 2011; Published online: March 2, 2012; DOI: 10.1002/mabi.201100456

Keywords: basic fibroblast growth factors; biomaterials; molecular recognition; osteoblasts; tissue engineering

[1] M. Vallet-Regí, E. Ruiz-Hernández, *Adv. Mater.* **2011**, *23*, 5177.
[2] M. Vallet-Regí, D. Arcos, *J. Mater. Chem.* **2005**, *15*, 1509.
[3] K. A. Hing, P. A. Revell, N. Smith, T. Buckland, *Biomaterials* **2006**, *27*, 5014.
[4] A. M. Pietak, J. W. Reid, M. J. Stott, M. Sayer, *Biomaterials* **2007**, *28*, 4023.
[5] E. S. Thian, J. Huang, S. M. Best, Z. H. Barber, R. A. Brooks, N. Rushton, W. Bonfield, *Biomaterials* **2006**, *27*, 2692.
[6] M. Bohner, *Biomaterials* **2009**, *30*, 6403.
[7] F. Balas, J. Pérez-Pariente, M. Vallet-Regí, *J. Biomed. Mater. Res., A* **2003**, *66*, 364.
[8] A. E. Porter, S. M. Best, W. Bonfield, *J. Biomed. Mater. Res., A* **2004**, *68*, 133.
[9] M. M. Dvorak, A. Siddiqua, D. T. Ward, D. H. Carter, S. L. Dallas, E. F. Nemeth, D. Riccardi, *Proc. Natl. Acad. Sci.* **2004**, *101*, 5140.
[10] F.-M. Chen, M. Zhang, Z.-T. Wu, *Biomaterials* **2010**, *31*, 6279.
[11] E. D. Miller, K. Li, T. Kanade, L. E. Weiss, L. M. Walker, P. G. Campbell, *Biomaterials* **2011**, *32*, 2775.
[12] E. D. Ker, A. S. Nain, L. E. Weiss, J. Wang, J. Suhan, C. H. Amon, P. G. Campbell, *Biomaterials* **2011**, *32*, 8097.
[13] M. Manzano, D. Lozano, D. Arcos, S. Portal-Núñez, C. López la Orden, P. Esbrit, M. Vallet-Regí, *Acta Biomater.* **2011**, *7*, 3555.
[14] S. S. Kelpke, R. Zinn, L. W. Rue, J. A. Thompson, *Biomed. Mater. Res., A* **2004**, *71*, 316.
[15] P. G. Campbell, E. D. Miller, G. W. Fisher, L. M. Walker, L. E. Weiss, *Biomaterials* **2005**, *6*, 6762.
[16] H. Shen, X. Hu, J. Bei, S. Wang, *Biomaterials* **2008**, *29*, 2388.
[17] M. S. Kim, Y. M. Shin, J.-H. Lee, S. I. Kim, Y. S. Nam, C. S. Shin, H. Shin, *Macromol. Biosci.* **2011**, *11*, 122.
[18] M. J. Feito, R. M. Lozano, M. Alcaide, C. Ramírez-Santillán, D. Arcos, M. Vallet-Regí, M. T. Portolés, *J. Mater. Sci.: Mater. Med.* **2011**, *22*, 405.
[19] G. Mabilleau, E. Aguado, I. C. Stancu, C. Cincu, M. F. Baslé, D. Chappard, *Biomaterials* **2008**, *29*, 1593.
[20] E. Wenk, A. R. Murphy, D. L. Kaplan, L. Meinel, H. P. Merkle, L. Uebersax, *Biomaterials* **2010**, *31*, 1403.
[21] A. Zieris, S. Prokoph, K. R. Levental, P. B. Welzel, M. Grimmer, U. Freudenberg, C. Werner, *Biomaterials* **2010**, *31*, 7985.
[22] L. Dailey, D. Ambrosetti, A. Mansukhani, C. Basilico, *Cytokine Growth Factor Rev.* **2005**, *16*, 233.
[23] P. J. Marie, *Gene* **2003**, *316*, 23.
[24] G. Xiao, D. Jiang, R. Gopalakrishnan, R. T. Franceschi, *J. Biol. Chem.* **2002**, *277*, 36181.
[25] K. Kubota, S. Iseki, S. Kuroda, S. Oida, T. Iimura, W. R. Duarte, K. Ohya, I. Ishikawa, S. Kasugai, *Bone* **2002**, *31*, 465.
[26] D. Arcos, J. Rodríguez-Carvajal, M. Vallet-Regí, *Chem. Mater.* **2004**, *16*, 2300.
[27] K. A. Wieghaus, S. M. Capitosti, C. R. Anderson, R. J. Price, B. R. Blackman, M. L. Brown, E. A. Botchwey, *Tissue Eng.* **2006**, *12*, 1903.
[28] S. Yang, Y.-S. Tian, Y.-J. Lee, F. H. Yu, H.-M. Kim, *Biomaterials* **2011**, *32*, 2851.
[29] M. Alcaide, M. C. Serrano, R. Pagani, S. Sánchez-Salcedo, A. Nieto, M. Vallet-Regí, M. T. Portolés, *J. Biomed. Mater. Res., A* **2009**, *8*, 539.
[30] A. Eapen, P. Sundivakkam, Y. Song, S. Ravindran, A. Ramachandran, C. Tiruppathi, A. George, *J. Biol. Chem.* **2010**, *47*, 36339.
[31] V. Knights, S. J. Cook, *Pharmacol. Ther.* **2010**, *125*, 105.
[32] D. R. Alessi, A. Cuenda, P. Cohen, D. T. Dudley, A. R. Saltiel, *J. Biol. Chem.* **1995**, *270*, 27489.
[33] C. Ge, G. Xiao, D. Jiang, R. T. Franceschi, *J. Cell. Biol.* **2007**, *176*, 709.
[34] H. Eda, K. Aoki, K. Marumo, K. Fujii, K. Ohkawa, *Biochem. Biophys. Res. Commun.* **2008**, *366*, 471.

PTHrP y el fragmento 107-111, denominado osteostatina, comparten con FGF-2 rutas de señalización implicadas en procesos de osteogénesis, promoviendo la formación ósea. Por este motivo, se ha evaluado si la adición de osteostatina soluble puede mejorar los efectos producidos por FGF-2 unido a SiHA sobre la proliferación y diferenciación de preosteoblastos MC3T3-E1 *in vitro*. Dado que FGF-2 induce además la angiogénesis al promover en osteoblastos la síntesis de factor de crecimiento de endotelio vascular (VEGF), en el presente estudio se ha analizado el efecto de los medios de MC3T3-E1 cultivados en presencia de SiHA/FGF-2 y/u osteostatina sobre la proliferación de células angiogénicas derivadas de progenitoras de endotelio de cerdo (EPCs).

Los resultados obtenidos se resumen a continuación y han dado lugar a la siguiente publicación:

- Lozano D, Feito MJ, Portal-Nuñez S, Lozano RM, Matesanz MC, Serrano MC, Vallet-Regí M, Portolés MT, Esbrit P. Osteostatin improves the osteogenic activity of fibroblast growth factor-2 immobilized on Si-doped hydroxyapatite in osteoblastic cells. Acta Biomaterialia 8:2770-2777, 2012.

Los preosteoblastos murinos MC3T3-E1 cultivados con SiHA/FGF-2 mostraron una proliferación incrementada respecto a los cultivados con SiHA, pero ésta no fue modificada por la adición de osteostatina soluble al cultivo. Para evaluar el efecto de estos factores sobre la diferenciación se analizó la expresión de un marcador temprano (Runx2) y un marcador tardío (osteocalcina) de este proceso. FGF-2 unido a SiHA ejerció un ligero estímulo de la expresión de ambas moléculas que fue significativamente incrementada por la adición de osteostatina al cultivo (**Figura 24**).

Durante la regeneración ósea, el sistema VEGF ejerce una función esencial tanto en la angiogénesis como en la osteogénesis. La expresión génica de VEGF y de sus receptores VEGFR1 y VEGFR2 fue analizada en preosteoblastos cultivados en presencia de SiHA/FGF-2 y osteostatina. Ambos factores incrementaron la expresión de todas estas moléculas, siendo superior el efecto producido por la acción combinada de SiHA/FGF-2 y osteostatina. Respecto a la expresión de receptores de FGF en MC3T3-E1, no se observó este efecto sinérgico probablemente debido a la sobreexpresión de FGFR1 y FGFR2 en este tipo celular.

Dado que FGF-2 y osteostatina estimulan la vía de las MAPKs para activar la expresión de genes implicados en la osteogénesis, en este estudio se han evaluado sus efectos sobre los niveles de calcio citosólico así como la fosforilación de ERK en preosteoblastos MC3T3-E1.

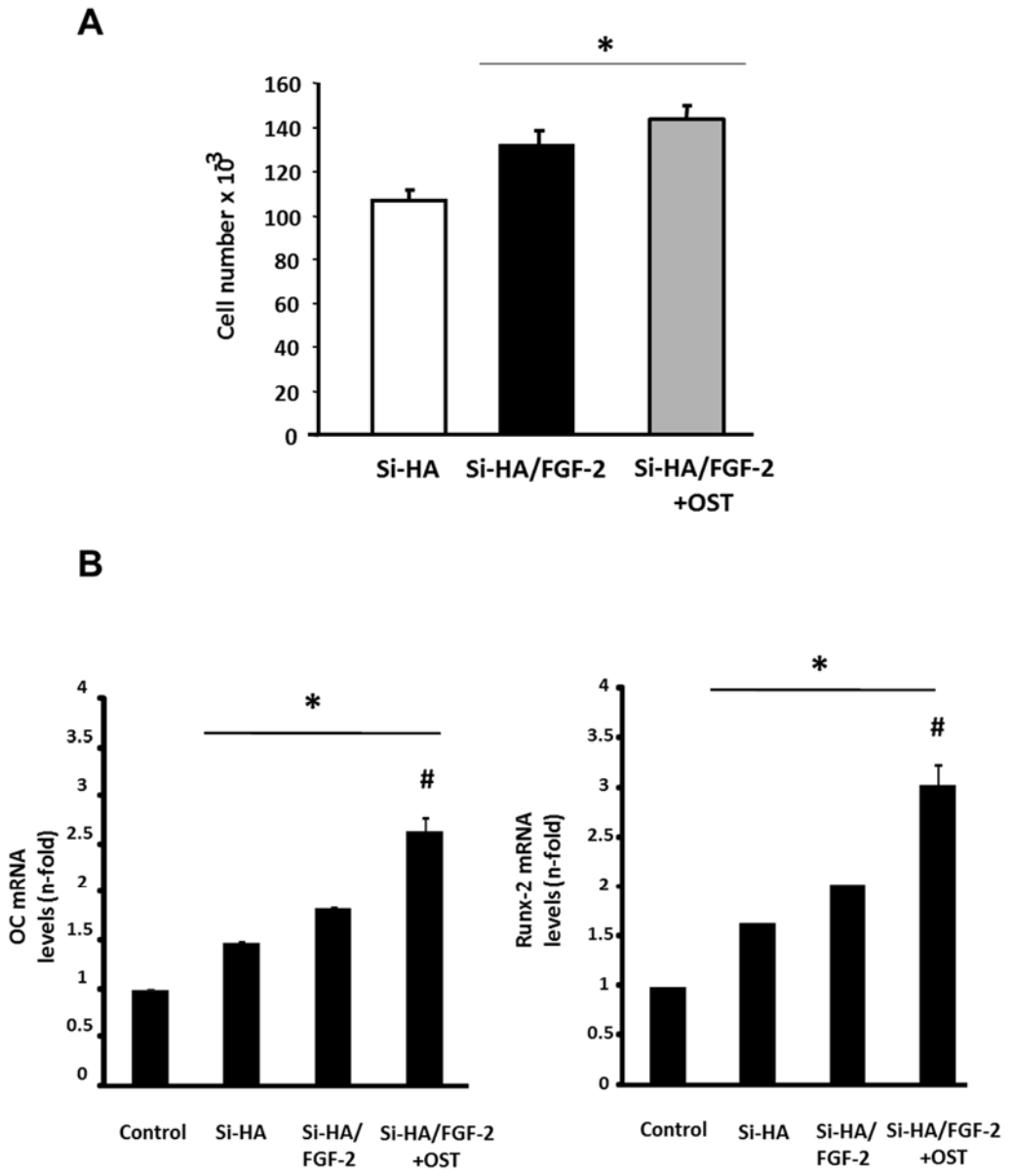

Figura 24. A) Proliferación de preosteoblastos MC3T3-E1 cultivados en presencia de SiHA, SiHA/FGF-2 y SiHA/FGF-2 en presencia de osteostina; B) Expresión de osteocalcina (OC) y Runx2 de preosteoblastos MC3T3-E1 cultivados en presencia de SiHA, SiHA/FGF-2 y SiHA/FGF-2 en presencia de osteostina . Gráfica procedente de [Lozano D *et al. 2012, Acta Biomater*].

El FGF-2/SiHA causó un rápido incremento de calcio citosólico (**Figura 25**) y mayor fosforilación de ERK. Ambos efectos fueron potenciados por la adición de osteostatina. El tratamiento de estos cultivos con U0126 y verapamil, inhibidor de ERK y antagonista de calcio respectivamente anularon el efecto sinérgico de ambos factores.

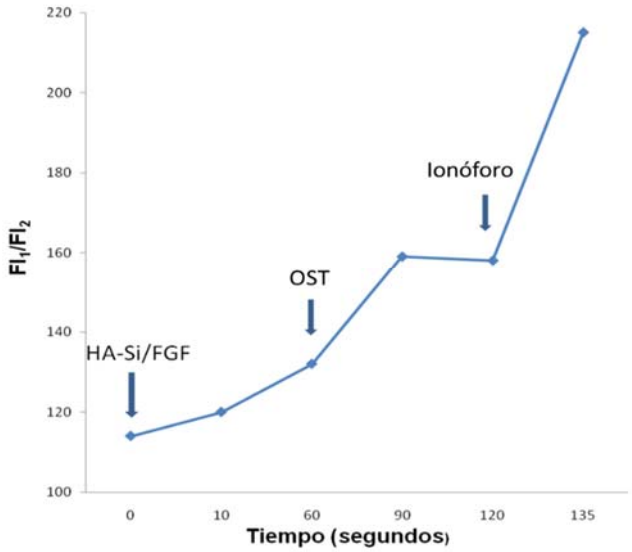

Figura 25. Incremento de los niveles intracelulares de Ca^{2+} tras la adición secuencial de FGF-2 unido a SiHA, osteostatina e ionóforo (este último control de la sonda Indo-1). Gráfica procedente de [Lozano D *et al. 2012, Acta Biomater*].

El estudio del efecto de los medios de MC3T3-E1 cultivados en presencia de SiHA/FGF-2 y/u osteostatina sobre células angiogénicas derivadas de progenitoras de endotelio de cerdo (EPCs), demostró un incremento de la proliferación de estas células producido por la acción de ambos factores pero no por la adición de cada uno por separado. La utilización de un anticuerpo anti-VEGF permitió comprobar que este efecto es específico de VEGF, al verse reducidos los niveles de proliferación (**Figura 26**).

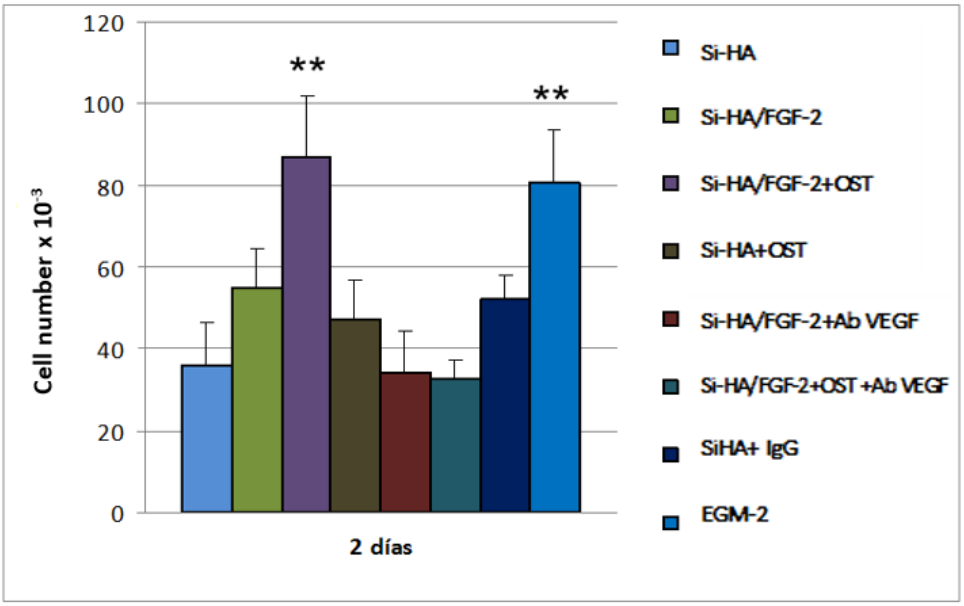

Figura 26. Proliferación de células angiogénicas cultivadas con medios de preosteoblastos MC3T3-E1 en presencia de SIHA/FGF-2 y/u osteostatina con y sin anticuerpos anti-VEGF. Gráfica procedente de [Lozano D *et al. 2012, Acta Biomater*].

Todos estos resultados demuestran que la acción de la osteostatina potencia los efectos de SiHA/FGF-2 mediante un mecanismo que implica la participación de las MAPKs y la movilización de calcio intracelular. La combinación de ambos factores supone una estrategia atractiva para futuros estudios de Ingeniería de Tejidos ósea.

Acta Biomaterialia 8 (2012) 2770–2777

Contents lists available at SciVerse ScienceDirect

Acta Biomaterialia

journal homepage: www.elsevier.com/locate/actabiomat

Osteostatin improves the osteogenic activity of fibroblast growth factor-2 immobilized in Si-doped hydroxyapatite in osteoblastic cells

Daniel Lozano [a,*], María José Feito [b], Sergio Portal-Núñez [a], Rosa María Lozano [c], María Concepción Matesanz [b], María Concepción Serrano [d], María Vallet-Regí [e,f], María Teresa Portolés [b], Pedro Esbrit [a]

[a] Laboratorio de Metabolismo Mineral y Óseo, Instituto de Investigación Sanitaria-Fundación Jiménez Díaz and Instituto de Salud Carlos III (RETICEF), Madrid, Spain
[b] Departamento de Bioquímica y Biología Molecular I, Universidad Complutense, Madrid, Spain
[c] Departamento de Biología Químico-Física, Centro de Investigaciones Biológicas-CSIC, Madrid, Spain
[d] Grupo de Materiales Bioinspirados, Instituto de Ciencia de Materiales-CSIC, Madrid, Spain
[e] Departamento de Química Inorgánica y Bioinorgánica, Madrid, Spain
[f] Centro de Investigación Biomédica en Red deBioingeniería, Biomateriales y Nanomedicina, Spain

ARTICLE INFO

Article history:
Received 28 November 2011
Received in revised form 30 March 2012
Accepted 2 April 2012
Available online 6 April 2012

Keywords:
Osteostatin
Fibroblast growth factor-2
Osteoblastic function
Parathyroid hormone-related protein
Si-based hydroxyapatite

ABSTRACT

Si-doped hydroxyapatite (Si-HA) is a suitable ceramic for the controlled release of agents to improve bone repair. We recently showed that parathyroid hormone-related protein (PTHrP) (107–111) (osteostatin) has remarkable osteogenic features in various in vitro and in vivo systems. Fibroblast growth factor (FGF)-2 modulates osteoblastic function and induces angiogenesis, and can promote osteoblast adhesion and proliferation after immobilization on Si-HA. In the present study we examined whether osteostatin might improve the biological efficacy of FGF-2-coated Si-HA in osteoblastic MC3T3-E1 cells in vitro. We found that Si-HA/FGF-2 in the presence or absence of osteostatin (100 nM) similarly increased cell growth (by about 50%). However, addition of the latter peptide to Si-HA/FGF-2 significantly enhanced gene expression of Runx2, osteocalcin, vascular endothelial growth factor (VEGF) and the VEGF receptors 1 and 2, without significantly affecting that of FGF receptors in these cells. Moreover, secreted VEGF in the MC3T3-E1 cell conditioned medium, which induced the proliferation of pig endothelial-like cells, was also enhanced by these combined factors. The synergistic action of osteostatin and Si-HA/FGF-2 on the VEGF system was abrogated by a mitogen-activated protein kinase inhibitor (U0126) and by the calcium antagonist verapamil. This action was related to an enhancement of alkaline phosphatase activity and matrix mineralization in MC3T3-E1 cells, and also in primary human osteoblastic cells. These in vitro data show that osteostatin increases the osteogenic efficacy of a Si-HA/FGF-2 biomaterial by a mechanism involving mitogen-activated protein kinases and intracellular Ca^{2+}. These findings provide an attractive strategy for bone tissue engineering.

1. Introduction

Si-doped hydroxyapatite (Si-HA) has biocompatibility, bioactivity and osteoconductivity properties, thus it has been proposed as a suitable matrix for the controlled release of biological agents to improve bone repair following fracture and other skeletal injuries [1]. The observed beneficial effects of Si substitution in this ceramic involve several passive and active mechanisms which have been critically reviewed by Bohner [2]. In addition, osteointegration of this type of material can be further improved by incorporation of growth factors which stimulate the repair mechanisms and thus functional restoration of the damaged tissue [3].

Recent findings indicate that parathyroid hormone-related protein (PTHrP) may affect bone formation and bone remodeling through distinct structural domains [4]. In this regard, the native C-terminal PTHrP (107–139) fragment has been shown to be a strong bone resorption inhibitor [5], but can also stimulate osteoblastic function both in vitro and in vivo [6–10]. The bioactivity of this fragment in bone appears to reside into its N-terminal domain, namely the pentapeptide known as osteostatin [6,11–14]. Of interest, osteostatin itself might be generated from PTHrP (107–139) upon proteolytic processing by the product of the PHEX gene (phosphate-regulating gene with homologies to endopeptidases on the X chromosome), which is abundant in osteoblasts [15]. Supporting the osteogenic action of this pentapeptide, we recently showed that its loading onto Si-based ceramics (including Si-HA) made these materials efficient in inducing cell growth and cell differentiation in

* Corresponding author. Tel.: +34 915504894.
E-mail address: dlozano@fjd.es (D. Lozano).

1742-7061/$ - see front matter © 2012 Acta Materialia Inc. Published by Elsevier Ltd. All rights reserved.
http://dx.doi.org/10.1016/j.actbio.2012.04.002

osteoblastic MC3T3-E1 cell cultures [13,16]. Interestingly, this bioactivity in vitro was similarly observed with osteostatin coated onto Si-HA scaffolds by either adsorption, and thus deliverable, or covalent immobilization, leaving free its N-terminus [16]. Moreover, osteostatin coating conferred osteoinduction properties to Si-based ordered SBA-15 mesoporous materials when implanted in a cavitary defect in the femoral epiphysis of healthy rabbits [17].

Fibroblast growth factors (FGFs) are a group of proteins which control the proliferation and differentiation of various cell types, including osteoblasts [18]. FGF-2 increases osteoblast proliferation and can also modulate osteoblast differentiation [19–22]. In this regard, we recently demonstrated that low doses ($\leqslant$1 ng ml^{-1}) of FGF-2 immobilized on Si-HA improved adhesion and proliferation of osteoblastic SaoS-2 osteosarcoma cells [23]. In addition, FGFs are strong inducers of angiogenesis [24]. This is of particular interest, since neovascularization is crucial to meet the oxygen and nutrient demands of cells involved in bone regeneration [25]. Hence, enhancement of bone growth by FGF-2 might be a result of increased osteoblastic growth and improved vascularization. Thus immobilization of FGF-2 on biomaterials would represent a promising approach for bone tissue engineering [26,27].

FGF-2 binding to specific tyrosine kinase receptors activates multiple signal transduction pathways involving mitogen-activated protein kinase (MAPK), phosphatidylinsositol-3 kinase (PI3K)-Akt and intracellular Ca^{+2}/protein kinase C in target cells, including osteoblasts [19,28]. In addition, both native PTHrP (107-139) and osteostatin have previously been shown to affect these signalling pathways in osteoblastic cells, related to various osteogenic effects [7,8,12]. Although the putative osteostatin receptor is presently unknown, these findings suggest that both FGF-2 and osteostatin appear to interact, at least in part, with common pathways in osteoblastic cells to promote bone formation.

In the present study, using the well-characterized non-transformed osteoblastic cell line MC3T3-E1, we extended our initial observations in an osteoblastic osteosarcoma cell line to confirm that FGF-2 maintains its osteogenic activity after immobilization on Si-HA. In addition, we aimed to evaluate whether addition of osteostatin would increase the activity of this biomaterial.

2. Materials and methods

2.1. FGF-2 immobilization on Si-HA

Si-HA with the nominal formula $Ca_{10}(PO_4)_{5.7}(SiO_4)_{0.3}(OH)_{1.7}\square_{0.3}$, where $\square$ represents vacancies at the hydroxyl position, was prepared by aqueous precipitation reaction of $Ca(NO_3)_2{\cdot}4H_2O$, $(NH_4)_2HPO_4$ and $Si(CH_3CH_2O)_4$ solutions, as previously described [29]. The precipitated Si-HA powder was treated at 700 °C to remove nitrates without altering the material structure, and elemental chemical analysis was carried out by fluorescence X-ray spectrometry. The particle size distribution of Si-HA powder in aqueous suspension showed a bimodal distribution centered at 10 and 50 μm [23,29].

The human full length FGF-2 (155 residues) used in this study was synthesized and purified by Dr. R.M. Lozano (Centro de Investigaciones Biológicas, Consejo Superior de Investigaciones Cientificas,

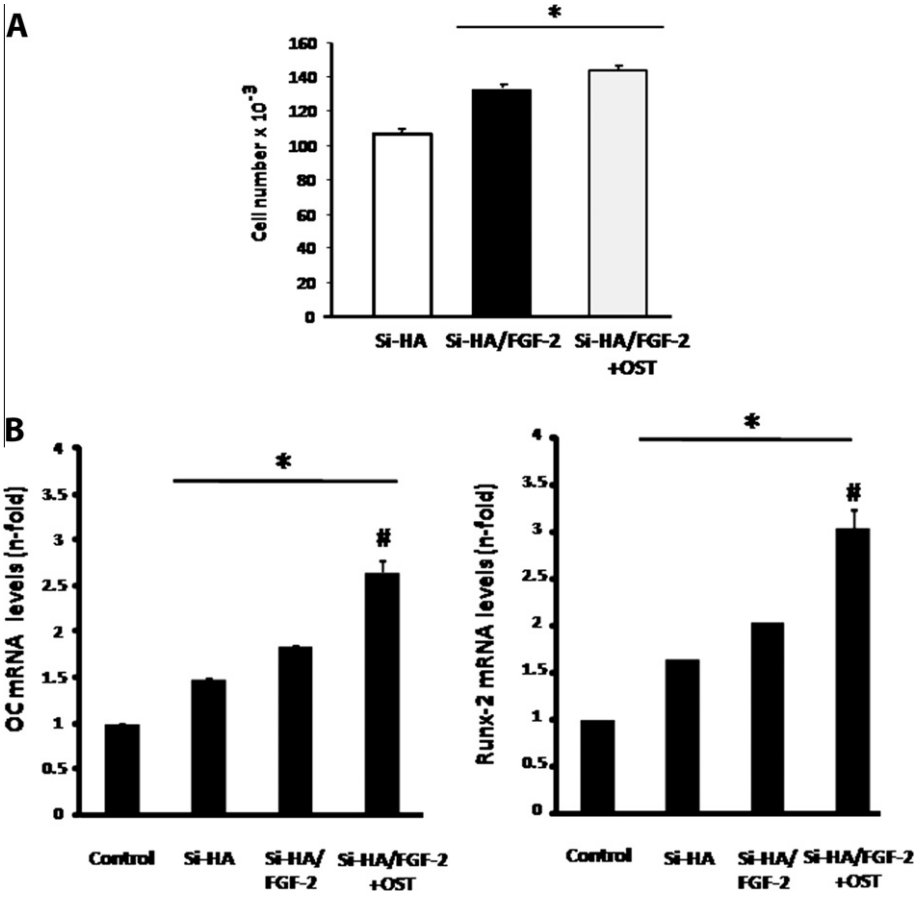

Fig. 1. (A) MC3T3-E1 cell proliferation in the presence of Si-HA, with or without immobilized FGF-2 alone or combined with 100 nM exogenous osteostatin (OST) after 4 days culture. (B) Changes in gene expression levels (assessed by real time PCR) of OC and Runx2 induced by Si-HA, with or without immobilized FGF-2 alone or combined with 100 nM exogenous osteostatin (OST) on day 4. Results are means ± SEM of at least three determinations in triplicate. $^{*}P < 0.05$ vs. Si-HA or control; $^{\#}P < 0.05$ vs. Si-HA/FGF-2.

Madrid, Spain), as described [23]. FGF-2 samples, at 1.4 mg ml^{-1} in 10 mM sodium phosphate (pH 7.2) containing 2 M NaCl, were stored at −20 °C. FGF-2 (200 μg) was adsorbed on powdered Si-HA (1 g) to a final volume of 6 ml in the aforementioned buffer with 50 mM NaCl. After slight rotation of the mix for 2 h at 4 °C it was lyophilized and maintained at −20 °C for subsequent assays. The Si-HA/FGF-2 ratio was calculated as the difference in protein concentration in the supernatants before and after FGF-2 coating onto the material using a value of 0.83 as the molar extinction coefficient at 280 nm of a 0.1% solution of FGF-2, at 25 °C, using a Perkin-Elmer spectrophotometer [23]. Sample scattering, measured as the absorbance at 340 nm, and buffer (10 mM sodium phosphate and 50 mM NaCl, pH 7.2) absorbance were subtracted from each sample. In this way the Si-HA/FGF-2 ratio was found to be 5 μg ng^{-1}.

2.2. Cell culture

The osteogenic capacity of the tested materials was examined using well-characterized murine preosteoblastic MC3T3-E1 cells (subclone 4, CRL-2593, ATCC, Mannassas, VA) as the experimental model [13,16]. Cells were seeded on 6-well plates at a density of 2×10^4 cells cm^{-2} and incubated with the tested agonists for different time periods in α-minimal essential medium (α-MEM) with 50 μg ml^{-1} ascorbic acid, 10 mM β-glycerophosphate, 10% fetal bovine serum (FBS), 100 μg ml^{-1} penicillin and 100 μg ml^{-1} streptomycin (differentiation medium) in a humidified 5% CO_2 atmosphere at 37 °C. The medium was replaced every other day. Human osteoblast-like (hOB) cells were isolated from trabecular bone explants obtained from knee samples discarded at the time of surgery on two osteoarthritic subjects (aged 69 and 80 years), as previously reported [7,8,30]. These subjects had no history of bone metabolic disorders. These cells were cultured in Dulbecco's modified Eagle's medium with 15% FBS and antibiotics, and used at passage 2.

Vascular endothelial growth factor (VEGF) secreted by MC3T3-E1 cells in response to the tested materials was examined using pig endothelial like cells at an early differentiation stage (EC_1), derived from endothelial progenitor cells (EPCs), as angiogenic cells expressing von Willebrand factor and endothelial NO synthase

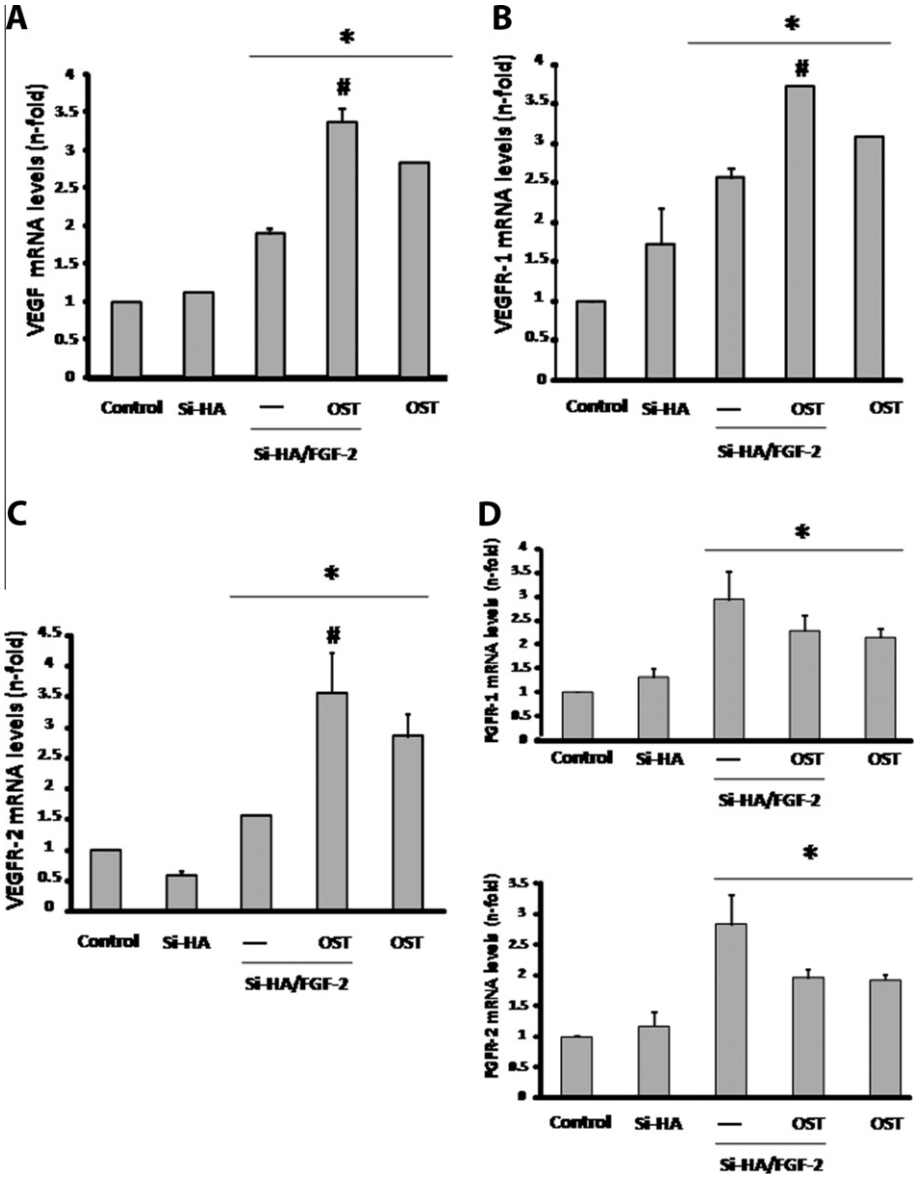

Fig. 2. Changes in gene expression levels (assessed by real time PCR) of VEGF, VEGFR-1 and VEGFR-2 (A–C), and FGFR-1 and FGFR -2 (D) induced by Si-HA, with or without immobilized FGF-2 alone or combined with 100 nM exogenous osteostatin (OST) or the latter peptide alone in MC3T3-E1 cells on day 4. Results are means ± SEM of at least three determinations in duplicate. $^{*}P < 0.05$ vs. control and Si-HA; $^{\#}P < 0.05$ vs. Si-HA/FGF-2 and OST alone.

[31]. EPCs are circulating premature cells which can differentiate into endothelial cells depending on the local environment and they can be used as an alternative to primary endothelial cells for tissue engineering [32]. To obtain EC_1 whole pig blood was diluted (50:50 vol.%) in phosphate-buffered saline, pH 7.2 (PBS), with 0.1% bovine serum albumin (BSA) and 0.6% sodium citrate. Mononuclear cells (MNCs) were isolated using a density gradient formed with Histopaque-1077 solution (Sigma-Aldrich, St Louis, MO) in Accuspin™ tubes (Sigma-Aldrich). After centrifugation at 800*g* for 30 min at room temperature the MNC layer was carefully collected and seeded in EGM-2 medium (endothelial growth medium containing hydrocortisone, FGF-2, VEGF, R3-insulin-like growth factor-1, ascorbic acid, epidermal growth factor and heparin (Lonza, Walkersville, MD)) in F75 polystyrene culture flasks (Corning Inc., Corning, NY) at a density of $2–3 \times 10^5$ cells cm^{-2} under a 5% CO_2 atmosphere at 37 °C. The culture medium was replaced at 96 h and then every 48 h for 2 weeks before addition of the MC3T3-E1 cell conditioned medium (see below).

2.3. Cell growth

For cell proliferation experiments, at 24 h after cell seeding FGF-2 (0.8 ng ml^{-1}) immobilized on powered Si-HA alone (5 μg) or combined with 100 nM exogenous osteostatin (Bachem, Bubendorf, Switzerland) was added to MC3T3-E1 cells for 4 days. These concentrations of each growth factor have been shown to maximally stimulate osteoblastic function [13,16,23]. Si-HA controls without the tested peptides were always included. In some experiments, after incubation as above for 5 days the medium conditioned by these cells for the last 48 h was removed and added to subconfluent EC_1 cells, in the presence or absence of a neutralizing rabbit polyclonal mouse $VEGF_{164}$ antibody (R&D, Minneapolis, MN) or non-immunogenic rabbit IgG (each at 0.5 μg ml^{-1}) for 2 days. Controls with EC_1 cells cultured in EGM-2 medium were also carried out as optimal cell growth conditions.

After incubation the attached cells were washed with PBS and then harvested using 0.25% trypsin–EDTA solution for 15 min. The reaction was stopped with culture medium and viable cells were counted by Trypan blue exclusion with a Neubauer hemocytometer. Alternatively, cells were centrifuged at 310*g* for 10 min and then resuspended in fresh medium for the analysis of apoptosis and the cell cycle in a LSR Beckton Dickinson flow cytometer [23].

2.4. Intracellular calcium transients

MC3T3-E1 cell suspensions (10^6 per ml) were incubated with 10 μM indo-1 AM (Enzo Life Sciences, Grupo Taper, Madrid, Spain) for 30 min at room temperature in the dark with shaking. Indo-1 was excited at 325 nm and the emitted fluorescence was measured with 380 nm long pass (FL1) and 424/44 nm band pass (FL2) filters following the sequential addition of FGF-2 (0.8 ng ml^{-1}) immobilized on powdered Si-HA and osteostatin (100 nM) in a LSR Beckton Dickinson flow cytometer. Thereafter 10 μM A-23187 ionophore (Enzo Life Sciences) was added as a positive control.

2.5. Real time PCR

MC3T3-E1 cells were incubated with the tested factors as described above in the presence or absence of 10 μM MAPK inhibitor U0126 (Promega, Madison, WI) or 50 μM calcium antagonist verapamil (Knoll Pharmaceutical, Madrid, Spain). These inhibitors were added 1 h prior to addition of the tested factors. 6 h or 4 days thereafter total MC3T3-E1 cell RNA was extracted with Trizol (Life Technologies, Rockville, MD). Gene expression was analyzed by real time PCR using an ABI Prism 7500 system (Applied Biosystems, Foster City, CA) and a described protocol [13]. Unlabeled mouse specific primers for Runx2, osteocalcin (OC), vascular endothelial growth factor (VEGF), VEGF receptors 1 and 2 (VEGFR-1 and VEGFR-2), FGF receptors 1 and 2 (FGFR-1 and FGFR-2), and TaqMan probes were obtained from Assay-by-Design (Applied Biosystems). The mRNA copy numbers were calculated for each sample using the cycle threshold (C_t) value. 18S rRNA, a housekeeping gene, was amplified in parallel with the tested genes. Fold change for the treatment was defined as the relative expression compared with that of the control and was calculated as $2^{-\Delta\Delta C_t}$, where $\Delta\Delta C_t = \Delta C_{treatment} - \Delta C_{control}$.

2.6. Western blot analysis

Cell total protein was extracted with 50 mM Tris–HCl, pH 7.5, 150 mM NaCl, 1 mM EDTA, 1% sodium deoxycholate, 1% NP-40, 1% sodium dodecyl sulfate (SDS), supplemented with the protease inhibitor cocktail P8340 (Sigma-Aldrich, St Louis, MO), and phosphatase inhibitor cocktail Set II 524625 (Calbiochem, La Jolla, CA). Protein concentration was measured using a bicinchoninic

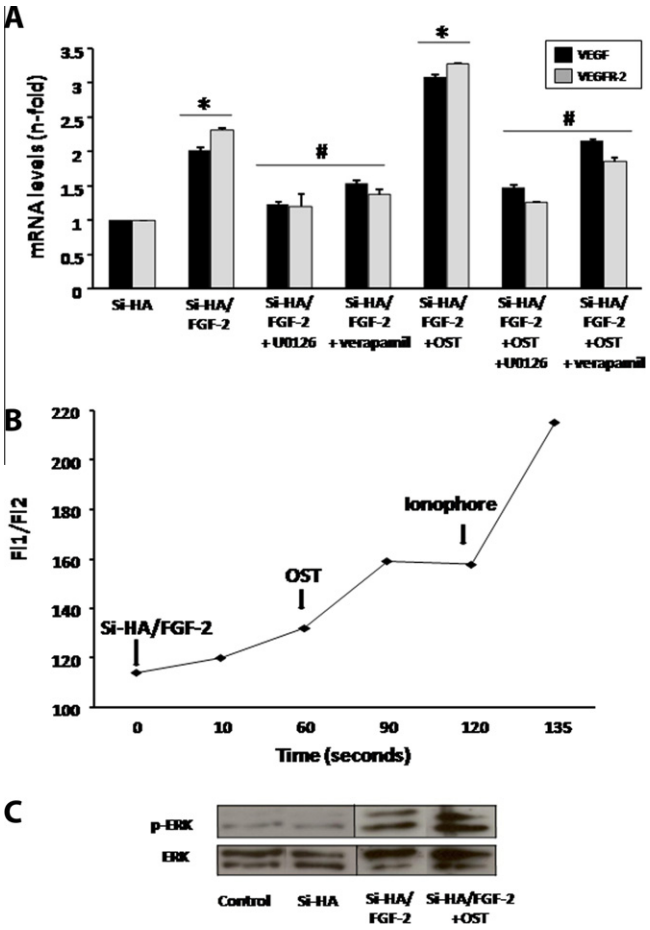

Fig. 3. (A) Changes in gene expression levels (analyzed by real time PCR) of VEGF and VEGFR-2 induced by Si-HA, with or without immobilized FGF-2 alone or combined with 100 nM exogenous osteostatin (OST), in the presence or absence of UO126 (at 10 μM) or verapamil (at 50 μM), after 6 h culture, in MC3T3-E1 cells. Results are means ± SEM of at least three determinations in duplicate. $^*P < 0.05$ vs. Si-HA; $^{\#}P < 0.05$ vs. Si-HA/FGF-2 and Si-HA/FGF-2 + OST. (B) Intracellular calcium transients in MC3T3-E1 cells. Points to trace the curve are the means of three independent measurements per time period. A-23187 ionophore (10 μM) was added at the end of the measurements as a control for the sensitivity of the assay. (C) ERK activation by the different tested biomaterials in MC3T3-E1 cells. Cells were incubated with these biomaterials for 30 min and then p-ERK and total ERK protein were assayed in cell protein extracts by Western blot as described in the text.

acid (BCA)-based protein assay (Pierce, Rockford, IL), using BSA as the standard. Proteins (20 μg per lane) were loaded on 12% polyacrylamide–SDS gels under reducing conditions. Detection of extracellular regulated kinase (ERK) and p-ERK was performed with rabbit polyclonal anti-ERK and anti-p-ERK antibodies (R&D systems, Minneapolis, MN) at 1:1000 and 1:500 dilutions, respectively, followed by incubation with a horseradish peroxidase-conjugated anti-rabbit IgG (Santa Cruz Biotechnology, Santa Cruz, CA) at 1:5000 dilution. Protein bands were developed with ECL™ Western blotting detection reagents (GE Healthcare, Chalfont St Giles, UK).

2.7. Mineralization assay

Matrix mineralization was measured by alizarin red staining after incubating MC3T3-E1 cells, in the presence or absence of neutralizing rabbit polyclonal mouse $VEGF_{164}$ antibody, or hOBs cells with the tested agonists for 12 and 18 days, respectively, as described [13,16]. The stain was dissolved with 10% cetylpyridinum chloride in 10 mM sodium phosphate, pH 7, measuring absorbance at 620 nm.

2.8. Alkaline phosphatase (ALP) activity

Following incubation with the agonists for different time periods the cells were washed with PBS and ALP activity was measured in cell extracts obtained with 0.1% Triton X-100 using p-nitrophenylphosphate as the substrate, as described previously [13]. ALP activity was normalized to cell protein content.

2.9. Statistical analysis

Results are expressed as means ± SEM. Statistical evaluation was carried out with analysis of variance and a post hoc test (Scheffé's) or Mann–Whitney test when appropriate. Statistical analysis was performed using the Statistical Package for the Social Sciences (SPSS v. 19). A value of $P < 0.05$ was considered significant.

3. Results and discussion

Recent strategies in tissue engineering and regenerative medicine have focused on the delivery of multiple growth factors and bioactive molecules from biomaterial-based platforms. The aim of such strategies is to provide an adequate spatial architecture and controlled release kinetics of the coated factors to target osteogenic cells to improve the healing process [3].

Previous results have shown that Si-HA can induce osteoblast proliferation [33], and this effect is improved by immobilizing FGF-2 on Si-HA scaffolds [23]. Moreover, recent studies have revealed that this immobilized factor activates intracellular signals which are crucial in stimulating osteoblast proliferation and differentiation [34]. We have also recently shown that osteostatin loading onto Si-HA induces both cell growth and the expression of various osteoblastic genes in MC3T3-E1 cells [16]. Thus the combination of Si-HA/FGF-2 and osteostatin might be envisioned as an alternative approach to stimulate bone regeneration. We have initially addressed this hypothesis by performing an in vitro study using a non-transformed osteoblastic cell line.

Fig. 1A shows MC3T3-E1 cell proliferation in the presence of a Si-HA material without (control) or with immobilized FGF-2 alone or combined with exogenously added osteostatin. In agreement with our previous results in Saos-2 human osteosarcoma cells [21], the Si-HA/FGF-2 biomaterial produced a significant increase in MC3T3-E1 proliferation, which was not significantly affected by the presence of osteostatin. On the other hand, apoptosis was unchanged and below 0.5% in the presence of any of these tested agents (not shown). Since osteostatin has mitogenic features in osteoblastic cells [6,13], the above result suggests that both FGF-2 and osteostatin might share a common mechanism to induce osteoblastic cell growth.

We next evaluated the capacity of the Si-HA/FGF-2 biomaterial to increase the expression of two markers corresponding to different osteoblast differentiation stages, Runx2 (early) and OC (late) [34], and possible interactions with osteostatin. We found that Si-HA alone increased the gene expression of both markers, and this effect was slightly improved by FGF-2 coating, but was significantly higher with osteostatin (Fig. 1B).

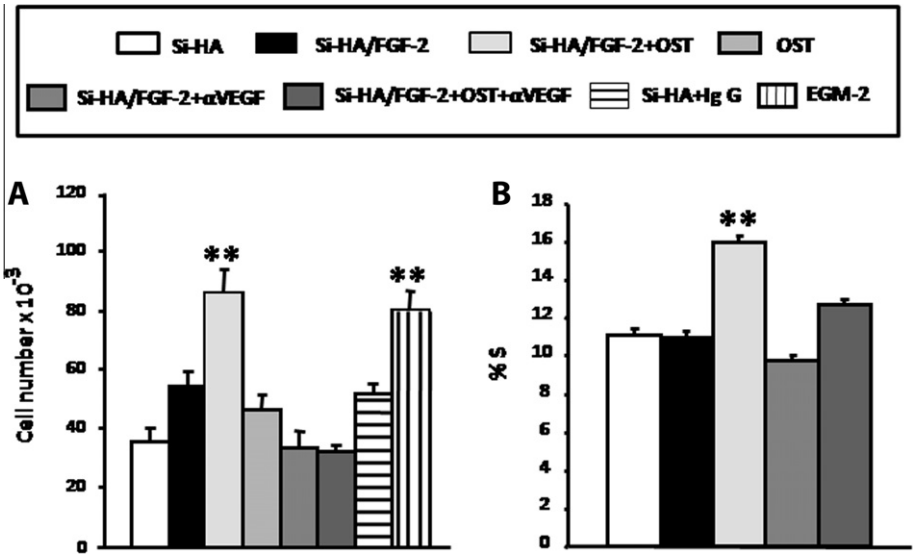

Fig. 4. Effect of MC3T3-E1 cell conditioned medium in the presence of Si-HA with or without FGF-2 alone or combined with 100 nM exogenous osteostatin (OST) or the latter peptide alone on (A) the EC_1 cell number and (B) the S phase of the EC_1 cycle on day 2. A neutralizing VEGF antibody (αVEGF) or non-immunogenic rabbit IgG was added in some experiments, as described in the text. EGM-2 medium was used as a positive control. Results are means ± SEM of at least three determinations in duplicate. $^{**}P < 0.01$ vs. all of the other conditions.

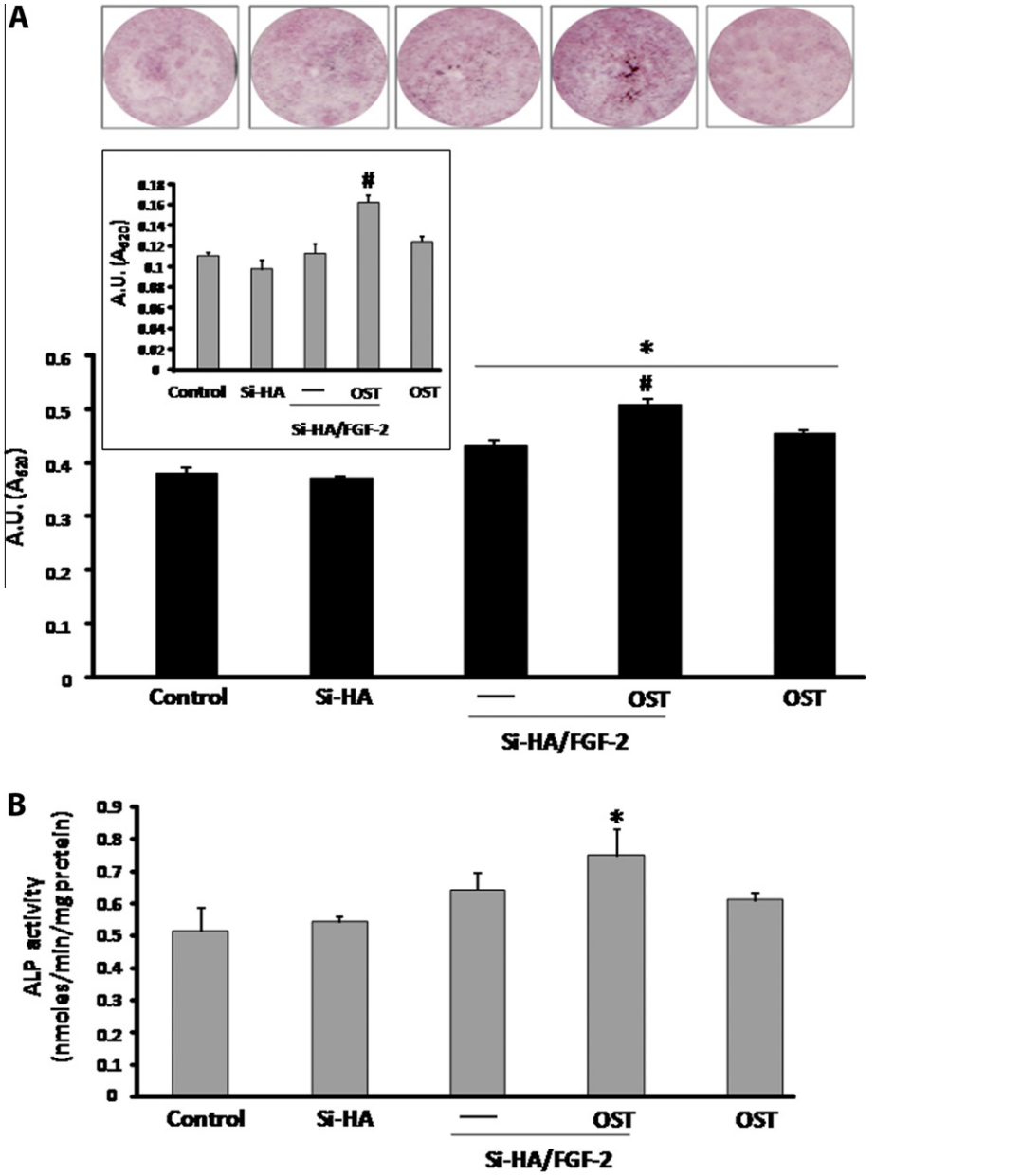

Fig. 5. Changes in mineralization and ALP activity in osteoblastic cells induced by Si-HA, with or without immobilized FGF-2 alone or combined with 100 nM exogenous osteostatin (OST) or by the latter peptide alone. (A) Mineralization was assessed by alizarin red staining; corresponding densitometric values and representative images of MC3T3-E1 cells on day 12 are shown. (Inset) These values for primary hOB cell cultures on day 18 are also depicted. (B) ALP activity was measured in MC3T3-E1 cell extracts on day 4, as described in the text. Results are means ± SEM of four determinations in duplicate. $^{*}P < 0.05$ vs. control and/or Si-HA; $^{\#}P < 0.05$ vs. Si-HA/FGF-2 and OST alone.

During bone regeneration angiogenesis plays a key role in the inflammatory response and callus development [35,36]. The VEGF system is overexpressed during bone healing, and is essential for both angiogenesis and osteogenesis, promoting the proliferation and differentiation of osteoprogenitors [36,37]. Therefore, we next evaluated the action of the tested agents on the VEGF system in osteoblastic cells. In contrast to Si-HA alone, FGF-2 coated onto this material as well as osteostatin were found to independently up-regulate VEGF, VEGFR-1 and VEGFR-2 gene expression in MC3T3-E1 cells, but this up-regulation was significantly higher with the combination of Si-HA/FGF-2 and osteostatin (Fig. 2A–C). In this regard, the latter peptide as well as the native PTHrP fragment, PTHrP (107-139), have been shown to interact with the VEGF system both in vivo and in vitro in osteoblastic cells [7–9,13,17,30]. In addition, we found herein that each single factor, Si-HA/FGF-2 or osteostatin, up-regulated the gene expression of FGFR-1 and FGFR-2, which are abundant in MC3T3-E1 cells [38,39], but their combination was no more efficient in these cells (Fig. 2D). The angiogenic potential of FGF-2 has also previously been characterized; this growth factor stimulates endothelial cells to produce both matrix metalloproteinases and VEGF and its receptors [40]. Interestingly in this context, VEGF and FGF-2 have shown a combined effect on angiogenesis, so that the addition of both factors to acellular collagen–heparin scaffolds enhances the early mature vasculature when subcutaneously implanted in rats [41,42].

MAPKs and intracellular Ca^{2+} have been demonstrated to play key roles in several osteogenic actions of both osteostatin and FGF-2 in osteoblastic cells [7,8,12,28]. In the present study the MAPK inhibitor U0126 as well as verapamil abrogated the synergistic induction of the VEGF system by the combined Si-HA/FGF-2 biomaterial and osteostatin in MC3T3-E1 cells (Fig. 3A). Moreover, as shown in Fig. 3B and C, this biomaterial was found

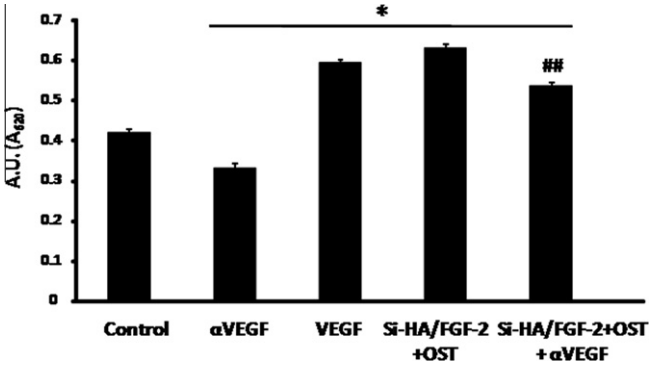

Fig. 6. Effect of a neutralizing VEGF antibody (αVEGF) on mineralization in the presence or absence of the different tested biomaterials in MC3T3-E1 cells. This antibody was added every other day throughout the time course (12 days). Mouse $VEGF_{164}$ (10 ng ml^{-1}) was used as a positive control. Results are means ± SEM of four determinations in duplicate. $^{*}P < 0.05$ vs. control; $^{\#\#}P < 0.05$ vs. Si-HA/FGF-2 + OST.

to trigger a rapid response of cytosolic Ca^{2+} and also stimulated p-ERK in MC3T3-E1 cells, indicating that FGF-2 maintains the capacity of Ca^{2+}/pERK signalling after immobilization on this ceramic [28,33]. Addition of osteostatin was shown to further increase this Ca^{2+} response, but ERK activation was only slightly greater than that triggered by the Si-HA/FGF-2 biomaterial (Fig. 3B and C). These data suggest that each factor is likely to interact with different receptors, but affect a common pathway involving p-ERK and intracellular Ca^{2+} to target the VEGF system in osteoblastic MC3T3-E1 cells.

In order to examine whether stimulation of VEGF gene expression by the tested growth factors had a consequence on VEGF secretion by MC3T3-E1 cells we used angiogenic EC_1 cells [31]. Medium conditioned by MC3T3-E1 cells for 2 days of the 5 day incubation period in the combined presence of Si-HA/FGF-2 and osteostatin, but not that containing each factor alone, increased EC_1 growth (Fig. 4A). This increase was similar to that induced by EGM-2 medium (as an optimal growth control) in these cells. VEGF in the MC3T3-E1 cell conditioned medium was responsible for this proliferative effect, since it was abolished by a neutralizing VEGF antibody but not by a non-immunogenic rabbit IgG (Fig. 4A). Since proliferation is dependent on cell cycle progression, the stimulatory effect of combined Si-HA/FGF-2 and osteostatin on EC_1 proliferation was confirmed by analysing the S phase of the MC3T3-E1 cell cycle (Fig. 4B).

A previous study has shown an important role of VEGF in promoting mineralization in primary cultures of hOBs [43]. Thus we here tested the possibility that the observed synergistic effect of combined Si-HA/FGF-2 and osteostatin on the VEGF system might also affect matrix mineralization in MC3T3-E1 cells. In fact, this was proven to be the case, since such a combination of factors was more efficient than each factor alone in stimulating both mineral deposition and ALP activity in these cells (Fig. 5A and B). This efficiency gain with both combined factors was similarly observed in primary hOB cells (Fig. 5A, inset). Moreover, this action was mimicked by exogenous $VEGF_{164}$ (10 ng ml^{-1}), and it was significantly inhibited, but not abolished, by a neutralizing VEGF antibody in MC3T3-E1 cells (Fig. 6). The latter might be due to a possible suboptimal dose of antibody used, which was based on that recommended by the antibody supplier as tested in a human umbilical vascular endothelial cells assay.

4. Conclusions

The present in vitro findings demonstrate for the first time that osteostatin can improve the osteogenic efficacy of a Si-HA/FGF-2 biomaterial in osteoblastic cells by stimulating osteoblastic function and their angiogenic potential. However, the majority of our results were obtained in the well-established osteoblastic cell line MC3T3-E1, and caution should be taken when translating these results to an in vivo situation. Taking this consideration into account, our data might have a pathophysiological impact in bone repair, strongly suggesting that the combination of these growth factors would be an attractive bone tissue engineering strategy.

Acknowledgements

We are indebted to Dr. Laura Saldaña (IdiPaz, Madrid) for providing primary hOB cells. This investigation was supported by grants from the Spanish Ministerio de Ciencia e Innovación (PI080922, PI11/00449, RETICEF RD06/0013/1002, MAT2008-00736, and MAT2008-06719-C03-02), Fundación de Investigación Médica Mutua Madrileña, and Comunidad Autónoma de Madrid (S2009 MAT-1472).

Appendix A. Figures with essential colour discrimination

Certain figures in this article, particularly Fig. 5, is difficult to interpret in black and white. The full colour images can be found in the on-line version, at doi:http://dx.doi.org/10.1016/j.actbio.2012.04.002.

References

[1] Vallet-Regí M, Arcos D. Silicon substituted hydroxyapatites. A method to upgrade calcium phosphate based implants. J Mater Chem 2005;15:1509–16.
[2] Bohner M. Silicon-substituted calcium phosphates – a critical review. Biomaterials 2009;30:6403–6.
[3] Chen F-M, Zhang M, Wu Z-F. Toward delivery of multiple growth factors in tissue engineering. Biomaterials 2010;31:6279–308.
[4] Bisello A, Horwitz MJ, Stewart AF. Parathyroid hormone-related protein: an essential physiological regulator of adult bone mass. Endocrinology 2004;145:3551–3.
[5] Cornish J, Callon KE, Nicholson GC, Reid IR. Parathyroid hormone-related protein-(107–139) inhibits bone resorption in vivo. Endocrinology 1997;38:1299–304.
[6] Cornish J, Callon KE, Lin C, Xiao C, Moseley JM, Reid IR. Stimulation of osteoblast proliferation by C-terminal fragments of parathyroid hormone-related protein. J Bone Miner Res 1999;14:915–22.
[7] de Gortázar AR, Alonso V, Alvarez-Arroyo MV, Esbrit P. Transient exposure to PTHrP (107–139) exerts anabolic effects through vascular endothelial growth factor receptor 2 in human osteoblastic cells in vitro. Calcif Tissue Int 2006;79:360–9.
[8] Alonso V, de Gortázar AR, Ardura JA, Andrade-Zapata I, Alvarez-Arroyo MV, Esbrit P. Parathyroid hormone-related protein (107–139) increases human osteoblastic cell survival by activation of vascular endothelial growth factor receptor-2. J Cell Physiol 2008;217:717–27.
[9] Lozano D, Fernández-de-Castro L, Portal-Núñez S, López-Herradón A, Dapía S, Gómez-Barrena E, et al. The C-terminal fragment of parathyroid hormone-related peptide promotes bone formation in diabetic mice with low turnover osteopenia. Br J Pharmacol 2011;162:1424–38.
[10] de Castro LF, Lozano D, Portal-Núñez S, Maycas M, De la Fuente M, Caeiro JR, et al. Comparison of the skeletal effects induced by daily administration of PTHrP (1–36) and PTHrP (107–139) to ovariectomized mice. J Cell Physiol 2012;227:1752–60.
[11] Fenton AJ, Kemp BE, Kent GN, Moseley JM, Zheng MH, Rowe DJ, et al. A carboxyl-terminal peptide from the parathyroid hormone-related protein inhibits bone resorption by osteoclasts. Endocrinology 1991;129:1762–8.
[12] Valín A, Guillén C, Esbrit P. C-terminal parathyroid hormone-related protein (PTHrP) (107–139) stimulates intracellular Ca^{2+} through a receptor different from the type 1 PTH/PTHrP receptor in osteoblastic osteosarcoma UMR 106 cells. Endocrinology 2001;142:2752–9.
[13] Lozano D, Manzano M, Doadrio JC, Salinas AJ, Vallet-Regí M, Gómez-Barrena E, et al. Osteostatin-loaded bioceramics stimulate osteoblastic growth and differentiation. Acta Biomater 2010;6:797–803.
[14] Cuthbertson RM, Kemp BE, Barden JA. Structure study of osteostatin PTHrP[Thr107](107–139). Biochim Biophys Acta 1999;1432:64–72.
[15] Boileau G, Tenenhouse HS, Desgroseillers L, Crine P. Characterization of PHEX endopeptidase catalytic activity: identification of parathyroid-hormone-related peptide 107–139 as a substrate and osteocalcin, PPi and phosphate as inhibitors. Biochem J 2001;355:707–13.
[16] Manzano M, Lozano D, Arcos D, Portal-Núñez S, López la Orden C, Esbrit P, et al. Comparison of the osteoblastic activity conferred on Si-doped hydroxyapatite scaffolds by different osteostatin coatings. Acta Biomater 2011;7:3555–62.

[17] Trejo CG, Lozano D, Manzano M, Doadrio JC, Salinas AJ, Dapía S, et al. The osteoinductive properties of mesoporous silicate coated with osteostatin in a rabbit femur cavity defect model. Biomaterials 2010;31:8564–73.
[18] Marie PJ. Fibroblast growth factor signaling controlling osteoblast differentiation. Gene 2003;316:23–32.
[19] Dailey L, Ambrosetti D, Mansukhani A, Basilico C. Mechanisms underlying differential responses to FGF signaling. Cytokine Growth Factor Rev 2005;16:233–47.
[20] Fei Y, Xiao L, Doetschman T, Coffin DJ, Hurley MM. Fibroblast growth factor 2 stimulation of osteoblast differentiation and bone formation is mediated by modulation of the Wnt signaling pathway. J Biol Chem 2011;286:40575–83.
[21] Kyono A, Avishai N, Ouyang Z, Landreth GE, Murakami S. FGF and ERK signaling coordinately regulate mineralization-related genes and play essential roles in osteocyte differentiation. J Bone Miner Metab 2012;30:19–30.
[22] Hughes-Fulford M, Li CF. The role of FGF-2 and BMP-2 in regulation of gene induction, cell proliferation and mineralization. J Orthop Surg Res 2011;6:8.
[23] Feito MJ, Lozano RM, Alcaide M, Ramírez-Santillán C, Arcos D, Vallet-Regí M, et al. Immobilization and bioactivity evaluation of FGF-1 and FGF-2 on powdered silicon-doped hydroxyapatite and their scaffolds for bone tissue engineering. J Mater Sci Mater Med 2011;22:405–16.
[24] Lazarous DF. The fibroblast growth factors and angiogenesis: basic considerations. Curr Interv Cardiol Rep 2001;3:213–7.
[25] Wieghaus KA, Capitosti SM, Anderson CR, Price RJ, Blackman BR, Brown ML, et al. Small molecule inducers of angiogenesis for tissue engineering. Tissue Eng 2006;12:1903–13.
[26] Mabilleau G, Aguado E, Stancu IC, Cincu C, Baslé MF, Chappard D. Effects of FGF-2 release from a hydrogel polymer on bone mass and microarchitecture. Biomaterials 2008;29:1593–600.
[27] Luong LN, Ramaswamy J, Kohn DH. Effects of osteogenic growth factors on bone marrow stromal cell differentiation in a mineral-based delivery system. Biomaterials 2012;33:283–94.
[28] Xiao G, Jiang D, Gopalakrishnan R, Franceschi RT. Fibroblast growth factor 2 induction of the osteocalcin gene requires MAPK activity and phosphorylation of the osteoblast transcription factor, Cbfa1/Runx2. J Biol Chem 2002;277:36181–7.
[29] Arcos D, Rodríguez-Carvajal J, Vallet-Regí M. Silicon incorporation in hydroxylapatite obtained by controlled crystallization. Chem Mater 2004;16:2300–8.
[30] Esbrit P, Alvarez-Arroyo MV, De Miguel F, Martín O, Martínez ME, Caramelo C. C-terminal parathyroid hormone-related protein increases vascular endothelial growth factor in human osteoblastic cells. J Am Soc Nephrol 2000;11:1085–92.
[31] Serrano MC, Pagani R, Ameer GA, Vallet-Regí M, Portolés MT. Endothelial cells derived from circulating progenitors as an effective source to functional endothelialization of NaOH-treated poly(ϵ-caprolactone) films. J Biomed Mater Res A 2008;87A:964–71.
[32] Walenta K, Friedrich EB, Sehnert F, Werner N, Nickenig G. In vitro differentiation characteristics of cultured human mononuclear cells-implications for endothelial progenitor cell biology. Biochem Biophys Res Commun 2005;333:476–82.
[33] Matesanz MC, Feito MJ, Ramírez-Santillán C, Lozano RM, Sánchez-Salcedo S, Arcos D, et al. Signaling pathways of immobilized FGF-2 on silicon-substituted hydroxyapatite. Macromol Biosci 2012;12:446–53.
[34] Chau JFL, Leong WF, Li B. Signaling pathways governing osteoblast proliferation, differentiation and function. Histol Histopathol 2009;24:1593–606.
[35] Towler DA. Vascular biology and bone formation: hints from HIF. J Clin Invest 2007;117:1477–80.
[36] Jacobsen KA, Al-Aql ZS, Wan C, Fitch JL, Stapleton SN, Mason ZD, et al. Bone formation during distraction osteogenesis is dependent on both VEGFR1 and VEGFR2 signaling. J Bone Miner Res 2008;23:596–609.
[37] Grellier M, Ferreira-Tojais N, Bourget C, Bareille R, Guillemot F, Amédée J. Role of vascular endothelial growth factor in the communication between human osteoprogenitors and endothelial cells. J Cell Biochem 2009;106:390–8.
[38] Shalhoub V, Ward SC, Sun B, Stevens J, Renshaw L, Hawkins N, et al. Fibroblast growth factor 23 (FGF23) and alpha-klotho stimulate osteoblastic MC3T3.E1 cell proliferation and inhibit mineralization. Calcif Tissue Int 2011;89:140–50.
[39] Haupt LM, Murali S, Mun FK, Teplyuk N, Mei LF, Stein GS, et al. The heparan sulfate proteoglycan (HSPG) glypican-3 mediates commitment of MC3T3-E1 cells toward osteogenesis. J Cell Physiol 2009;220:780–91.
[40] Presta M, Dell'Era P, Mitola S, Moroni E, Ronca R, Rusnati M. Fibroblast growth factor/fibroblast growth factor receptor system in angiogenesis. Cytokine Growth Factor Rev 2005;16:159–78.
[41] Nillesen STM, Geutjes PJ, Wismans R, Schalkwijk J, Daamen WF, van Kuppevelt TH. Increased angiogenesis in acellular scaffolds by combined release of FGF2 and VEGF. J Controlled Release 2006;116:e88–90.
[42] Nillesen STM, Geutjes PJ, Wismans R, Schalkwijk J, Daamen WF, van Kuppevelt TH. Increased angiogenesis and blood vessel maturation in acellular collagen–heparin scaffolds containing both FGF2 and VEGF. Biomaterials 2007;28:1123–31.
[43] Mayer H, Bertram H, Lindenmaier W, Korff T, Weber H, Weich H. Vascular endothelial growth factor (VEGF-A) expression in human mesenchymal stem cells: autocrine and paracrine role on osteoblastic and endothelial differentiation. J Cell Biochem 2005;95:827–39.

Con el reciente desarrollo de la nanotecnología y dado que las apatitas de hueso de mamífero son nanocristalinas, se ha propuesto la utilización de SiHA nanocristalina, con mayor área de superficie y mejores respuestas biológicas. En la presente Tesis Doctoral se han evaluado los efectos de hidroxiapatita nanocristalina (nano-HA) e hidroxiapatita nanocristalina sustituida con silicio (nano-SiHA) sobre células implicadas en la inmunidad innata y adquirida, dada la importancia de la respuesta inflamatoria en el proceso de regeneración ósea tras la implantación de cualquier biomaterial.

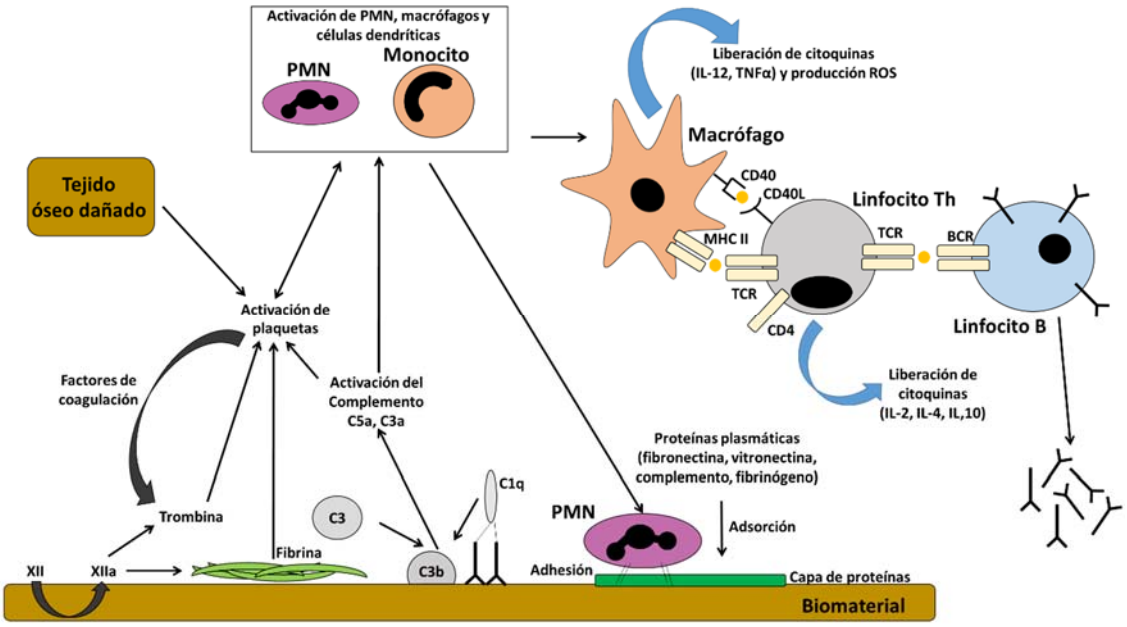

Figura 27. Proceso inflamatorio y principales células de la inmunidad innata y adquirida . Esquema procedente de [*Franz S et al. 2011, Biomaterials*].

En los primeros momentos tras la implantación de un biomaterial en un tejido, proteínas de los fluídos fisiológicos y de la sangre se adsorben a la superficie de los mismos y activan la cascada de coagulación, el sistema del complemento, las plaquetas y las células implicadas en la respuesta inmune. La unión de proteínas séricas y el efecto de los biomateriales en el sistema inmune son aspectos esenciales para la evaluación de su biocompatibilidad, determinando su aceptación o rechazo (**Figura 27**). Por esta razón, en el presente estudio se evaluó la adsorción de albúmina de suero bovino (BSA) sobre nano-HA y nano-SiHA pulverizadas, así como el efecto de la interacción de estas cerámicas con macrófagos (principales componentes de la respuesta inmune innata) y linfocitos T (células específicas de la respuesta inmune adaptativa).

Los resultados obtenidos se resumen a continuación y han dado lugar a la siguiente publicación:

- Matesanz MC, Feito MJ, Oñaderra M, Ramírez-Santillán C, daCasa C, Arcos D, Vallet-Regí M, Rojo JM, Portolés MT. Early *in vitro* response of macrophages and T lymphocytes to nanocrystalline hydroxyapaties. Journal of Colloid and Interface Science 416: 59–66, 2014.

Los perfiles de adsorción de BSA sobre nano-HA y nano-SiHA fueron similares, demostrando que la sustitución con silicio no modifica la interacción de proteínas con HA.

Dado que los macrófagos son células implicadas en la inmunidad innata y, por tanto, esenciales para el éxito de un implante, se evaluó el efecto de 1 mg/ml de nano-HA y nano-SiHA sobre macrófagos murinos RAW 264.7 y macrófagos primarios de peritoneo de ratón cultivados durante 3 días en presencia de estos materiales. Los parámetros de biocompatiblidad analizados fueron: morfología celular, proliferación, viabilidad, apoptosis, liberación de lactato deshidrogenasa (LDH) y contenido en especies reactivas de oxígeno (ROS) como indicador de estrés oxidativo. Los resultados mostraron un retraso en la proliferación de macrófagos primarios y células RAW 264.7 en contacto con ambos materiales aunque presentaron altos valores de viabilidad. Estas apatitas nanocristalinas no indujeron apoptosis, ni liberación de LDH al medio. Tampoco produjeron estrés oxidativo en estas células.

Puesto que los macrófagos son las principales células fagocíticas del sistema inmune, se analizó su capacidad fagocítica en presencia de nano-HA y nano-SiHA. Tanto RAW 264.7 como los macrófagos murinos conservaron dicha actividad pero se vio disminuida por la presencia de material, salvo en macrófagos murinos tratados con nano-HA. Es de destacar que la actividad fagocítica de las células primarias fue mucho más elevada que la de la línea celular RAW 264.7. Este hecho puede asociarse a la menor sensibilidad de los macrófagos murinos a nano-HA.

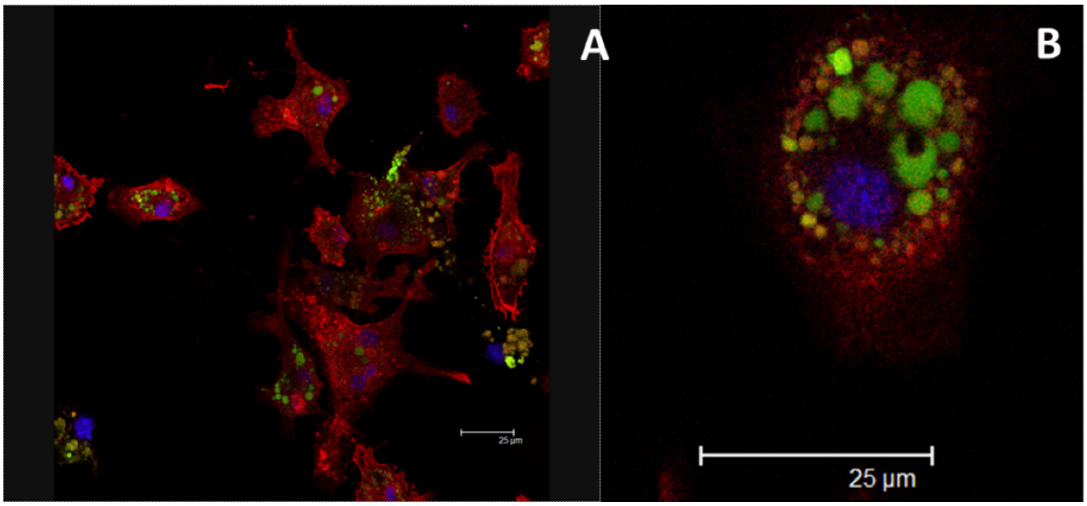

Figura 28. Evaluación morfológica de la fagocitosis de bolas de látex recubiertas de anti-IgG-FITC (verde) en macrófagos murinos primarios cultivados en presencia de nano-SiHA (A). Detalle de las partículas fagocitadas (B). Gráfica procedente de [Matesanz MC *et al. 2014, J. Colloid Interface Sci*].

Los cultivos de células primarias son un modelo experimental más parecido a la situación *in vivo*. La interleuquina 6 (IL-6) y el factor de necrosis tumoral α (TNFα) son las principales citoquinas proinflamatorias, por lo que juegan un papel esencial en el proceso de inflamación. Por estos motivos, se ha evaluado la liberación de ambas moléculas al medio extracelular en cultivos de macrófagos primarios de ratón en contacto con nano-HA y nano-SiHA. Estos materiales generaron un incremento en la secreción de las citoquinas proinflamatorias IL-6 y TNF-α. Sin embargo, la liberación de IL-6 fue más pronunciada en contacto con nano-SiHA y los niveles de TNF-α fueron más altos en el caso de los cultivos con nano-HA.

Por otra parte, los linfocitos T están implicados en la inmunidad adquirida y juegan un papel importante en el proceso inflamatorio, regulando el comportamiento de macrófagos. Por esta razón, se evaluó el efecto de 1 mg/ml de nano-HA y nano-SiHA sobre la proliferación, viabilidad y ciclo celular de linfocitos "syngeneic-reactive D10" (SR.D10) como modelo experimental, ya que estas células son linfocitos murinos derivados de células Th2 $CD4^+$ [*Ojeda G et al. 1995, Cell Immunol*]. Los resultados obtenidos no mostraron alteraciones de la proliferación y viabilidad celular de linfocitos SR.D10 en contacto con estos materiales. Sin embargo, se observó un incremento de la fase de apoptosis acompañado de un descenso de la fase de síntesis y mitosis.

Todos estos resultados evidencian la respuesta temprana de células inmunes a estos materiales y sugieren que tras la implantación *in vivo* de los mismos podría inducirse la activación del sistema inmune innato.

Journal of Colloid and Interface Science 416 (2014) 59–66

Contents lists available at ScienceDirect

Journal of Colloid and Interface Science

www.elsevier.com/locate/jcis

Early *in vitro* response of macrophages and T lymphocytes to nanocrystalline hydroxyapatites

María Concepción Matesanz [a], María José Feito [a], Mercedes Oñaderra [a], Cecilia Ramírez-Santillán [a], Carmen da Casa [a], Daniel Arcos [b,c], María Vallet-Regí [b,c], José María Rojo [d], María Teresa Portolés [a,*]

[a] Department of Biochemistry and Molecular Biology I, Faculty of Chemistry, Universidad Complutense, 28040 Madrid, Spain
[b] Department of Inorganic and Bioinorganic Chemistry, Faculty of Pharmacy, UCM, Instituto de Investigación Sanitaria Hospital 12 de Octubre i+12, 28040 Madrid, Spain
[c] Networking Research Center on Bioengineering, Biomaterials and Nanomedicine, CIBER-BBN, Spain
[d] Department of Cellular and Molecular Medicine, Centro de Investigaciones Biológicas, CSIC, 28040 Madrid, Spain

ARTICLE INFO

Article history:
Received 10 September 2013
Accepted 24 October 2013
Available online 9 November 2013

Keywords:
Biocompatibility
Cytokine
Hydroxyapatite
Lymphocyte
Macrophage

ABSTRACT

Hypothesis: Synthetic hydroxyapatite (HA) and Si substituted hydroxyapatite (SiHA) are calcium phosphate ceramics currently used in the field of dentistry and orthopaedic surgery. The preparation of both biomaterials as polycrystalline solid pieces or grains formed by nanocrystallites has awakened a great interest to enhance the bioactive behavior due to the microstructural defects and the higher surface area. The study of the macrophage and lymphocyte behavior in contact with nanocrystalline HA and SiHA will allow to elucidate the immune response which conditions the success or rejection of these biomaterials.
Experiments: HA and SiHA granules (with sizes of tens of microns) have been prepared by controlled aqueous precipitation avoiding subsequent high temperature sintering. HA and SiHA granules were constituted by crystallites smaller than 50 nm. The effects of both nanocrystalline materials on immune system have been evaluated with macrophages (main components of innate immune system) and T lymphocytes (specific cells of adaptive response) after short-term culture as *in vitro* models of the early immune response.
Findings: Significant decreases of macrophage proliferation and phagocytic activity, increased production of inflammatory cytokines (IL-6, TNF-α) and T lymphocyte apoptosis, were induced by these nanocrystalline ceramics suggesting that, after *in vivo* implantation, they induce significant effects on immune responses, including an early activation of the innate immune system.

1. Introduction

Immediately after biomaterial-tissue contact, blood and interstitial fluid proteins adsorb to the biomaterial surface and activate the coagulation cascade, complement system, platelets and immune cells [1,2]. Thus, the evaluation of serum proteins adsorption and the biomaterial effects on immune system are essential aspects of biocompatibility assessment [3,4]. The immune response comprises both innate and adaptive defence mechanisms which co-ordinately activate different cell populations. Neutrophils, monocytes and macrophages are critical cellular components of the innate immune response, carrying out phagocytosis and producing reactive oxygen species, antimicrobial peptides, and inflammatory mediators [5]. The adaptive response is mediated by antigen-specific lymphocytes (T and B cells) and by their products, which include inflammatory cytokines and antibodies. Although the interaction of immune cells with biomaterials has been considered negative for a long time, specific cell responses may be beneficial for biomaterial integration and improve implant performance [6]. Recent studies demonstrate the potential of biomaterials to modulate immune cell function suggesting the possibility of designing biomaterials capable of eliciting appropriate immune responses at implantation sites [7].

Because of its similarity to the mineral component of bone, synthetic hydroxyapatite (HA) is a calcium phosphate ceramic widely used in the field of dentistry and orthopaedic surgery with different purposes. Its main applications are grafting for small bone defects, coatings of metallic prostheses and periodontal implants, and as scaffolds for bone tissue engineering [8]. Silicon substituted hydroxyapatites (SiHAs) have attracted the attention of many researchers [9–13] and have recently been incorporated to the biomaterials market as Actifuse ABX™ (Apatech Ltd., UK) for

* Corresponding author. Address: Departamento de Bioquímica y Biología Molecular I, Facultad de Ciencias Químicas, Universidad Complutense, 28040 Madrid, Spain. Fax: +34 1 394 41 59.
E-mail addresses: conchitamatesanz@hotmail.com (M.C. Matesanz), mjfeito@pdi.ucm.es (M.J. Feito), monaderr@bio.ucm.es (M. Oñaderra), cecilia27884@hotmail.com (C. Ramírez-Santillán), cdacasa_19991@hotmail.com (C. da Casa), arcosd@farm.ucm.es (D. Arcos), vallet@farm.ucm.es (M. Vallet-Regí), jmrojo@cib.csic.es (J.M. Rojo), portoles@quim.ucm.es (M.T. Portolés).

0021-9797/$ - see front matter © 2013 Elsevier Inc. All rights reserved.
http://dx.doi.org/10.1016/j.jcis.2013.10.045

spinal, orthopedic, periodontal, oral and craniomaxillofacial applications. SiHAs are intended to improve the bone formation compared to non-substituted HA, in terms of better bioactivity, higher osteoclastic resorption activity, enhanced bone in growth, and bone implant coverage. This performance improvement could be due to the higher solubility at the grain boundary [9,10] and the osteogenic action of silicon in the early stages of bone formation [14]. SiHA approved for clinical use and most of HA based implants, undergo a sintering process at high temperatures to increase the density and improve the mechanical properties. This thermal treatment yields polycrystalline pieces or granulates constituted by large SiHA crystals, having dimensions of several micrometers depending on the crystal direction considered. Moreover, the crystalline growth comprises a reduction of porosity and surface area. In the last years, the possibility of enhancing the bioceramics bioreactivity through their preparation with low temperature methods has been suggested [15]. Avoiding the high temperature sintering process (commonly about 1200 °C), nanocrystalline pieces and grains can be prepared. The associated higher surface area and smaller crystal size could provide very interesting bioresponses, especially in SiHA as the osteogenic effect of silicon is mainly explained by its location at the crystals boundaries [9,10].

As essential processes after biomaterial-tissue contact, the albumin adsorption to both nanocrystalline HA and SiHA as well as the effects of these materials on different immune cells have been evaluated in the present study. With this objective, murine macrophages (main components of innate immune system) and T lymphocytes (specific cells involved in adaptive response) have been cultured for three days in direct contact with these nanocrystalline hydroxyapatites, as an *in vitro* model of the early immune response to both materials. Different cell parameters as morphology, proliferation, phagocytic activity, viability, lactate dehydrogenase release (LDH), apoptosis, intracellular reactive oxygen species (ROS), cell cycle phases, and cytokine (IL-6 and TNF-α) production were determined as markers of biocompatibility and specific response of both cell types.

2. Materials and methods

2.1. Nanocrystalline hydroxyapatite and silicon substituted hydroxyapatite synthesis

Samples of pure and silicon substituted HA were prepared by aqueous precipitation reaction of $Ca(NO_3)_2{\cdot}4H_2O$, $(NH_4)_2HPO_4$ and $Si(CH_3CH_2O)_4$ solutions. The amounts of reactants were calculated on the assumption that silicon would be substituted by phosphorus. Two different compositions have been prepared with nominal formula $Ca_{10}(PO_4)_{6-x}(SiO_4)_x(OH)_{2-x}$, with $x = 0$ and 0.25 for nano-HA and nano-SiHA samples, respectively. 1 M $Ca(NO_3)_2{\cdot}4H_2O$ solution was added to $(NH_4)_2HPO_4$ and TEOS solutions of stoichiometric concentration to obtain the compositions described above. The mixture was stirred for 12 h at 80 °C. During the reaction the pH was continuously adjusted to 9.5 to ensure constant conditions during the synthesis. The samples were treated at 700 °C under air atmosphere to remove the nitrates without introducing important changes in the crystallite size respect to the as precipitated powder. The HA and Si-HA grains thus obtained have a diameter ranging in size between 10 and 100 μm, as determined by means of a Sedigraph 5100 equipment (data not shown).

2.2. Chemical, structural and microstructural studies of nano-HA and nano-SiHA

Elemental chemical analysis was carried out by fluorescence X-ray spectrometry for P, Si and Ca. XRD patterns were collected with a Philips PW 1730 X-ray diffractometer using Cu Kα radiation with a step size of 0.02 $2\theta^\circ$ and 8 s of counting time. In order to determine the crystalline and microstructural characteristic of both samples, Rietveld refinements were carried out over the XRD patterns collected. The refinements were performed using the atomic position set and the space group of the HA structure $P6_3/m$, no 176 [16] by means of computer program FullProf 2000.

2.3. Adsorption of bovine serum albumin (BSA)

Adsorption experiments were carried out with 10 mg of either nano-HA or nano-SiHA granulates incubated with different concentrations of BSA (Sigma) in PBS and moderately shaken for 5 h at 37 °C. Incubation of 24 h showed no significant difference in the amount of protein adsorbed. Controls with the same BSA concentration but without material were carried out. After incubation time, the supernatant obtained was analyzed by UV–Vis spectroscopy and the adsorbed protein amount was calculated as the difference in protein concentration before and after BSA adsorption, using a value of 0.667 as coefficient E (0.1%, 279 nm, 1 cm).

2.4. Isolation and culture of murine peritoneal macrophages

Normal macrophages were obtained from the peritoneum of untreated mice as described elsewhere [17]. Briefly, BALB/c mice were killed, and the skin was removed from the abdominal area. Mice were then injected intraperitoneally with 4–5 ml of phosphate buffered saline (PBS) using an 18 gauge needle. Without extracting the needle, the abdomen was gently massaged and then as much fluid from the peritoneum as possible was slowly withdrawn with the syringe. The peritoneal cells were washed in PBS before use. All procedures were approved by Institutional Animal Care and Use Committees.

2.5. Cell culture

RAW-264.7 cells or mouse peritoneal macrophages at a density of 10^5 cells/ml were seeded in 6 well culture plates in 2 ml of Dulbecco's Modified Eagle Medium (DMEM) supplemented with 10% heat-inactivated fetal bovine serum (FBS) and 1 mM L-glutamine. SR.D10 cells [18] derived from the murine $CD4^+$ Th2 cell line D10.G4.1 [19] were cultured in suspension in Click's medium supplemented with 10% FBS containing 5 U/ml mrIL-2, 10 U/ml mrIL-4, and 25 pg/ml mrIL-1 (IL medium) as previously described [18,19]. After 3 days culture in the presence or the absence of 1 mg/ml of either nano-HA or nano-SiHA, cells were collected in order to determine the number of cells. The attached RAW-264.7 cells were washed with PBS and harvested using cell scrapers. Murine peritoneal macrophages were washed with PBS and detached with PBS/1 mM EDTA at 4 °C. After these procedures, 10 μl of the suspensions of these cell types and 10 μl of SR.D10 lymphocytes were counted with a Neubauer hemocytometer in the presence of 0.2% Trypan Blue, which stains the dead cells, for the analysis of cell proliferation. Then, cell suspensions were centrifuged at 310g for 10 min and resuspended in fresh medium for the analysis of different parameters by Flow Cytometry as described below (Section 2.8).

2.6. Morphological studies by confocal microscopy

After fixation with 3.7% paraformaldehyde in PBS, samples were permeabilized with 0.1% Triton X-100, preincubated with PBS containing 1% BSA and incubated with rhodamine phalloidin to stain F-actin filaments. After cell nuclei staining with 3 μM DAPI, cells were examined by a LEICA SP2 Confocal Laser Scanning Microscope. The fluorescence of rhodamine was excited at 540 nm and

measured at 565 nm. DAPI fluorescence was excited at 405 nm and measured at 420–480 nm. To observe the phagocytosis of Latex Beads-Rabbit IgG-FITC by macrophages, cells were incubated as described below (Section 2.8.3), fixed with paraformaldehyde and the FITC fluorescence was detected with filters for excitation and emission at 485 and 535 nm, respectively.

2.7. Lactate dehydrogenase (LDH) measurement

LDH was measured in the culture medium by an enzymatic method at 340 nm (Bio-Analítica) using a Beckman DU 640 UV–Visible spectrophotometer.

2.8. Flow cytometry studies

After cell detachment (Section 2.5) and incubation with the different probes (as it is described below) the conditions for the data acquisition and analysis were established using negative and positive controls with the CellQuest Program of Becton Dickinson and these conditions were maintained during all the experiments. Each experiment was carried out three times and single representative experiments are displayed. For statistical significance, at least 10,000 cells were analyzed in each sample and the mean of the fluorescence emitted by these single cells was used.

2.8.1. Apoptosis detection

Cell suspensions were incubated with 5 μg/ml Hoechst 33258 for 30 min in darkness. Hoechst fluorescence was excited at 350 nm and measured at 450 nm in a LSR Becton Dickinson Flow Cytometer. The percentage of cells in each cycle phase was calculated with the CellQuest Program of Becton Dickinson and the $SubG_1$ fraction was used as indicative of apoptosis.

2.8.2. Intracellular reactive oxygen species (ROS) content and cell viability

Cells were incubated for 30 min with 100 μM DCFH/DA. DCF fluorescence was excited by a 15 mW laser tuning to 488 nm and was measured with a 530/30 band pass filter in a FACScalibur Becton Dickinson Flow Cytometer. Cell viability was determined by propidium iodide (PI, 0.005%) exclusion test to stain the DNA of dead cells.

2.8.3. Phagocytosis assays

The phagocytosis of Latex Beads-Rabbit IgG-FITC by macrophages was evaluated by the Phagocytosis Assay Kit (IgG FITC) of Cayman Chemical Company. Cells were incubated overnight with 1 μg/ml LPS (*E. coli* 055:B5) and Latex Beads-Rabbit IgG-FITC after treatment with the materials. FITC fluorescence was excited by a 15 mW laser tuning to 488 nm and measured with a 530/30 band pass filter in a FACScalibur Becton Dickinson Flow Cytometer.

2.9. Inflammatory cytokine detection

The amounts of TNF-α, and IL-6 in the culture medium were quantified by ELISA (Gen-Probe, Diaclone), carried out according to the manufacturer's instructions.

2.10. Measurement of Ca^{2+} levels in the culture medium

To know the effect of hydroxyapatite (HA) and silicon-doped hydroxyapatite (SiHA) on Ca^{2+} levels in the culture medium, Ca^{2+} was analyzed with an ILyte Electrolyte Analyzer.

2.11. Statistics

Data are expressed as means ± standard deviations of one representative experiment out of three experiments carried out in triplicate. Statistical analysis was performed using the Statistical Package for the Social Sciences (SPSS) version 19 software. Statistical comparisons were made by analysis of variance (ANOVA). Scheffé test was used for *post hoc* evaluations of differences among groups. $P < 0.05$ was considered as statistically significant.

3. Results and discussion

3.1. Chemical, structural and microstructural properties of nano-HA and nano-SiHA

The Ca, P and Si contents of the HA and SiHA granules, determined by elemental chemical analysis (Table 1), show that the experimental cationic composition is very similar to the theoretical one, indicating that the synthesis method applied allows the incorporation of the silicon into the precipitated powder of nano-SiHA. XRD patterns were collected for nano-HA and nano-SiHA samples, exhibiting almost identical profiles which are presented in Fig. 1. All the diffraction maxima correspond to the reflections of an apatite phase. Table 2 shows the lattice parameters and the sizes of the crystallites calculated using the apparent sizes along the different directions, obtained from the microstructural parameters calculated from the Rietveld refinements. Table 2 shows the data along [100] and [001] directions as well as the mean crystallite size. The crystallite sizes indicate an anisotropic growth along the *c* axis, [001] direction, resulting in crystallites with needle-like shapes similar to those found in the mineral component of bone [20]. Nano-HA crystallites are 48.2 nm and 27.6 nm in size for the longest and shortest dimensions, respectively. Besides, nano-SiHA crystallites are 32.9 nm and 19.1 nm for the same dimensions, thus indicating that the silicon incorporation seems to play a role on the crystalline growth decreasing the crystal size. Independently of the dimension considered, the crystallites of both samples are smaller than 50 nm, confirming that the grains of nano-HA and nano-SiHA are polycrystalline particles formed by numerous nanocrystallites.

3.2. Adsorption of bovine serum albumin (BSA) to nano-HA and nano-SiHA

Blood proteins are important factors in determining the *in vivo* acceptance of biomaterials [1]. The protein adsorption depends on the physico-chemical properties of the material [21] and is a key point in the initial cellular response to a biomaterial after implantation, affecting the cellular adhesion, differentiation and extracellular matrix production [1]. Since albumin is the most abundant serum protein, a comparative evaluation of the adsorption of different BSA concentrations on nano-HA and nano-SiHA surface was carried out. Both nanocrystalline hydroxyapatites showed similar BSA adsorption profiles (Fig. 2), thus indicating that the incorporation of the silicon does not change the binding affinity and the maximum amount of protein adsorbed.

Table 1
Experimental Ca, P and Si content (% in weight) obtained by X-ray fluorescence spectroscopy. Theoretical values are indicated below in brackets.

Sample	Ca	P	Si
Nano-HA	39.5 (39.9)	17.8 (18.5)	0.0 (0.0)
Nano-SiHA	39.2 (40.1)	17.2 (17.8)	0.6 (0.7)

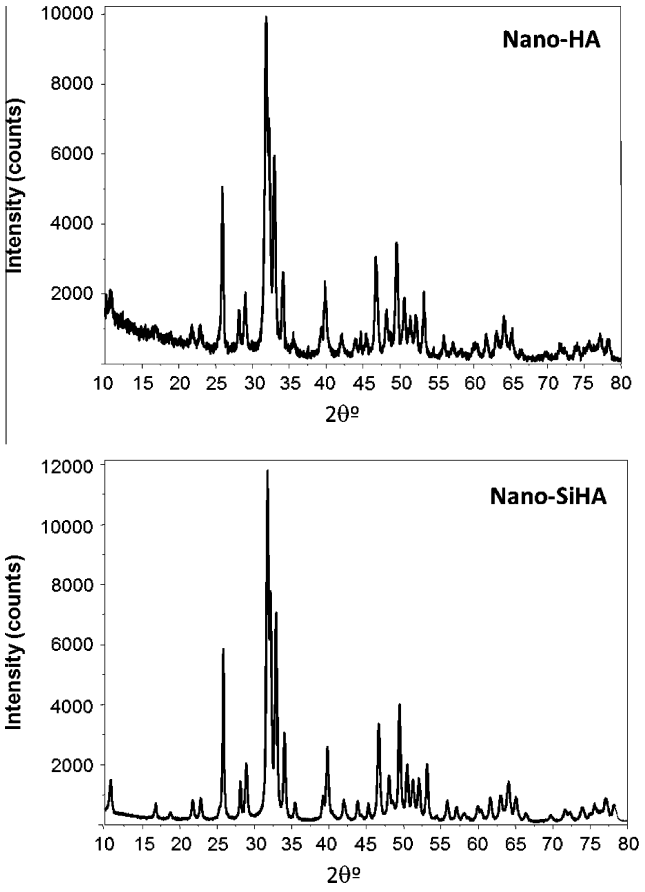

Fig. 1. Experimental (circles) and calculated (solid line) powder X-ray diffraction pattern for (up) nano-HA and (down) nano-SiHA.

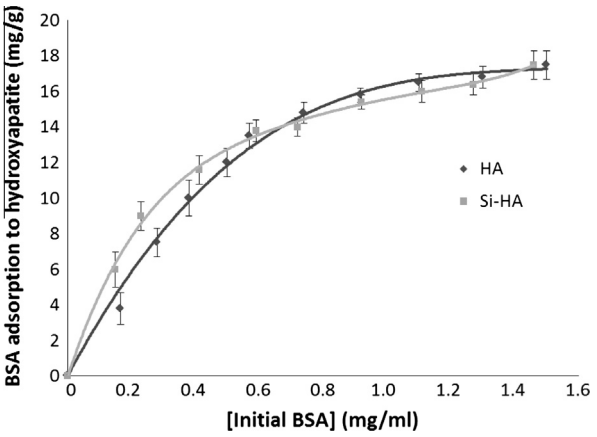

Fig. 2. BSA adsorption profiles on nano-HA and nano-SiHA after 5 h treatment.

3.3. In vitro effects of nano-HA and nano-SiHA on immune cells

To know the nano-HA and nano-SiHA effects on immune system, macrophages and T lymphocytes were used as *in vitro* models of innate and adaptive immune response, respectively.

3.3.1. Macrophage response to nano-HA and nano-SiHA

The macrophage capability of playing both positive and negative roles in disease processes and tissue remodelling after injury, has been recently related to the diverse and context dependent macrophage phenotypes [6]. Thus, macrophages can be classified in two types: proinflammatory and microbicidal ones (M1) and immunomodulatory and reparative ones (M2) [22]. The host response to biomaterials depends on the balance between the M1 and M2 phenotypes, with participation of diverse specific cytokines. RAW-264.7 is a mouse macrophage cell line retaining many of the characteristics of macrophages *in vivo* [23]. Fig. 3 shows the results concerning proliferation and phagocytic activity of murine RAW-264.7 macrophages after 3 days of treatment with either nano-HA or nano-SiHA (1 mg/ml). RAW-264.7 growth was significantly delayed by both hydroxyapatites in comparison with cells cultured in the absence of material (Fig. 3A, $p < 0.005$). Both materials also produced a significant decrease in phagocytic activity of RAW-264.7 cells ($p < 0.005$), although these cells continued phagocyting when in contact with either nano-HA or nano-SiHA (Fig. 3B). No significant alterations in cell viability and $SubG_1$ fraction reveal that neither nano-HA nor nano-SiHA induced apoptosis of RAW-264.7 cells (Table 3). No significant changes of reactive oxygen species, widely used as macrophage signaling mediators [24], were observed after treatment with these materials, thus indicating the absence of oxidative stress in RAW-264.7 macrophages (Table 3). The integrity of plasma membrane was demonstrated because no significant increase of LDH levels in the culture medium was detected (Table 3). No morphological alterations induced by these nanocrystalline hydroxyapatites on these cells were observed (Fig. 4). Studies with other cell types showed that silicon-doped hydroxyapatite has biocompatibility and mechanical properties comparable to HA but improved bioactivity which enhances bone tissue growth rate [11,25–27]. Previous experiments carried out with human Saos-2 osteoblasts cultured for 4 days in the presence of 1 mg/ml of either nano-HA or nano-SiHA demonstrated that this cell type proliferated in contact with both materials, but the cell number was significantly lower than in controls. However, the number of Saos-2 cells in contact with nano-SiHA was significantly higher than with nano-HA, indicating that these cells grow better in the presence of nano-SiHA. This result was also observed by Scanning Electron Microscopy (SEM) when Saos-2 osteoblasts were cultured for 4 days on surface of both nano-HA and nano-SiHA disks. SEM images demonstrated that Saos-2 cells adhere to the nano-SiHA disks, proliferate and colonize their surface better than on HA disks. Although low levels of apoptosis were obtained in human Saos-2 osteoblasts after contact with these materials, this cell type showed a slight increase of cell apoptosis in the presence of nano-HA (2.1%) in comparison to nano-SiHA (0.4%) and control cells (0.3%). Intracellular ROS content did not show alteration in the presence of these materials, thus indicating no oxidative stress [11].

Table 2
Lattice parameters and crystallite sizes obtained from Rietveld refinements.

Sample	Lattice parameters (Å)	Crystallite size along [100] (nm)	Crystallite size along [001] (nm)	Mean crystallite size[a] (nm)
Nano-HA	a = 9.4209 (1) c = 6.8841 (1)	27.6	48.2	30 (8)
Nano-SiHA	a = 9.4236 (1) c = 6.8875 (1)	19.1	32.9	22 (6)

[a] The values in brackets for mean crystallite size do not make reference to the measurement errors, but are an estimation of the crystal size anisotropy.

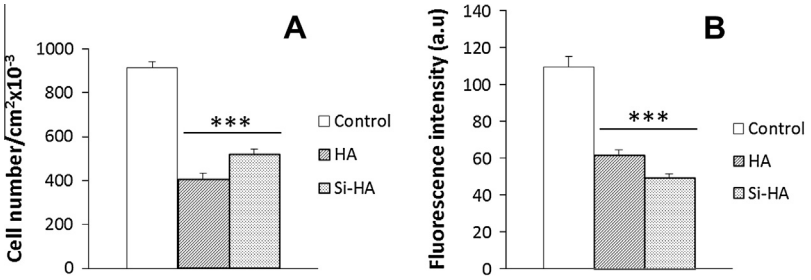

Fig. 3. Effects of nano-HA and nano-SiHA on proliferation (A) and phagocytosis (B) of murine RAW-264.7 macrophages after 3 days treatment. $^{***}p < 0.005$.

Table 3
Effects of nano-HA and nano-SiHA on cell viability, apoptosis, ROS production and LDH release into the culture medium of murine RAW-264.7 macrophages after 3 days treatment.

	Control	Nano-HA	Nano-SiHA
Viability (%)	83.3 ± 1.8	77.1 ± 3.1	84.3 ± 0.1
Apoptosis (%)	2.6 ± 0.3	1.4 ± 0.1	1.9 ± 1.3
ROS (a.u.)	403.1 ± 104.0	310.8 ± 75.6	308.9 ± 105.5
LDH (U/L)	16.1 ± 2.9	25.8 ± 11.8	22.2 ± 8.2

To evaluate the effects of these nanocrystalline hydroxyapatites on a cellular model more similar to the *in vivo* situation, fresh murine macrophages were obtained from the peritoneum of untreated mice and were cultured for 3 days in the presence of either nano-HA or nano-SiHA (1 mg/ml) to measure cell proliferation, phagocytic activity and release of inflammatory cytokines (IL-6, TNF-α). Fig. 5A shows a significant proliferation decrease of fresh murine macrophages induced by both hydroxyapatites ($p < 0.005$). Nano-SiHA material also produce a significant decrease in phagocytosis of these cells ($p < 0.005$) whose activity is not affected by nano-HA (Fig. 5B). In spite of this decrease induced by SiHA, fresh macrophages continue phagocyting when they are in contact with this material (Fig. 6A and B). The different effect of nano-HA on RAW and fresh macrophages can be due to the higher values of phagocytosis obtained with fresh macrophages which always showed higher fluorescence values (Fig. 5B) than RAW macrophages (Fig. 3B). This fact can be associated with a lower sensitivity to nano-HA of fresh macrophages although the phagocytic activity of these cells was affected by nano-SiHA.

Since the hydroxyapatite bioactivity could produce the sequestration of calcium in the extracellular medium, and taking into account that the Ca^{2+} ion plays a crucial role in cell processes [28], Ca^{2+} levels were measured in the culture medium. Fig. 7 shows a significant Ca^{2+} decrease in the culture medium produced by both nano-HA and nano-SiHA, more pronounced with nano-SiHA, in agreement with the higher bioactivity of this material [27]. The observed sequestration of extracellular calcium can be partially responsible of the lower proliferation produced by nano-HA and nano-SiHA, as it has been described in other cell types [29]. Concerning the possible effect of extracellular calcium depletion on phagocytosis, some studies have shown that macrophages can still phagocyte in the absence of calcium through Fc receptor mediated pathways [30]. On the other hand, the changes

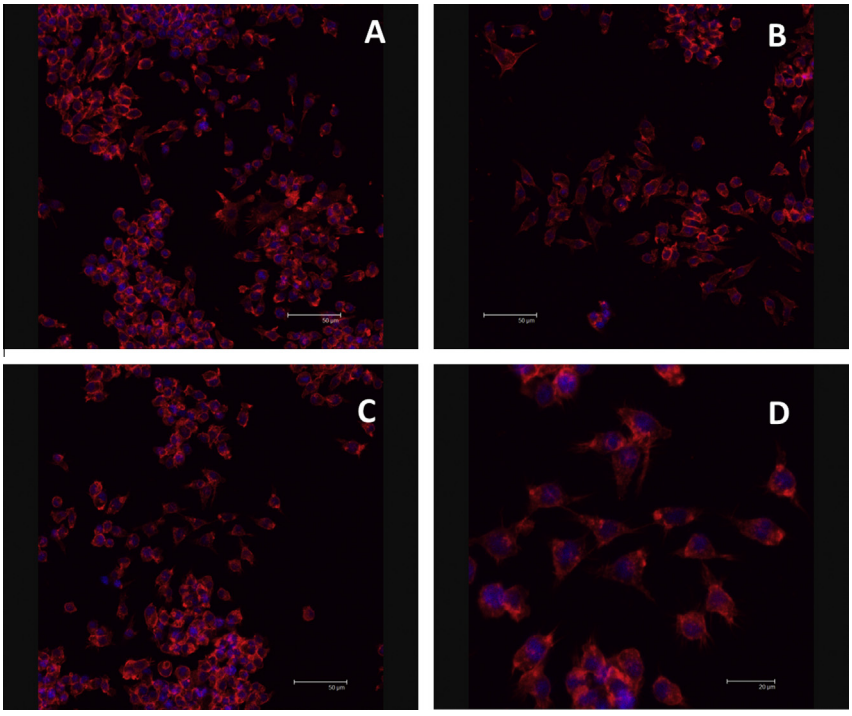

Fig. 4. Morphology evaluation by confocal microscopy of murine RAW-264.7 macrophages after 3 days treatment with nano-HA (B) and nano-SiHA (C). Controls without material are also included (A). Detail of RAW-264.7 cells in the presence of nano-SiHA (D).

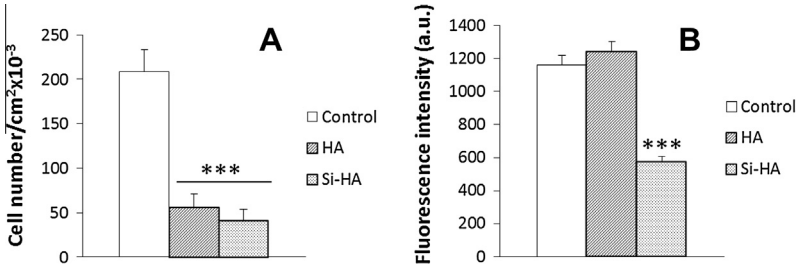

Fig. 5. Effects of nano-HA and nano-SiHA on proliferation (A) and phagocytosis (B) of murine fresh macrophages after 3 days treatment. $^{***}p < 0.005$.

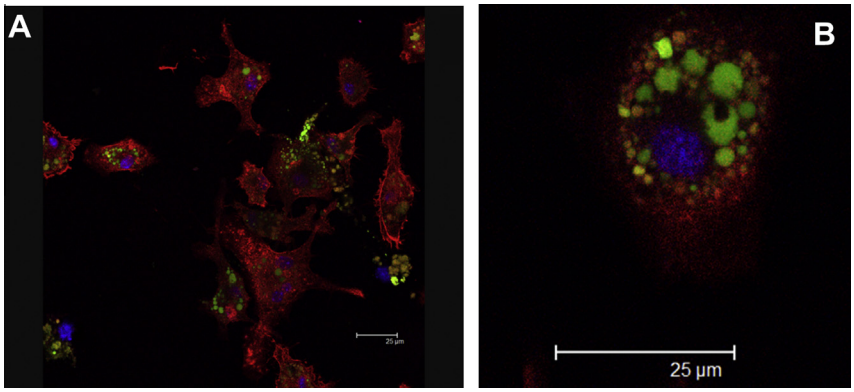

Fig. 6. Morphology evaluation by confocal microscopy of phagocytosis of rabbit IgG-FITC-coated latex beads (in green) by murine fresh macrophages after 3 days treatment with nano-SiHA. (A) Panoramic image. (B) Detail of the macrophage phagocyting activity. (For interpretation of the references to colour in this figure legend, the reader is referred to the web version of this article.)

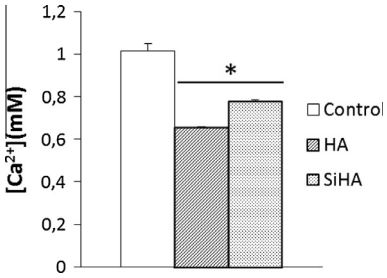

Fig. 7. Effects of nano-HA and nano-SiHA on Ca^{2+} levels in the culture medium after 3 days treatment. $^{*}p < 0.05$.

due to depletion of extracellular calcium could be decreased *in vivo* by the dynamic flow conditions of the body fluids [31].

It is well known that interleukin 6 (IL-6) and tumor necrosis factor alpha (TNF-α) are major inflammatory cytokines and play a crucial role in infection, inflammation and stress responses. For this reason, the release of IL-6 and TNF-α by fresh mouse macrophages was measured after 3 days of treatment with these materials. Fig. 8A shows significant increases of IL-6 induced by nano-HA ($p < 0.05$) and nano-SiHA ($p < 0.005$). Both materials also triggered a significant TNF-α increase (Fig. 8B), which was more pronounced with nano-HA ($p < 0.005$) than with nano-SiHA ($p < 0.05$). These results evidence the early *in vitro* response of macrophages to both nanocrystalline hydroxyapatites, suggesting that, after *in vivo* implantation, these biomaterials might induce activation of the innate immune system and production of pro-inflammatory cytokines. Although further studies are needed to elucidate the long-term response of macrophages to these materials, an *in vivo* study evidenced the moderate IL-6 and IL-8 expression in bone cells and rich IL10-containing cells distribution after 8 months of hydroxyapatite implantation [32]. This fact reveals the switch of pro-inflammatory macrophage phenotype (M1) to reparative phenotype (M2) expressing high levels of IL-10 [6] and indicates the resolution of inflammatory phase at longer times.

3.3.2. Lymphocyte response to nano-HA and nano-SiHA

T lymphocytes also play an important regulatory role in the resolution of the inflammatory process through local secretion of cytokines and chemokines, many of which are known to affect macrophage polarization [6]. In order to know the nano-HA and nano-SiHA effects on T lymphocytes as specific cells involved in adaptive immune response, SR.D10 cells were cultured in the presence of these materials (1 mg/ml). SR.D10 [18] is a clone obtained from the murine $CD4^+$ Th2 cell line D10.G4.1 [19] specific for Conalbumin fragment 134–146, bound to $I\text{-}A^k$ class II major histocompatibility complex molecules. SR.D10 cells provide a convenient system to test *in vitro* lymphocyte activation which has been largely used as a model of T cell proliferation and signalling [33,34]. These T cells have been previously used for biocompatibility testing of different bioceramics [4]. Although non-significant differences were observed on proliferation and viability of SR.D10 lymphocytes after 3 days treatment (Fig. 9A and B), a significant increase of Sub G_1 fraction, indicative of cell apoptosis, is produced by both hydroxyapatites. This effect is accompanied by significant decreases of both S and G2M fractions (Fig. 10).

Programmed cell death (apoptosis) is a key mechanism for regulating lymphocyte number. In T lymphocytes, two major mechanisms have been described involving: (a) the activation of T cell through Fas, which leads to the caspase-8 and caspase-3 induction, and (b) the loss of mitochondrial integrity controlled by members of the BcL-2 family proteins [35]. Other molecules that regulate this death process include the leukocyte common antigen CD45, which has been shown to be essential for normal signaling through the T cell receptor (TCR) and for modulating signaling through

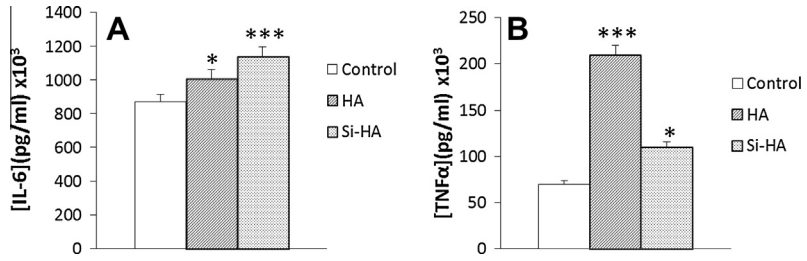

Fig. 8. Effects of nano-HA and nano-SiHA on IL-6 (A) and TNF-α (B) release by murine fresh macrophages after 3 days treatment. $^{*}p < 0.05$, $^{***}p < 0.005$.

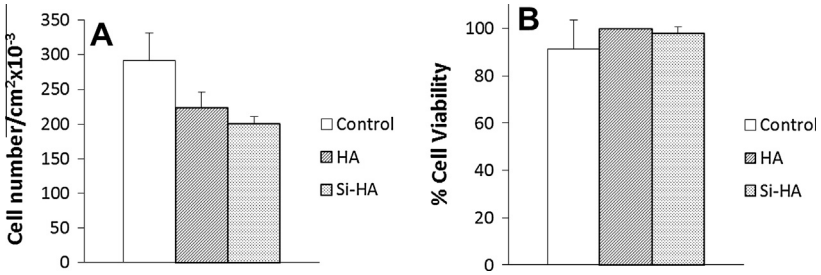

Fig. 9. Effects of nano-HA and nano-SiHA on proliferation (A) and viability (B) of SR.D10 lymphocytes after 3 days treatment.

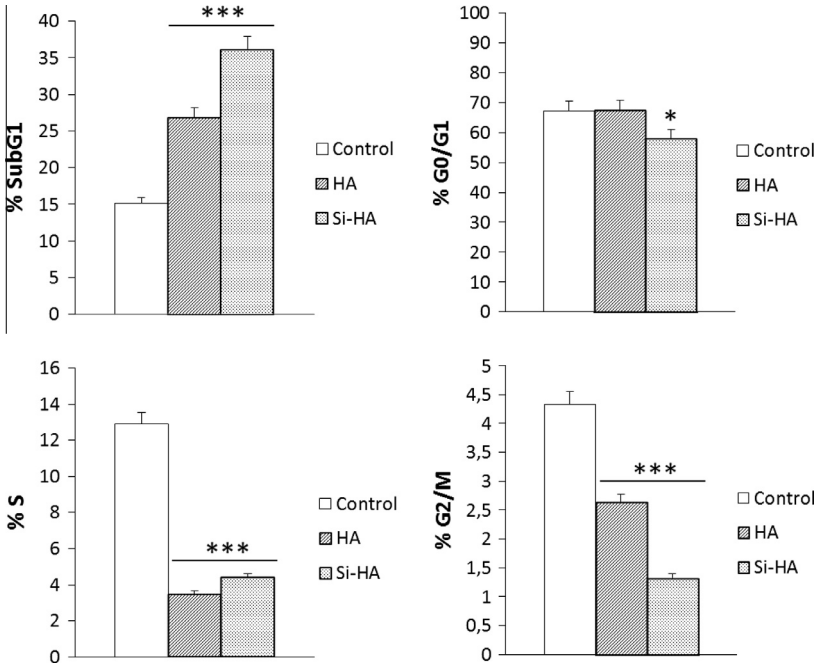

Fig. 10. Effects of nano-HA and nano-SiHA on cell cycle phases of SR.D10 lymphocytes after 3 days treatment. $^{*}p < 0.05$, $^{***}p < 0.005$.

cytokine receptors [50]. SR.D10 "syngeneic-reactive D10", is a variant of the murine $CD4^{+}$ T helper cell clone which is hyperreactive to TCR dependent and-independent stimuli. This hyperreactivity is related to the expression of several cell surface molecules involved in T cell activation as CD45 RB receptor, abundantly expressed in SR.D10 [18]. The high levels of T cell apoptosis observed in the present study could be explained by the abundant expression of this receptor that favors this death process through Fas and TCR-induced apoptosis [36]. The presence of either nano-HA or nano-SiHA produces a significant increase of SR.D10 apoptosis probably through these mechanisms.

All these studies and previous results obtained with many different biomaterials demonstrate different cellular responses which are dependent on each biomaterial and depending on each cell type [37–39].

4. Conclusions

The *in vitro* evaluation of the early immune response to nanocrystalline hydroxyapatites evidences significant decreases of macrophage proliferation and phagocytic activity. These biomaterials also induce the production of the pro-inflammatory cytokines IL-6 and TNF-α by murine fresh macrophages and trigger apoptosis mechanisms in SR.D10 T lymphocytes. The study of the early immune response is the first step to know whether a phenotypic

switch of pro-inflammatory (M1) to reparative macrophages (M2) occurs in the presence of these materials. The results obtained will be used in further studies to elucidate the long-term response of immune cells to these nanocrystalline hydroxyapatites which conditions the biomaterial success or rejection. The detection of specific macrophage markers and cytokines will allow a better understanding of the effects at longer times of these biomaterials on the equilibrium of these two distinct macrophage subsets which represents a key factor for establishing their applicability for bone Tissue Engineering.

Acknowledgments

This study was supported by research grants from Comunidad de Madrid through the project S2009/MAT-1472 and the Ministerio de Ciencia e Innovacion (MICINN) through the projects MAT2012-35556 and CSO2010-11384-E (Agening Network of Excellence). J.M. Rojo is supported by Grant PI10/00650 from "Plan Estatal I+D+i, ISCIII-Subdirección General de Evaluación y Fomento de la Investigación, Ministerio de Economía y Competitividad (MINECO), Spain. M.C. Matesanz is greatly indebted to MICINN for the predoctoral fellowship. The authors wish to thank also to Javier Linares for technical assistance and to the staff of the Cytometry and Fluorescence Microscopy Center of the Universidad Complutense de Madrid (Spain).

References

[1] C.J. Wilson, R.E. Clegg, D.I. Leavesley, M.J. Pearcy, Tiss. Eng. 11 (2005) 1–18.
[2] M.B. Gorbet, M.V. Sefton, Biomaterials 25 (2004) 5681–5703.
[3] M.J. Smith, K.L. White Jr., D.C. Smith, G.L. Bowlin, Biomaterials 30 (2009) 149–159.
[4] M. Alcaide, P. Portolés, A. López-Noriega, D. Arcos, M. Vallet-Regí, M.T. Portolés, Acta Biomater. 6 (2010) 892–899.
[5] R. Medzhitov, C.A. Janeway Jr., N. Engl. J. Med. 343 (2000) 338–344.
[6] B.N. Brown, B.D. Ratner, S.B. Goodman, S. Amar, S.F. Badylak, Biomaterials 33 (2012) 3792–3802.
[7] S. Franz, S. Rammelt, D. Scharnweber, J.C. Simon, Biomaterials 32 (2011) 6692–6709.
[8] S.V. Dorozhkin, Biomaterials 31 (2010) 1465–1485.
[9] M. Vallet-Regí, D. Arcos, J. Mater. Chem. 15 (2005) 1509–1516.
[10] A.E. Porter, N. Patel, J.N. Skepper, S.M. Best, W. Bonfield, Biomaterials 24 (2003) 4609–4620.
[11] M.C. Matesanz, M.J. Feito, C. Ramírez-Santillán, R.M. Lozano, S. Sánchez-Salcedo, D. Arcos, M. Vallet-Regí, M.T. Portolés, Macromol. Biosci. 12 (2012) 446–453.
[12] A. Balamurugan, A.H.S. Rebelo, A.F. Lemos, J.H.G. Rocha, J.M.G. Ventura, J.M.F. Ferreira, Dent. Mater. 24 (2008) 1374–1380.
[13] D. Arcos, J. Rodríguez-Carvajal, M. Vallet-Regí, Chem. Mater. 16 (2004) 2300–2308.
[14] E.M. Carlisle, Calcif. Tiss. Int. 33 (1981) 27–34.
[15] S.V. Dorozhkin, Materials 2 (2009) 1975–2045.
[16] M.I. Kay, R.A. Young, A.S. Posner, Nature 204 (1964) 1050–1052.
[17] B.B. Mishell, J.M. Shiigi, Preparation of Mouse Cell Suspensions, in: B.B. Mishell, J.M. Shiigi (Eds.), Selected Methods in Cellular Immunology, WH Freeman & Co., San Francisco, 1980, pp. 1–28.
[18] G. Ojeda, M. Ronda, S. Ballester, R. Díez-Orejas, M.J. Feito, L. García-Albert, J.M. Rojo, P. Portolés, Cell. Immunol. 164 (1995) 265–278.
[19] J. Kaye, S. Porcelli, J. Tite, B. Jones, C.A. Janeway Jr., J. Exp. Med. 158 (1983) 836–856.
[20] R.A. Robinson, J. Bone. Joint Surg. Am. 34 (1952) 389–476.
[21] A. Rosengren, E. Pavlovic, S. Oscarsson, A. Krajewski, A. Ravaglioli, A. Piancastelli, Biomaterials 23 (2002) 1237–1247.
[22] P.M. Kou, J.E. Babensee, J. Biomed. Mater. Res. A 96 (2011) 239–260.
[23] J. Scheel, S. Weimans, A. Thiemann, E. Heisler, M. Hermann, Toxicol. In Vitro 23 (2009) 531–538.
[24] M. Nagata, Curr. Drug Targets Inflamm. Aller. 4 (2005) 503–504.
[25] M. Vallet-Regí, E. Ruiz-Hernández, Adv. Mater. 23 (2011) 5177–5218.
[26] E.S. Thian, J. Huang, S.M. Best, Z.H. Barber, R.A. Brooks, N. Rushton, W. Bonfield, Biomaterials 27 (2006) 2692–2698.
[27] A.M. Pietak, J.W. Reid, M.J. Stott, M. Sayer, Biomaterials 28 (2007) 4023–4032.
[28] B. Zhivotovskya, S. Orreniusa, Cell. Calcium 50 (2011) 211–221.
[29] M.M. Dvorak, A. Siddiqua, D.T. Ward, D.H. Carter, S.L. Dallas, E.F. Nemeth, D. Riccardi, Proc. Natl. Acad. Sci. USA 101 (2004) 5140–5145.
[30] T.M. Jesse, J.A. Swanson, J. Leukoc. Biol. 72 (2002) 677–684.
[31] H.M. da Silva, M. Mateescu, C. Damia, E. Champion, G. Soares, K. Anselme, Colloids Surf. B: Biointerf. 80 (2010) 138–144.
[32] M. Pilmane, G. Salms, A. Skagers, Int. J. Oral Maxillofac. Surg. 40 (2001) 1211–1218.
[33] R. Díez-Orejas, S. Ballester, M.J. Feito, G. Ojeda, G. Criado, M. Ronda, P. Portolés, J.M. Rojo, EMBO J. 13 (1994) 90–99.
[34] J.M. Rojo, C.A. Janeway Jr., J. Immunol. 140 (1988) 1081–1088.
[35] Z. Liu, R. Dawes, S. Petrova, P.C.L. Beverley, E.Z. Tchilian, Int. Immunol. 18 (2005) 959–966.
[36] M. Ramaswamy, A.C. Cruz, S.Y. Cleland, M. Deng, S. Price, V.K. Rao, R.M. Siegel, Cell Death Differ. 18 (2011) 712–720.
[37] M.C. Serrano, R. Pagani, M. Vallet-Regí, J. Peña, A. Rámila, I. Izquierdo, M.T. Portolés, Biomaterials 25 (2004) 5603–5611.
[38] M. Alcaide, P. Portolés, A. López-Noriega, D. Arcos, M. Vallet-Regí, M.T. Portolés, Acta Biomater. 6 (2010) 892–899.
[39] M. Cicuéndez, M.T. Portolés, I. Izquierdo-Barba, M. Vallet-Regí, Chem. Mater. 24 (2012) 1100–1106.

El remodelado óseo, proceso esencial para el correcto funcionamiento del hueso, es dependiente de procesos de formación y resorción llevados a cabo por osteoblastos y osteoclastos respectivamente. Un incremento en la actividad resortiva de los osteoclastos puede dar lugar a patologías como la osteoporosis. Esta enfermedad implica la desmineralización y pérdida generalizada de la masa ósea, así como un deterioro de la microarquitectura del hueso produciendo una mayor susceptibilidad a fracturas óseas que disminuyen enormemente la calidad de vida. La alteración del proceso de remodelado óseo durante la osteoporosis no se conoce con detalle, por lo que son numerosos los estudios dirigidos a la búsqueda de un tratamiento efectivo. Una posibilidad es la implantación de biomateriales en hueso osteoporótico que sean capaces de detener el proceso y estimular la regeneración del tejido. Sin embargo, aún no existe ningún biomaterial aprobado en clínica para esta aplicación biomédica.

Los osteoclastos y los macrófagos proceden de células madre hematopoyéticas (HSCs) que dan lugar a células mononucleares circulantes denominadas unidades formadoras de colonias de granulocitos y macrófagos (CFU-GM) cuya proliferación es estimulada por el factor estimulador de colonias (M-CSF). Por otra parte, el ligando del receptor activador del factor nuclear κB (RANKL) es producido por osteoblastos para estimular la diferenciación de osteoclastos (**Figura 11**).

Por todo ello, en la presente Tesis Doctoral se ha puesto a punto la diferenciación de osteoclastos a partir de macrófagos murinos RAW 264.7 cultivados durante 21 días en contacto con M-CSF y RANKL sobre discos de nano-HA y nano-SiHA, analizando diversos parámetros de diferenciación y la actividad resortiva sobre dichos soportes.

Los resultados obtenidos se resumen a continuación y han dado lugar a la siguiente publicación:

- **Matesanz MC, Linares J, Lilue I, Sánchez-Salcedo S, Feito MJ, Arcos D, Vallet-Regí M, Portolés MT. Nanocrystalline silicon substituted hydroxyapatite effects on osteoclast differentiation and resorptive activity. Journal of Materials Chemistry B, 2:2910-2919, 2014.**

El estudio de diferentes parámetros de osteoclastogénesis mediante microscopía confocal como la existencia de múltiples núcleos, numerosos podosomas y formación del anillo de actina en la zona de sellado para el proceso de resorción, demuestró un retraso en la diferenciación osteoclástica sobre nano-SiHA respecto a nano-HA. Las células cultivadas sobre nano-HA contaban con 4-5 núcleos, un anillo de actina más marcado y unos podosomas más organizados que en las células cultivadas sobre discos de nano-SiHA (1-2 núcleos). Altos niveles de viabilidad y baja apoptosis fueron observados en contacto con ambos materiales.

La observación de las cavidades de resorción mediante SEM indicó una disminución de la actividad resortiva de las células cultivadas sobre nano-SiHA respecto a nano-HA, ya que en contacto con nano-HA, se obtuvieron huellas de mayor tamaño que las encontradas sobre discos de nano-SiHA, de morfología esférica (**Figura 29**).

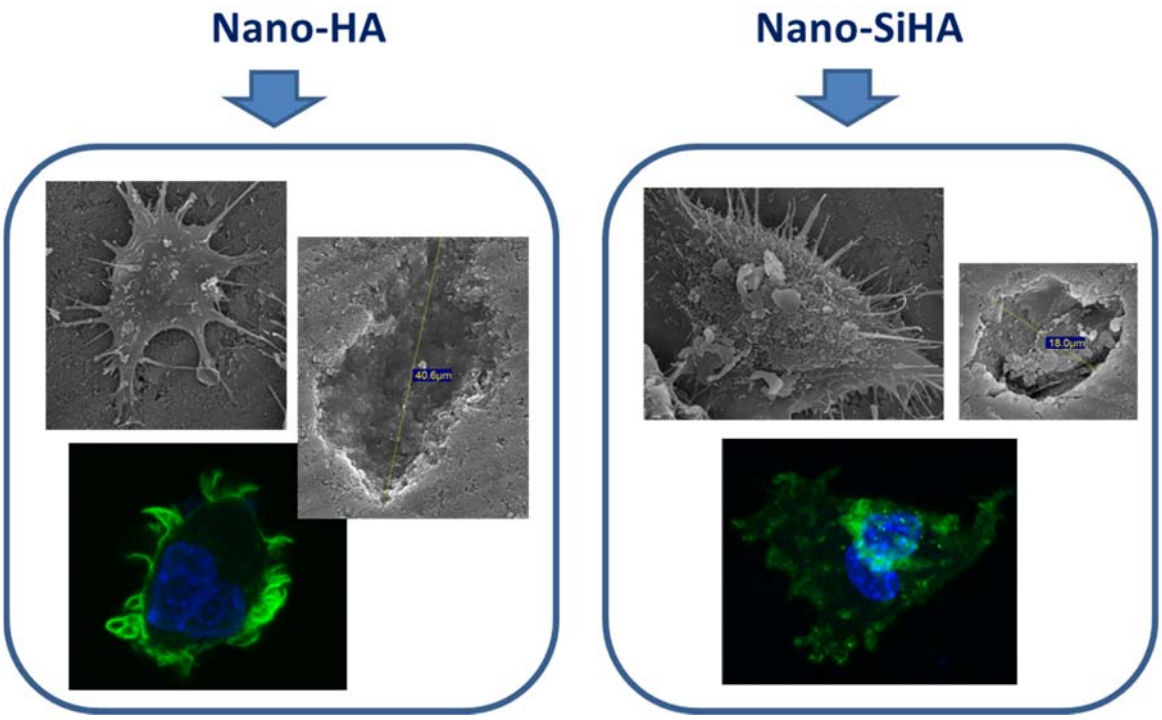

Figura 29. Diferenciación y actividad resortiva de osteoclastos sobre nano-HA y nano-SiHA. Gráfica procedente de [*Matesanz MC et al. 2014, J Mater Chem*].

Otros parámetros evaluados (contenido intracelular de ROS, calcio intracelular, liberación de citoquinas IL-6 y TNFα) mostraron incrementos en presencia de nano-SiHA relacionados con el retraso observado en el proceso de diferenciación.

Estos datos demuestran que el silicio afecta a etapas tardías de la diferenciación y a la fusión de los osteoclastos, causando una inhibición significativa de la osteoclastogénesis y de la actividad resortiva *in vitro*, sin disminuir la viabilidad celular ni producir apoptosis.

Todos estos resultados, junto con los obtenidos con osteoblastos y células de la respuesta inmune, indican el elevado potencial de nano-SiHA como biomaterial biocompatible para la modulación del remodelado óseo, previniendo la resorción y estimulando la formación de hueso en los lugares de implantación del material para tratamiento de procesos osteoporóticos y de regeneración ósea.

Journal of Materials Chemistry B

PAPER

Nanocrystalline silicon substituted hydroxyapatite effects on osteoclast differentiation and resorptive activity

Cite this: *J. Mater. Chem. B*, 2014, **2**, 2910

María Concepción Matesanz,[a] Javier Linares,[ac] Isabel Lilue,[a] Sandra Sánchez-Salcedo,[bc] María José Feito,[a] Daniel Arcos,[bc] María Vallet-Regí[bc] and María Teresa Portolés*[a]

Received 29th November 2013
Accepted 10th March 2014

DOI: 10.1039/c3tb21697g

www.rsc.org/MaterialsB

In the present study, the effects of nanocrystalline hydroxyapatite (nano-HA) and nanocrystalline Si-substituted hydroxyapatite (nano-SiHA) on osteoclast differentiation and resorptive activity have been evaluated *in vitro* using osteoclast-like cells. The action of these materials on proinflammatory and reparative macrophage populations was also studied. Nano-SiHA disks delayed the osteoclast differentiation and decreased the resorptive activity of these cells on their surface, as compared to nano-HA samples, without affecting cell viability. Powdered nano-SiHA also induced an increase of the reparative macrophage population. These results along with the beneficial effects on osteoblasts previously observed with powdered nano-SiHA suggest the potential of this biomaterial for modulating the fundamental processes of bone formation and turnover, preventing bone resorption and enhancing bone formation at implantation sites in treatment of osteoporotic bone and in bone repair and regeneration.

1. Introduction

Bone is a dynamic tissue in continuous remodelling which depends on resorption and new bone formation processes carried out by osteoclasts and osteoblasts respectively, working together in basic multicellular units. The main purpose of bone remodelling is to repair micro-fractures and maintain mineral homeostasis by providing access to stores of calcium and phosphate.[1] Imbalances in bone turnover lead to bone loss and development of osteoporosis and ultimately fracture. Thus, osteoclasts, as principal bone-resorbing cells, are involved in the pathogenesis of various bone diseases, including osteoporosis.[2,3] Severe bone loss due to excessive bone resorption is also observed in bacterial infection-related inflammatory diseases, such as periodontitis, osteomyelitis, and some types of arthritis.[4] Osteoclasts are multinucleated giant cells which differentiate from hematopoietic stem cells (HSCs) through different consecutive steps regulated by several growth factors and cytokines expressed by different cell types present in bone.[5–7] HSCs give rise to circulating mononuclear cells termed colony forming unit-granulocyte/macrophage (CFU-GM) whose proliferation is stimulated by macrophage/monocyte-colony forming factor (M-CSF), maintaining a pool of mononuclear cells in monocyte/macrophage lineage which are osteoclast precursors.[8,9] These mononuclear precursors are attracted to the resorption sites, where they will then attach onto the bone matrix to differentiate into prefusion osteoclasts with the stimulation of M-CSF and the receptor activator of nuclear factor kappa-B ligand (RANKL). RANKL is a protein found on the surface of the osteoblastic lineage cells, which may also be cleaved into a soluble form by metalloproteinases. RANKL interacts with its receptor, RANK, expressed on the surface of hematopoietic precursor cells thereby promoting osteoclast formation and maintaining their viability and activity. The continuous stimulation of M-CSF and RANKL induces the further differentiation of the prefusion osteoclasts which, by fusion, become multinucleated cells. The formation of a "ruffled membrane", critical for bone resorption, is also stimulated by RANKL which promotes the survival of mature osteoclasts.[8,10] Resorption implies an initial tight attachment of osteoclasts to the bone surface to create the "sealing zone", rich in F-actin. The osteoclast thus isolates the resorptive space from the surrounding bone.[11,12] The ruffled border is formed by fusion of intracellular acidic vesicles which form finger-like projections inside the sealing zone. The vesicles contain a cocktail of matrix-degrading enzymes (such as cathepsin K), hydrogen ions (H^+) and chloride ions (Cl^-) which are released into the resorption lacunae and are responsible for acidification to a pH of around 4.5.[13–15] This process produces the dissolution of the bone mineral component and enhances the enzymatic activity on the organic matrix. The degraded bone matrix is

[a]*Department of Biochemistry and Molecular Biology I, Faculty of Chemistry, UCM, 28040-Madrid, Spain. E-mail: portoles@quim.ucm.es*

[b]*Department of Inorganic and Bioinorganic Chemistry, Faculty of Pharmacy, UCM, Instituto de Investigación Sanitaria Hospital 12 de Octubre i+12, 28040-Madrid, Spain*

[c]*Networking Research Center on Bioengineering, Biomaterials and Nanomedicine, CIBER-BBN, Spain*

endocytosed from the resorption lacunae and transported by transcytotic carriers to the functional secretory domain, where it is released into the extracellular environment.[16,17] Although these mechanisms of osteoclast action for bone resorption are well known, the bone remodelling process is not yet completely understood when osteoporosis is present.[18] Pathological fractures are the natural consequence of osteoporosis and, for this reason, much attention has been paid to fracture prevention through pharmacological and physical therapies. However, less attention has been directed at the study of orthopaedic biomaterials behaviour when implanted in osteoporotic bone.[19] In fact, there are no clinically approved biomaterials specifically tailored for application in osteoporotic bones. Certainly, there are some examples of medical devices for osteosynthesis with special designs, but they are made of the same biomaterials as the conventional ones.[19] Biomaterials that enhance the osteogenic function while decreasing the osteoclast-mediated resorption would be of great interest in fabricating implants specially tailored for osteoporotic patients. In this sense, nanocrystalline silicon substituted hydroxyapatites (nano-SiHA) could play a significant role for this biomedical purpose. In 1999, Gibson *et al.* proposed SiHA as an improved bioceramic with respect to stoichiometric hydroxyapatite.[20] Thereafter, *in vivo* studies demonstrated that the bioactivity of HA was improved with the incorporation of Si.[21] This fact is explained in terms of a higher solution-mediated degradation of the apatite phase due to the silicate presence within the crystalline structure, higher solubility at the grain boundary and an up-regulation in osteoblast cell metabolism in the early stages of bone formation.[22–27] Since then, Si-substituted HAs have attracted the attention of many researchers and have recently been incorporated to the biomaterials market for spinal, orthopaedic, periodontal, oral and craniomaxillofacial applications. SiHAs approved for clinical use are highly crystalline bioceramics treated at high temperatures. However, the possibility of enhancing the bioceramics bioreactivity through their preparation as nanocrystalline compounds has been suggested.[28,29] Higher surface area and smaller crystal size could thus provide very interesting bioresponses, especially in SiHA as the osteogenic effect of silicon is mainly explained by its location at the crystal boundaries.[22,23]

In vitro cell cultures help to understand the interaction of bone remodeling cells with biomaterials.[30] In the case of SiHA based bioceramics, the majority of *in vitro* studies are focused on the interaction of sintered and highly crystalline Si-HA with osteoblasts,[31–33] and little is known about the interaction of highly crystalline SiHA with bone resorbing osteoclasts.[34,35] The interactions of nanocrystalline SiHA with osteoblasts have been also studied by Thian *et al.*[28,36] However, to the best of our knowledge, there are no studies concerning osteoclast interactions with nanocrystalline SiHA. Since bone remodelling depends on resorption and new bone formation processes carried out by osteoclasts and osteoblasts respectively, in the present study we aimed to know the behaviour of osteoclasts on both nano-HA and nano-SiHA disks, evaluating their differentiation and resorptive activity *in vitro*. The results herein presented open new possibilities for tailoring biomaterials specially aimed for osteoporotic bone treatment.

On the other hand, cells with osteoclastogenic potential also exist in blood and peripheral hematopoietic organs and a common progenitor for osteoclasts, macrophages, and dendritic cells from murine bone marrow has been recently characterized.[37] The capacity of macrophages to play both positive and negative roles in disease processes and tissue remodeling after injury has been recently related to the balance between the proinflammatory (M1) and immunomodulatory/reparative (M2) macrophage phenotypes, with participation of diverse specific cytokines.[38,39] Recent studies demonstrate the potential of biomaterials to modulate the immune cell function, suggesting the possibility of designing biomaterials capable of eliciting appropriate immune responses at implantation sites.[40]

Previous studies have shown that Saos-2 osteoblasts grow better on nanocrystalline SiHA (nano-HA) disks than on nanocrystalline HA (nano-HA) disks. Since bone remodelling depends on resorption and new bone formation processes carried out by osteoclasts and osteoblasts respectively, in the present study we aimed to know the behaviour of osteoclasts on both nano-HA and nano-SiHA disks, evaluating their differentiation and resorptive activity *in vitro*. With this purpose, osteoclast-like cells have been differentiated for the first time on these substrates by treatment of RAW-264.7 macrophages with M-CSF and RANKL. The U0126 inhibitor of MAPKs (MEK) was used to potentiate the differentiation process.

2. Materials and methods

2.1. Nanocrystalline hydroxyapatite and silicon substituted hydroxyapatite synthesis

Samples of pure and silicon substituted HA were prepared by aqueous precipitation reaction of $Ca(NO_3)_2 \cdot 4H_2O$, $(NH_4)_2HPO_4$ and tetraethyl orthosilicate $Si(CH_3CH_2O)_4$ (TEOS) solutions. The amounts of reactants were calculated on the assumption that phosphorus would be substituted by silicon. Two different compositions have been prepared with nominal formula $Ca_{10}(PO_4)_{6-x}(SiO_4)_x(OH)_{2-x}$, with $x = 0$ and 0.25 for nano-HA and nano-SiHA samples, respectively, as previously reported by Arcos *et al.*[26] Briefly, 1 M $Ca(NO_3)_2 \cdot 4H_2O$ solution was added to $(NH_4)_2HPO_4$ and TEOS solutions of stoichiometric concentration to obtain the compositions described above. The mixture was stirred for 12 hours at 80 °C. During the reaction the pH was continuously adjusted to 9.5 to ensure constant conditions during the synthesis. The as-precipitated powders were milled, sieved and treated at 700 °C for 2 hours under an air atmosphere to remove the nitrates without introducing important changes in the crystallite size with respect to the as-precipitated powder. The HA and Si-HA particles thus obtained have a diameter ranging in size from 10 to 100 micrometers, as could be measured with a particle size analyser Sedigraph 5100 (data not shown). X-ray diffraction (XRD) patterns were recorded with a Philips X'Pert diffractometer using the Cu Kα radiation (wavelength 1.5406 Å). Crystallite sizes were calculated using the Scherrer equation for different diffraction maxima. The XRD pattern collected from a well crystallized LaB_6 sample was used as standard.

2.2. Preparation of nano-HA and nano-SiHA disks

Fractions of 300 mg of the as-precipitated powders of HA and Si-HA materials were milled, sieved and pressed into disk-shape (11 mm diameter, 2 mm height) by means of 3 tons of uniaxial pressing. Thereafter the disks were treated at 700 °C for two hours under an air atmosphere.

2.3. Culture of RAW-264.7 macrophages and treatment with nano-HA or nano-SiHA

RAW-264.7 cells were seeded on 6 well culture plates (CULTEK S.L.U., Madrid, Spain) at a density of 10^5 cells per ml in Dulbecco's Modified Eagle Medium (DMEM) supplemented with 10% fetal bovine serum (FBS, Gibco, BRL), 1 mM L-glutamine (BioWhittaker Europe, Belgium), penicillin (200 μg ml^{-1}, BioWhittaker Europe, Belgium), and streptomycin (200 μg ml^{-1}, BioWhittaker Europe, Belgium), under a CO_2 (5%) atmosphere at 37 °C for 24 h. Then, 1 mg ml^{-1} of either nano-HA or nano-SiHA were added to cultured RAW-264.7 and maintained under a CO_2 (5%) atmosphere at 37 °C for 24 h. Parallel control experiments were carried out in the absence of material. After this treatment, the attached cells were washed with PBS and harvested using cell scrapers. Then, 10 μl of the cell suspensions were counted with a Neubauer hemocytometer for the analysis of cell proliferation and cell suspensions were centrifuged at 310 × *g* for 10 min and resuspended in fresh medium for the analysis of different parameters by flow cytometry as described below (Section 2.6).

2.4. Osteoclast differentiation on nano-HA and nano-SiHA disks

Murine RAW-264.7 macrophages were seeded on either nano-HA or nano-SiHA disks, previously introduced into 24 well culture (CULTEK S.L.U., Madrid, Spain), at a density of 2×10^4 cells per ml in Dulbecco's Modified Eagle Medium (DMEM) supplemented with 10% fetal bovine serum (FBS, Gibco, BRL), 1 mM L-glutamine (BioWhittaker Europe, Belgium), penicillin (200 μg ml^{-1}, BioWhittaker Europe, Belgium), and streptomycin (200 μg ml^{-1}, BioWhittaker Europe, Belgium). In order to stimulate osteoclast differentiation, 40 ng ml^{-1} of mouse RANK Ligand recombinant protein (TRANCE/RANKL, carrier-free, BioLegend, San Diego), 25 ng ml^{-1} recombinant human macrophage-colony stimulating factor (M-CSF, Millipore, Temecula) and U0126 (5 μM Promega, Madison, WI, USA) were added to the culture medium. Cells were cultured under a CO_2 (5%) atmosphere and at 37 °C for 21 days, renewing culture medium every 5–7 days. After 21 days culture on nano-HA and nano-SiHA disks, cells were washed with PBS, harvested using PBS-EDTA over 10 min and counted using a Neubauer hemocytometer. Cell suspensions were then centrifuged at 310 × *g* for 10 min and resuspended in fresh medium for the analysis of different parameters by flow cytometry as described below (Section 2.5).

2.5. Flow cytometry studies

After incubation with different probes, as is described below, the conditions for the data acquisition and analysis were established using negative and positive controls with the CellQuest Program of Becton Dickinson. These conditions were maintained for all the experiments. At least 10 000 cells were analyzed in each sample.

2.5.1. Cell cycle analysis and apoptosis detection. Cell suspensions were incubated with Hoechst 33258 (PolySciences, Inc., Warrington, PA) (Hoechst 5 μg ml^{-1}, ethanol 30%, and BSA 1% in PBS), used as a nucleic acid stain, for 30 min at room temperature in darkness. The fluorescence of Hoechst was excited at 350 nm and the emitted fluorescence was measured at 450 nm in a LSR Becton Dickinson Flow Cytometer. The cell percentage in each cycle phase: G0/G1, S and G2/M was calculated with the CellQuest Program of Becton Dickinson and the SubG1 fraction was used as indicative of apoptosis.

2.5.2. Intracellular reactive oxygen species (ROS) content and cell viability. Cells were incubated at 37 °C for 30 min with 100 μM 2′,7′-dichlorofluorescein diacetate (DCFH/DA, Serva, Heidelberg/Germany) for directly measuring the intracellular content of ROS. DCFH/DA is diffused into cells and is deacetylated by cellular esterases to non-fluorescent DCFH, which is rapidly oxidized to highly fluorescent DCF by ROS. To measure the intracellular reactive oxygen species (ROS), the DCF fluorescence was excited using a 15 mW laser tuned to 488 nm and the emitted fluorescence was measured with a 530/30 band pass filter in a FACScalibur Becton Dickinson Flow Cytometer. Cell viability was determined by the propidium iodide (PI) exclusion test and flow cytometry after addition of PI (0.005% in PBS, Sigma-Aldrich Corporation, St. Louis, MO, USA) to stain the DNA of dead cells.

2.5.3. Intracellular calcium content. Cell suspensions were incubated with the probe Indo-1 AM at a concentration of 10 μM for 30 min at room temperature, in darkness and with shaking. The fluorescence of Indo-1 was excited at 325 nm and the emitted fluorescence was measured with 380 nm long pass (FL1) and 424/44 nm band pass (FL2) filters in a LSR Becton Dickinson flow cytometer. After all the measurements, 10 μM A-23187 ionophore (Enzo Life Sciences) was added in order to test the sensitivity of the assay.

2.6. Morphological studies by confocal microscopy

Cells cultured on nano-HA and nano-SiHA disks were fixed with 3.7% paraformaldehyde in PBS for 10 min, washed with PBS and permeabilized with 0.1% Triton X-100 for 3 to 5 min. The samples were then washed with PBS and preincubated with PBS containing 1% BSA for 20 to 30 min. Then cells were incubated for 20 min with FITC phalloidin (Dilution 1 : 40, Molecular Probes) to stain F-actin filaments. Samples were then washed with PBS and the cell nuclei were stained with DAPI (4′-6-diamidino-2′-phenylindole, 3 μM in PBS, Molecular Probes). After staining and washing with PBS, cells were examined using a LEICA SP2 Confocal Laser Scanning Microscope. The fluorescence of FITC was excited at 488 nm and the emitted fluorescence was measured at 491–586 nm. DAPI fluorescence was excited at 405 nm and measured at 420–480 nm.

2.7. Morphological studies by scanning electron microscopy

Scanning electron microscopy and EDX spectroscopy were carried out with a JEOL JSM-6400 scanning electron

microscope. Since gold coatings overlap with the phosphorous signal in the EDX analysis, Nano-HA and Nano-SiHA disks were coated with graphite.

Cells cultured on nano-HA and nano-SiHA disks were fixed with glutaraldehyde (2.5% in PBS) for 45 min. Sample dehydration was performed by slow water replacement using a series of ethanol solutions (30, 50, 70, 90%) for 15 min with the final dehydration in absolute ethanol for 30 min, allowing samples to dry at room temperature and under vacuum. Afterwards, the pieces were mounted on stubs and coated in a vacuum with gold-palladium.

2.8. Observation of osteoclast resorption cavities by scanning electron microscopy

To observe the geometry of resorption cavities produced by osteoclasts on the surface of nano-HA and nano-SiHA disks, cells were detached after 21 days culture on these biomaterials and disks were dehydrated, coated with gold-palladium (as in Section 2.8) and examined with a JEOL JSM-6400 scanning electron microscope.

2.9. Inflammatory cytokine detection

The amounts of TNF-α and IL-6 in the culture medium were quantified by ELISA (Gen-Probe, Diaclone), carried out according to the manufacturer's instructions.

2.10. Statistics

Data are expressed as means + standard deviations of one representative experiment out of three experiments carried out in triplicate. Statistical analysis was performed using the Statistical Package for the Social Sciences (SPSS) version 19 software. Statistical comparisons were made by analysis of variance (ANOVA). The Scheffé test was used for *post hoc* evaluations of differences among groups. In all of the statistical evaluations, $p < 0.05$ was considered as statistically significant.

3. Results and discussion

Bone remodelling depends on the balance between osteoblastic bone formation and osteoclastic bone resorption. Differentiation and activity of both osteoblasts and osteoclasts are precisely regulated processes and can greatly be influenced by the presence of a biomaterial.[1] Thus, silicate nanoparticles have been recently used in an animal model to stimulate bone growth by inhibiting osteoclasts while enhancing the activity of osteoblasts.[41] However, little is known about the effects on osteoclast differentiation/activity produced by the majority of biomaterials designed for bone tissue. Silicon substituted hydroxyapatites (Si-HA) are among the most interesting calcium phosphates for bone repair with comparable biocompatibility and mechanical properties to hydroxyapatite (HA) but improved bioactivity which enhances the bone tissue growth rate.[22–24,36,42] The beneficial actions of Si-substituted calcium phosphates have been recently revised, but the majority of studies concerning the Si effects have focused on bone formation and osteoblasts.[31–33,43–47] In the present study, taking into account that osteoclasts are derived from a monocyte/macrophage precursor,[37] the *in vitro* effects of nanocrystalline hydroxyapatite (nano-HA) and nanocrystalline silicon substituted hydroxyapatite (nano-SiHA) on murine RAW-264.7 macrophages were analyzed, as was the capacity of these cells to differentiate into mature osteoclasts on the surface of these biomaterials in the presence of soluble RANKL and M-CSF in the culture medium.

Fig. 1A and B depict the scanning electron micrographs obtained from disks of nano-HA and nano-SiHA, respectively. Both surfaces show large and irregular particles ranging in size between 10 and 50 micrometers. These particles do not show the typical polyhedral morphology of highly crystalline ceramics treated at high temperature. In contrast, they exhibit irregular shapes with incomplete sintered grain boundaries, as would correspond to pressed powders treated at temperatures below the sintering point.

SEM observations of the surfaces at higher magnifications (Fig. 1C and D) show that the large grains are formed by nanoparticles leaving porosity at the nanoscale. This is due to the low thermal treatment, which is clearly insufficient to lead to the crystal growth of the as-precipitated nanocrystalline powders. The micrographs also evidence the presence of macropores (larger than 50 nm) and surface defects that, from a qualitative point view, seem to be more numerous in nano-SiHA (Fig. 1D). Fig. 1E and F show the EDX spectra for nano-HA and nano-SiHA, which agree with the chemical compositions expected for the nominal formulae $Ca_{10}(PO_4)_6(OH)_2$ and $Ca_{10}(PO_4)_{5.7}(SiO_4)_{0.3}(OH)_{1.7}$.

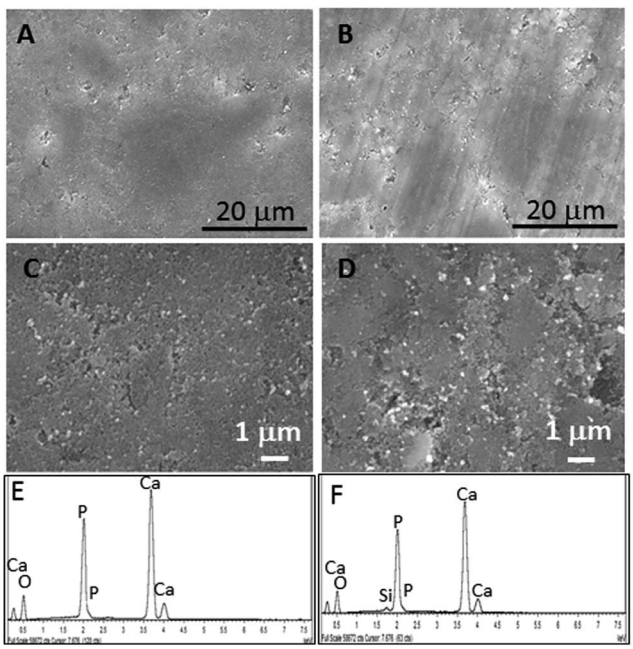

Fig. 1 Scanning electron micrographs (magnification × 2000) obtained from disks of nano-HA (A) and nano-SiHA (B). Scanning electron micrographs (magnification × 10 000) obtained from disks of nano-HA (C) and nano-SiHA (D). EDX spectra corresponding to nano-HA (E) and nano-SIHA (F).

Fig. 2 shows the XRD patterns collected from nano-HA and nano-SiHA after being treated at 700 °C. The XRD patterns indicate that both samples are composed of a unique single apatite phase without the presence of secondary calcium phosphates, such as α or β tricalcium phosphates, which could modify the materials solubility. The averaged crystallite size values were 30.0 nm and 24.8 nm for nano-HA and nano-SiHA, respectively. These crystallite sizes indicate that both samples remain as nanocrystalline apatites after the thermal treatment at 700 °C.

Fig. 3A shows macrophage proliferation values after 1 day culture with either nano-HA or nano-SiHA (1 mg ml^{-1} in powder form). As can be observed, both materials produced a significant decrease of RAW-264.7 cell proliferation in comparison with controls in the absence of material. This effect has been previously observed using cultured L929 fibroblasts, Saos-2 osteoblasts and MC3T3-E1 preosteoblasts.[24,48]

Increased reactive oxygen species (ROS) formation has been described in response of macrophages to different hydroxyapatite dispersions.[49] When the intracellular ROS content of RAW-264.7 macrophages was evaluated by flow cytometry with the probe DCFH/DA, after 1 day treatment with either nano-HA or nano-SiHA, a significant increase induced by nano-HA was observed at this short time of culture. However, macrophages treated with nano-SiHA showed lower ROS values than control (Fig. 3B), thus indicating a beneficial action of Si-substituted material in agreement with other studies.[22–24,36,42,43]

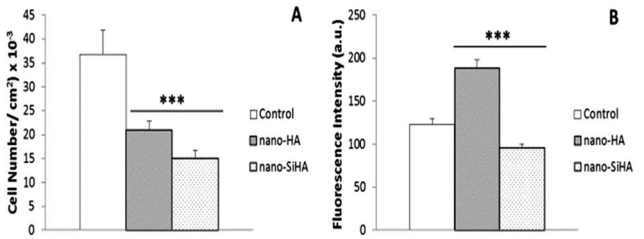

Fig. 3 Effect of 1 mg ml^{-1} of powdered nano-HA and nano-SiHA on proliferation (A) and intracellular ROS content (B) of RAW-264.7 macrophages after 1 day treatment. Control experiments without material were carried out in parallel. ***$p < 0.005$.

To know the possible effects of these biomaterials on macrophage phenotypes, the analysis of two RAW-264.7 cell populations, with high and low intracellular ROS contents, was carried out in the samples by flow cytometry after DCFH labelling. As can be observed in Fig. 4, the percentage of low ROS population is significantly higher in control and nano-SiHA samples than in nano-HA treated cells, whereas the high ROS population is significantly higher in nano-HA compared with nano-SiHA and control. The two populations observed can be related to the proinflammatory (M1, high ROS) and reparative (M2, low ROS) macrophage phenotypes, whose balance has been involved in the macrophage capacity to play both negative and positive roles in disease processes and tissue remodelling after injury.[38,39] Although further studies are necessary to establish the effects of these nanocrystalline hydroxyapatites on macrophage polarization, the results obtained suggest the beneficial role of nano-SiHA which could favour the reparative population with low ROS content. In this sense, recent studies suggest the potential of biomaterials to modulate immune response at implantation sites.[40]

In order to evaluate the action of nano-HA and nano-SiHA on osteoclast differentiation and resorptive activity *in vitro*,

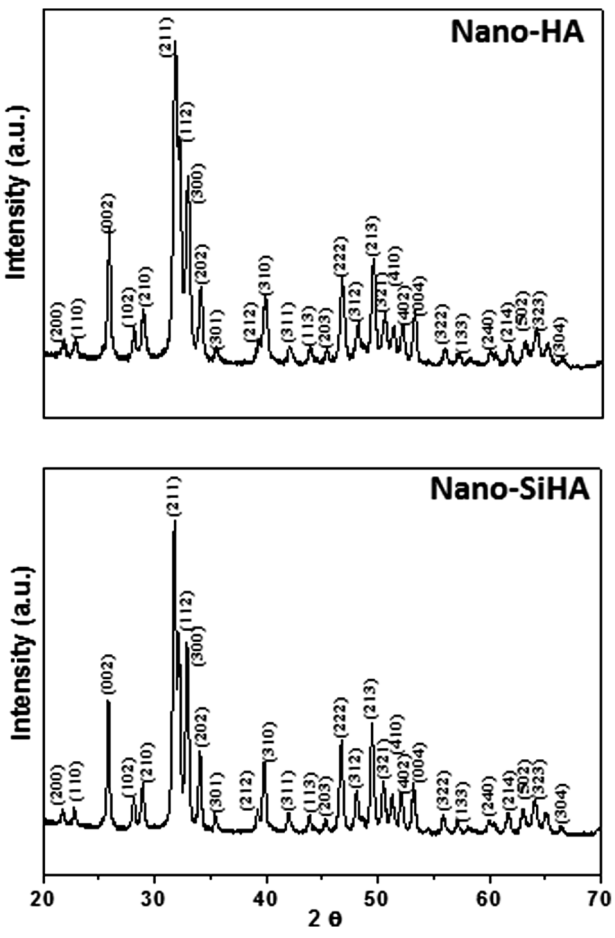

Fig. 2 XRD patterns of nano-HA and nano-SiHA. Miller indices corresponding to an apatite phase are indicated.

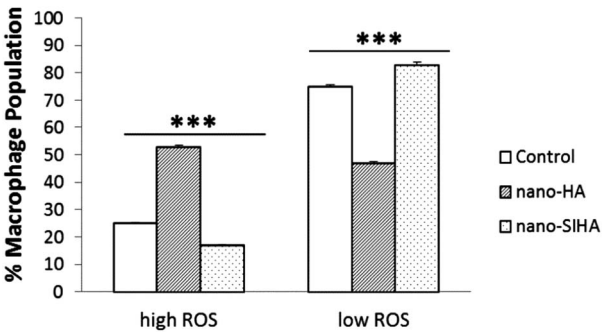

Fig. 4 Effect of 1 mg ml^{-1} of powdered nano-HA and nano-SiHA on RAW-264.7 macrophage populations concerning intracellular ROS content after 1 day treatment. Control experiments without material were carried out in parallel. ***$p < 0.005$.

osteoclasts were differentiated by treatment of RAW-264.7 macrophages with M-CSF and RANKL on the surface of disks prepared with these biomaterials. The U0126 inhibitor of MAPKs (MEK) was used to potentiate the differentiation process.[50] As can be observed in Fig. 5 and 6, continuous stimulation with these factors induces osteoclast-like cell differentiation on both materials by fusion of macrophagic precursors leading to multinucleated cells (asterisks indicate the nuclei in the insets of Fig. 5A and B, and in Fig. 6D). The formation of long and numerous finger-like projections (podosomes) was also observed (thin arrows in Fig. 5C and D and Fig. 6), as well as the F-actin ring which allows creation of the "sealing zone" (thick arrows in Fig. 5B and 6C), which is critical for bone resorption.

All these morphological characteristics reveal osteoclastogenesis on these nanocrystalline hydroxyapatites in agreement with other studies carried out with carbonate-substituted hydroxyapatite.[51] However, some differences were observed between osteoclast-like cells differentiated on nano-HA and nano-SiHA disks. A higher number of nuclei per cell was observed on the nano-HA surface (asterisks in the insets of Fig. 5A and B) than on nano-SiHA disks (asterisks in Fig. 6D). The statistical analysis of the multinucleated cells showed 10% of multinucleated cells on both materials. However, in contact with nano-SiHA, these multinucleated cells contain two nuclei and the multinucleated cells on nano-HA disks contain four or five nuclei. Although the formation of the F-actin ring and podosomes, related to the definition of the sealing zone, was observed on both materials, more organized podosomes were evident in the cells differentiated on nano-HA (thin arrows in Fig. 5C and D) than on nano-SiHA (thin arrows in Fig. 6C).

All these results reveal that nano-SiHA produces a delay in the osteoclastogenesis probably due to the presence of Si. In this sense, experiments with RAW-264.7 macrophages demonstrate that Si affects the late stages of differentiation and fusion of osteoclasts, causing a significant inhibition of osteoclast phenotypic gene expressions, osteoclast formation and bone resorption *in vitro*.[52]

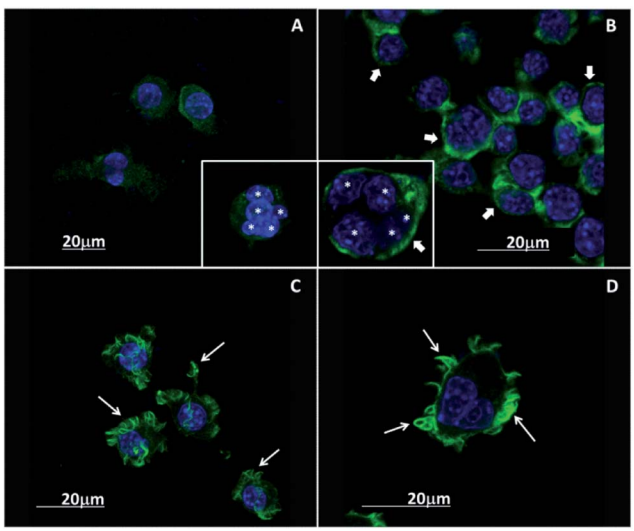

Fig. 5 Morphology evaluation by confocal microscopy of osteoclast-like cells cultured on nano-HA disks, stained with DAPI (for the visualization of the cell nuclei) and FITC phalloidin (for the visualization of cytoplasmic F-actin filaments). Asterisks indicate the nuclei, thin arrows the podosomes and thick arrows the F-actin ring of the "sealing zone".

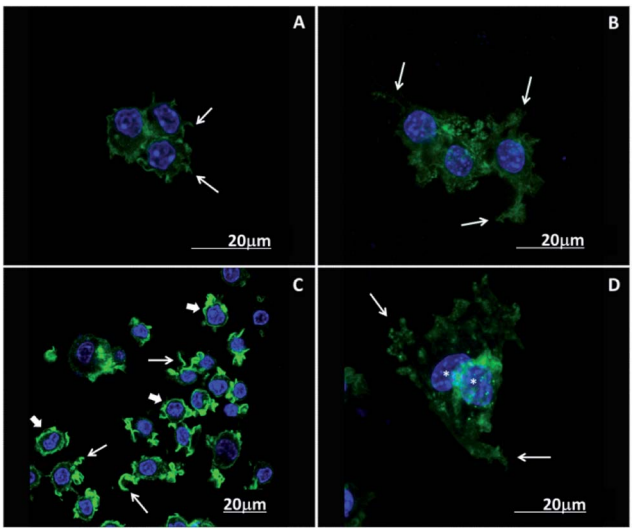

Fig. 6 Morphology evaluation by confocal microscopy of osteoclast-like cells cultured on nano-SiHA disks, stained with DAPI (for the visualization of the cell nuclei) and FITC phalloidin (for the visualization of cytoplasmic F-actin filaments). Asterisks indicate the nuclei, thin arrows the podosomes and thick arrows the F-actin ring of the "sealing zone".

Fig. 7 shows the proliferation (A) and cell viability (B) of osteoclast-like cells differentiated on nano-HA and nano-SiHA disks. As it can be observed in Fig. 7A, the cell growth on the nano-SiHA surface was significantly lower than that on nano-HA disks after 21 days. However, high viability values on both biomaterials (up 80%) were obtained (Fig. 7B). The significant decrease of osteoclast proliferation produced by nano-SiHA, probably due to the presence of Si, is in agreement with the powdered nano-SiHA action on RAW-264.7 cells (Fig. 3A), and can be related to the same origin of both cell types from a monocyte/macrophage precursor.[37] Previous results have shown a significant Ca^{2+} decrease in the culture medium produced by both nano-HA and nano-SiHA, more pronounced with nano-SiHA, in agreement with the higher bioactivity of this material.[42,53] The observed sequestration of extracellular calcium can

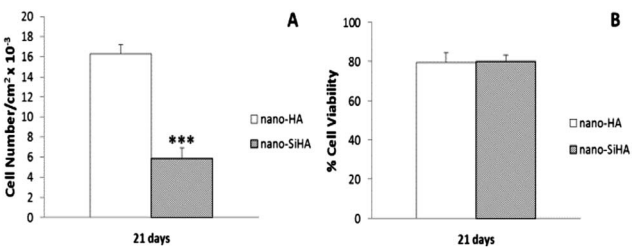

Fig. 7 Proliferation (A) and cell viability (B) of osteoclast-like cells cultured on nano-HA and nano-SiHA disks. ***$p < 0.005$.

be partially responsible for the lower proliferation of osteoclasts on nano-SiHA observed in the present study. Recently, it has been observed that bioglass 45S5 particles cause a significant reduction of osteoclast-like cells in both the marrow cultures and RAW-264.7 cells, suggesting a direct inhibitory effect of Si on the osteoclast precursors that is not due to cell toxicity.[52] However, previous studies with Saos-2 osteoblasts showed that the number of Saos-2 cells after 4 days culture in contact with nano-SiHA was significantly higher than with nano-HA, indicating that this cell type grows better in the presence of nano-SiHA. This result was also observed by Scanning Electron Microscopy (SEM) when Saos-2 osteoblasts were cultured for 4 days on the surface of both nano-HA and nano-SiHA disks. SEM images demonstrated that Saos-2 cells adhere to the nano-SiHA disk, proliferate and colonize its surface better than on nano-HA disks.[24] Previous studies also showed that osteoblasts cultured on the nano-SiHA surface showed the typical bone cell morphology, cube-shape, and big sized, joining other cells to construct a net through strong cellular union.[24] Adhesion and proliferation processes are good indicators of the cell response that could be expected when a biomaterial is used *in vivo*. Thus, the previous results obtained with osteoblasts cultured on nano-SiHA disks indicate a good biocompatibility and an adequate interaction of osteoblasts with nano-SiHA materials.

Since proliferation is dependent on the cell cycle progression, in which cells pass through the G_0/G_1 phase (quiescence/gap 1) to the S phase (synthesis) and finally to the G_2/M phase (gap 2 and mitosis), the cell cycle phases of osteoclast-like cells cultured on nano-HA disks and nano-SiHA disks were analysed. No significant changes were observed (Fig. 8), demonstrating that these materials do not produce toxicity on osteoclast-like cells, in agreement with the results obtained from the propidium iodide exclusion test (Fig. 7B). The analysis of the SubG1 fraction, corresponding to cells with fragmented DNA, reveals low apoptosis levels induced by both materials (Fig. 8) but slightly higher on nano-SiHA than on nano-HA (Fig. 9A).

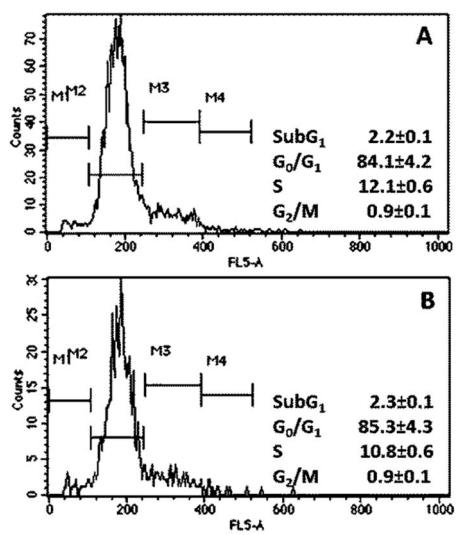

Fig. 8 Effect on cell cycle phases of osteoclast-like cells cultured on nano-HA disks (A) and nano-SiHA disks (B).

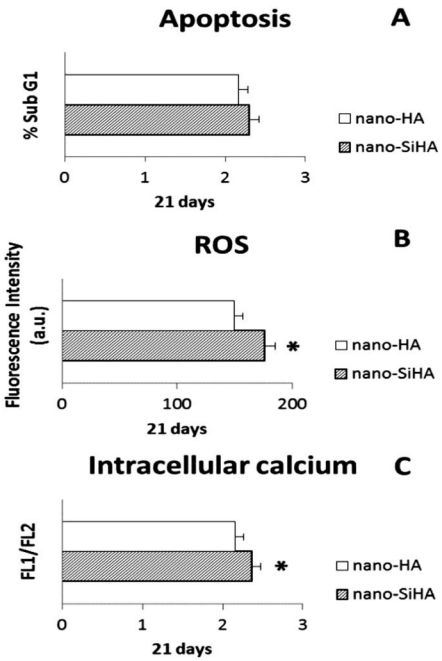

Fig. 9 Effect on apoptosis (A), ROS production (B) and cytosolic Ca^{2+} (C) of osteoclast-like cells cultured on nano-HA and nano-SiHA disks. *$p < 0.05$.

Intracellular ROS and Ca^{2+} play essential roles in osteoclastogenesis.[54] Thus, following stimulation with RANKL, the pre-osteoclasts increase intracellular ROS by activation of NADPH oxidase (Nox) homologs or by increased mitochondria ROS production, which subsequently induced long lasting Ca^{2+} oscillations.[54–56] In the present study both intracellular ROS and Ca^{2+} contents of osteoclast-like cells cultured on nano-HA disks and nano-SiHA disks were analyzed by flow cytometry and higher values of both parameters were obtained in cells cultured on nano-SiHA than on nano-HA (Fig. 9B and C). These results could suggest the existence of a differentiation delay produced by nano-SiHA on RAW-264.7 cells, in agreement with the morphological characteristics observed by confocal microscopy (Fig. 5 and 6).

Fig. 10 shows the morphology of RAW-264.7 macrophages differentiated into osteoclast-like cells cultured on nano-HA disks (Fig. 10A and B) and nano-SiHA disks (Fig. 10C and D), as determined by Scanning Electron Microscopy (SEM). These SEM studies demonstrate the presence of cells attached on both surfaces, presenting typical characteristics of osteoclasts with many longer podosomes.

In order to evaluate the geometry of the resorption cavities left by osteoclast-like cells cultured on nano-HA and nano-SiHA samples, the surfaces of these materials were analyzed by SEM after cell detachment. As can be observed in Fig. 11, osteoclasts cultured on nano-HA disks demonstrate higher resorptive activity (Fig. 11A and B) than on nano-SiHA disks (Fig. 11C and D) after 21 days culture in the presence of RANKL, M-CSF and U0126. Resorption cavities on the nano-HA surface present higher size than on the nano-SiHA surface which shows spherical cavities (inset in Fig. 11D). The statistical analysis of

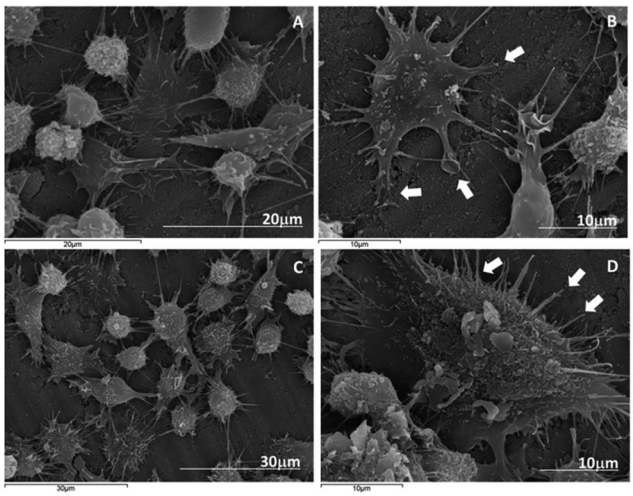

Fig. 10 Morphology evaluation by scanning electron microscopy of osteoclast-like cells cultured on nano-HA disks (A and B) and nano-SiHA disks (C and D).

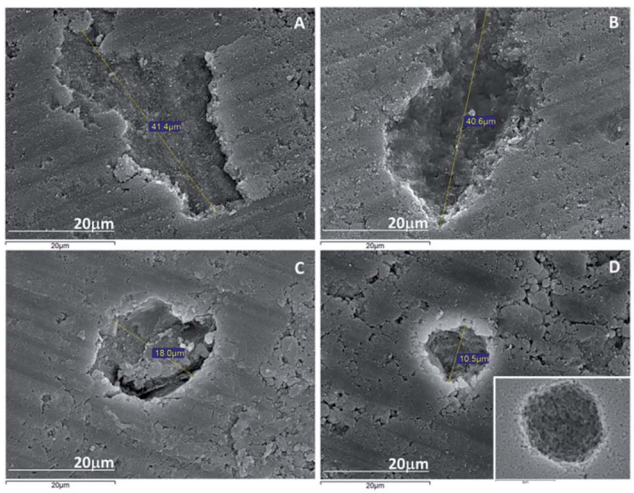

Fig. 11 Morphology evaluation by scanning electron microscopy of the resorption cavities left by osteoclast-like cells cultured on nano-HA disks (A and B) and nano-SiHA disks (C and D).

the cave size showed values of 10 ± 1.7 μm on nano-SiHA and 32.5 ± 9.7 μm on nano-HA (**$p < 0.01$). Concerning the resorption of nanocrystalline calcium phosphates by osteoclast-like cells, Detsch *et al.* have recently showed that nano-HA with low carbonate content strongly stimulated the differentiation and resorption of these cells on its surface when compared with carbonate-rich samples.[12]

Resorption implies an initial tight attachment of osteoclasts to the disk surface to create the "sealing zone", rich in F-actin, which isolates the resorptive space from the surrounding material.[11,12] The ruffled border is formed by fusion of intracellular acidic vesicles which contain enzymes (such as cathepsin K), Cl^- and H^+ ions which are released into the resorption lacunae for the acidification to a pH of around 4.5.[13–15] This process produces the dissolution of the material,

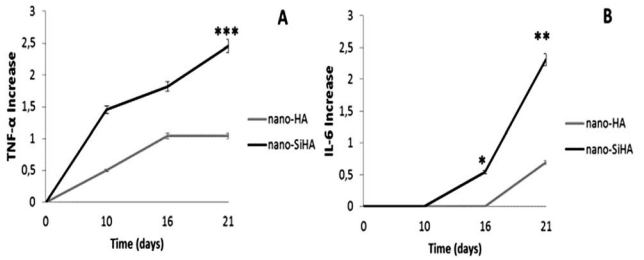

Fig. 12 Effects on TNF-α (A) and IL-6 (B) release to culture medium of osteoclast-like cells cultured on nano-HA and nano-SiHA disks. *$p < 0.05$, **$p < 0.01$, ***$p < 0.005$.

which is then endocytosed from the resorption cavity and transported to the secretory domain for releasing into the extracellular environment.[16,17]

Many different stimuli have been shown to regulate Ca^{2+} concentrations in osteoclasts and extracellular acidification has been described to cause a decrease in intracellular Ca^{2+} concentration in isolated chicken osteoclasts.[57] The lower Ca^{2+} content observed in the present study with osteoclast-like cells cultured on nano-HA disks in comparison to cells cultured on nano-SiHA samples (Fig. 9C) can be related to higher extracellular acidification produced by these cells on the nano-HA surface than on the nano-SiHA surface, as demonstrated by the geometry of the resorption cavities observed on this material (Fig. 11A and B).

Since it has been found that osteoclast differentiation is induced by tumor necrosis factor (TNF)-α and IL-6,[58,59] these cytokines were evaluated in the culture medium of RAW-264.7 macrophages at different times during the differentiation into osteoclast-like cells on nano-HA disks and nano-SiHA disks. As can be observed, both TNF-α (Fig. 12A) and IL-6 (Fig. 12B) levels increased progressively in the culture medium during osteoclast differentiation. The values of both cytokines were always significantly higher in the presence of nano-SiHA than nano-HA.

Taking into account that TNF-α and IL-6 modulate osteoclastogenesis, the increase of these cytokines in the presence of nano-SiHA could be explained by a higher secretion as a response to stimulate the differentiation process which is delayed on this material. However, in mouse bone marrow-derived macrophages (BMMs), IL-6 decreased osteoclast formation and bone-resorption ability.[60] Taking into account the results obtained with BMMs, the nano-SiHA effects on osteoclastogenesis and resorption activity observed in the present study, could also be caused by an increase of IL-6 induced by this material (Fig. 12B). Other cytokines as TNF-α and IL-1β, showed various responses according to the phase of osteoclast maturation and the concentration of each cytokine and RANKL.[60]

4. Conclusions

Since bone is a dynamic tissue in continuous remodelling which depends on resorption and new bone formation

processes carried out by osteoclasts and osteoblasts respectively, in the present study we aimed to know the behaviour of osteoclasts on both nano-HA and nano-SiHA disks, evaluating for the first time the differentiation and the substrate resorption carried out by this cell type on both substrates. This study demonstrates that nanocrystalline Si-substituted hydroxyapatite delays the osteoclast differentiation and decreases the resorptive activity of these cells on their surface, as compared to nanocrystalline hydroxyapatite, without affecting cell viability. Furthermore, the demonstrated increase of the reparative macrophage population, along with the beneficial effects on osteoblasts previously observed with powdered nano-SiHA, suggests the potential of this biomaterial for modulating the fundamental processes of bone formation and turnover, preventing bone resorption and enhancing bone formation at implantation sites in treatment of osteoporotic bone and in bone repair and regeneration.

Acknowledgements

This study was supported by research grants from Comunidad de Madrid through the project S2009/MAT-1472 and the Ministerio de Ciencia e Innovacion (MICINN) through the projects MAT2012-35556 and CSO2010-11384-E (Agening Network of Excellence). M. C. Matesanz and J. Linares are greatly indebted to MICINN and CIBER-BBN respectively for predoctoral fellowships. The authors wish to also thank the staff of the Cytometry and Fluorescence Microscopy Centre of the Universidad Complutense de Madrid (Spain) and ICTS National Centre for Electron Microscopy (Spain).

Notes and references

1 P. Pivonka, J. Zimak, D. W. Smith, B. S. Gardiner, C. R. Dunstan, N. A. Sims, T. J. Martin and G. Mundy, *Bone*, 2008, **43**, 249–263.
2 S. C. Manolagas, *Aging*, 1998, **10**, 182–190.
3 T. Luhmann, O. Germershaus, J. Groll and L. Meinel, *J. Controlled Release*, 2012, **161**, 198–213.
4 S. P. Nair, S. Meghji, M. Wilson, K. Reddi, P. White and B. Henderson, *Infect. Immun.*, 1996, **64**, 2371–2380.
5 X. Feng, *Gene*, 2005, **350**, 1–13.
6 H. K. Väänänen and T. Laitala-Leinonen, *Arch. Biochem. Biophys.*, 2008, **473**, 132–138.
7 G. J. Atkins, D. R. Haynes, S. M. Geary, M. Loric, T. N. Crotti and D. M. Findlay, *Bone*, 2000, **26**, 653–661.
8 T. Suda, N. Takahashi, N. Udagawa, E. Jimi, M. T. Gillespie and T. J. Martin, *Endocr. Rev.*, 1999, **20**, 345–357.
9 S. L. Teitelbaum, M. M. Tondravi and F. P. Ross, *J. Leukocyte Biol.*, 1997, **61**, 381–388.
10 S. Wang and W. S. El-Deiry, *Oncogene*, 2003, **22**, 8628–8633.
11 J. E. Aubin, *J. Bone Miner. Res.*, 1992, **7**, 365–368.
12 R. Detsch, D. Hagmeyer, M. Neumann, S. Schaefer, A. Vortkamp, M. Wuelling, G. Ziegler and M. T. Epple, *Acta Biomater.*, 2010, **6**, 3223–3233.
13 A. Qin, T. S. Cheng, N. J. Pavlos, Z. Lin, K. R. Dai and M. H. Zheng, *Int. J. Biochem. Cell Biol.*, 2012, **44**, 1422–1435.
14 H. K. Väänänen, Y. K. Liu, P. Lehenkari and T. Uemara, *Mater. Sci. Eng., C*, 1998, **6**, 205–209.
15 H. C. Blair, S. L. Teitelbaum, R. Ghiselli and S. Gluck, *Science*, 1989, **245**, 855–857.
16 H. C. Blair and N. A. Athanasou, *Histol. Histopathol.*, 2004, **19**, 189–199.
17 S. L. Teitelbaum, *Science*, 2000, **289**, 1504–1508.
18 H. Namkung-Matthai, R. Appleyard, J. Jansen, H. Lin, S. Maastricht, M. Swain, R. S. Mason, G. A. Murrell, A. D. Diwan and T. Diamond, *Bone*, 2001, **28**, 80–86.
19 D. Arcos, A. R. Boccaccini, M. Bohner, A. Díez-Pérez, M. Epple, E. Gómez-Barrena, A. Herrera, J. A. Planell, L. Rodríguez-Mañas and M. Vallet-Regí, *Acta Biomater.*, 2014, **10**, 1793–1805.
20 I. R. Gibson, S. M. Best and W. Bonfield, *J. Biomed. Mater. Res.*, 1999, **44**, 422–428.
21 N. Patel, S. M. Best, W. Bonfield, I. R. Gibson, K. A. Hing, E. Damien and P. A. Revell, *J. Mater. Sci.: Mater. Med.*, 2002, **13**, 1199–1206.
22 M. Vallet-Regí and D. Arcos, *J. Mater. Chem.*, 2005, **15**, 1509–1516.
23 A. E. Porter, N. Patel, J. N. Skepper, S. M. Best and W. Bonfield, *Biomaterials*, 2003, **24**, 4609–4620.
24 M. C. Matesanz, M. J. Feito, C. Ramírez-Santillán, R. M. Lozano, S. Sánchez-Salcedo, D. Arcos, M. Vallet-Regí and M. T. Portolés, *Macromol. Biosci.*, 2012, **12**, 446–453.
25 A. Balamurugan, A. H. Rebelo, A. F. Lemos, J. H. Rocha, J. M. Ventura and J. M. Ferreira, *Dent. Mater.*, 2008, **24**, 1374–1380.
26 D. Arcos, J. Rodríguez-Carvajal and M. Vallet-Regí, *Chem. Mater.*, 2004, **16**, 2300–2308.
27 E. M. Carlisle, *Calcif. Tissue Int.*, 1981, **33**, 27–34.
28 E. S. Thian, Z. Ahmad, J. Huang, M. J. Edirisinghe, S. N. Jayasinghe, D. C. Ireland, R. A. Brooks, N. Rushton, W. Bonfield and S. M. Best, *Acta Biomater.*, 2010, **6**, 750–755.
29 S. V. Dorozhkin, *Materials*, 2009, **2**, 1975–2045.
30 M. Fini, G. Giavaresi, P. Torricelli, V. Borsaria, R. Giardino, A. Nicolini and A. Carpi, *Biomed. Pharmacother.*, 2004, **58**, 487–493.
31 C. M. Botelho, R. A. Brooks, S. M. Best, M. A. Lopes, J. D. Santos, N. Rushton and W. Bonfield, *J. Biomed. Mater. Res., Part A*, 2006, **79**, 723–730.
32 H. Marques da Silva, M. Mateescu, C. Damia, E. Champion, G. Soares and K. Anselme, *Colloids Surf., B*, 2010, **80**, 138–144.
33 M. Honda, K. Kikushima, Y. Kawanobe, T. Konishi, M. Mizumoo and M. Aizawa, *J. Mater. Sci.: Mater. Med.*, 2012, **23**, 2923–2932.
34 C. M. Botelho, R. A. Brooks, G. Spence, I. McFarlane, M. A. Lopes, S. M. Best, J. D. Santos, N. Rushton and W. Bonfield, *J. Biomed. Mater. Res., Part A*, 2006, **78**, 709–720.
35 G. Lehmann, I. Cacciotti, P. Palmero, L. Montanaro, A. Bianco, L. Campagnolo and A. Camaioni, *Biomed. Mater.*, 2012, **7**, 055001.
36 E. S. Thian, J. Huang, S. M. Best, Z. H. Barber, R. A. Brooks, N. Rushton and W. Bonfield, *Biomaterials*, 2006, **27**, 2692–2698.

37 C. E. Jacome-Galarza, S. K. Lee, J. A. Lorenzo and H. L. Aguila, *J. Bone Miner. Res.*, 2013, **28**, 1203–1213.
38 B. N. Brown, B. D. Ratner, S. B. Goodman, S. Amar and S. F. Badylak, *Biomaterials*, 2012, **33**, 3792–3802.
39 P. M. Kou and J. E. Babensee, *J. Biomed. Mater. Res., Part A*, 2011, **96**, 239–260.
40 S. Franz, S. Rammelt, D. Scharnweber and J. C. Simon, *Biomaterials*, 2011, **32**, 6692–6709.
41 G. R. Beck, S. W. Ha, C. E. Camalier, M. Yamaguchi, Y. Li, J. K. Lee and M. N. Weitzman, *Nanomedicine: Nanotechnology, Biology and Medicine*, 2012, **8**, 793–803.
42 A. M. Pietak, J. M. Reid, M. J. Stott and M. Sayer, *Biomaterials*, 2007, **28**, 4023–4032.
43 M. Bohner, *Biomaterials*, 2009, **30**, 6403–6406.
44 O. Tsigkou, J. R. Jones, J. M. Polak and M. M. Stevens, *Biomaterials*, 2009, **30**, 3542–3550.
45 D. M. Reffitt, N. Ogston, R. Jugdaohsingh, H. F. Cheung, B. A. Evans, R. P. Thompson, J. J. Powell and G. N. Hampson, *Bone*, 2003, **32**, 127–135.
46 M. Wiens, X. Wang, H. C. Schroder, U. Kolb, U. Schlossmacher, H. Ushijima and W. E. Müller, *Biomaterials*, 2010, **31**, 7716–7725.
47 S. Zou, D. Ireland, R. A. Brooks, N. Rushton and S. Best, *J. Biomed. Mater. Res., Part B*, 2009, **90**, 123–130.
48 M. J. Feito, R. M. Lozano, M. Alcaide, C. Ramírez-Santillán, D. Arcos, M. Vallet-Regí and M. T. Portolés, *J. Mater. Sci.: Mater. Med.*, 2011, **22**, 405–416.
49 C. Albrecht, A. M. Scherbart, D. van Berlo, C. M. Braunbarth, R. P. Schins and J. Scheel, *Toxicol. In Vitro*, 2009, **23**, 520530.
50 H. Hotokezaka, E. Sakai, K. Kanaoka, K. Saito, K. Matsuo, H. Kitaura and N. Yoshida, *J. Biol. Chem.*, 2002, **277**, 47366–47372.
51 G. Spence, N. Patel, R. Brooks and N. Rushton, *J. Biomed. Mater. Res., Part A*, 2009, **90**, 217–224.
52 Z. Mladenović, A. Johansson, B. Willman, K. Shahabi, E. Björn and M. Ransjö, *Acta Biomater.*, 2014, **10**, 406–418.
53 M. C. Matesanz, M. J. Feito, M. Oñaderra, C. Ramírez-Santillán, C. da Cas, D. Arcos, M. Vallet-Regí, J. M. Rojo and M. T. Portolés, *J. Colloid Interface Sci.*, 2014, **416**, 59–66.
54 M. S. Kim, Y. M. Yang, A. Son, Y. S. Tian, S. I. Lee, S. W. Kang, S. Muallem and D. M. Shin, *J. Biol. Chem.*, 2010, **285**, 6913–6921.
55 X. He, G. Andersson, U. Lindgren and Y. Li, *Biochem. Biophys. Res. Commun.*, 2010, **401**, 356–362.
56 S. Srinivasan, A. Koenigstein, J. Joseph, L. Sun, B. Kalyanaraman, M. Zaidi and N. G. Avadhani, *Ann. N. Y. Acad. Sci.*, 2010, **1192**, 245–252.
57 S. Y. Hwang and J. W. Putney Jr, *Biochim. Biophys. Acta*, 2011, **1813**, 979–983.
58 H. Kitaura, N. Nagata, Y. Fujimura, H. Hotokezaka, M. Tatamiya, N. Nakao, N. Yoshida and K. Nakayama, *Immunol. Lett.*, 2003, **88**, 193–198.
59 N. Rozen, S. Ish-Shalom, A. Rachmiel, H. Stein and D. Lewinson, *Bone*, 2000, **26**, 469–474.
60 S. Moon, I. E. Ahn, H. Jung, H. Yi, J. Kim, Y. Kim, S. K. Kwok, K. S. Park, J. K. Min, S. H. Park, H. Y. Kim and J. H. Ju, *Int. J. Mol. Med.*, 2013, **31**, 769–777.

REFERENCIAS DEL CAPÍTULO I

1. Arcos D, Vallet-Regí M. Bioceramics for drug delivery. Acta Materialia, 61(3):890-911, 2013.
2. Arcos D, Boccaccini AR, Bohner M, Díez-Pérez A, Epple M, Gómez-Barrena E, Herrera A, Planell JA, Rodríguez-Mañas L, Vallet-Regí M. The relevance of biomaterials to the prevention and treatment of osteoporosis. Acta Biomaterialia, 10(5):1793-1805, 2014.
3. Balamurugan A, Rebelo AHS, Lemos AF, Rocha JHG, Ventura JMG, Ferreira JMF. Suitability evaluation of sol-gel derived Si-substituted hydroxyapatite for dental and maxillofacial applications through *in vitro* osteoblasts response. Dental Materials, 24:1374-1380, 2008.
4. Beck BR, Snow CM. Bone health across the lifespan--exercising our options. Exercise and Sport Sciences Reviews, 31(3):117-122, 2003.
5. Brey EM, Uriel S, Greisler HP, McIntire LV. Therapeutic neovascularization: contributions from bioengineering. Tissue Engineering, 11(3-4):567-584, 2005.
6. Carlisle E. Si: an essential element for the chick. Science, 178:619-621, 1972.
7. Cech D. Prevention of osteoporosis: From infancy through older adulthood. Hong Kong Physiotherapy Journal 2012, 30:6-12.
8. Chan CK, Kumar TS, Liao S, Murugan R, Ngiam M, Ramakrishnan S. Biomimetic nanocomposites for bone graft applications. Nanomedicine London, 1(2):177-188, 2006.
9. Chan R, Woo J, Leung J. Effects of food groups and dietary nutrients on bone loss in elderly Chinese population The Journal of Nutrition Health and Aging, 15(4):287-294, 2011.
10. Chen W, Zhou H, Weir MD, Tang M, Bao C, Xu HH. Human embryonic stem cell-derived mesenchymal stem cell seeding on calcium phosphate cement-chitosan-RGD scaffold for bone repair. Tissue Engineering Part A, 19(7-8):915-927, 2013.
11. Chesnut CH 3rd, Silverman S, Andriano K, Genant H, Gimona A, Harris S, Kiel D, LeBoff M, Maricic M, Miller P, Moniz C, Peacock M, Richardson P, Watts N, Baylink D. A randomized trial of nasal spray salmon calcitonin in postmenopausal women with established osteoporosis: the prevent recurrence of osteoporotic fractures study. PROOF Study Group. The American Journal of Medicine, 109(4):267-276, 2000.
12. Cranney A, Tugwell P, Zytaruk N, Robinson V, Weaver B, Adachi J, Wells G, Shea B, Guyatt G; Osteoporosis Methodology Group and The Osteoporosis Research Advisory Group. Meta-analyses of therapies for postmenopausal osteoporosis. IV. Meta-analysis of raloxifene for the prevention and treatment of postmenopausal osteoporosis. Endocrine Reviews, 23(4):524-528, 2002.

13. Dailey L, Ambrosetti D, Mansukhani A, Basilico C. Mechanisms underlying differential responses to FGF signalling. Cytokine and Growth Factors Reviews, 16(2):233-247, 2005.

14. DeBar LL, Ritenbaugh C, Aickin M, Orwoll E, Elliot D, Dickerson J, Vuckovic N, Stevens VJ, Moe E, Irving LM. Youth: a health plan-based lifestyle intervention increases bone mineral density in adolescent girls. Archives of Pediatrics and Adolescens Medicine, 160(12):1269-1276, 2006.

15. Dorozhkin SV. Nanodimensional and Nanocrystalline Apatites and Other Calcium Orthophosphates in Biomedical Engineering, Biology and Medicine. Materials, 2(4), 1975-2045, 2009.

16. Eastell R. Osteoporosis. Medicine 41(10):586-591, 2013.

17. Estrugo-Devesa A, Gómez-Vaquero C, López-López J. Osteoporosis y enfermedades orales. Medicina Clínica 140(4):169-174.

18. Feito MJ, Lozano RM, Alcaide M, Ramírez-Santillán C, Arcos D, Vallet-Regí M, Portolés MT. Immobilization and bioactivity evaluation of FGF-1 and FGF-2 on powdered silicon-doped hydroxyapatite and their scaffolds for bone tissue engineering. Journal of Materials Science: Materials in Medicine, (2):405-416, 2011.

19. Gates BJ, Sonnett TE, Duvall CA, Dobbins EK. Review of osteoporosis pharmacotherapy for geriatric patients. The American Journal of Geriatric Pharmacotherapy, 7(6):293-323, 2009.

20. Guerra-García MM, Rodríguez-Fernández JB, Puga-Sarmiento E, Charle-Crespo MÁ, Gomes-Carvalho CS, Prejigueiro-Santás A. [Incidence of hip fractures due to osteoporosis in relation to the prescription of drugs for their prevention and treatment in Galicia, Spain]. Atención Primaria, 43(2):82-88, 2011.

21. Heini PF, Berlemann U, Kaufmann M, Lippuner K, Fankhauser C, van Landuyt P. Augmentation of mechanical properties in osteoporotic vertebral bones--a biomechanical investigation of vertebroplasty efficacy with different bone cements. European Spine Journal, 10(2):164-171, 2001.

22. Hernlund E, Svedbom A, Ivergård M, Compston J, Cooper C, Stenmark J, McCloskey EV, Jönsson B, Kanis JA. Osteoporosis in the European Union: medical management, epidemiology and economic burden. A report prepared in collaboration with the International Osteoporosis Foundation (IOF) and the European Federation of Pharmaceutical Industry Associations (EFPIA). Archives of Osteoporosis, 8(1-2):136, 2013.

23. Hsu WL, Chen CY, Tsauo JY, Yang RS. Balance control in elderly people with osteoporosis. Journal of Formosan Medical Association, 113(6):334-339, 2014.

24. Ing-Lorenzini K, Desmeules J, Plachta O, Suva D, Dayer P, Peter R. Low-energy femoral fractures associated with the long-term use of bisphosphonates: a case series from a Swiss university hospital. Drug Safety, 32(9):775-785, 2009.

25. Jaye M, Schlessinger J, Dionne CA. Fibroblast growth factor receptor tyrosine kinases: molecular analysis and signal transduction. Biochimica et Biophysica Acta, 1135(2):185-199, 1992.

26. Jonca F, Ortéga N, Gleizes PE, Bertrand N, Plouët J. Cell release of bioactive fibroblast growth factor 2 by exon 6-encoded sequence of vascular endothelial growth factor. The Journal of Biological Chemistry, 272(39):24203-24209, 1997.

27. Khosla S, Riggs BL. Pathophysiology of age-related bone loss and osteoporosis. Endocrinology and Metabolism Clinics of North America, 34(4):1015-1030, 2005.

28. Kim HW, Kim HE, Salih V. Stimulation of osteoblast responses to biomimetic nanocomposites of gelatin-hydroxyapatite for tissue engineering scaffolds. Biomaterials, 26(25):5221-5230, 2005.

29. Kwong FN, Harris MB. Recent developments in the biology of fracture repair. Journal of the American Academy of Orthopaedic Surgeons, 16(11):619-625, 2008.

30. Layman H, Spiga MG, Brooks T, Pham S, Webster KA, Andreopoulos FM. The effect of the controlled release of basic fibroblast growth factor from ionic gelatin-based hydrogels on angiogenesis in a murine critical limb ischemic model. Biomaterials, 28(16):2646-2654, 2007.

31. Lehenkari PP, Kellinsalmi M, Näpänkangas JP, Ylitalo KV, Mönkkönen J, Rogers MJ, Azhayev A, Väänänen HK, Hassinen IE. Further insight into mechanism of action of clodronate: inhibition of mitochondrial ADP/ATP translocase by a nonhydrolyzable, adenine-containing metabolite. Molecular Pharmacology, 61(5):1255-1262, 2002.

32. Lenart BA, Neviaser AS, Lyman S, Chang CC, Edobor-Osula F, Steele B, van der Meulen MC, Lorich DG, Lane JM. Association of low-energy femoral fractures with prolonged bisphosphonate use: a case control study. Osteoporosis International, 20(8):1353-1362, 2009.

33. Lewandrowski KU, Bondre SP, Wise DL, Trantolo DJ. Enhanced bioactivity of a poly(propylene fumarate) bone graft substitute by augmentation with nano-hydroxyapatite. Bio-Medical Materials and Engineering, 13(2):115-124, 2003.

34. Lozano D, Sánchez-Salcedo S, Portal-Núñez S, Vila M, López-Herradón A, Ardura JA, Mulero F, Gómez-Barrena E, Vallet-Regí M, Esbrit P. Parathyroid hormone-related protein (107-111) improves the bone regeneration potential of gelatin-glutaraldehyde biopolymer-coated hydroxyapatite. Acta Biomaterialia, 10(7):3307-3316, 2014.

35. Mabilleau G, Aguado E, Stancu IC, Cincu C, Baslé MF, Chappard D. Effects of FGF-2 release from a hydrogel polymer on bone mass and microarchitecture. Biomaterials. 29(11):1593-1600, 2008.

36. Malkin I, Karasik D, Livshits G, Kobyliansky E. Modelling of age-related bone loss using cross-sectional data. Annals of Human Biology, 29(3):256-270, 2002.

37. Manzano M, Lozano D, Arcos D, Portal-Núñez S, Orden CL, Esbrit P, Vallet-Regí M. Comparison of the osteoblastic activity conferred on Si-doped hydroxyapatite scaffolds by different osteostatin coatings. Acta Biomaterialia, 7(10):3555-3562, 2011.

38. Manzano M, Vallet-Regí M. Revisiting bioceramics: Bone regenerative and local drug delivery systems. Progress in Solid State Chemistry, 40(3):17-30, 2012.

39. Marie PJ. Fibroblast growth factor signaling controlling bone formation: an update. Gene, 498(1):1-4, 2012.

40. Marini F, Brandi ML. Pharmacogenetics of osteoporosis. Best Practice and Research Clinical Endocrinology and Metabolism, 28(6):783-793, 2014.

41. Mastrogiacomo M, Muraglia A, Komlev V, Peryin F, Rustichelli F, Crovace A, Cancedda R. Tissue engineering of bone: search for a better scaffold. Orthodontics and Craniofacial Research, 8:277-284, 2005.

42. Mellibovsky L, Díez A. Qué significa la calidad ósea. Seminarios de la Fundación Nacional de Reumatología, 7(4):165,176, 2006.

43. Mikołajczyk T, Rabiej S, Boguń M. Analysis of the structural parameters of polyacrylonitrile fibers containing nanohydroxyapatite. Journal of Applied Polymer Science, 101(1):760-765, 2006.

44. Nakamura T, Hara Y, Tagawa M, Tamura M, Yuge T, Fukuda H, Nigi H. Recombinant human basic fibroblast growth factor accelerates fracture healing by enhancing callus remodeling in experimental dog tibial fracture. Journal of Bone and Mineral Research, 13(6):942-949, 1998.

45. Nanes MS, Kallen CB. Osteoporosis Seminars in Nuclear Medicine, 44(6):439-450, 2014.

46. Ojeda G, Ronda M, Ballester S, Díez-Orejas R, Feito MJ, García-Albert L, Rojo JM, Portolés P. A hyperreactive variant of a CD4+ T cell line is activated by syngeneic antigen presenting cells in the absence of antigen. Cellular Immunology, 164:265-278, 1995.

47. Ornitz DM, Marie PJ. FGF signaling pathways in endochondral and intramembranous bone development and human genetic disease. Genes & Development, 16(12):1446-1465, 2002.

48. Palin E, Liu H, Webster TJ. Mimicking the nanofeatures of bone increases bone-forming cell adhesion and proliferation. Nanotechnology, 16(9):1828-1835, 2005.

49. Pasco JA, Henry MJ, Korn S, Nicholson GC, Kotowicz MA. Morphometric vertebral fractures of the lower thoracic and lumbar spine, physical function and quality of life in men. Osteoporosis International, 20(5):787-792, 2009.

50. Pietak AM, Reid JW, Stott MJ, Sayer M. Silicon substitution in the calcium phosphate bioceramics. Biomaterials, 28:4023-4032, 2007.

51. Porter AE, Patel N, Skepper JN, Best SM, Bonfield W. Comparison of *in vivo* dissolution processes in hydroxyapatite and silicon-substituted hydroxyapatite bioceramics. Biomaterials, 24:4609-4620, 2003.

52. Porter AE, Patel, N, Skepper JN, Best SM, Bonfield W. Effect of sintered silicate silicate-substituted hydroxyapatite on remodelling processes at the bone-implant interface. Biomaterials, 25: 3303-3314, 2004.

53. Richards JB, Zheng HF, Spector TD. Genetics of osteoporosis from genome-wide association studies: advances and challenges. Nature Reviews Genetics 13:576-588, 2012.

54. Riggs BL, Melton Iii LJ 3rd, Robb RA, Camp JJ, Atkinson EJ, Peterson JM, Rouleau PA, McCollough CH, Bouxsein ML, Khosla S. Population-based study of age and sex differences in bone volumetric density, size, geometry, and structure at different skeletal sites. Journal of Bone and Mineral Research, 19(12):1945-1954, 2004.

55. Rogers MJ. New insights into the molecular mechanisms of action of bisphosphonates. Current Pharmaceutical Design, 9(32):2643-2658, 2003.

56. Sachse A, Wagner A, Keller M, Wagner O, Wetzel WD, Layher F, Venbrocks RA, Hortschansky P, Pietraszczyk M, Wiederanders B, Hempel HJ, Bossert J, Horn J, Schmuck K, Mollenhauer J. Osteointegration of hydroxyapatite-titanium implants coated with nonglycosylated recombinant human bone morphogenetic protein-2 (BMP-2) in aged sheep. Bone, 37(5):699-710, 2005.

57. Sato M, Webster TJ. Nanobiotechnology: implications for the future of nanotechnology in orthopedic applications. Expert Review of Medical Devices, 1(1):105-14, 2004.

58. Sato M, Sambito MA, Aslani A, Kalkhoran NM, Slamovich EB, Webster TJ. Increased osteoblast functions on undoped and yttrium-doped nanocrystalline hydroxyapatite coatings on titanium. Biomaterials, 27(11):2358-2369, 2006.

59. Schnettler R, Alt V, Dingeldein E, Pfefferle HJ, Kilian O, Meyer C, Heiss C, Wenisch S. Bone ingrowth in bFGF-coated hydroxyapatite ceramic implants. Biomaterials, 24(25):4603-4608, 2003.

60. Solomon KD, Ong JL. Vascular endothelial growth factor attachment to hydroxyapatite via self-assembled monolayers promotes angiogenic activity of endothelial cells. Thin Solid Films, 537:256-262, 2013.

61. Sumner DR, Turner TM, Urban RM, Leven RM, Hawkins M, Nichols EH, McPherson JM, Galante JO. Locally delivered rhTGF-beta2 enhances bone ingrowth and bone regeneration at local and remote sites of skeletal injury. Journal of Orthopaedic Research, 19(1):85-94, 2001.

62. Tella SH, Gallagher JC. Prevention and treatment of postmenopausal osteoporosis. The Journal of Steroid Biochemistry and Molecular Biology, 142:155-170, 2014.

63. Thian ES, Huang J, Best SM, Barber ZH, Brooks RA, Rushton N, Bonfield W. The response of osteoblasts to nanocrystalline silicon-substituted hydroxyapatite thin films. Biomaterials, 27:2692-2698, 2006.

64. Thian ES, Ahmad Z, Huang J, Edirisinghe MJ,Jayasinghe SN, Ireland DC, Brooks RA, Rushtond N, Bonfield W, Best SM. The role of surface wettability and surface charge of electrosprayed nanoapatites on the behaviour of osteoblasts. Acta Biomaterialia 6:750–755, 2010.

65. Trejo CG, Lozano D, Manzano M, Doadrio JC, Salinas AJ, Dapía S, Gómez-Barrena E, Vallet-Regí M, García-Honduvilla N, Buján J, Esbrit P. The osteoinductive properties of mesoporous silicate coated with osteostatin in a rabbit femur cavity defect model. Biomaterials, 31(33):8564-8573, 2010.

66. Tsurushima H, Marushima A, Suzuki K, Oyane A, Sogo Y, Nakamura K, Matsumura A, Ito A. Enhanced bone formation using hydroxyapatite ceramic coated with fibroblast growth factor-2. Acta Biomaterialia, 6(7):2751-2759, 2010.

67. Vallet-Regí M, Arcos D. Silicon substituted hydroxyapatites. A method to upgrade calcium phosphate based implants. Journal of Materials Chemistry, 15:1509-1516, 2005.

68. Vallet-Regí M. Biocerámicas: evolución y aplicaciones. Anales de la Real Sociedad Española de Química, 107(1):28-35, 2011.

69. Wang J, Shaw LL. Nanocrystalline hydroxyapatite with simultaneous enhancements in hardness and toughness. Biomaterials, 30(34):6565-6572, 2009.

70. Webster TJ, Ergun C, Doremus RH, Siegel RW, Bizios R. Specific proteins mediate enhanced osteoblast adhesion on nanophase ceramics. Journal of Biomedical Materials Research, 51(3):475-483, 2000.

71. Webster TJ, Ergun C, Doremus RH, Siegel RW, Bizios R. Enhanced osteoclast-like cell functions on nanophase ceramics. Biomaterials, 22(11):1327-1333, 2001.

72. Yang JH, Kim HJ, Kim SE, Yun YP, Bae JH, Kim SJ, Choi KH, Song HR. The effect of bone morphogenic protein-2-coated tri-calcium phosphate/hydroxyapatite on new bone formation in a rat model of femoral distraction osteogenesis. Cytotherapy, 14(3):315-326, 2012.

73. Yu L, Li Y, Zhao K, Tang Y, Cheng Z, Chen J, Zang Y, Wu J, Kong L, Liu S, Lei W, Wu Z. A novel injectable calcium phosphate cement-bioactive glass composite for bone regeneration. PLoS One, 8(4):e62570, 2013.

74. Zhou DS, Zhao KB, Li Y, Cui FZ, Lee IS. Repair of Segmental Defects with Nano-hydroxyapatite/Collagen/PLA Composite Combined with Mesenchymal Stem Cells. Journal of Bioactive and Compatible Polymers September, 21: 373-384, 2006.

Capítulo II

Nanopartículas de óxido de grafeno para tratamiento antitumoral por hipertermia

1. PROPIEDADES Y APLICACIONES BIOMÉDICAS DEL ÓXIDO DE GRAFENO

A pesar de su naturaleza anfipática, el óxido de grafeno (GO) presenta elevada hidrofilicidad debido al gran número de grupos hidroxilo, carboxilo y epóxido de su superficie (**Figura 4**), que hacen de este material el más relevante de su grupo de cara a posibles aplicaciones biomédicas, ya que aumentan su solubilidad, facilitando su manejo, y permiten la unión de diversas biomoléculas.

Las nanopartículas de óxido de grafeno (**nano-GO**), debido a su pequeño tamaño y dimensión lateral inferior a los 20 nm, presentan además la capacidad de introducirse en las células. A través de los grupos presentes en su superficie, las nano-GO pueden establecer numerosas **interacciones a nivel molecular**:

- *Adsorción de iones y moléculas de pequeño tamaño*: Gracias a su naturaleza anfipática, nano-GO y sus derivados funcionalizados son materiales adecuados para transportar diferentes moléculas en sistemas biológicos [*Cote LJ et al. 2011, Pure Appl Chem*]. La adsorción sobre su superficie se ve especialmente favorecida en moléculas de baja solubilidad, cierta hidrofobicidad o carga positiva y en moléculas con enlaces π que permiten establecer interacciones π-π con nano-GO. Esta característica puede dar lugar a la depleción de micronutrientes y a la presencia de artefactos en ensayos con sondas moleculares. Por otra parte, este tipo de interacciones hace posible cargar el nanomaterial con drogas de pequeño tamaño [*Yang X et al. 2011, J Mater Chem*] para la liberación controlada de fármacos [*Sánchez VC et al. 2012, Chem Res Toxicol*]. Estudios con doxorrubicina unida a nano-GO/PEG a través de interacciones π-π de apilamiento molecular mostraron la resorción del fármaco en el endosoma, donde el pH ácido vuelve a la molécula más hidrofílica y soluble [*Sun X et al. 2008, Nano Res*]. Iones metálicos como Mg^{2+} o Cu^{2+} pueden ser adsorbidos por GO y nano-GO por quelación [*Tung VC et al. 2009, Nat Nanotechnol; Yang ST et al. 2010, J Colloid Interface Sci; Ren H et al. 2010, ACS Nano*].

- *Interacciones con ácidos nucleicos:* La interacción se produce a través de las bases nitrogenadas mediante fuerzas hidrofóbicas e interacciones π-π de apilamiento [*Wu M et al. 2011, Langmuir*] que superan la repulsión electrostática producida por la carga negativa del ADN y del GO. Este tipo de interacción ocurre preferentemente en los ácidos nucleicos de cadena sencilla. Sin embargo, en los de doble cadena las bases quedan hacia el interior, dificultando la unión al material. Por otra parte, el nano-GO tiene la ventaja de proteger a los ácidos nucleicos de la acción de las nucleasas [*Lu CH et al. 2010, Chem Commun (Camb); Wang Y et al. 2010, J Am Chem Soc*]. Estas características hacen atractiva la utilización de GO como soporte para la liberación controlada de ácidos nucleicos y en biosensores, siendo especialmente interesante el

empleo de nano-GO por su mayor dispersibilidad, estabilidad coloidal, incorporación celular y menor toxicidad [*Sánchez VC et al. 2012, Chem Res Toxicol*]. Se ha descrito el intercalamiento de nano-GO entre los pares de bases del ADN gracias a su estructura plana, lo que permite el acercamiento de átomos de cobre unidos a los grupos carboxilo a zonas del ADN vulnerables para la escisión oxidativa [*Ren H et al. 2010, ACS Nano*].

- *Interacciones con proteínas:* La adsorción proteica parece mediar la incorporación celular y las respuestas tóxicas de los nanomateriales [*Nel AE et al. 2009, Nat*]. A diferencia del papel protector que muestra el material frente a las nucleasas, el nano-GO no impide la acción de las proteasas, debido posiblemente a la diferente geometría y conformación de las moléculas adsorbidas (ácidos nucléicos o proteínas). Por esta causa, se utiliza nano-GO para sensores de actividad proteasa (por ejemplo trombina), basados en la adsorción de péptidos marcados fluoresecentemente sobre este nanomaterial que actuan como sustrato de dicha actividad [*Zhang M et al. 2011, Chem Commun (Camb)*].

- *Reacciones oxidativas*: Estudios con glutatión, demuestran la actividad catalítica del GO para la reacción entre este antioxidante y el O_2, dependiente del área de superficie y del desorden estructural [*Liu X et al. 2011, Small*]. Esto demuestra la capacidad del GO para mediar el daño oxidativo en sistemas biológicos.

- *Degradación biológica*: Los nanomateriales de carbono como el GO se caracterizan por su resistencia a la degradación, lo que aumenta su persistencia en organismos vivos. Sin embargo, GP Kotchey et al. mostraron la susceptibilidad del GO de sufrir oxidaciones por peróxido de hidrógeno y peroxidasa de rábano [*Kotchey GP et al. 2011, ACS Nano*].

Las numerosas **aplicaciones biomédicas** propuestas para el óxido de grafeno pueden clasificarse de la siguiente manera:

- *Liberación de fármacos:* La gran superficie del material así como los grupos carboxilo e hidroxilo de su estructura permiten la unión de diversas moléculas insolubles en agua como fármacos antiinflamatorios o antitumorales por conjugación química o adsorción [*Shen H et al. 2012, Theranostics*]. Este tipo de fármacos menos hidrofílicos incrementan su solubilidad a pH ácido, por lo que se produce su liberación en los lisosomas celulares tras el proceso de endocitosis [*Sánchez VC et al. 2012, Chem Res Toxicol*].

Los primeros estudios *in vitro* de unión de fármacos antitumorales a nano-GO se llevaron a cabo con el inhibidor de la topoisomerasa I, SN-38, unido mediante interacciones no covalentes π-π. Esta combinación produjo una elevada citotoxicidad en células HCT-116 de carcinoma colorrectal humano, mil veces más potente que la obtenida con CPT-11 (camptotecina), un fármaco antitumoral soluble en agua aprobado por la FDA y utilizado en el

tratamiento del cáncer de colon [*Liu Z et al. 2008, J Am Chem Soc*]. Estudios con células humanas de linfoma de Burkitt Raji-B tratadas con GO al que se había unido covalentemente Rituxan (anticuerpo monoclonal frente a CD20, receptor expresado en las células B de este linfoma) o doxorrubicina por adsorción física, mostraron una mayor inhibición del crecimiento celular comparado con estos fármacos administrados de forma libre [*Sun X et al. 2008, Nano Res*]. Puesto que ciertas células tumorales expresan receptores de ácido fólico, recientemente se ha unido ácido fólico a GO en combinación con doxorrubicina y CPT-11 como posible tratamiento antitumoral. Al poner en contacto esta combinación con células humanas de cáncer de mama MCF-7 (que expresan receptores de ácido fólico) y con células epiteliales de adenocarcinoma alveolar A549 (sin estos receptores), el tratamiento fue más efectivo en las células MCF-7 [*Shen H et al. 2012, Theranostics*].

- *Vehículos para Terapia Génica:* El grafeno puede modificarse químicamente para permitir la unión y liberación controlada de secuencias génicas, protegiéndolas frente a la acción de nucleasas. La unión de polietilenimina (PEI, con grupos amino cargados positivamente) a óxido de grafeno permite la interacción electrostática con plásmidos de DNA para los procesos de transfección y expresión de los genes que contenga el plásmido. Estudios de transfección en células HeLa con el plásmido de la proteína verde fluorescente (EGFP) unido a GO-PEI muestran menor citotoxicidad y mayor eficacia en la expresión de dicha proteína respecto a PEI-EGFP libre de GO [*Feng L 2011, Nanoscale*]. En ensayos similares utilizando la secuencia génica de la luciferasa unida a GO-PEI, se observó también mayor eficacia de transfección que en ausencia de GO [*Chen B et al. 2011, J Mater Chem*].

La liberación de RNA de silenciamiento (siRNA) es otra interesante aplicación del GO con un gran potencial en Biomedicina. Estudios de L Zhang *et al*. muestran una excelente y efectiva liberación de doxorrubicina y de siRNA dirigido frente al oncogen Bcl-2, incrementando significativamente la citotoxicidad en células HeLa y produciendo un efecto sinérgico que aumenta la eficacia de este tratamiento antitumoral [*Zhang L et al. 2011, Small*].

- *Técnicas de bioimagen y biosensores:* El grafeno presenta fotoluminiscencia que puede ser utilizada para diferentes técnicas de bioimagen [*Chien et al 2012, Angew Chem Int Ed Engl*]. Recientemente, partículas de GO menores de 10 nm (*graphene quantum dots*) han comenzado a estudiarse por la fluorescencia intrínseca que exhiben [*Bacon M et al. 2014, Part Part Syst Charact*].

Varios tipos de grafeno han sido utilizados como biosensores para la detección de moléculas como la trombina, ATP, oligonucleótidos, aminoácidos y dopamina. Algunos de estos sensores se han desarrollado haciendo uso de la capacidad de *quenching* del grafeno para transferencia de energía por resonancia de fluorescencia. Por otro lado, se han ideado

nanoplataformas de grafeno para espectrometría de masas y secuenciación de DNA [*Shen H et al. 2012, Theranostics*]. Recientes estudios demuestran el potencial del GO como sensor para la detección temprana de cáncer [*Feng L et al. 2013, Adv Mater*].

- *Materiales antibacterianos:* Se han desarrollado con éxito algunos estudios que demuestran la actividad antimicrobiana del GO y del óxido de grafeno reducido (GOr) como los llevados a cabo por O Akhavan et al. Diferente actividad antibacteriana y citotoxicidad ha sido observada para GO y GOr en dependencia de las características físico-químicas de ambos y del modelo experimental utilizado. Debido a las propiedades de su membrana externa, las bacterias Gram negativas como *Escherichia coli* son más resistentes a nanopartículas de GO depositadas sobre acero inoxidable que las bacterias Gram positivas como *Staphylococcus aureus* [*Akhavan O et al. 2010, ACS Nano*].

- *Andamios para Ingeniería Tisular:* Ciertos estudios sobre grafeno están encaminados hacia su utilización como refuerzo en andamios para crecimiento celular con aplicación en Ingeniería Tisular. Películas de GO permiten la adhesión y el crecimiento de fibroblastos NIH-3T3 sobre su superficie sin causar toxicidad [*Ryoo SR et al. 2010, ACS Nano*]. Las combinaciones de grafeno/quitosano, con mejores propiedades mecánicas que el quitosano, han sido utilizadas para la fabricación de soportes que favorecen la proliferación de células madre mesenquimales humanas (hMSCs) estimulando su diferenciación hacia células óseas en presencia de factores osteogénicos [*Nayak et al. 2011, ACS Nano*]. Resultados similares se han obtenido con preosteoblastos murinos MC3T3-E1 que son capaces de adherirse y proliferar en mayor medida sobre andamios de GO/quitosano que sobre los de quitosano, llegando a colonizar el interior de los poros de dichos andamios [*Depan et al. 2011, Acta Biomater*]. Otros estudios con hidrogeles preparados con polivinilalcohol (PVA) a los que se les adiciona GO han mostrado una clara mejora de las propiedades mecánicas del material y ausencia de toxicidad en osteoblastos [*Zhang L et al. 2011, J Mater Chem*].

- *Terapia antitumoral por hipertermia:* Actualmente hay un amplio conocimiento de la Biología del cáncer y, con ello, grandes avances en la terapia antitumoral. Sin embargo, el éxito de los tratamientos actuales está limitado por la complejidad de los mecanismos de progresión del tumor y su vascularización, así como por la toxicidad y resistencia a los fármacos antitumorales, lo que hace indispensable el estudio de tratamientos alternativos a la quimioterapia y a la radioterapia. Recientemente, está cobrando gran importancia la utilización de nanopartículas con este fin, entre las que se encuentra el nano-GO.

Para que las nanopartículas puedan ser utilizadas con fines terapeúticos, son imprescindibles una serie de requisitos básicos como el transporte por el torrente sanguíneo hasta las células diana, la entrada a través de la membrana plasmática de las mismas, una rápida

filtración renal y el adecuado aclaramiento a través del sistema retículo-endotelial [*Hubbell JA et al. 2012, Science*]. Se requiere un tiempo de circulación en sangre suficiente para asegurar la liberación en los tejidos diana, para lo cual se puede aumentar la solubilidad del material mediante su funcionalización, ya sea no covalente con moléculas anfifílicas o covalente mediante oxidaciones y reacciones de cicloadición. Uno de los métodos de funcionalización del nano-GO más frecuentes es mediante la unión de PEG, que incrementa su dispersión y estabilidad en medio acuoso [*Sun X et al. 2008, Nano Res; Liu Z et al. 2008, J Am Chem Soc*]. De esta manera se puede incrementar el tiempo de circulación en sangre, aunque se reduce la interacción con superficies biológicas y, sumado al aumento de tamaño, puede disminuir la incorporación celular. Las células no fagocíticas internan nanopartículas de forma variable dependiendo del tipo celular y de las dimensiones de las mismas. Partículas entre 150 y 200 nm son generalmente endocitadas mediante receptores, mientras que escapan de la incorporación en macrófagos, ya que éstos fagocitan partículas de gran tamaño. Resultados recientes en nuestro grupo han mostrado la participación de diferentes mecanismos en la incorporación del nano-GO/PEG/FITC dependiendo del tipo celular analizado, destacando la macropinocitosis como mecanismo general de incorporación del material [*Linares J et al. 2014, ACS Appl Mater Interfaces,* ANEXO].

Uno de los acontecimientos esenciales para el desarrollo de un tumor es el estímulo de la angiogénesis. Cuando el tumor es suficientemente grande como para que las células que lo componen sufran hipoxia, se desencadenan mecanismos de respuesta que conducen a la síntesis de nuevos vasos. Esta nueva vasculatura es desordenada e irregular, con una mayor presión interna que da lugar a un flujo convectivo que, junto con la gran densidad intersticial de la estructura y la masa sólida que comprime los vasos, dificulta la difusión de fármacos al centro del tumor [*Chauhan VP et al. 2011, Annu Rev Chem Biomol Eng*]. Sin embargo, debido a este hecho, las nanopartículas tienen un mayor tiempo de retención, lo que se conoce como **efecto de permeabilidad y retención aumentada** (*enhanced permeability and retention effect* o efecto EPR) [*Gonçalves G et al. 2013, Adv Healthc Mater*]. Los estudios actuales combinan las características del efecto EPR con la unión de GO a péptidos o anticuerpos que actúan como ligandos de moléculas características de las células tumorales. Con esta estrategia las nanopartículas se dirigen específicamente al tumor, evitando efectos adversos en las células normales circundantes [*Day ES et al. 2009, J Biomed Eng*; *Gonçalves G et al. 2013, Adv Healthc Mater*].

La inyección de nano-GO funcionalizado con PEG y marcado fluorescentemente en ratones con tumores xenogénicos demostró acumulación del material en los tumores tras 24 horas de la administración, una baja incorporación en el sistema retículo-endotelial y ausencia

de toxicidad a corto plazo. El material se acumuló además en hígado y bazo, seguido de un aclaramiento gradual tras un periodo de 3-15 días. A los 3 meses de la administración de dosis de 20 mg/kg, el material había sido completamente eliminado [*Yang K et al. 2011, ACS Nano*]. Sin embargo, en estudios realizados *in vivo* en los que se inyectaron 0,4 mg de GO a ratones, se generaron granulomas en varios órganos llegando a causar la muerte en el 50% de los casos [*Wang K et al. 2011, Nanoscale Res Lett*]. En dicho estudio, dosis superiores a 50 μg/ml indujeron toxicidad *in vitro* en fibroblastos humanos. Sin embargo, dosis inferiores no provocaron alteraciones *in vivo* ni *in vitro*, mostrando que este efecto es dosis-dependiente. Otros estudios mostraron una toxicidad mínima a dosis de 50 μg/ml en diferentes tipos celulares con menor incorporación del material [*Chang Y et al. 2011, Toxicol Lett*].

En la actualidad están descritos casos de toxicidad por inhalación crónica de materiales no fibrosos y planos, de morfología similar al grafeno, aunque son todavía escasos los estudios sobre la toxicidad de este último. El grado de toxicidad pulmonar vendrá determinado por la orientación de la nanopartícula y la región en que se deposite, ya que en las regiones alveolares existen células mucosas ciliadas que reducen el tiempo de retención. Sin embargo, según se profundiza en el pulmón, el número de estas células disminuye y aumenta la proporción de macrófagos alveolares, haciendo que el tiempo de retención del material sea mayor [*Sánchez VC et al. 2012, Chem Res Toxicol*]. Los macrófagos alveolares cuando no pueden fagocitar el material se fusionan dando lugar a células gigantes para rodear al material y encapsularlo, pudiendo generarse granulomas [*Kunkel SL et al. 1998, Semin Respir Infect*].

Ensayos con células de mamífero muestran que las células diana de este material en el pulmón son los macrófagos alveolares, las células epiteliales y los fibroblastos [*Card JW et al. 2008, Am J Physiol Lung Cell Mol Physiol*]. Los resultados obtenidos demuestran que la toxicidad depende del tipo de material, de la dosis utilizada y del tipo celular.

Todos los estudios concluyen que la generación de especies reactivas de oxígeno (ROS) por parte de las células que entran en contacto con el material es el mecanismo principal desencadenante de la toxicidad del GO. En células neuronales se ha visto daño mitocondrial tras 4-24 horas de exposición a dosis de 10 μg/ml [*Zhang Y et al. 2010, ACS Nano*].

La modificación de la superficie del GO podría ser una herramienta para disminuir estos efectos negativos y conseguir una mayor eficacia en el tratamiento del tumor mediante la unión de fármacos, así como promover su degradación tras la eliminación de la droga.

El GO funcionalizado con PEG se ha propuesto como candidato para la *terapia antitumoral por hipertermia* debido a su capacidad para incorporarse en las células y a su absorción en el infrarrojo cercano (700-900 nm), rango de longitudes de onda de máxima penetración de manera no invasiva, conocido como **ventana terapéutica**, que ofrece la

posibilidad de tratar patologías sin dañar a las células sanas alrededor del tejido afectado [*Weissleder R 2001, Nat Biotechnol*]. Está descrito que, tras la administración de GO, con una radiación de 808 nm y 2 W/cm^2, se produce calentamiento y la ablación del tumor en ratones. Después de 90 días todo el material ha sido eliminado por el organismo [*Yang K et al. 2010, Nano Lett*]. A Sahu et al. llevaron a cabo estudios *in vitro* e *in vivo* con nano-GO recubierto de plurónico (etileno-propileno) y acomplejado con azul de metileno (fotosensibilizador cargado positivamente). En cultivos celulares se observó una mayor incorporación en las células tumorales que en las normales y mayor toxicidad en las células que internaron el nanomaterial al incidir con NIR. En ratones se detectó una gran acumulación de nano-GO en el tumor, produciéndose la ablación del mismo al irradiar con el láser [*Sahu A et al. 2013, Biomaterials*]. Por otra parte, recientemente se administró nano-GO combinado con ácido fólico a ratones con un tumor inducido, observándose mayor biodistribución en el tumor a medida que se incrementaba la dosis de ligando, acompañada de una disminución del tamaño del tumor más acusada tras la irradiación NIR [*Lee JH et al. 2015, J Control Release*]. Finalmente, en estudios con nano-GO funcionalizado con PEG unido mediante puentes disulfuro y cargado con doxorrubicina, se observó una mayor liberación del fármaco en células A549 que se veía favorecida con la irradiación NIR [*Xiong H et al. 2014, J Photochem Photobiol B*].

2. TUMORES ÓSEOS

El **osteosarcoma** es el tumor primario más común en hueso, tanto en niños como en adultos. Este tumor deriva de células mesenquimales dando lugar a una formación aberrante del osteoide [*Gill J et al. 2013, Pharmacol Ther*]. La gran mayoría de estos tumores son de alto grado de malignidad (80-90%), y a su vez pueden ser clasificados según el tipo celular alterado. Los más frecuentes son de tipo osteoblástico, condroblástico y fibroblástico [*Gorlick R, 2009, Cancer Treat Res*].

Los osteosarcomas también se pueden generar de forma secundaria como consecuencia de otras alteraciones preexistentes, como la enfermedad de Paget, o de la radioterapia [*Bielack S et al. 2009, Ann Oncol*].

La incidencia de esta enfermedad en la Unión Europea es de 0,2-3 casos de cada 100.000 por año, por lo que no se considera una patología frecuente en seres humanos [*Bielack S et al. 2009, Ann Oncol*]. Sin embargo, se encuentra entre los tipos de cáncer más comunes en adolescentes, solo superado por linfomas y tumores cerebrales. Presenta dos picos de distribución: el primero en la adolescencia y el segundo en torno a los 70-80 años de vida del

individuo. La aparición durante la adolescencia puede deberse a la alta tasa de proliferación de las células óseas durante el crecimiento [*Ottaviani G et al. 2009, Cancer Treat Res*]. La aparición de osteosarcoma en menores de 5 años es extremadamente baja, suponiendo el 1% de los enfermos de osteosarcoma [*Kager L et al. 2010, Cancer*]. Se ha establecido una mayor incidencia en individuos de sexo masculino (60%) [*Bielack S et al. 2009, Ann Oncol*]. La tasa de supervivencia a 5 años es del 68%, independientemente del sexo del paciente. Sin embargo, la edad sí es un factor determinante en la supervivencia, siendo ésta menor en pacientes adultos [*Ottaviani G et al. 2009, Cancer Treat Res*].

Aún cuando no existe un conocimiento claro sobre los factores que desencadenan este tumor, se han identificado dos genes cuya mutación parece estar implicada en la acumulación de defectos genéticos que finalmente desencadena el proceso tumoral: una mutación hereditaria del gen que codifica para retinoblastoma y una mutación autosómica recesiva de p53 [*Entz-Werle N et al. 2003, Br J Cancer*]. La mayor parte de estos tumores aparecen en la articulación de la rodilla incluyendo la parte distal del fémur (43%) o la parte proximal de la tibia (23%). La región proximal del húmero representa el 10% de los casos [*Bielack SS et al. 2002, J Clin Oncol*]. Dentro del hueso, esta patología suele desarrollarse en la metáfisis, próxima a la placa de crecimiento óseo [*Gill J et al. 2013, Pharmacol Ther*].

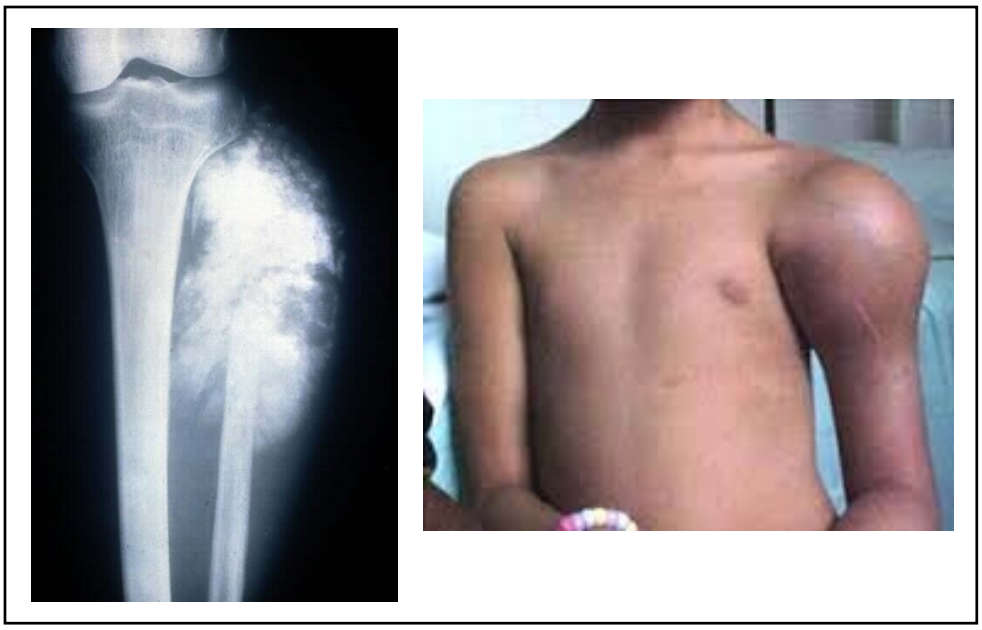

Figura 30. Radiografía de paciente de osteosarcoma en rodilla y foto de niño con tumor en el hombro. Imágenes procedentes de http://biospecimens.cancer.gov/meeting/brnsymposium/2011/Posters/Lana-508.pdf y http://www.illumina.com/documents/seminars/presentations/2009_06_mezazepeda_leonardo.pdf

El tratamiento más frecuente, antes de la aparición de la quimioterapia, consistía en la amputación del miembro afectado. Sin embargo, en la gran mayoría de los casos se desarrollaban metástasis durante el año posterior al diagnóstico [*Marcove RC et al. 1970, J Bone Joint Surg Am*], demostrando la existencia de éstas en el momento de la manifestación del proceso tumoral (15-20%). El 85% de las metástasis macroscópicas se originan en el pulmón, seguido de otras localizaciones óseas y en menor medida en nódulos linfáticos [*Bielack SS et al. 2002, J Clin Oncol*]. También existen una serie de micrometástasis que son difíciles de detectar por los métodos convencionales [*Bacci G et al. 2003, Ann Oncol*]. Incluso en los casos de osteosarcoma localizado, la tercera parte de los pacientes desarrollan tumores recurrentes en los 2-3 años posteriores [*Kempf-Bielack B et al. 2005, J Clin Oncol*].

A partir de los años 80 fue validado el efecto beneficioso de fármacos quimioterapéuticos por el *Multi-Institutional Osteosarcoma Study* (MIOS), estudio en el que de forma aleatoria se aplicó a pacientes de osteosarcoma un tratamiento de quimioterapia, posterior a la amputación localizada. Estos pacientes mostraban un claro aumento en su supervivencia a los dos años (66%) respecto a aquellos que solo habían sufrido la intervención quirúrgica (17%) [*Link MP et al. 1986, N Engl J Med*]. Hoy en día, se administra la quimioterapia en dos fases: qumioterapia neo-adyuvante pre-operatoria (unas 10-12 semanas anterior a la intervención quirúrgica) y adyuvante post-operatoria (durante unas 12-29 semanas) [*Gill J et al. 2013, Pharmacol Ther*]. En la actualidad, existen principalmente varios agentes quimioterapéuticos en el tratamiento de osteosarcoma: metotrexato a altas dosis con leucovorin, doxorrubicina, cisplatina e ifosfamida [*Ferrari S et al. 2007, Curr Opin Oncol*]. Independientemente de la quimioterapia, es necesaria la cirugía para la completa curación del tumor. Sin embargo, se recurre a la cirugía conservativa en la mayoría de los casos y se evita la amputación [*Luetke A et al. 2014, Cancer Treat Rev*].

Los tumores óseos se consideran resistentes a radioterapia. Sin embargo, este tratamiento es utilizado cuando se trata de tumores que no pueden someterse a la cirugía. En esos casos, se ha comprobado que ciertos agentes quimioterapéuticos como la ifosfamida o la cisplatina aumentan la efectividad de la radioterapia local [*Errani C et al. 2011, Expert Rev Anticancer* Ther]. Sin embargo, se debe tener en cuenta que este tipo de fármacos causan en muchos casos toxicidad a corto y a largo plazo [*Hattinger CM et al. 2010, Expert Opin Emerg Drugs*], produciendo alopecia, inmunosupresión, náuseas, vómitos e incluso la muerte, como se ha descrito en algunos casos de tratamiento con doxorrubicina [*Muñoz A et al. 2009, Clin Transl Oncol*]. Debido a los problemas que puede ocasionar la terapia antitumoral convencional, otros tratamientos como la quimioembolización, angioembolización, crioterapia, ablación por radiofrecuencia y ablación térmica, están siendo considerados [*Errani C et al. 2011, Expert Rev*

Anticancer Ther]. Entre estas posibles alternativas, la terapia antitumoral por fototermia presenta un amplio potencial y, por este motivo, se encuentra actualmente en fase de estudio. Gracias a la capacidad de las nanopartículas de óxido de grafeno (nano-GO) para absorber radiación infrarroja cercana (NIR) y el efecto EPR previamente comentado, este nanomaterial posee un gran potencial para su posible aplicación en el campo de la Biomedicina.

OBJETIVOS

1. Evaluación *in vitro* de la cinética de incorporación de nanopartículas de óxido de grafeno funcionalizadas con polietilenglicol y marcadas con isotiocianato de fluoresceína (nano-GO/PEG/FITC) en diferentes tipos celulares.
2. Análisis de la biocompatibilidad *in vitro* de nano-GO y de su localización intracelular.
3. Estudio del efecto de la hipertermia inducida por nano-GO sobre la línea celular de osteosarcoma humano Saos-2 y evaluación de las condiciones de tiempo y potencia de exposición a luz NIR para el control de la muerte celular.

OBJECTIVES

1. *In vitro* evaluation of the incorporation kinetics of graphene oxide nanoparticles functionalized with poly(ethylene glycol) and labeled with fluorescein isothiocyanate (nano-GO/PEG/FITC) in different cell types.
2. Analysis of the *in vitro* biocompatibility and intracellular localization of nano-GO.
3. Study of the nano-GO induced hyperthermia effect on the human osteosarcoma-derived cell line Saos-2 and evaluation of the NIR exposure conditions (time and power) to control cell death.

RESULTADOS

El uso de nanopartículas para inducir hipertermia como terapia antitumoral alternativa a la quimioterapia y radioterapia está siendo ampliamente estudiado en los últimos años. Las nanopartículas de óxido de grafeno (nano-GO) presentan gran potencial para su aplicación biomédica en este campo debido a las propiedades únicas de su estructura, especialmente por su capacidad de absorber radiación infrarroja cercana (808 nm) generando energía vibracional y, como consecuencia, provocar un aumento de temperatura de forma local. La ausencia de cromóforos que absorban a esta longitud de onda en la mayoría de sistemas biológicos permite inducir la muerte selectiva de las células tumorales tras la incorporación de nano-GO, sin causar daño en las células sanas adyacentes (ventana terapéutica). Esta propiedad unida a su forma bidimensional, tamaño nanométrico y excelentes propiedades mecánicas y eléctricas hacen al nano-GO un nanomaterial único para este tipo de tratamiento.

En la presente Tesis Doctoral se han utilizado nanopartículas de óxido de grafeno funcionalizadas con polietilenglicol y marcadas con isotiocianato de fluoresceína (nano-GO/PEG/FITC) con el objetivo de evaluar *in vitro* su cinética de incorporación en diferentes tipos celulares, su biocompatibilidad y localización intracelular, así como para inducir hipertermia sobre la línea celular de osteosarcoma humano Saos-2. La síntesis y caracterización del material han sido previamente desarrolladas por el Departamento de Química Inorgánica y Bioinorgánica de la Universidad Complutense de Madrid en colaboración con el TEMA-Mechanical Engineering Department de la Universidad de Aveiro (Portugal). El aprendizaje de estos procesos por María de la Concepción Matesanz Sancho ha sido realizado bajo la supervisión de la Dra. Mercedes Vila durante la estancia predoctoral en la Universidad de Aveiro (3 meses) y las características de estos métodos se detallan a continuación.

- Síntesis y caracterización de nano-GO/PEG/FITC

La **obtención** de nano-GO se llevó a cabo a partir de la exfoliación de grafito de alta pureza mediante el método de Hummers modificado [*Gonçalves G et al. 2009, Chem Mater*; *Marcano DC et al. 2010, ACS Nano*]. Brevemente, se mezclan 5 g de grafito y 3,8 g de $NaNO_3$ en un soporte sumergido en hielo, añadiendo a continuación 169 ml de H_2SO_4 y agitando hasta alcanzar la homogeneidad. Gradualmente se añaden 22,5 g de $KMnO_4$ mientras la mezcla se mantiene en agitación y sumergida en hielo. Tras dos horas se retira del hielo y se deja en agitación 5-7 días para que tenga lugar el proceso de oxidación. La mezcla resultante se añade a 500 ml de una solución de 5wt% H_2SO_4 durante una hora mientras está siendo continuamente

agitada. Tras dos horas de agitación se añade a la mezcla 30wt% H_2O_2 y se deja en agitación otras dos horas.

La **purificación** se lleva a cabo mediante dispersión y precipitación por adición de 500 ml de solución acuosa 3wt% H_2SO_4 y 0,5%wt% H_2O_2. Tras repetidos procesos de filtración y eliminación del sobrenadante (unas diez veces) se dispersan 0,5 ml de la mezcla en 500 ml de agua desionizada y se ultrasónica para separar las diferentes capas, obteniéndose una suspensión de GO exfoliado. Finalmente, se procede a la liofilización del material.

A continuación se procede a la **activación** del GO. Para ello se suspenden 50 mg de GO por cada 12,5 ml de H_2O y se sónica durante 45 minutos. A esta solución se le adiciona NaOH (2,5 mg en 37,5 ml de H_2O) y, sobre esta mezcla, 2,5 g de $ClCH_2COOH$. Se deja la mezcla en un baño de ultrasonidos durante 3 horas. Al finalizar la sonicación se procede a la eliminación de sales mediante centrifugación, previa adición de HCl para recuperar el pH anterior a la adición de NaOH (pH 5,2).

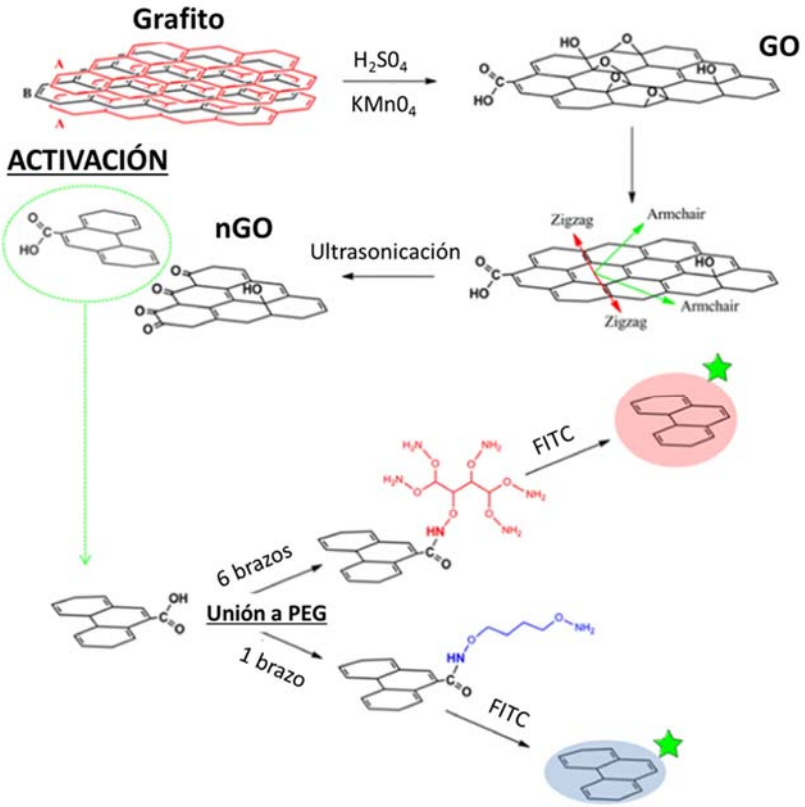

Figura 31. Esquema de la síntesis de óxido de grafeno. Esquema procedente de Vila et al. (Nanotechnology 23: 465103(9pp), 2012).

Una vez que el GO está activo se realiza la funcionalización con PEG para evitar agregados de las nanopartículas y para la posterior unión de otras moléculas. Para ello se hace reaccionar con 1-etil-3-(3-dimetilaminopropil)carbodiimida) (EDAC) de manera que por cada 50

mg de GO (disueltos en 40 ml de agua miliQ) se adicionan 0,11 g de EDAC (disueltos en 5 ml de agua miliQ). Tras 3 horas de agitación vigorosa se añade la mezcla a 0,83 g de PEG previamente disueltos en 25 ml de agua miliQ y se deja en agitación durante 48 horas a temperatura ambiente. A continuación de este proceso se procede a los correspondientes lavados y centrifugaciones para eliminar el exceso de reactivo.

Gracias a la unión de PEG a las nanopartículas de óxido de grafeno se puede proceder al **marcaje fluorescente** del material con moléculas como el FITC que permiten realizar el seguimiento del material en los estudios celulares. Para ello, se redispersan 100 mg de GO-PEG y 20 mg de FITC en 200 ml de tampón fosfato y se deja en agitación durante una noche. Al igual que en el proceso de unión del PEG, se debe proceder a numerosos lavados para eliminar el exceso de FITC. Terminado el proceso de síntesis, se puede liofilizar el material para su mejor conservación hasta su utilización.

Cualquier biomaterial que va a ser utilizado con un fin terapéutico debe presentar reproducibilidad en su proceso de síntesis, por lo que es necesaria la **caracterización** y comprobación de las propiedades del material obtenido.

Técnicas frecuentemente utilizadas en el proceso de caracterización son la Dispersión dinámica de luz (DLS), el potencial Z y la Espectrofotometría Infrarroja por Transformada de Fourier (FTIR).

La técnica de DLS permite obtener un perfil de distribución del tamaño hidrodinámico de las nanopartículas de estudio, en este caso nano-GO, mediante la medida de la dispersión de un haz de luz monocromática incidente, analizada por un programa informático como Zetasizer. Según se avanza en el proceso de síntesis el tamaño de partícula va disminuyendo debido a los procesos de sonicación, con la excepción del GO-PEG que debido a la unión de éste último, da lugar a un aumento del nanosistema. La distribución de tamaños que se suele obtener una vez unido el PEG oscila entre 10 y 120 nm, encontrándose la mayoría de las nanopartículas alrededor de los 40 nm.

Otra medida de caracterización del material es el potencial Z que nos indica la carga superficial del material y se calcula como la diferencia de potencial entre el medio de dispersión y la capa estacionaria de fluido unido a la partícula dispersada. La importancia de este parámetro está en su relación con la estabilidad de las dispersiones coloidales, ya que un alto potencial zeta para moléculas y partículas pequeñas implica estabilidad al no tender a la agregación. Por tanto, puede dar idea del grado de repulsión entre partículas adyacentes, cargadas de manera similar en una dispersión. Por el contrario, valores bajos de potencial zeta indican un posible proceso de floculación. En nuestro caso se obtuvieron valores negativos de potencial zeta debido a las

cargas de los grupos carboxilo e hidroxilo. Con la unión de PEG el potencial zeta se hace menos negativo al estar presentes en la nanopartícula grupos amino.

Los datos obtenidos en la presente estancia se muestran a continuación en la **Tabla 1**:

Tabla 1. Tamaño y Potencial Zeta de GO, GO-COOH, GO-PEG y GO-PEG-FITC

	GO	**GO-COOH**	**GO-PEG**	**GO-PEG-FITC**
Size (nm)	243,87±1,96	153,77±1,04	396,23±3,93*	392,40±15,52*
Potencial Zeta (mV)	-40,47±0,64	-38,7±0,89	-34,03±0,42	-23,87±1,07

*Los datos de tamaño de nanopartícula son más grandes que los que habitualmente se obtienen

La espectroscopía FTIR se ha utilizado para obtener un espectro infrarrojo de absorción del nano-GO. La técnica se denomina así debido a la transformada de Fourier que se requiere para convertir los datos brutos en el espectro real. Esta técnica permite identificar los grupos funcionales de un material ya que cada uno vibra en una frecuencia determinada conocida, dando lugar a un espectro con la información de los elementos que lo componen. Las moléculas que reaccionan con IR siempre presentan el mismo pico distintivo de energía, de modo que pueden ser fácilmente identificadas a partir de la gráfica.

Los resultados mostraron grupos funcionales de oxígeno en la superficie del nano-GO además de un alargamiento de la banda de vibración C-O (1100-1150 cm^{-1}) y una contribución de C-H (2800 cm^{-1}), que indica claramente la presencia de PEG unido a la nanopartícula de GO.

Con el objetivo de evaluar *in vitro* la cinética de incorporación de nano-GO/PEG/FITC en diferentes tipos celulares, fibroblastos murinos L929, osteoblastos humanos Saos-2, preosteoblastos murinos MC3T3-E1 y macrófagos murinos RAW 264.7 fueron cultivados durante varios tiempos en presencia de 0,075 mg/ml de este material funcionalizado de forma lineal (nano-1-GO con un brazo de PEG) o ramificada (nano-6-GO con seis brazos de PEG). La incorporación de nano-1-GO y nano-6-GO fue analizada comparativamente para conocer los efectos que las diferencias de carga de estas nanopartículas pueden producir en su incorporación celular.

Los resultados obtenidos se resumen a continuación y han dado lugar a la siguiente publicación.

- Vila M, Portolés MT, Marques PAAP, Feito MJ, Matesanz MC, Ramírez-Santillán C, Gonçalves G, Cruz SMA, Nieto-Peña A, Vallet-Regi M. Cell uptake survey of pegylated nano graphene oxide. Nanotechnology, 23: 465103(9pp), 2012.

Mediante la caracterización del material se observó una distribución de tamaño hidrodinámico entre 10 y 120 nm, con el máximo número de partículas localizado alrededor de los 40 nm. El análisis por Microscopía de Fuerza Atómica (AFM) mostró un grosor de las nanopartículas de unos 2 nm, correspondiente a 3 ó 4 capas de nano-GO (**Figura 32**).

El potencial Z fue -37,8 ± 8 mV para nano-GO activado sin PEG, -30,5 ± 3 mV para nano-1-GO y -8,05 ± 4 mV para nano-6-GO. Estos resultados demostraron que la funcionalización con PEG disminuye la carga negativa de las nanopartículas.

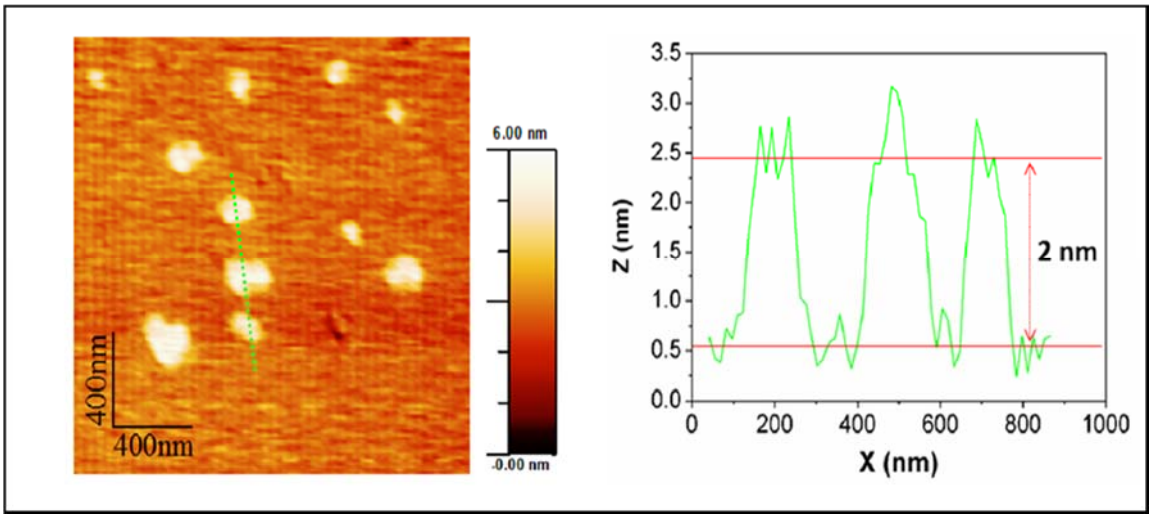

Figura 32. Caracterización de nano-GO por AFM. Imágenes procedentes de [*Matesanz MC et al. 2013, Biomaterials*].

La cantidad de nano-GO internado por fibroblastos murinos L929, osteoblastos humanos Saos-2, preosteoblastos murinos MC3T3-E1 y macrófagos murinos RAW 264.7 fue detectada mediante citometría de flujo, observándose que el grado y la velocidad de incorporación dependen del tipo celular. Estudios de quenching con Trypan Blue demostraron que el nanomaterial no se encontraba adsorbido en la superficie de las células sino que fue internado en todos los casos. Las células de linaje osteoblástico presentaron el mayor grado de incorporación, mientras que con fibroblastos y macrófagos se obtuvieron niveles menores de captación del material (**Figura 33**), estabilizándose a las 24 horas en todos los casos. La línea de osteosarcoma humano Saos-2 presentó mayor incorporación que la de preosteoblastos MC3T3-E1 de ratón. Este resultado sugiere que mediante el control del tiempo de incorporación y la posterior irradiación del material *in vivo*, se podría afectar principalmente a las células tumorales produciendo menores efectos en las células sanas adyacentes.

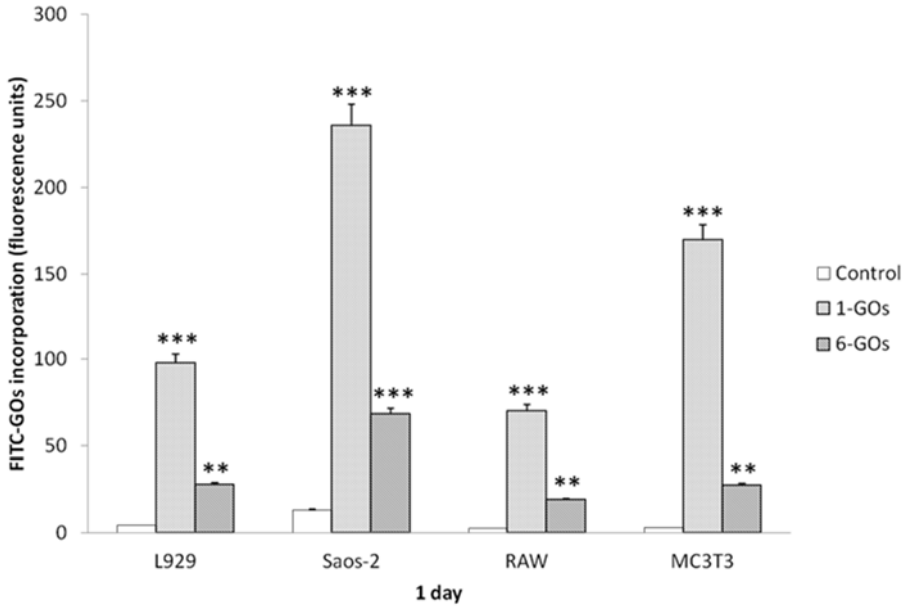

Figura 33. Incorporación de nano-1-GO y nano-6-GO en fibroblastos L929, osteoblastos Saos-2, macrófagos RAW 264.7 y preosteoblastos MC3T3-E1. Imágenes procedentes de [*Vila M et al. 2012, Nanotechnology*].

Al estudiar la influencia de la carga de la superficie y del tamaño de partícula en la internación del material con nano-1-GO y nano-6-GO, se observó que en todos los tipos celulares analizados la incorporación de nano-1-GO es significativamente superior que con nano-6-GO a pesar de que el mayor número de ramificaciones implica una carga menos negativa (**Figura 33**). Esto parece deberse al mayor número de ramificaciones de PEG del nano-6-GO, demostrando que es el tamaño y no la carga el factor determinante para la incorporación de estas nanopartículas.

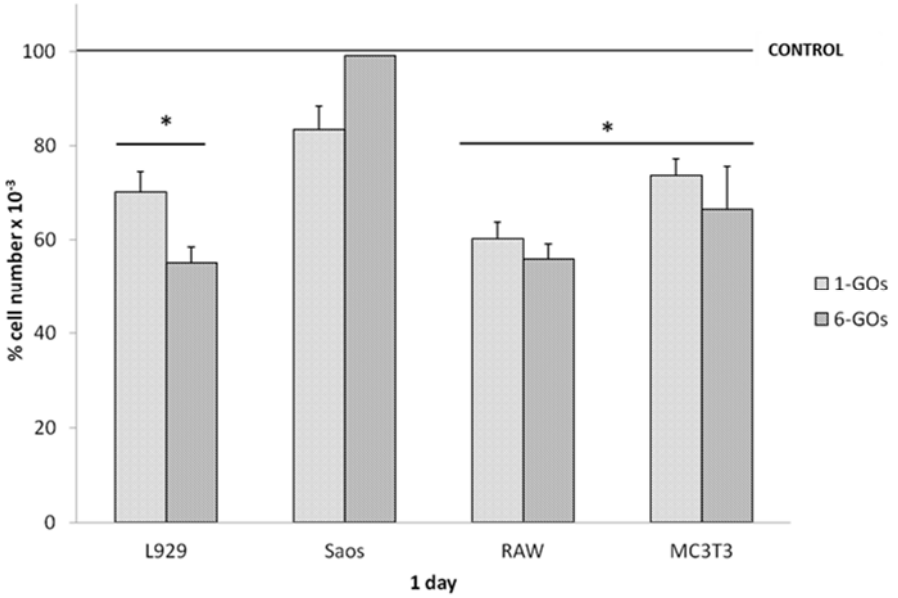

Figura 34. Porcentaje de proliferación de fibroblastos L929, osteoblastos Saos-2, macrófagos RAW 264.7 y preosteoblastos MC3T3-E1 cultivados en presencia de nano-1-GO y nano-6-GO respecto a sus respectivas células control. Imágenes procedentes de [*Vila M et al. 2012, Nanotechnology*].

Las células fueron capaces de proliferar en contacto con ambos nanomateriales, aunque presentaron cierto retraso respecto al control excepto en el caso de Saos-2 tratados con nano-6-GO (**Figura 34**). A pesar de la menor incorporación de nano-6-GO, se obtuvieron efectos similares para los dos materiales sobre los parámetros de biocompatibilidad analizados, indicando mayor toxicidad de 6-GOs sobre la función celular.

Estos estudios demuestran que la incorporación de nano-GO depende de la funcionalización del material y del tipo celular, observándose valores superiores de internación con nano-1-GO en células óseas, especialmente en las procedentes de osteosarcoma humano.

Nanotechnology **23** (2012) 465103 (9pp) doi:10.1088/0957-4484/23/46/465103

Cell uptake survey of pegylated nanographene oxide

M Vila[1,2], M T Portolés[3], P A A P Marques[4], M J Feito[3], M C Matesanz[3], C Ramírez-Santillán[3], G Gonçalves[4], S M A Cruz[4], A Nieto[1,2] and M Vallet-Regi[1,2]

[1] Inorganic and Bioinorganic Chemistry Department, Universidad Complutense de Madrid, 28040, Spain
[2] Centro de Investigación Biomédica en Red. Bioingeniería, Biomateriales y Nanomedicina, CIBER-BBN, Spain
[3] Department of Biochemistry and Molecular Biology I, Universidad Complutense Madrid, 28040, Spain
[4] TEMA-NRD, Mechanical Engineering Department, University of Aveiro, 3810-193 Aveiro, Portugal

E-mail: mvila@farm.ucm.es

Received 25 June 2012, in final form 7 September 2012
Published 23 October 2012
Online at stacks.iop.org/Nano/23/465103

Abstract
Graphene and more specifically, nanographene oxide (GO) has been proposed as a highly efficient antitumoral therapy agent. Nevertheless, its cell uptake kinetics, its influence in different types of cells and the possibility of controlling cellular internalization timing, is still a field that remains unexplored. Herein, different cell types have been cultured *in vitro* for several incubation periods in the presence of 0.075 mg ml^{-1} pegylated GO solutions. GO uptake kinetics revealed differences in the agent's uptake amount and speed as a function of the type of cell involved. Osteoblast-like cells GO uptake is higher and faster without resulting in greater cell membrane damage. Moreover, the dependence on the commonly used PEG nature (number of branches) also influences the viability and cell uptake speed. These facts play an important role in the future definition of timing parameters and selective cell uptake control in order to achieve an effective therapy.

S Online supplementary data available from stacks.iop.org/Nano/23/465103/mmedia

(Some figures may appear in colour only in the online journal)

Introduction

The exciting advances in the preparation of nanosystems with applications in the medical field have led to new challenges in the design of smart materials capable of meeting the clinical demands, mainly after finding that the introduction of nanosystems into living cells is possible by shuttling various cargoes across cellular membranes without producing cytotoxicity.

Nanoparticles have been proposed for locally releasing highly toxic drugs directly into tumors, while reducing the unwanted side effects of aggressive treatments, and to target tumors using the intrinsic capacities of different nanomaterials applied as new treatments [1]. For example, their capacity to induce localized heating within tumors is being exhaustively explored. Approaches to nanoparticle-mediated thermal therapy include absorption of infrared light, radio frequency ablation, and magnetically induced heating [2, 3].

Among carbon based materials, following closely and taking over from carbon nanotubes (CNTs), graphene and more specifically, graphene oxide (GO), represents one of the most promising 'nanoparticles' of the past few years. Its small two-dimensional shape [4], as well as its properties, low cost and easy processing, makes this nanomaterial a promising nanoparticle for medical applications where large-scale production is needed [5–8]. Its unique structure is useful for applications in drug delivery and its strong NIR optical absorption ability in the 700–1100 nm range (the 'therapeutic window', which allows non-invasive, harmless and skin penetrating irradiation) is particularly attractive for performing photodynamic therapies [9] or for the induction of

cell hyperthermia in tumor treatments as a minimally invasive alternative to surgery (photothermal therapy) [10].

The *in vitro* toxicity of GO towards human cells appears to be lower than that of CNT and it has been proposed as a potential cancer biomarker sensor, drug delivery particle and as nanoplatforms for cancer-selective drug delivery [10, 11]. There have been several recent works where the *in vitro* and *in vivo* behavior of fluorescent-labeled polyethylene glycol (PEG) functionalized GO and CNTs were studied by using mouse models, showing its potential to be used as a highly efficient *in vivo* photothermal therapy agent [12–14]. As is already well known, PEG has been approved for human use by the FDA, is non-toxic and can be eliminated by a combination of renal and hepatic pathways [15], thus making it an ideal carrier in pharmaceutical applications, having the lowest level of protein or cellular absorption of any known polymer. Nevertheless, although the research experiments have taken giant strides, the uptake kinetics of these pegylated GO nanosheets, their influence in different types of cells, PEG nature effects, and the possibility of controlling cellular internalization, are still fields that remain unexplored. There is an urgent need to define the potential of GO to be internalized and to interact by representative cells in order to assess the potential risk/gain associated with this nanotechnology.

With the purpose of finding and understanding the possible diverse biological responses of different cell types (for the first time orientated to the treatment of bone cancer) to this GO uptake, a kinetic study of GO nanosheet internalization has been performed in osteoblasts, preosteoblasts, fibroblasts, and macrophages as experimental cell models which subsist in the same environment. The influence that both the different timing and the cell nature has on the amount of GO internalized by different cell types has been seen for the first time. Moreover, the effects of PEG branching on cell uptake were elucidated by comparing a branched PEG ligand to the PEG linear version. The obtained results must be taken into account in order to know how the process of the therapy will take place and how cells surrounding the tumor could be affected in a photothermal therapy treatment.

1. Experimental details

1.1. GO nanosheet preparation

GO nanosheets of approximately 100 nm have been obtained from exfoliation of high-purity graphite in an acidic medium by a modified Hummers method [16]. Briefly, 2 g of graphite (99.99%; Sigma-Aldrich) was dispersed into a flask containing 50 ml of concentrated H_2SO_4 and 7 g of $KMnO_4$ and the solution was magnetically stirred for 2 h. After that, the solution was treated with H_2O_2 until the gas evolution ceased, then the resultant suspension was thoroughly washed, first with HCl solution (0.1 mol dm^{-3}) and then with distilled water by filtration and centrifugation. The resulting GO suspension was then dialyzed until a pH of 7 was reached.

1.2. GO nanosheet functionalization

After 3 h of further ultrasonic treatment to reduce the lateral size (50–100 nm), 50 ml of graphite oxide in water (∼1 mg ml^{-1}) was activated with 2.5 g of chloroacetic acid (Cl–CH_2–COOH) under strongly basic conditions (2.5 g NaOH), in order to promote –COOH groups at its surface, and bath sonicated for 3 h. The resulting GO solution was neutralized and purified by repeated rinsing and filtration. Activated GO was then functionalized by covalent bonding with non-toxic and non-immunogenic polymers poly (ethylene Glycol-amine) (PEG) to avoid the intercession with cellular functions or target immunogenicities and to decrease aggregation. A diimide activation was performed by adding (EDAC:1-Ethyl-3-(3-dimethylaminopropyl) carbodiimide hydrochloride, Sigma Inc. 0.106 g) to 45 ml of GO aqueous solution (1 mg ml^{-1}) and stirring vigorously for 3 h. Afterwards this solution was added to a 25 ml solution of polyethylene glycol-amine (11 mg ml^{-1}) and the reaction was allowed to take place for 48 h. Excess PEG was removed by centrifuge filtration. GO water suspensions were systematically washed by centrifugation through MWCO Amicon filters with a 100 kDa molecular weight cutoff. Different branched PEG polymers were attached following the same route; 1 arm PEG bis (3-aminopropyl) terminated 1.5 kDa (Sigma) and 6 arm branched PEG amine 15 kDa (SunBio Inc.) samples, named 1-GOs and 6-GOs respectively, in order to study the influence of surface charge and polymer size on the uptake process.

All GOs were marked with fluorescein isocyanate (FITC) covalent bonded to the PEG in order to control and follow the GOs during the different steps in the *in vitro* cell internalization studies. Pegylated GOs were redispersed in a pH 7.5 phosphate buffer (0.02 M) (0.5 mg ml^{-1}) and reacted with the amine reactive dye FITC. The reaction was allowed to take place overnight at room temperature to avoid light. Excess dye molecules were removed by centrifugation filtration through 100 kDa MWCO Amicon filters and washed away with water more than 10 times, until no noticeable color remained in the filtrate solution. (See scheme of figure 1.) Afterwards, pegylated and fluorescein labeled GOs were lyophilized.

The amino content of the GOs was determined at every synthesis step by quantitative analysis of the amino groups in order to monitor the chemical modifications [17]. This procedure was carried out by protecting the amino groups with highly fluorescent fluorenylmethyloxycarbonyl chloride (FMOC-Cl), followed by intensive washing steps, cleaving the protective group, and subsequently measuring the UV–vis absorption. As other groups present on the GO nanosheets (e.g. hydroxyl radicals) could also react with the FMOC, an initial sample was also measured to evaluate the residual signal. Table 1 gives the data corresponding to the GOs.

1.3. GO nanosheet characterization

The size, structure and properties of the GO nanosheets have been evaluated using different techniques. Transmission

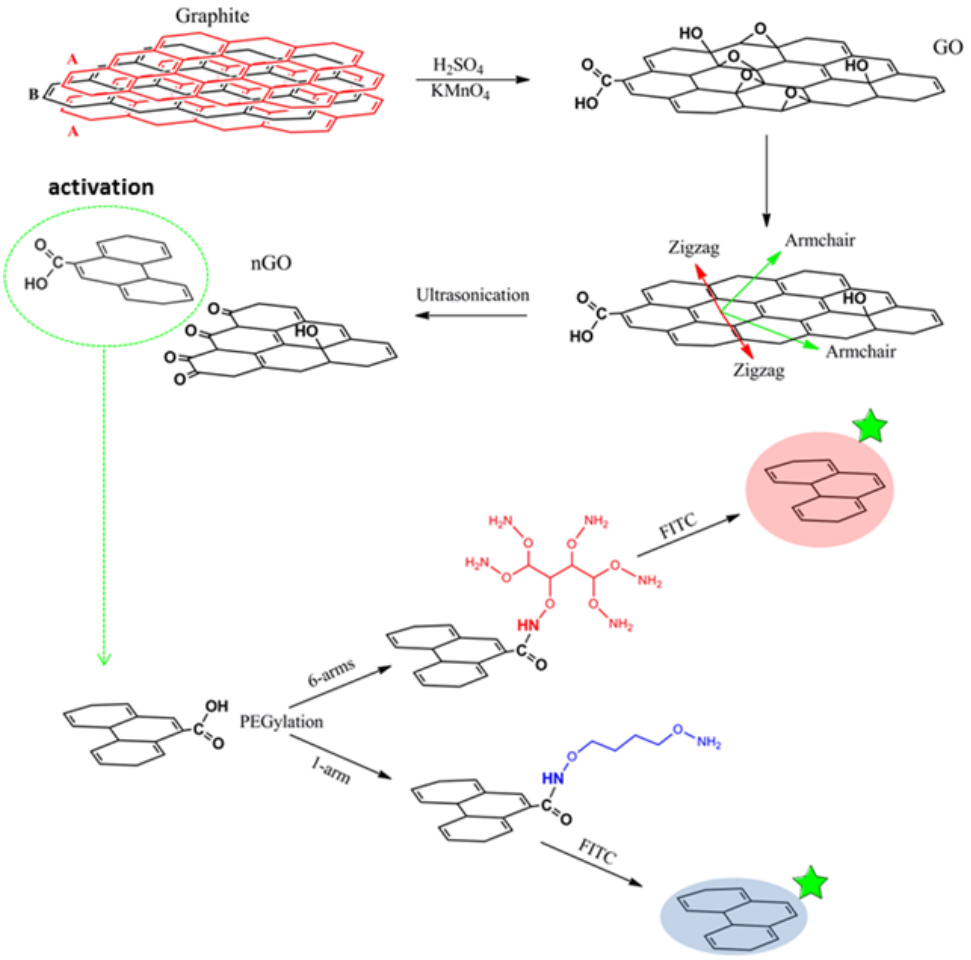

Figure 1. Schematic illustration of GO exfoliation and pegylation by differently branched PEG.

Table 1. Quantitative analysis of amine content (10^{-5} mmol mg^{-1}).

	GO	GO-PEG	GO-PEG-FTIC
1-GO	1.3	1.52	1.47
6-GO	1.3	2.71	2.17

electron microscopy (TEM) was performed using a 200 kV JEOL JEM 2100. GO nanosheets deposited on mica substrates were analyzed using an atomic force microscope (AFM) (VEECO Multimode; USA). Fourier transform infrared spectroscopy (FTIR) was performed with a Nicolet Nexus spectrometer using the KBr pellet method. 5 mg of each sample was added to 10 ml milliQ water (solution pH 7.8) and centrifuged (3500 rpm) for 10 min to analyze the Z-potential and particle size of the supernatant particles, following the same procedure as the material used on the experiment. Zeta potential (ζ) and dynamic light scattering particle size analysis DLS measurements were performed on pH 5 solutions in a Zetasizer Nano Series instrument equipped with a 633 nm 'red' laser from Malvern Instruments, with reproducibility being verified by collection and comparison of sequential measurements. Z-average sizes of three sequential measurements were collected at room temperature and analyzed.

1.4. GOs incorporation studies and cell proliferation studies

Four different types of cells were chosen for the *in vitro* studies. Human Saos-2 osteoblasts, murine MC3T3-E1 preosteoblasts, murine L929 fibroblasts and murine RAW-264.7 macrophages were seeded on six-well culture plates (CULTEK S.L.U., Madrid, Spain), at a density of 105 cells ml^{-1} in either DMEM (for Saos-2, L929 and RAW-264.7 cells) or α-MEM (for MC3T3-E1 cells) supplemented with 10% fetal bovine serum (FBS, Gibco, BRL), 1 mM L-glutamine (BioWhittaker Europe, Belgium), penicillin (200 μg ml^{-1}, BioWhittaker Europe, Belgium), and streptomycin (200 μg ml^{-1}, BioWhittaker Europe, Belgium), under a CO_2 (5%) atmosphere and at 37 °C for 24 h. To evaluate the GOs incorporation by cells in suspension, Saos-2, L929 and RAW-264.7 cultures were washed with Phosphate Buffer Saline (PBS) and the attached cells were harvested using either 0.25% trypsin-EDTA solution for 5 min (for Saos-2 and L929 cells) or cell scrapers designed for harvesting cells (for RAW-264.7 cells). The trypsin action was stopped with culture medium, cells were centrifuged at 310*g* for 10 min and resuspended in fresh medium. Cell suspensions were incubated in the presence of 0.075 mg ml^{-1} GOs solutions (concentration within the range of previously optimized published results [18]) dispersed in supplemented

DMEM for 30, 60 and 150 min in order to evaluate the incorporation of GOs by flow cytometry.

To evaluate the incorporation of GOs by cultured cells, 0.075 mg ml^{-1} GOs solutions dispersed in supplemented DMEM material were added to cultured Saos-2, MC3T3-E1, L929 and RAW-264.7 for different times. After 30 min, 2, 6 and 24 h culture in the presence of this material, cells were harvested, as indicated above, and the incorporation of GOs was evaluated by flow cytometry. In order to determine the effects of GOs on cell proliferation, cells were counted with a Neubauer hemocytometer after harvesting. Controls without material were always carried out.

The conditions for the data acquisition and analysis of flow cytometry were established using negative and positive controls with the CellQuest Program of Becton Dickinson and these conditions were maintained during all the experiments. Each experiment was carried out three times and single representative experiments are displayed. For statistical significance, at least 10 000 cells were analyzed in each sample and the mean of the fluorescences emitted by these single cells was used.

To measure the GOs incorporation by different cell types after treatment with this material, cells were cultured and harvested as explained earlier. Then, the fluorescence of FITC was excited by a 15 mW laser tuned to 488 nm and the emitted fluorescence was measured with a 530/30 band pass filter in a FACScalibur Becton Dickinson flow cytometer.

To evaluate the internalization of GOs material, Trypan Blue (40 μg ml^{-1}) was added to cell suspensions before the flow cytometric analysis to quench the fluorescence produced by the FITC label of GOs adsorbed on the exterior surface of cells.

1.5. Cytotoxicity studies

A major concern in biomaterials science is always the possible toxicity of the tested materials. Cell viability of cells cultured in the presence of the investigated materials was determined by addition of propidium iodide (PI; 0.005% in PBS, Sigma-Aldrich Corporation, St. Louis, MO, USA) to stain the DNA of dead cells. The fluorescence of PI was excited by a 15 mW laser tuned to 488 nm and the emitted fluorescence was measured with a 670 nm long pass filter in a FACScalibur Becton Dickinson flow cytometer.

The plasma membrane integrity was evaluated in terms of the lactate dehydrogenase released (LDH). LDH was measured in the culture medium by an enzymatic method at 340 nm (Bio-Analítica, S.L.) using a Beckman DU 640 UV–visible spectrophotometer. The medium was collected after every culture time and centrifuged at 12 000*g* at 4 °C. The enzymatic assay was performed in the supernatant.

Data are expressed as means + standard deviations of a representative of three experiments carried out in triplicate. Statistical analysis was performed using the Statistical Package for the Social Sciences (SPSS) version 19 software. Statistical comparisons were made by analysis of variance (ANOVA). A Scheffé test was used for post hoc evaluations of differences among groups. In all of the statistical evaluations, $p < 0.05$ was considered as statistically significant.

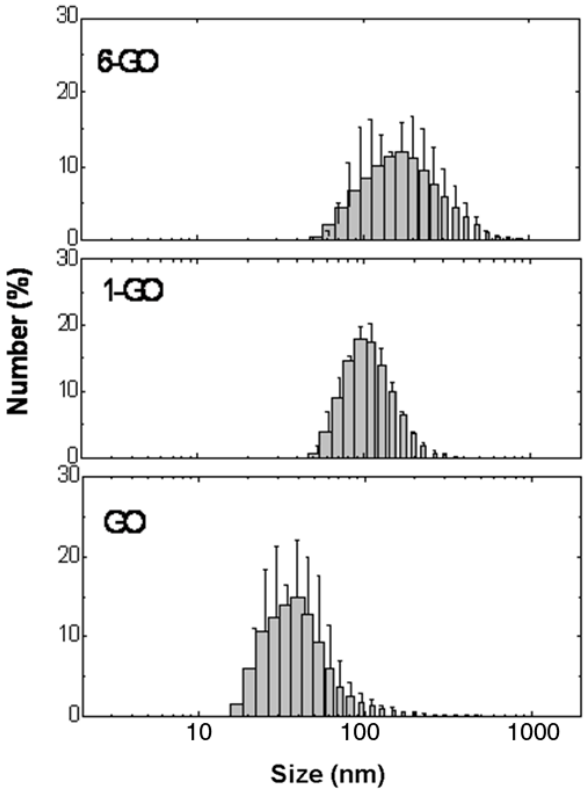

Figure 2. Activated GOs particle size distribution obtained by DLS.

1.6. Confocal microscopy studies

To observe the incorporation of GOs by confocal microscopy, human Saos-2 osteoblasts, murine MC3T3-E1 preosteoblasts, murine L929 fibroblasts and murine RAW-264.7 macrophages were seeded on glass coverslips and cultured in the presence of GOs material for 24 h. Controls without material were always carried out. Cells were washed with PBS and fixed with 3.7% paraformaldehyde in PBS for 10 min. After washing with PBS, cells were examined by a LEICA SP2 confocal laser scanning microscope.

2. Results and discussion

2.1. GO nanosheet characterization

The chemical exfoliation of graphite in aqueous media, subsequent chemical activation and size separation by centrifugation, resulted in sheets of graphene oxide (GO) with an hydrodynamic size distribution in the range approximately 10–120 nm with the maximum number of particles located around 40 nm (figure 2). As can be seen in the figure from data obtained by DLS, and as it was expected based on the molecular weights and shapes of the branched and linear PEG [19], the hydrodynamic particle size increases with the increasing number of branches of the PEG, shifting the maximum hydrodynamic size from 40 nm for GO, to 95 and 190 nm for the pegylated 1-GOs and 6-GOs respectively.

The thin structure of the GO sheet and its smooth surface are confirmed by TEM, although some corrugation

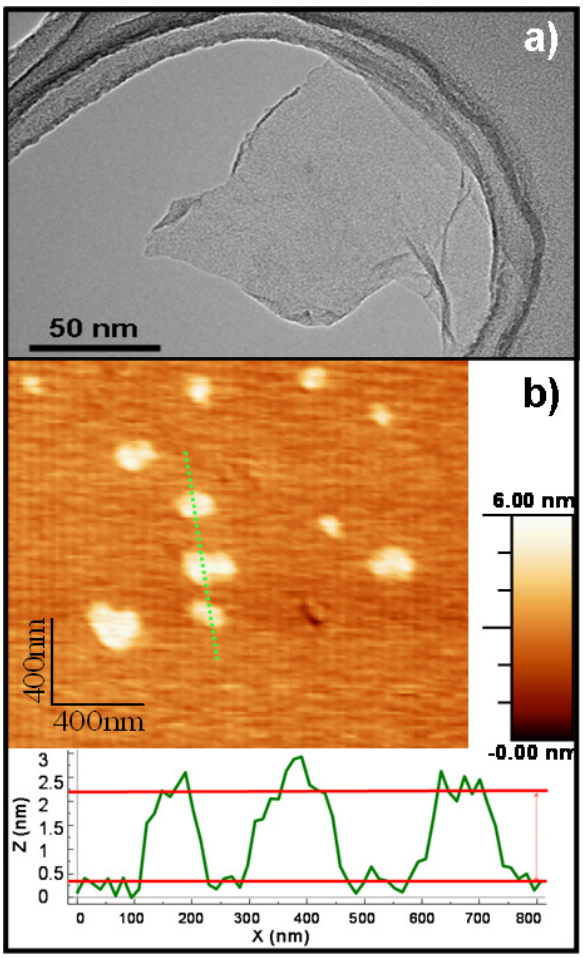

Figure 3. (a) Transmission electron micrograph of activated GO nanosheets. (b) AFM topographic image of dispersed GO nanosheets. The graph represents the thickness profile from the green line of the AFM image.

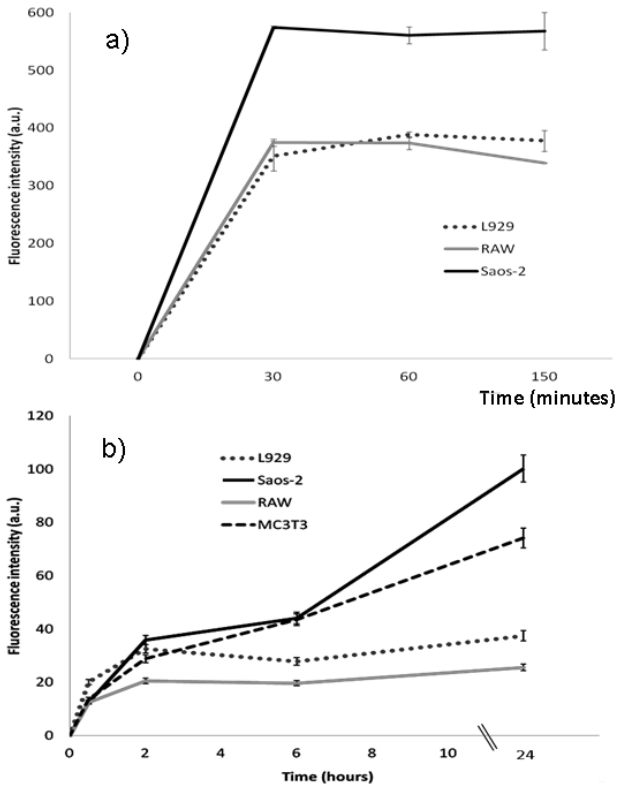

Figure 4. (a) Incorporation of 1-GOs labeled with FITC by human Saos-2 osteoblasts, murine L929 fibroblasts and murine RAW-264.7 macrophages in suspension for different times. (b) Incorporation of 1-GOs labeled with FITC by human Saos-2 osteoblasts, murine L929 fibroblasts, murine RAW-264.7 macrophages and murine MC3T3-E1 preosteoblasts in culture for different times.

is detected, suggesting a flexible structure of the GO sheets. Regarding the size, the results are in the range of those obtained with DLS analysis. A representative GO sheet is shown in figure 3(a), displaying a well exfoliated thin nanosheet. AFM was used [16] to measure the size and thickness of the individual GO nanosheets. The average thickness of GO was around 2 nm, corresponding to nanosheets with 3 or 4 layers, and the size range of nanosheets measured matched the higher range obtained with DLS.

Graphene oxide surfaces subjected to a successful pegylation procedure were monitored by FTIR spectra and resulted in the presence of oxygen functionalities at the GO surface plus the C–O stretch vibration band (110–150 cm^{-1}) and the strong C–H stretch peak (2800 cm^{-1}), clearly indicating the presence of the PEG on the GO sample. (Figure 1 supporting information available at stacks.iop.org/Nano/23/465103/mmedia.)

Values of the amine quantification used to give a direct measure of the average quantity of amines before and after fluorescent labeling on each 1 arm or 6 arm pegylated GOs are shown in table 1. In addition, differences between the 1-GOs and 6-GOs are shown by the zeta potential of aqueous suspensions of each sample. The results show that –COOH activated GO sheets are highly negatively charged -37.8 ± 8 mV, which can be attributed to the presence of oxygen species at the surface of GO. As soon as the PEG is attached to the GO sheets, the zeta potential changes slightly, to -30.5 ± 3 mV, for the case of the 1 arm PEG, and to -8.05 ± 4 mV, for the 6 arm PEG. This fact confirms the existence of the positive amino ended branches which change the GO electrostatic nature, being less negative for the 6 arm PEG.

2.2. *GOs uptake*

The use of GOs for medical application requires the evaluation of their interaction with different cell types in order to know the internalization kinetics and the cell response to this material. The GO nanosheet cell uptake was evaluated, first of all, with suspensions of human Saos-2 osteoblasts, murine L929 fibroblasts and murine RAW-264.7 macrophages after short incubation periods. As a first approach, cell suspensions were incubated for 30, 60 and 150 min with only 1-GOs (as said above all particles are labeled with FITC) and the amount of cell-associated fluorescence was detected by flow cytometry. As can be observed in figure 4(a), these three cell types incorporate 1-GOs quickly, showing stable

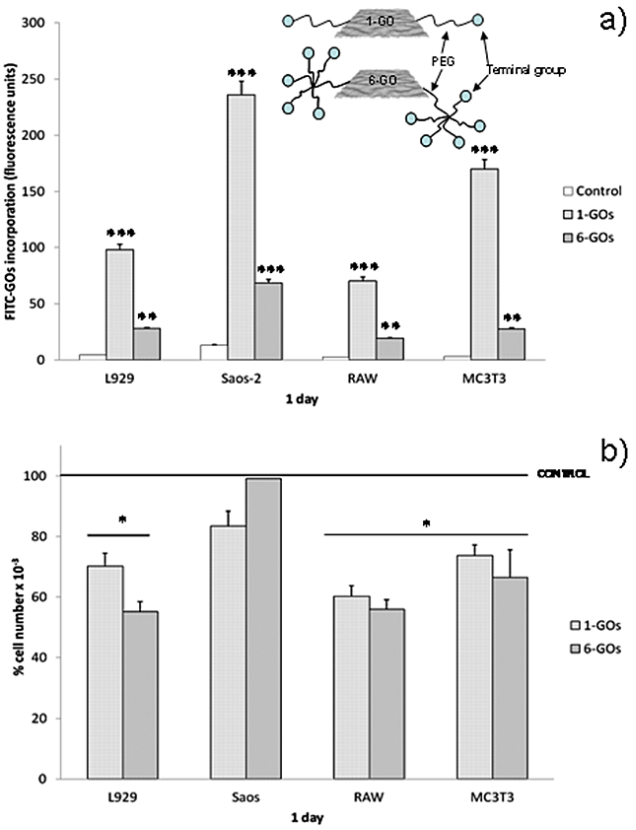

Figure 5. (a) Incorporation of 1-GOs and 6-GOs labeled with FITC by cultured human Saos-2 osteoblasts, murine L929 fibroblasts, murine RAW-264.7 macrophages and murine MC3T3-E1 preosteoblasts after a 1 day treatment. Controls represent the basal fluorescence values in the absence of GOs. (b) Effect of 1-GOs and 6-GOs on proliferation of cultured human Saos-2 osteoblasts, murine L929 fibroblasts, murine RAW-264.7 macrophages and murine MC3T3-E1 preosteoblasts after a 1 day treatment. The cell number is given as a percentage relative to the controls (100%) carried out in the absence of material.

levels of fluorescence during these incubation periods. The results revealed that GOs uptake by human osteoblasts was higher than by the other cell types. The same study was then carried out in cell cultures for longer times (30 min, 2, 6 and 24 h) with Saos-2, L929 and RAW-264.7 and also murine MC3T3-E1 preosteoblasts to compare information on non-carcinogenic osteoblast cell line behavior with the previous fast uptake showed by the tumoral osteoblast-like line.

Figure 4(b) indicates again that GOs uptake by Saos-2 osteoblasts is higher than GOs incorporation in fibroblasts and macrophages, which show almost constant fluorescence values in a time independent manner after 2 h treatment. MC3T3-E1 preosteoblasts show similar GOs incorporation to osteoblasts after 6 h, confirming the faster uptake kinetics in these two bone cell types, which even continue incorporating GOs at longer times (24 h).

As macrophages are phagocytic cells, it was expected that their GOs internalization would be lower in comparison with other cell lines. It has been already reported that escaping phagocytic uptake is induced by maintaining the particle size around 150 nm, as this kind of cell favors the uptake of large particles and a Z potential below 15. Moreover, the PEG has nonfouling or protein resistant properties and was specifically included to limit the interaction with biological interfaces, in order to decrease particle uptake by macrophages and increase their circulation time. Also, particles of small sizes might exhibit a high level of exocytosis [20, 21]. On the other hand, non-phagocytic cells favor the uptake of small particles. Endocytic pathways involved in particle uptake have been investigated in these types of cell [22, 23] showing that they use more than one pathway to internalize particles, but it is assumed that particles up to 200 nm are internalized mainly by (receptor-mediated) endocytosis. It is known that the cellular uptake of nanoparticles is dependent on cell line as particle binding depends on cell surface properties which are vital to their interaction with particles. It has been already reported [21] for polymeric nanoparticles that fibroblasts have one of the lowest nanoparticle uptake rates. Moreover, the fact that Saos-2 cells have a higher and faster uptake than MC3T3 could be related to their tumoral nature. Saos-2 is a human osteosarcoma cell line with osteoblastic properties such as production of a mineralized matrix, high levels of alkaline phosphatase, PTH receptors coupled to adenylate cyclase and the presence of osteonectin. The osteoblastic cell line MC3T3-E1 has been established from a C57BL/6 mouse calvaria. These cells are preosteoblasts and have the capacity to differentiate into osteoblasts and osteocytes, forming calcified bone tissue *in vitro*.

The different behavior of tumoral versus non-tumoral cells—although this must be further studied—suggests that the internalization and posterior application of the NIR irradiation could affect bone cells through the control of GO cell uptake timing, mainly through the irradiation efficiency (as is directly related to the amount of GOs uptaken), reducing the number of healthy cells affected, as their uptake is lower and slightly slower. This last process could be even more retarded by surface decoration methods.

To know the influence of surface charge and pegylated GO particle size on the GOs uptake process, a comparative study with 1-GOs and 6-GOs was carried out by culturing Saos-2, MC3T3-E1, L929 and RAW-264.7 cells for 1 day in the presence of both materials separately. The cell uptake behavior shown in figure 5(a), demonstrated that 1-GOs incorporation is significantly higher than 6-GOs uptake by all cell types.

This is in agreement with the fact explained above that non-phagocytic cells favor the uptake of smaller particles, as is the case of 1-GO. Moreover, as is expected, the more highly branched PEG might be limiting in a higher grade the interaction with biological surfaces (useful to avoid their removal by the macrophages), and it seems that this fact is also limiting the uptake by targeted cells. These results indicate that there might be a limit of PEG size and number of branches (also directly related to surface charge) in arriving at a compromise which is still highly efficient for uptake by targeted cells.

Moreover, following the same trend as was mentioned above, osteoblasts show the most pronounced GOs incorporation in both cases.

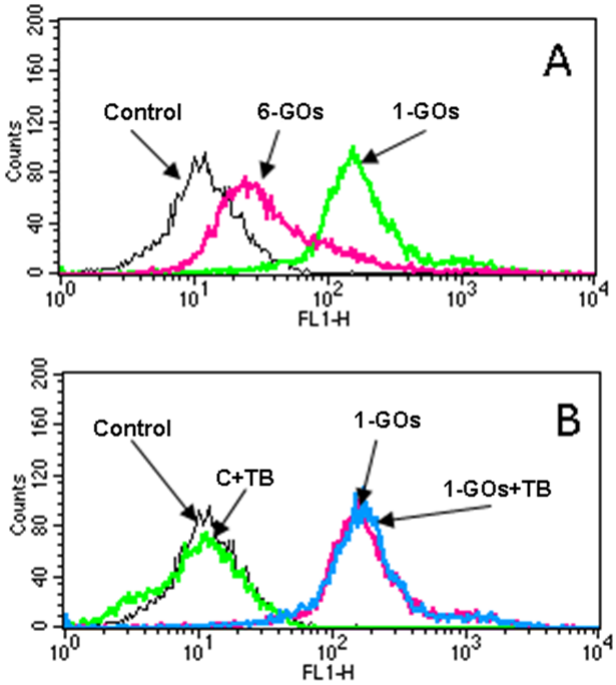

Figure 6. (a) Fluorescence profiles of cultured Saos-2 osteoblasts treated for 1 day with 1-GOs and 6-GOs in comparison with control cells in the absence of GOs. (b) Effect of Trypan Blue (TP) on fluorescence profiles of cultured Saos-2 osteoblasts treated for 1 day with 1-GOs and control cells in the absence of 1-GOs.

Since the cellular responses to GOs are still poorly understood, the effects of both 1-GOs and 6-GOs on cell proliferation were analyzed after 1 day treatment of cultured Saos-2, MC3T3-E1L929 and RAW-264.7 cells. A significant delay of cell proliferation was observed after both treatments with all cells types except with Saos-2 osteoblasts, which do not show alterations of the growth rate (figure 5(b)). In spite of the lower incorporation of 6-GOs in MC3T3-E1, L929 and RAW-264.7 cells in comparison with 1-GOs uptake by these cell types (figure 4), 6-GOs and 1-GOs produce similar effects on the proliferation of each cell type, suggesting that 6-GOs can induce more alterations on cell function than 1-GOs.

The internalization of GOs was confirmed by flow cytometry, after adding Trypan Blue to quench the fluorescence [24] produced by the GOs adsorbed on the exterior surface of cells. Representing these cell uptake fluorescence profiles only for Saos-2 in figure 6(a) with control cells in the absence of GOs, it was demonstrated that similar profiles were obtained both with and without Trypan Blue (figure 6(b)), indicating that both 1-GOs and 6-GOs are completely cell internalized.

It has been found that densely coating nanomaterial surfaces with PEG [25] increases *in vivo* particle circulation times, likely by resisting clearance via the reticuloendothelial system (RES), but it is important to assess the branch number dependence on the cell uptake process [11]. It is known that PEG [19] branching reduces dynamic viscosity and, although in most of the works published a high branch number is applied because of the possibilities of decorating it with more molecules, it may have influences on cellular uptake due to changes on particle hydrodynamic size and surface charge.

Although it has been reported that for most particles a positive charge at their surface enhances the cellular internalization [26, 27] rate due to preferred contact with the negatively charged cell surface via their electrostatic interaction [28], in this case, the less negative charged particles are those of the 6 arm PEG, which are also the least internalized. Moreover, although the cellular uptake depends on the charged nature of the particles, this fact also being cell dependent (due to distinct surface properties), the behavior of internalization for the greater proportion of the 1-GOs is similar for all the cell lines studied. This fact suggests that the particle size difference between the two materials seems to be the determining factor for the differences in the amount of particle uptake. It has been reported that the internalization inside cells depends directly on the absolute size and/or volume of the particles and that, in the 100–200 nm range, they have an optimum size for the uptake to be faster [29]. This faster uptake of particles of high aspect ratio has been attributed to the multivalent cationic interactions with cells that are available in particles, because of the larger surface areas in contact with the cell membrane. Nevertheless, nanoparticles with larger sizes need a stronger driving force and additional energy in the cellular internalization process. It has also been reported that particles with sizes greater than 150 nm could have an slower internalization by non-phagocytic cells by nonspecific endocytosis [21, 30]. Moreover, it is not only size that matters, as shape-dependent uptake might also dominate the uptake process for particles with varying geometries [31, 32]. The fact that rod-like particles (and linear shaped ones) proved to interact better with the cell membrane and that adsorptive endocytosis plays a major role could also be an important reason why 1-GOs internalize faster than 6-GOs. (Inset of figure 5(a).)

Following this study, the morphology of all cell types was studied by confocal microscopy (figure 7).

As can be observed, the highest fluorescence intensity is obtained in Saos-2 cells, in agreement with the incorporation studies by flow cytometry. The subcellular distribution of graphene inside each cell type seems very different. L929 fibroblasts and RAW macrophages show a diffuse FITC-GO signal, mainly localized on the cell membrane and in the cytoplasm. However, in Saos osteoblasts and MC3T3 preosteoblasts, the signal seems located on microtubules. Although further studies are needed to determine why the FITC-GO localization depends on cell type, the observed differences could be due to the different function of each cell type, which could determine the cytoskeleton characteristics and dynamics. The cytoskeleton presents microfilaments, microtubules and intermediate filaments which are responsible for cell shape and motility. It is well known that the cytoskeleton is extremely dynamic and these filament systems are able to lengthen or shorten very rapidly in order to change cell shape (such as during phagocytosis in macrophages), complete cell division, or migrate. Macrophages are immune cells with a specialized

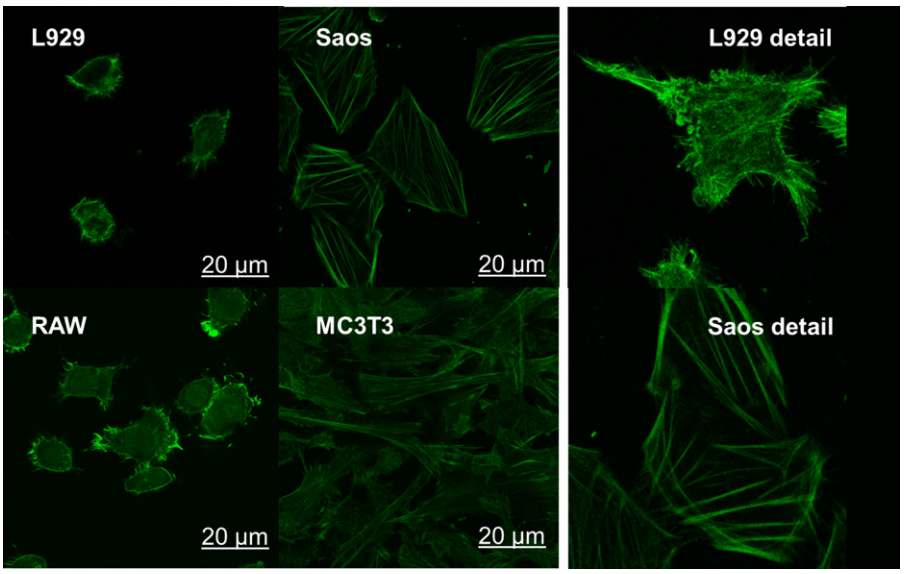

Figure 7. Incorporation of GOs by cultured human Saos-2 osteoblasts, murine MC3T3-E1 preosteoblasts, murine L929 fibroblasts and murine RAW-264.7 macrophages after 1 day treatment observed by confocal microscopy. Controls without material were always carried out.

capacity for cell migration and phagocytosis. Fibroblasts are the most common cells in connective tissue and maintain the structural integrity of this tissue by continuously secreting extracellular matrix proteins. Osteoblasts and preosteoblasts are involved in bone-forming, bone-remodeling and mechano-transduction processes. Thus, the different cell functions of the celltypes used in this study could be the cause of the differences seen by confocal microscopy.

As the evaluation of the plasma membrane integrity is one of the most common ways to measure cell viability and cytotoxic effects, this parameter was analyzed through propidium iodide exclusion and lactate dehydrogenase release to the culture medium. Table 2 shows the cell viability values measured for cultured Saos-2, MC3T3-E1, L929 and RAW-264.7 cells after both GOs treatments for 1 day. High viability levels are obtained in all cases, revealing that the GOs dose used in this study does not induce plasma membrane damage. These results are in agreement with the absence of significant changes induced by GOs in the lactate dehydrogenase release to the culture medium (figure 2 supporting information available at stacks.iop.org/Nano/23/465103/mmedia). These results indicate that the experiments were performed within the concentration range and time period where no cytotoxicity occurred.

Table 2. Effect of 1-GOs and 6-GOs on cell viability of cultured human Saos-2 osteoblasts, murine L929 fibroblasts, murine RAW-264.7 macrophages and murine MC3T3-E1 preosteoblasts after a 1 day treatment.

	Control	1-GOs	6-GOs
L929	97.2 ± 0.2	97.1 ± 0.3	97.6 ± 0.2
Saos-2	97.0 ± 0.1	93.2 ± 0.3	94.1 ± 0.9
RAW	95.2 ± 0.5	88.4 ± 4.4	88.8 ± 0.6
MC3T3	97.8 ± 0.1	95.4 ± 0.4	97.1 ± 0.2

3. Conclusions

A kinetic study of GO nanosheet (GOs) internalization has been performed for the first time in osteoblasts, preosteoblasts, fibroblasts, and macrophages as experimental cell models which subsist in the same environment. The influence that the different timing or culture cell nature has on the amount of GO internalized by different cell types has been studied, showing that osteoblast cell uptake is faster compared with the other cell types. Moreover, PEG branching effects on cell uptake were assessed by comparing internalization of a branched PEG ligand to the PEG linear version, and it has been found that 1 arm pegylated GO is internalized in a greater proportion than 6 arm pegylated GO. Moreover it has been suggested that even with the high viability levels obtained in all cases, revealing that the GOs doses used in this study do not induce plasma membrane damage, 6-GOs can induce more alterations to cell function than 1-GOs. The tumoral cell uptake has proved to be faster and the internalization speed has been proved to depend on the cell type. Moreover, this effect could be emphasized by a proper surface decoration method.

The obtained results must be taken into account in order to understand how a future therapy process could take place and how the cells surrounding the tumor might be affected in a therapy treatment.

Acknowledgments

The work has been financially supported by the Spanish CICYT through project MAT-2008-00736, Spanish National CAM project S2009/MAT-1472 and the Network of Excellence CSO2010-11384-E. M Vila thanks the Spanish Ministry for the RyC grant and the FSE. M C Matesanz thanks the MICINN for the pre-doctoral fellowship. The authors also

wish to thank the Electron Microscopy, Confocal Microscopy and Cytometry Center of the Universidad Complutense de Madrid (Spain). P Marques thanks the Ciencia 2007 Program, G Gonçalves thanks Iberian Nanotechnology Laboratory (INL) for a PhD grant and S M A Cruz thanks FCT for the PhD grant (SFRH/BD/68598/2010).

References

[1] Torchilin V P 2006 *Nanoparticulates as Drug Carriers* (London: Imperial College Press)
[2] Day E S, Morton J G and West J L 2009 Nanoparticles for thermal cancer therapy *J. Biomech. Eng.* **131** 074001
[3] Fischer K, Gedroyc W and Jolesz F A 2010 Focused ultrasound as a local therapy for liver cancer *Cancer J.* **16** 118–24
[4] Melucci M *et al* 2010 Facile covalent functionalization of graphene oxide using microwaves: bottom–up development of functional graphitic materials *J. Mater. Chem.* **20** 9052–60
[5] Bai S and Shen X 2012 Graphene–inorganic nanocomposites *RSC Adv.* **2** 64–98
[6] Zhang L, Liang J, Huang Y, Ma Y, Wang Y and Chen Y 2009 Size-controlled synthesis of graphene oxide sheets on a large scale using chemical exfoliation *Carbon* **47** 3365–8
[7] Huang X, Qi X, Boey F and Zhang H 2012 Graphene-based nanocomposites *Chem. Soc. Rev.* **41** 666–86
[8] Loh K P, Bao Q, Eda G and Chhowalla M 2010 Graphene oxide as a chemically tunable platform for optical applications *Nature Chem.* **2** 1015–23
[9] Wang K, Ruan J, Song H, Zhang J, Wo Y, Guo S and Cui D 2011 Biocompatibility of graphene oxide *Nanoscale Res. Lett.* **6** 1–8
[10] Markovic Z M *et al* 2011 *In vitro* comparison of the photothermal anticancer activity of graphene nanoparticles and carbon nanotubes *Biomaterials* **32** 1121–9
[11] Liu Z, Robinson J T, Sun X and Dai H 2008 PEGylated nanographene oxide for delivery of water-insoluble cancer drugs *J. Am. Chem. Soc.* **130** 10876–7
[12] Sun X, Liu Z, Welsher K, Robinson J T, Goodwin A, Zaric S and Dai H 2008 Nano-graphene oxide for cellular imaging and drug delivery *Nano Res.* **1** 203–12
[13] Yang K, Zhang S, Zhang G, Sun X, Lee S-T and Liu Z 2010 Graphene in mice: ultrahigh *in vivo* tumor uptake and efficient photothermal therapy *Nano Lett.* **10** 3318–23
[14] Shi Kam N W, O'Connell M, Wisdom J A and Dai H 2005 Carbon nanotubes as multifunctional biological transporters and near-infrared agents for selective cancer cell destruction *Proc. Natl Acad. Sci. USA* **102** 11600–5
[15] Hooftman G, Herman S and Schacht E 1996 Poly (ethylene glycol)s with reactive endgroups II. Practical consideration for the preparation of protein-PEG conjugates *J. Bioact. Compat. Polym.* **11** 135–59
[16] Gonçalves G, Marques P A A P, Granadeiro C, Nogueira H I S, Singh M K and Grácio J 2009 Surface modification of graphene nanosheets with gold nanoparticles: the role of oxygen moieties at graphene surface on gold nucleation and growth *Chem. Mater.* **21** 4796–802
[17] Yoon T J *et al* 2006 Specific targeting, cell sorting, and bioimaging with smart magnetic silica core–shell nanomaterials *Small* **2** 209–15
[18] Dong H, Zhao Z, Wen H, Li Y, Shen A, Pilger F, Lin C and Shi D 2010 Poly(ethylene glycol) conjugated nano. Graphene oxide for photodynamic therapy *Sci. China Chem.* **53** 1–7
[19] Navath R S, Wang B, Kannan S, Romero R and Kannan R M 2010 Stimuli-responsive star polyethylene glycol conjugates for improved intracellular delivery of N-acetyl cysteine in neuroinflammation *J. Control. Release* **19** 447–56
[20] Slowing I, Trewyn B G and Lin B S Y 2006 Effect of surface functionalization of MCM-41-type mesoporous silica nanoparticles on the endocytosis by human cancer cells *J. Am. Chem. Soc.* **128** 14792–3
[21] Cortez C, Tomaskovic-Crook E, Johnston A P R, Scott A M, Nice E C, Heath J K and Caruso F 2007 Influence of size, surface, cell line and kinetic properties on the specific binding of A33 antigen-targeted multilayered particles and capsules to colorectal cancer cells *ACS Nano* **1** 93–102
[22] He C, Hu Y, Yin L, Tang C and Yin C 2010 Effects of particle size and surface charge on cellular uptake and biodistribution of polymeric nanoparticles *Biomaterials* **31** 3657–66
[23] Gratton S E, Napier M E, Ropp P A, Tian S and DeSimone J M 2008 Microfabricated particles for engineered drug therapies: elucidation into the mechanisms of cellular internalization of PRINT particles *Pharm. Res.* **25** 2845–52
[24] Busch W *et al* 2010 *J. Nanopart. Res.* **13** 293–310
[25] Wang H, Robinson J T, Li X and Dai H 2009 Solvothermal reduction of chemically exfoliated graphene sheets *J. Am. Chem. Soc.* **131** 9910–1
[26] Halamoda Kenzaoui B, Vilà M R, Miquel J M, Cengelli F and Juillerat-Jeanneret L 2012 Evaluation of uptake and transport of cationic and anionic ultrasmall iron oxide nanoparticles by human colon cells *Int. J. Nanomed.* **7** 1275–86
[27] Chen L, Mccrate J M, Lee J C-M and Li H 2011 The role of surface charge on the uptake and biocompatibility of hydroxyapatite nanoparticles with osteoblast cells *Nanotechnology* **22** 105708
[28] Yue Z G, Wei W, Lv P P, Yue H, Wang L Y, Su Z G and Ma G H 2011 Surface charge affects cellular uptake and intracellular trafficking of chitosan-based nanoparticles *Biomacromolecules* **12** 2440–6
[29] Yin Win K and Feng S S 2005 Effects of particle size and surface coating on cellular uptake of polymeric nanoparticles for oral delivery of anticancer drugs *Biomaterials* **26** 2713–22
[30] Conner S D and Schmid S L 2003 Regulated portals entry into the cell *Nature* **422** 37–44
[31] Alemdaroglu F E, Alemdaroglu N C, Langguth P and Herrmann A 2008 Cellular uptake of DNA block copolymer micelles with different shapes *Macromol. Rapid Commun.* **29** 326–9
[32] DeSimone J M 2008 The effect of particle design on cellular internalization pathways *Proc. Natl Acad. Sci. USA* **105** 11613–8

Nano-GO está considerado como un nanomaterial muy prometedor para diferentes aplicaciones biomédicas. Sin embargo, poco se conoce acerca de la respuesta celular a este material. Por tanto, una vez conocida la cinética de incorporación del material se estudió su biocompatibilidad en osteoblastos humanos Saos-2, preosteoblastos murinos MC3T3-E1 y macrófagos murinos RAW 264.7 cultivados en contacto con nano-1-GO y nano-6-GO. Los materiales utilizados fueron marcados con FITC para conocer su localización intracelular.

Los resultados obtenidos se resumen a continuación y han dado lugar a la siguiente publicación:

- Matesanz MC, Vila M, Feito MJ, Linares J, Gonçalves G, Vallet-Regi M, Marques PAAP, Portolés MT. The effects of graphene oxide nanosheets localized on F-actin filaments on cell cycle alterations. Biomaterials, 34:1562-1569, 2013.

Los resultados mostraron que tras la internación de estos materiales (significativamente mayor de nano-1-GOs y especialmente incrementada en células de linaje osteoblástico), las nanopartículas se asocian a los filamentos de actina, induciendo alteraciones en el ciclo celular, apoptosis y estrés oxidativo. Sin embargo, no se afectaron la membrana plasmática, el tamaño y la complejidad celular.

El contenido intracelular de ROS se vio incrementado en todos los casos, excepto en osteoblastos Saos-2 en contacto con 1-GOs, indicando la inducción de estrés oxidativo. Las nanopartículas de GO produjeron alteraciones en el ciclo celular, observándose un ligero incremento de la fracción SubG1 indicativa de apoptosis en todos los casos, excepto en MC3T3-E1 cultivadas en presencia de nano-6-GO. Las células MC3T3-E1 y RAW 264.7 presentaron un claro incremento de la fase G0/G1 en detrimento de la fase S, sugiriendo una parada del ciclo celular producido por la incorporación del material, principalmente en los macrófagos en los que este efecto se acentuó a las 72 horas de cultivo. Las células de linaje osteoblástico (Saos-2 y MC3T3-E1) presentaron un descenso de la fase G2/M, revelando la alteración de la capacidad mitótica que puede explicar la disminución de la proliferación.

Estudios de microscopía confocal revelaron la localización de estas nanopartículas asociadas a los filamentos de actina en todos los casos (**Figuras 35** y **36**). Dado que dichos filamentos son esenciales para el progreso de las diferentes fases del ciclo celular, la interacción del material con la actina podría ser la causa de las alteraciones observadas en este parámetro.

En contacto con ambos materiales se observó un descenso en los niveles de IL-6 secretada al medio por osteoblastos Saos-2, más pronunciado a las 72 horas de cultivo con nano-6-GO.

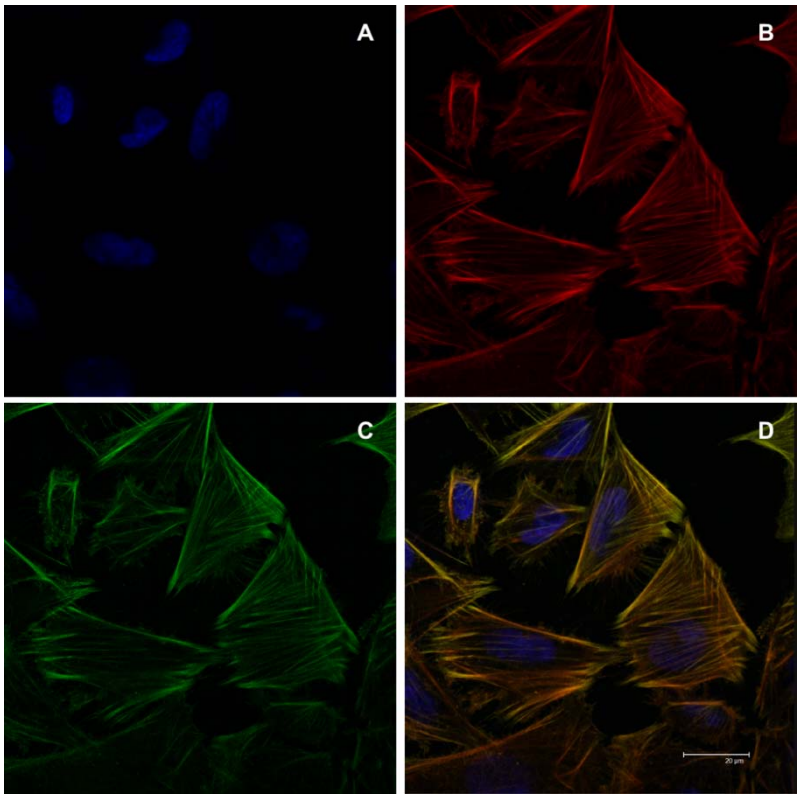

Figura 35. Osteoblastos Saos-2 cultivados en presencia de nano-GO observados por Microscopía Confocal. A) marcaje de los núcleos con DAPI, **B)** marcaje de los filamentos de actina con faloidina-rodamina, **C)** nano-GO marcado con FITC, **D)** superposición de A, B y C. Imágenes procedentes de [*Matesanz MC et al. 2013, Biomaterials*].

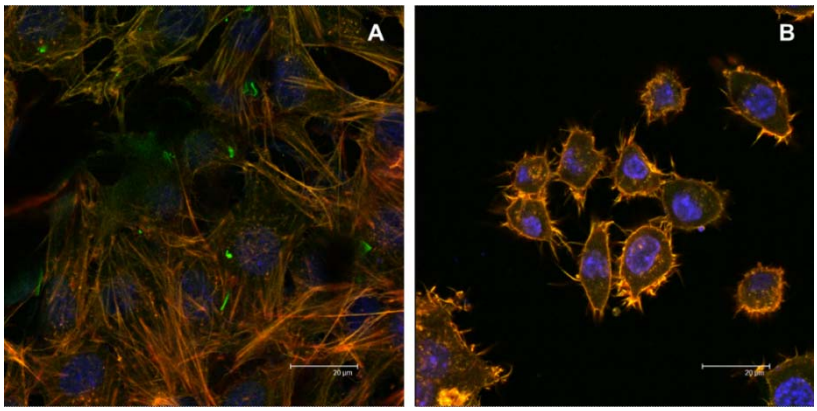

Figura 36. Preosteoblastos MC3T3-E1 (A) y macrófagos RAW 264.7 (B) cultivados en presencia de nano-GO observados por Microscopía Confocal. Imágenes procedentes de [*Matesanz MC et al. 2013, Biomaterials*].

Todos estos resultados deben ser tomados en consideración para los estudios de terapia fototérmica ya que algunos de los efectos citotóxicos producidos por el material podrían utilizarse como un factor sinérgico para conseguir la destrucción de las células tumorales.

Biomaterials 34 (2013) 1562–1569

Contents lists available at SciVerse ScienceDirect

Biomaterials

journal homepage: www.elsevier.com/locate/biomaterials

The effects of graphene oxide nanosheets localized on F-actin filaments on cell-cycle alterations

María-Concepción Matesanz [a], Mercedes Vila [b,c], María-José Feito [a], Javier Linares [a], Gil Gonçalves [d], María Vallet-Regi [b,c], Paula-Alexandrina A.P. Marques [d], María-Teresa Portolés [a,*]

[a] Department of Biochemistry and Molecular Biology I, Faculty of Chemistry, Universidad Complutense, 28040 Madrid, Spain
[b] Department of Inorganic and Bioinorganic Chemistry, Faculty of Pharmacy, Universidad Complutense, 28040 Madrid, Spain
[c] Networking Research Center on Bioengineering, Biomaterials and Nanomedicine, CIBER-BBN, Spain
[d] TEMA-NRD, Mechanical Engineering Department, University of Aveiro, 3810-193 Aveiro, Portugal

ARTICLE INFO

Article history:
Received 10 October 2012
Accepted 1 November 2012
Available online 22 November 2012

Keywords:
Actin
Biocompatibility
Interleukin
Macrophage
Nanoparticle
Osteoblast

ABSTRACT

Graphene oxide (GO) is considered to be a promising nanomaterial for biomedical applications due to its small two-dimensional shape besides its electrical and mechanical properties. However, only a few data concerning the cell responses to this material have been described and the GO biocompatibility has not been yet fully assessed. In the present study, graphene oxide nanosheets (GOs) decorated with 1-arm (1-GOs) and 6-arm (6-GOs) poly(ethylene glycol-amine) (PEG) have been incubated with cultured Saos-2 osteoblasts, MC3T3-E1 preosteoblasts and RAW-264.7 macrophages to analyze several key cell markers for *in vitro* biocompatibility evaluation. The results demonstrate that, after internalization, GO nanosheets are localized on F-actin filaments inducing cell-cycle alterations, apoptosis and oxidative stress in these cell types. The observed GOs effects must be considered in further studies focused on photothermal cancer therapy as a synergistic factor.

1. Introduction

Nanomedicine is focused in searching new nanosystems for biomedical applications and the research approaches in this area include various nanoparticles which are being investigated as they offer unique advantages. Among all nanoparticles, graphene is a single-atom-thick sheet of sp^2-hybridized carbon atoms that has attracted great interest in the world of nanotechnology because of its excellent properties as flexibility, elasticity, mechanical resistance and its ability to conduct electricity [1–3]. Although current graphene research is mainly focused on nanoelectronics [4], the use of graphene for biomedical applications such as drug delivery [5,6], tissue engineering [7,8] and hyperthermia cancer therapy [9–11] has been recently proposed. The induction of hyperthermia on graphene for cancer treatment is possible due to the energy transfer produced during the irradiation of the material with light of wavelength in the near infrared (NIR) region (~890 nm), generating vibrational energy. Its strong NIR absorption thus generates sufficient heat for cell destruction (40 °C) [10,11] and it is called photothermal therapy. Graphene is classified depending on its properties such as surface area, number of layers, lateral dimension, surface chemistry and purity [2]. Graphene oxide (GO) is one of the most important graphene derivatives in terms of applications, and has been extensively studied in the recent years [2]. GO is known to have carboxylate groups on the periphery that provide pH dependent negative surface charge and colloidal stability [12]. The basal surfaces contain hydroxyl and epoxide functional groups as well as hydrophobic domains capable of π–π interactions. Although GO colloids are soluble in water, they need further functionalization with molecules like poly(ethylene glycol-amine) (PEG) which let the material become dispersible and highly stable in aqueous solutions [5,13]. Recent studies demonstrate the applicability of graphene with magnetic properties and fluorescence as a multifunctional marker for *in vitro* and *in vivo* studies with HeLa cells and zebrafish respectively [14]. *In vivo* tests in mice show that, after intravenous administration, GO is mainly located in lung, liver and spleen, causing some toxicity in these tissues [15]. However, other authors showed no toxicity after three months of injection of GO (20 mg/kg) in this animal model [16]. In human lung epithelial cells, GO doses over 50 μg/mL show no toxicity *in vitro* [17], but higher GO concentrations cause a dose-dependent oxidative stress in these cells and a slight loss of cell viability. In fact, most studies agree that GO promotes cytotoxicity mainly through ROS generation in a dose-dependent manner [14,18–20]

* Corresponding author. Fax: +34 1 394 41 59.
E-mail address: portoles@quim.ucm.es (M.-T. Portolés).

0142-9612/$ – see front matter © 2012 Elsevier Ltd. All rights reserved.
http://dx.doi.org/10.1016/j.biomaterials.2012.11.001

inducing oxidative stress. All these results demonstrate that further studies are needed to examine in more detail the interaction between GO and cells before applying this material with medical purposes.

In the present study, different cell types were selected to evaluate their behavior after being in contact with pegylated graphene nanosheets (GOs). Thus, human osteosarcoma Saos-2 cells (as tumor cell line), murine MC3T3-E1 preosteoblasts (as undifferentiated osteoblast-like cells) and murine RAW-264.7 macrophages (as immune cells) were used as experimental models. To know the influence of its surface charge and particle size on cell functions, GOs decorated with 1-arm (1-GOs) and 6-arm (6-GOs) branched PEG were studied. Both GOs were marked with fluorescein isocyanate to measure their uptake and intracellular localization. Different biocompatibility parameters as reactive oxygen species (ROS) production, plasma membrane integrity, cell-cycle phases, apoptosis and light scattering properties were measured by flow cytometry after 1 day treatment. Moreover, the effects of GOs on cell proliferation, cell morphology and cytokine release were also analyzed.

2. Material and methods

2.1. GO nanosheet preparation and characterization

GO nanosheets have been prepared following the method previously published by the authors [21]. Basically, GO nanosheets of c.a. 100 nm were obtained from exfoliation of high purity graphite in acidic medium by a modified Hummers method [22]. The resulting GO suspension was then dialyzed until a pH of 7, activated to promote −COOH groups at its surface, and functionalized by covalent bonding with non-toxic and non-immunogenic polymers poly(ethylene Glycol-amine) (PEG) to avoid the intercession with cellular functions or target immunogenicities and to decrease aggregation. Different branched PEG polymer were attached following the same route, 1-arm PEG bis(3-aminopropyl) terminated (1.5 kDa) and 6-arm branched PEG amine (15 kDa). The samples named 1-GOs and 6-GOs respectively were marked with the amine reactive dye fluorescein isocyanate (FITC) covalent bonded to the PEG. Transmission electron microscopy (TEM) was performed on a 200 kV JEOL JEM 2100. GO nanosheets were analyzed by atomic force microscopy (AFM, VEECO multimode; USA.) and Fourier transform infrared spectroscopy (FTIR, Nicolet Nexus spectrometer). Zeta-potential (ζ) and dynamic light scattering particle size analysis DLS measurements were also performed in pH 5 solutions in a Zetasizer Nano Series instrument equipped with a 633 nm "red" laser from Malvern Instruments with reproducibility being verified by collection and comparison of sequential measurements. *Z*-average sizes of three sequential measurements were collected at RT and analyzed.

2.2. Cell culture for FITC-GO nanosheet incorporation and cell proliferation studies

Saos-2 osteoblasts, MC3T3-E1 preosteoblasts and RAW-264.7 macrophages were seeded at a density of 10^5 cells/mL in culture medium supplemented with 10% FBS, 1 mM L-glutamine, penicillin, streptomycin, under a 5% CO_2 atmosphere and at 37 °C for 24 h in contact with 75 μg/mL FITC-GO material. Then, the attached cells were harvested using either 0.25% trypsin-EDTA (in Saos-2 and MC3T3-E1 cells) or cell scrapers (in RAW-264.7 cells) and counted with a Neubauer hemocytometer. The fluorescence of FITC-GO was excited at 488 nm and measured with a 530/30 band pass filter in a FACScalibur Becton Dickinson flow cytometer.

2.3. Intracellular reactive oxygen species (ROS) content and cell viability

After culture with GO material and detachment, cells were incubated with 100 μM 2′,7′-dichlorofluorescein diacetate (DCFH/DA) (37 °C for 30 min). DCF fluorescence was excited at 488 nm and measured with a 530/30 band pass filter in a FACScalibur Becton Dickinson flow cytometer. In these assays, the basal green fluorescence of FITC-GOs associated to cells in the absence of DCFH/DA, was subtracted from the total fluorescence values (FITC-GOs plus DCF), in order to measure only the DCF fluorescence due to the DCFH oxidation by ROS. Cell viability was determined by addition of propidium iodide (PI; 0.005% in PBS). The PI exclusion indicates the plasma membrane integrity.

2.4. Cell-cycle analysis and apoptosis detection

After culture with GO material and detachment, cells were incubated for 30 min with Hoechst 33258. Hoechst fluorescence was excited at 350 nm and measured at 450 nm in a LSR Becton Dickinson flow cytometer. The fluorescence of Hoechst was excited at 350 nm and the emission was measured at 450 nm in a LSR Becton Dickinson flow cytometer. The cell percentage in each cycle phase: G_0/G_1, S and G_2/M was calculated with the CellQuest Program of Becton Dickinson and the $SubG_1$ fraction was used as indicative of apoptosis.

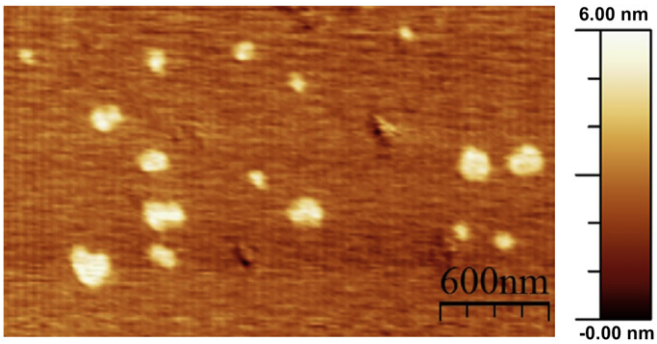

Fig. 1. AFM topographic image of GOs.

2.5. Cell size and complexity

Forward angle (FSC) and side angle (SSC) scatters were indicative of cell size and complexity respectively using a FACScalibur Becton Dickinson flow cytometer.

2.6. Confocal microscopy studies

Cells were seeded on glass coverslips and cultured in the presence of FITC-GO material for 24 h, fixed with 3.7% paraformaldehyde in PBS, permeabilizated with 0.1% Triton X-100 and preincubated with PBS containing 1% BSA. Then, cells were incubated for 20 min with rhodamine-phalloidin (1:40), stained with 4′-6-diamidino-2′-phenylindole (DAPI, 3×10^{-6} M in PBS) and examined using a Leica SP2 Confocal Laser Scanning Microscope. Rhodamine fluorescence was excited at 540 nm and measured at 565 nm. DAPI fluorescence was excited at 405 nm and measured at 420–480 nm. FITC fluorescence was excited at 488 nm and measured at 491–586 nm.

2.7. Inflammatory cytokine detection

IL-1β, TNF-α, and IL-6 cytokines released by cells to the culture medium were quantified by ELISA with a Gen-Probe Diaclone kit.

2.8. Statistics

Data are expressed as means + standard deviations of a representative of three experiments carried out in triplicate. Statistical analysis was performed using the Statistical Package for the Social Sciences (SPSS) version 19 software. Statistical comparisons were made by analysis of variance (ANOVA). Scheffé test was used for *post hoc* evaluations of differences among groups. In all of the statistical evaluations, $p < 0.05$ was considered as statistically significant.

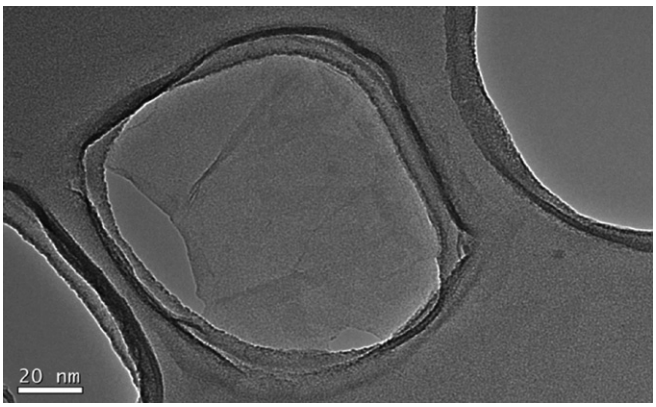

Fig. 2. Transmission electron micrograph of activated GOs.

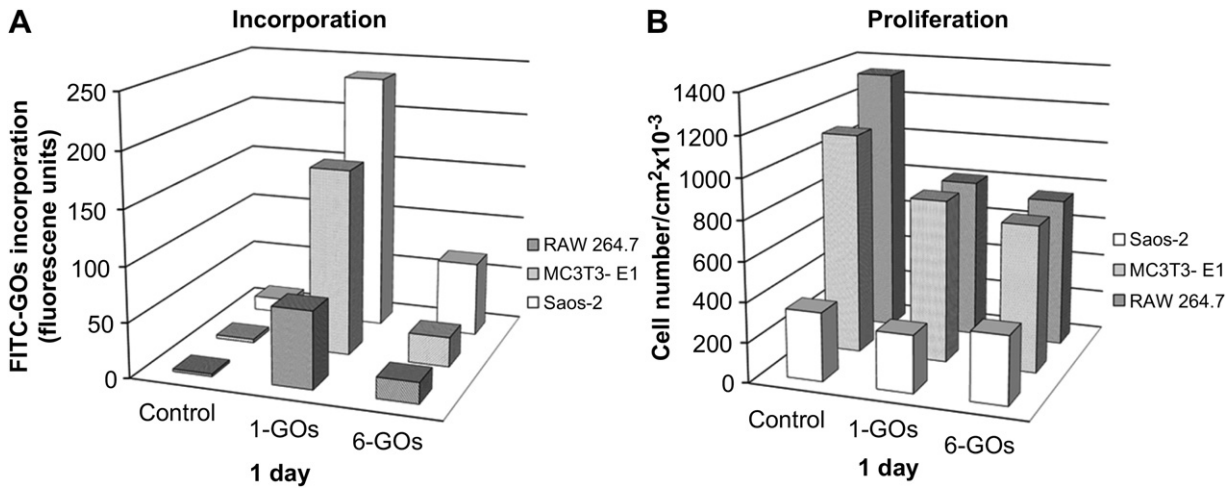

Fig. 3. GOs incorporation (A) and effects on proliferation (B) of human Saos-2 osteoblasts, murine MC3T3-E1 preosteoblasts and murine RAW-264.7 macrophages after 1 day treatment. Controls without GOs were also carried out.

Table 1
Effect of 1-GOs and 6-GOs on cell viability of human Saos-2 osteoblasts, murine MC3T3-E1 preosteoblasts and murine RAW-264.7 macrophages after 1 day treatment. Controls without GOs were also carried out. Statistical significance: $^{*}p < 0.05$, $^{***}p < 0.005$.

	Control	1-GOs	6-GOs
Saos-2	96.24 ± 0.65	94.73 ± 0.28*	94.91 ± 0.28*
MC3T3-E1	97.67 ± 0.66	94.47 ± 2.08*	97.60 ± 0.32*
RAW-264.7	89.55 ± 0.33	84.05 ± 0.30***	83.67 ± 1.02***

3. Results and discussion

Although graphene oxide (GO) is considered the most promising "nanoparticle" for biomedical applications due to its small two-dimensional shape besides its electrical and mechanical properties, only a few data concerning the cell responses to this material have been described [23–25] and the GO biocompatibility has not been yet fully assessed [2,15]. In the present study, graphene oxide nanosheets (GOs) decorated with 1-arm (1-GOs) and 6-arm (6-GOs) PEG have been incubated with different cultured cell types to analyze several key cell markers for *in vitro* biocompatibility evaluation.

A complete characterization of the material has been previously published by our group [21]. As a brief description, GOs have shown in AFM to be thin, of 3–4 layers of graphene with an average thickness around 1.8 nm (Fig. 1) as confirmed by TEM (Fig. 2). Particle sizes observed are in agreement with the range obtained by DLS analysis, showing a hydrodynamic size distribution in the range of c.a. 10–120 nm with a maximum located around 40 nm.

The GOs functionalization by covalent bonding with either 1-arm or 6-arm PEG was carried out to decrease aggregation processes. As it was expected, hydrodynamic particle size increased with the increasing number of branches of the PEG, shifting the maximum hydrodynamic size from 40 nm of the GO, to 95 and 190 nm for the 1-arm and 6-arm pegylated GO respectively. These samples, named 1-GOs and 6-GOs, respectively, were marked with fluorescein isocyanate (FITC) covalent bonded to the PEG to

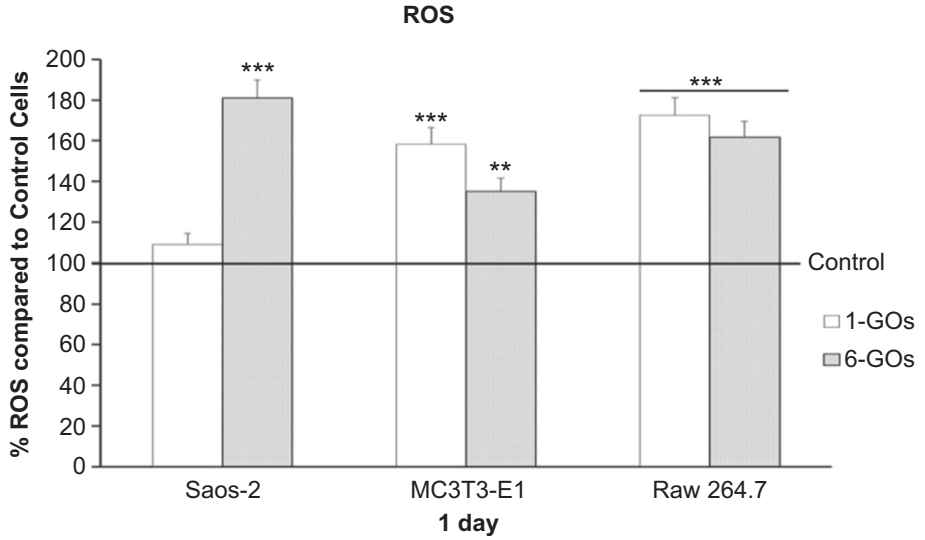

Fig. 4. GOs effects on ROS production of human Saos-2 osteoblasts, murine MC3T3-E1 preosteoblasts and murine RAW-264.7 macrophages after 1 day treatment. This production is referred as percentage in relation to the controls (100%) carried out without GOs. Statistical significance: $^{**}p < 0.01$, $^{***}p < 0.005$.

evaluate the GOs uptake by three cell types with specific functions: two osteoblastic cell lines in diverse stages of differentiation and a macrophagic cell type. Saos-2 osteoblasts are a human osteosarcoma cell line usually employed as experimental model for *in vitro* studies [26,27] due to its osteoblastic properties as production of mineralized matrix, high levels of alkaline phosphatase, PTH receptors coupled to adenylate cyclase and osteonectin presence [28]. The preosteoblastic cell line MC3T3-E1 has been established from a C57BL/6 mouse calvaria and has the capacity to differentiate into osteoblasts and osteocytes forming calcified bone tissue *in vitro*. On the other hand, RAW-264.7 cells are functional macrophages with the ability of pinocytose and phagocytose [29] as immune cells.

Fig. 3A shows the incorporation differences between both GOs in human Saos-2 osteoblasts, murine MC3T3-E1 preosteoblasts and murine RAW-264.7 macrophages after 1 day treatment. As it has been discussed in previous work [21], the results evidence higher 1-GOs uptake than 6-GOs incorporation in all cases and reveal that the cell associated GOs amount also depends on the cell type. Thus, the osteoblastic cell lines Saos-2 and MC3T3-E1 internalize more GOs than macrophages, obtaining the highest uptake in Saos-2 cells.

Both facts are related with non-phagocytic cells preference for the uptake of smaller particles and with the PEG having nonfouling or protein resistant properties that were specifically included lo limit the interaction with biological interfaces in order to decrease particle uptake by macrophages for increasing their circulation time.

Moreover, this behavior could be due to the characteristics of this human osteosarcoma cell line and this fact may have a great interest for future studies with GOs for selective photothermal anti-

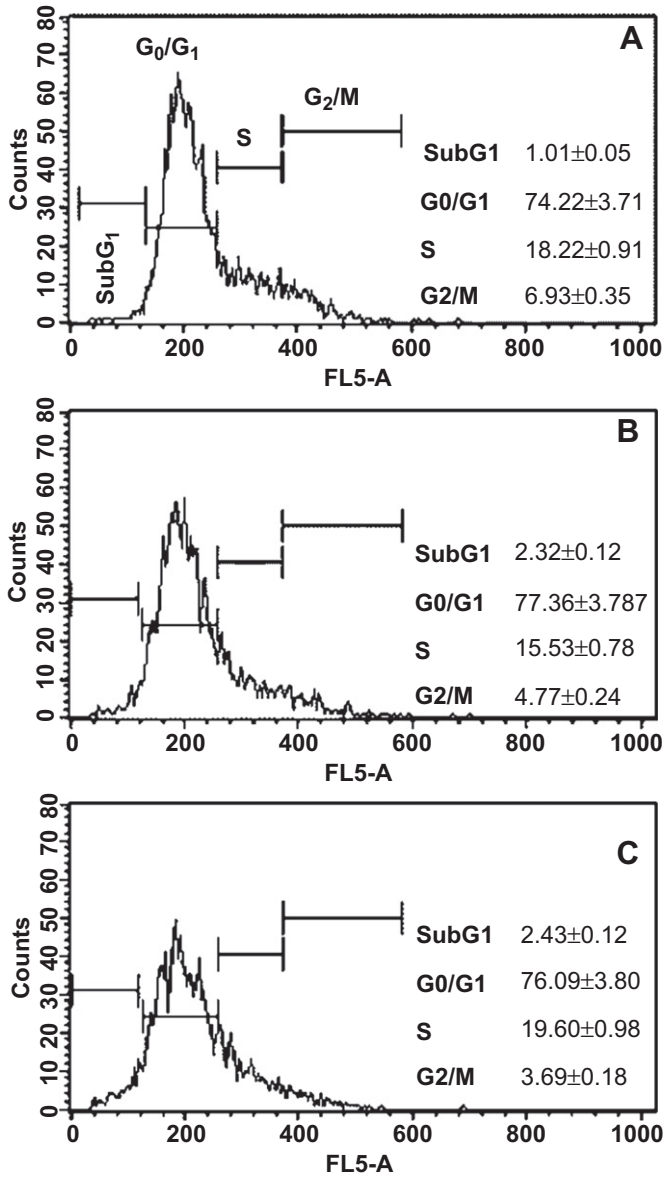

Fig. 5. GOs effects on cell-cycle phases of human Saos-2 osteoblasts after 1 day treatment. A) Control cells without GOs; B) and C) cells treated with 1-GOs and 6-GOs, respectively.

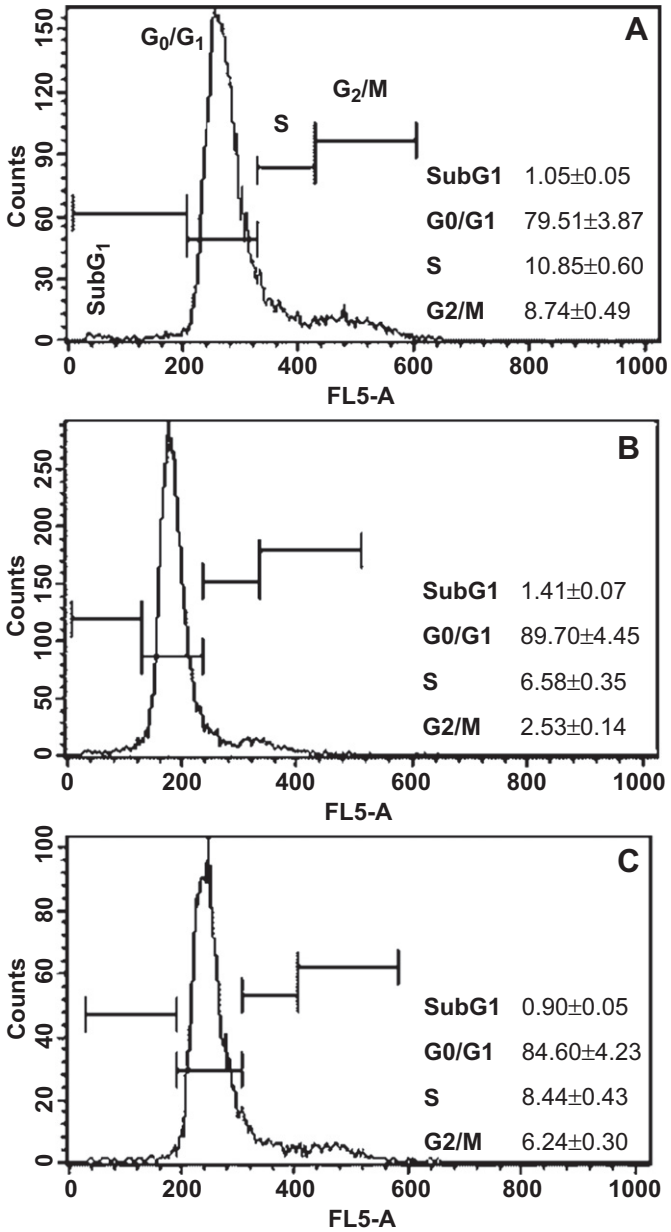

Fig. 6. GOs effects on cell-cycle phases of murine MC3T3-E1 preosteoblasts after 1 day treatment. A) Control cells without GOs; B) and C) cells treated with 1-GOs and 6-GOs, respectively.

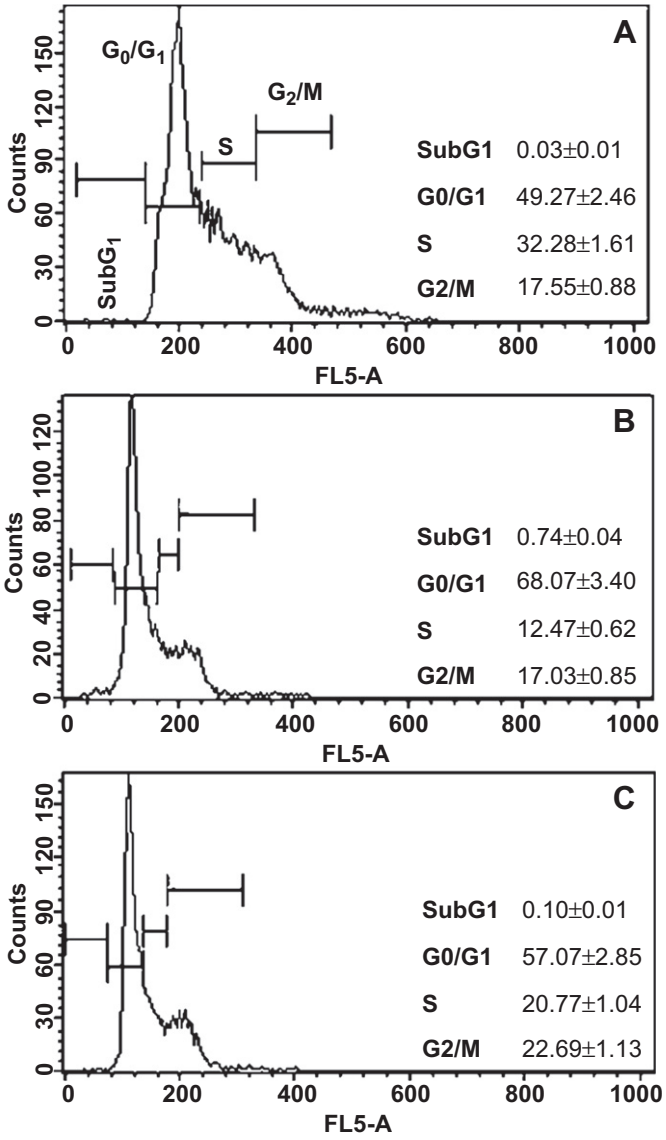

Fig. 7. GOs effects on cell-cycle phases of murine RAW-264.7 macrophages after 1 day treatment. A) Control cells without GOs; B) and C) cells treated with 1-GOs and 6-GOs, respectively.

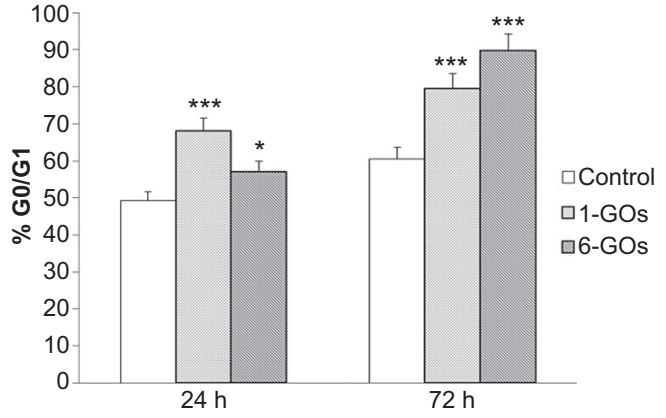

Fig. 8. GOs effects on G_0/G_1 cell-cycle phase of murine RAW-264.7 macrophages after 24 h and 72 h treatments with 1-GOs and 6-GOs. Control without GOs were also carried out. Statistical significance: $^{*}p < 0.05$, $^{***}p < 0.005$.

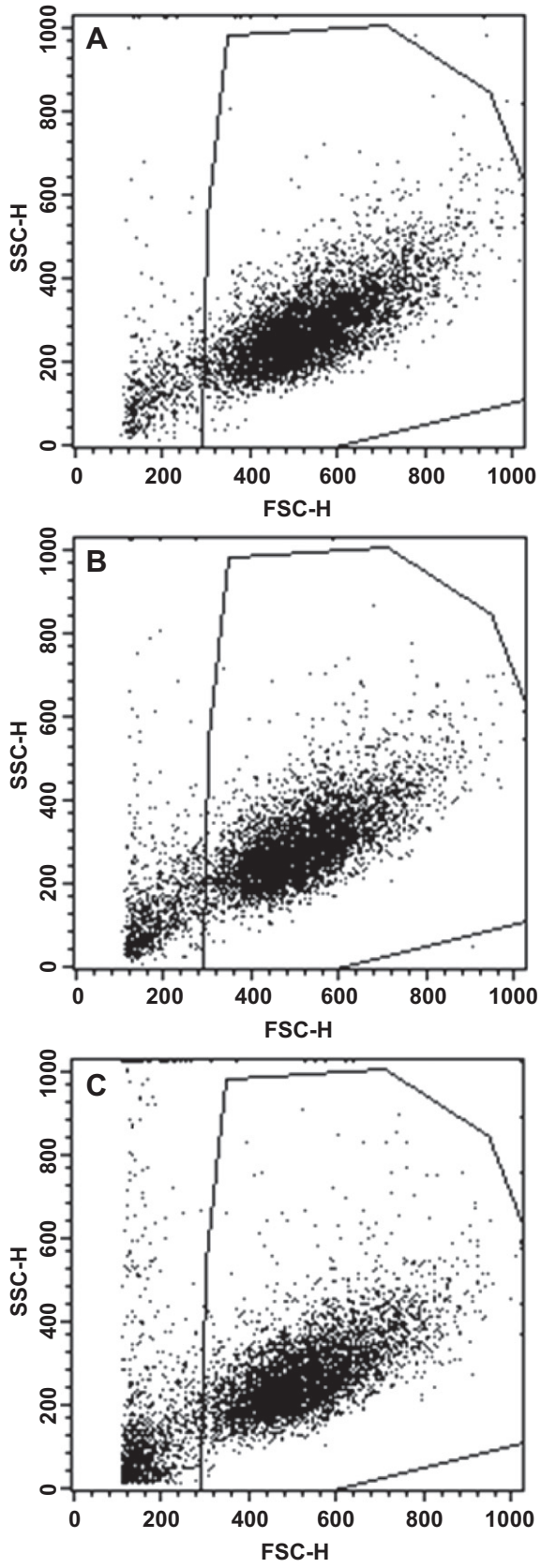

Fig. 9. GOs effects on light scattering properties of human Saos-2 osteoblasts after 1 day treatment. A) control cells without GOs; B) and C) cells treated with 1-GOs and 6-GOs, respectively. Forward angle (FSC) and 90° side angle (SSC) light scatters were analyzed by flow cytometry as a measurement of cell size and internal complexity, respectively.

cancer therapy, once the GOs uptake kinetics of different cell types is well known.

The effects of GOs incorporation on the proliferation of Saos-2, MC3T3-E1 and RAW-264.7 cells were also evaluated after 1 day treatment. Although these three cell types can proliferate in contact with both 1-GOs and 6-GOs materials, a slight growth delay induced by GOs is observed in comparison with the respective control cells cultured on tissue culture plastic (Fig. 3B). Some authors have recently evaluated the interaction of cells with graphene films and scaffolds observing that these substrates promote adherence of human osteoblasts [23] and accelerate the osteogenic differentiation of human mesenchymal stem cells [25]. However, the growth delay observed in the present study is probably due to the different interaction of cells with nanosized particles of GO, instead of surfaces, which is affecting their proliferation rate. On the other hand, high values of cell viability evaluated by propidium iodide (PI) exclusion were obtained, and this parameter remains over 80–90% in all cases (Table 1). This exclusion test demonstrates the plasma membrane integrity which avoids the PI penetration for intracellular DNA staining. Although recent studies indicate that the direct interaction between GOs and cells can result in physical damage to the plasma membrane, this effect is largely attenuated when GO is incubated with fetal bovine serum (FBS) due to the extremely high protein adsorption ability of GO [20].

Since direct or indirect generation of reactive oxygen species (ROS) and oxidative stress induction are the leading toxicity mechanisms proposed for engineered nanomaterials [2], the effects of 1-GOs and 6-GOs on intracellular ROS content of Saos-2, MC3T3-E1 and RAW-264.7 cells were studied after 1 day treatment with the probe DCFH/DA. Fig. 4 reveals that GOs materials produce significant increases ($^{***}p < 0.005$ and $^{**}p < 0.01$) of ROS levels in all cell types except 1-GOs in Saos-2 cells. In these assays, the basal green fluorescence of FITC-GOs associated to cells in the absence of DCFH/DA, was subtracted in order to measure only the DCF fluorescence due to the DCFH oxidation by ROS.

Recent toxicological studies with multifunctional graphene have revealed non-cytotoxic results in HeLa cells without significant amounts of ROS and apoptosis [14]. However, pristine graphene can induce cytotoxicity in RAW-264.7 macrophages through the depletion of the mitochondrial membrane potential and the increase of ROS, triggering apoptosis by activation of the mitochondrial pathway through the MAPKs and the TGF-beta-related signaling pathways [30].

Considering both the proliferation delay and the enhanced ROS production induced by GOs in the present study, it was also of interest to analyze the effects of these materials on the cell-cycle phases and apoptosis of Saos-2, MC3T3-E1 and RAW-264.7 cells. Proliferation is dependent on the cell-cycle progression, in which

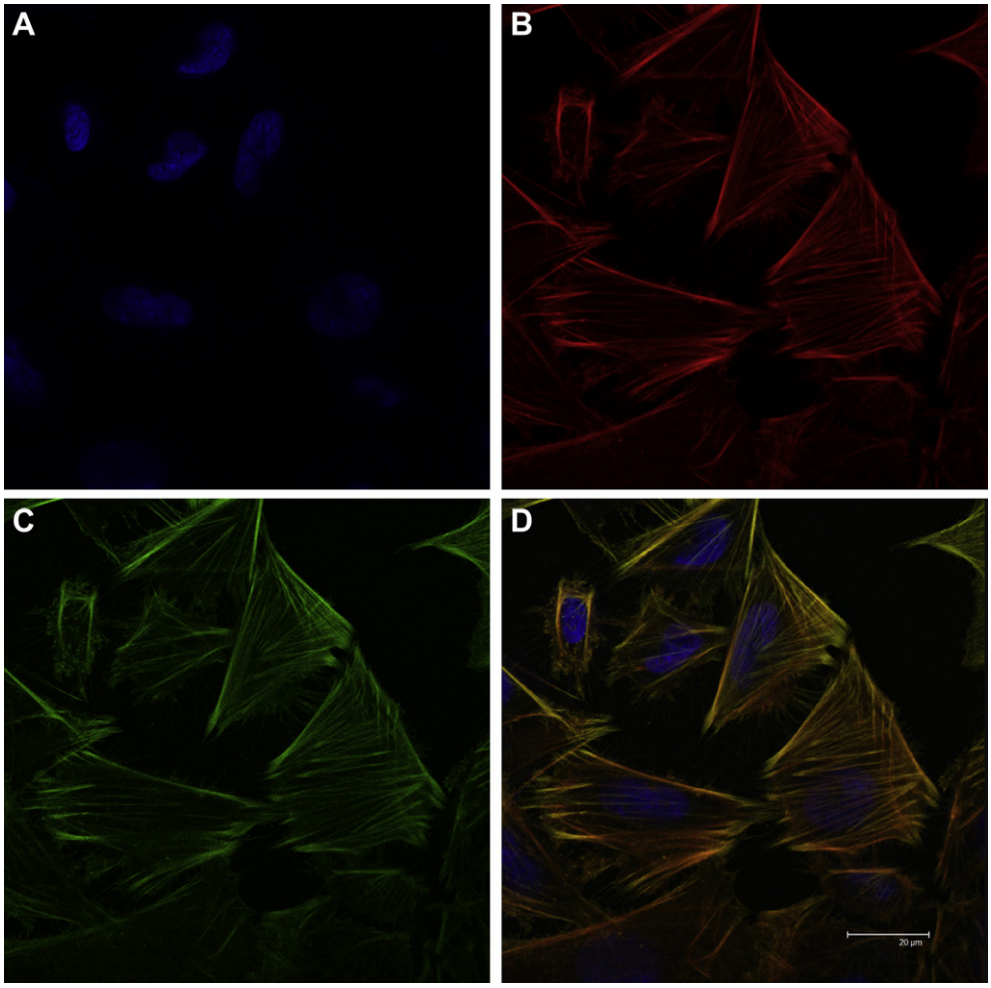

Fig. 10. Morphology evaluation by confocal microscopy of cultured human Saos-2 osteoblasts after 1 day treatment with GOs. Cells were stained with DAPI (A) for the visualization of the cell nuclei in blue, rhodamine-phalloidin (B) for the visualization of cytoplasmic F-actin filaments in red and FITC-GOs for the visualization of GOs in green (C). Fig. 10 D shows the whole composition with the three stainings revealing that FITC-GOs colocalizes with rhodamine-phalloidin resulting in yellow/orange coloration. Controls without GOs were also carried out. (For interpretation of the references to color in this figure legend, the reader is referred to the web version of this article.)

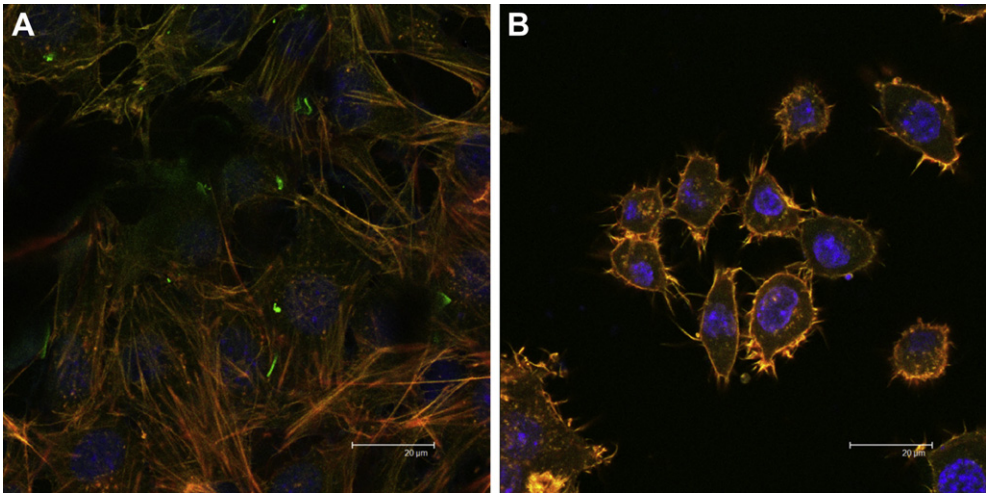

Fig. 11. Morphology evaluation by confocal microscopy of cultured murine MC3T3-E1 preosteoblasts (A) and murine RAW-264.7 macrophages (B) after 1 day treatment with GOs. Cells were stained with DAPI for the visualization of the cell nuclei in blue, rhodamine-phalloidin for the visualization of cytoplasmic F-actin filaments in red and FITC-GOs for the visualization of GOs in green. Figure shows the whole composition with the three stainings revealing that FITC-GOs colocalizes with rhodamine-phalloidin resulting in yellow/orange coloration. Controls without GOs were also carried out. (For interpretation of the references to color in this figure legend, the reader is referred to the web version of this article.)

cells pass through the G_0/G_1 phase (Quiescence/Gap 1) to the S phase (Synthesis) and finally to the G_2/M phase (Gap 2 and Mitosis). $SubG_1$ fraction corresponds to cells with fragmented DNA and it is indicative of apoptosis. Figs. 5–7 show the cycle profiles and cell percentages in each cycle phase of these three cell types after 1 day culture in the presence of 1-GOs (Figs. 5–7B) and 6-GOs (Figs. 5–7C). Controls without materials were always carried out (Figs. 5–7A). As it can be observed, the effects of these materials on cell proliferation are accompanied by some cell-cycle alterations. $SubG_1$ fraction shows a slight but significant apoptosis increase ($^{***}p < 0.005$) induced by both GOs in all cell types except by 6-GOs in MC3T3-E1 cells. The G_0/G_1 percentages of MC3T3-E1 preosteoblasts and RAW-264.7 macrophages are significantly increased ($^{***}p < 0.005$) by treatment with both GOs in comparison with control values in the absence of GOs. These G_0/G_1 increases are accompanied by significant decreases of S fractions, thus indicating a G_0/G_1 cell-cycle phase arrest induced by GOs in these two cell types, mainly in the macrophagic cell line which showed a more pronounced G_0/G_1 arrest after 72 h treatment (Fig. 8). Saos-2 and MC3T3-E1 cells show a significant decrease of G_2/M phase ($^{***}p < 0.005$) which can be also related to the observed growth delay and reveals an alteration of the capacity for mitotic division. In many cases, apoptosis and cell-cycle arrest are connected [31]. Generally, the eukaryotic cell-cycle progression is regulated by sequential activation and subsequent inactivation of a series of cyclin-dependent kinases (Cdks) during the corresponding phases. Cellular responses such as cell-cycle arrest or apoptosis depend on the toxicants (which can produce either activation or inhibition of cell checkpoints), the cell type and where cells are in the cell-cycle when they encounter these damaging agents. Since some anti-cancer treatments are based on cell-cycle arrest and induction of apoptosis [32,33], the GOs effects on cell-cycle observed in the present study must be considered in further studies focused on photothermal cancer therapy and it may be used as a synergistic factor that could be deliberately increased in targeted anti-cancer treatments.

When light scattering properties of these three cell types cultured in contact with GOs were evaluated by flow cytometry, no cell size or complexity alterations were observed. Fig. 9 shows these parameters measured through forward angle (FSC) and 90° side angle (SSC) light scatters respectively with human Saos-2 osteoblasts after 1 day GOs treatment. Results concerning MC3T3-E1 and RAW-264.7 cells also demonstrate no differences between GOs treated and control cells (data not shown).

Confocal microscopy techniques were carried out to evaluate the Saos-2, MC3T3-E1 and RAW-264.7 morphology in the presence of GOs and to study its intracellular localization. The typical characteristics of osteoblasts, preosteoblasts and macrophages are observed in the presence of FITC-GOs (in green), rhodamine-phalloidin (to stain F-actin filaments in red) and DAPI (for nuclear staining in blue) (Fig. 10A–C). The present study demonstrates that GOs materials are co-localized with rhodamine-phalloidin (resulting in yellow/orange coloration), evidencing that internalized GO nanosheets are positioned closed to F-actin filaments (Figs. 10D and 11). This fact can be related to the observed alterations produced by GOs materials on cell cycle (Figs. 5–7) because it is well established that actin microfilaments have to be intact for G_1 progression, S phase entry and mitotic division [34].

Cytokines are oxidative stress-sensitive generated molecules which can act as pivotal ROS mediators with an important role in the maintenance of cellular homeostasis [35]. Since interleukin-6 (IL-6) has been shown to protect against different compound-

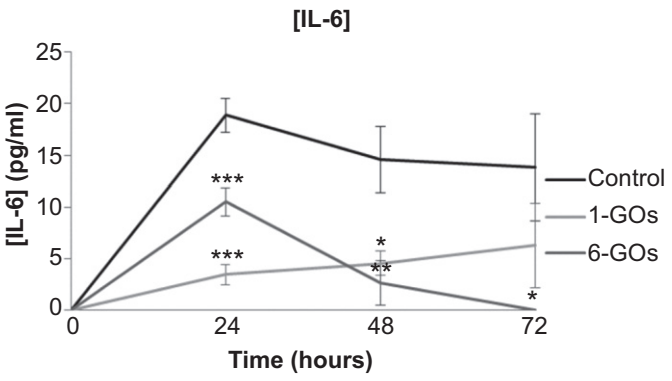

Fig. 12. GOs effects on IL-6 release by cultured human Saos-2 osteoblasts after 24, 48 and 72 h treatment. Controls without material were also carried out.

induced cytotoxicity [36], the production of this proinflammatory cytokine was evaluated in the culture medium after treatment of cells with both GOs during different times. As it can be observed in Fig. 12, both materials seem to affect the cytokine production by Saos-2 cells showing a significant decrease of IL-6 levels more pronounced after 72 h treatment with 6-GO. No significant alterations were detected in the other cell types (data not shown).

4. Conclusions

In this study Saos-2 osteoblasts, MC3T3-E1 preosteoblasts and RAW-264.7 macrophages were cultured with GO nanosheets (GOs) decorated with 1-arm (1-GOs) and 6-arm (6-GOs) PEG to analyze several key cell markers for *in vitro* biocompatibility evaluation. After internalization, GOs are localized on F-actin filaments inducing cell-cycle alterations, apoptosis and oxidative stress. These GOs effects must be considered in further studies focused on photothermal cancer therapy as a synergistic factor.

Acknowledgments

This study was supported by research grants from Comunidad de Madrid (S2009/MAT-1472), Spanish CICYT (MAT-2008-00736) and the Network of Excellence CSO2010-11384-E. M.C. Matesanz is greatly indebted to MICINN for the predoctoral fellowship. M.Vila thanks the Spanish Ministry for the RyC grant and the FSE. P. Marques thanks to the Ciencia 2007 Program and G. Gonçalves thanks to Iberian Nanotechnology Laboratory (INL) for a PhD grant. The authors wish to thank also to the staff of the Cytometry and Fluorescence Microscopy Center of the Universidad Complutense de Madrid (Spain) for the assistance in the flow cytometry and confocal microscopy studies.

References

[1] Novoselov KS, Geim AK, Morozov SV, Jiang D, Zhang Y, Dubonos SV, et al. Electric field effect in atomically thin carbon films. Science 2004;306:666–9.
[2] Sanchez VC, Jachak A, Hurt RH, Kane AB. Biological interactions of graphene-family nanomaterials: an interdisciplinary review. Chem Res Toxicol 2012;25:15–34.
[3] Geim AK. Graphene: status and prospects. Science 2009;324:1530–4.
[4] Ruoff R. Graphene: calling all chemists. Nat Nanotechnol 2008;3:10–1.
[5] Sun X, Liu Z, Welsher K, Robinson JT, Goodwin A, Zaric S, et al. Nano-graphene oxide for cellular imaging and drug delivery. Nano Res 2008;1:203–12.
[6] Zhang L, Xia J, Zhao Q, Liu L, Zhang Z. Functional graphene oxide as a nanocarrier for controlled loading and targeted delivery of mixed anticancer drugs. Small 2010;6:537–44.
[7] Fan H, Wang L, Zhao K, Li N, Shi Z, Ge Z, et al. Fabrication, mechanical properties, and biocompatibility of graphene-reinforced chitosan composites. Biomacromolecules 2010;11:2345–51.
[8] Depan D, Girase B, Shah JS, Misra RD. Structure-process-property relationship of the polar graphene oxide-mediated cellular response and stimulated growth of osteoblasts on hybrid chitosan network structure nanocomposite scaffolds. Acta Biomater 2011;7:3432–45.
[9] Huang P, Xu C, Lin J, Wang C, Wang X, Zhang C, et al. Folic acid-conjugated graphene oxide loaded with photosensitizers for targeting photodynamic therapy. Theranostics 2011;1:240–50.
[10] Yang K, Zhang S, Zhang G, Sun X, Lee ST, Liu Z. Graphene in mice: ultrahigh *in vivo* tumor uptake and efficient photothermal therapy. Nano Lett 2010;10:3318–23.
[11] Kam NW, O'Connell M, Wisdom JA, Dai H. Carbon nanotubes as multifunctional biological transporters and near-infrared agents for selective cancer cell destruction. Proc Natl Acad Sci U S A 2005;102:11600–5.
[12] Park S, An J, Jung I, Piner RD, An SJ, Li X, et al. Colloidal suspensions of highly reduced graphene oxide in a wide variety of organic solvents. Nano Lett 2009;9:1593–7.
[13] Liu Z, Robinson JT, Sun X, Dai H. PEGylated nanographene oxide for delivery of water-insoluble cancer drugs. J Am Chem Soc 2008;130:10876–7.
[14] Gollavelli G, Ling YC. Multi-functional graphene as an *in vitro* and *in vivo* imaging probe. Biomaterials 2012;33:2532–45.
[15] Wang K, Ruan J, Song H, Zhang J, Wo Y, Guo S, et al. Biocompatibility of graphene oxide. Nanoscale Res Lett 2011;6:8.
[16] Yang K, Wan J, Zhang S, Zhang Y, Lee ST, Liu Z. *In vivo* pharmacokinetics, long-term biodistribution, and toxicology of PEGylated graphene in mice. ACS Nano 2011;5:516–22.
[17] Chang Y, Yang ST, Liu JH, Dong E, Wang Y, Cao A, et al. *In vitro* toxicity evaluation of graphene oxide on A549 cells. Toxicol Lett 2011;200:201–10.
[18] Liu X, Sen S, Liu J, Kulaots I, Geohegan D, Kane A, et al. Antioxidant deactivation on graphenic nanocarbon surfaces. Small 2011;4(7):2775–85.
[19] Zhang Y, Ali SF, Dervishi E, Xu Y, Li Z, Casciano D, et al. Cytotoxicity effects of graphene and single-wall carbon nanotubes in neural phaeochromocytoma-derived PC12 cells. ACS Nano 2010;4:3181–6.
[20] Hu W, Peng C, Lv M, Li X, Zhang Y, Chen N, et al. Protein corona-mediated mitigation of cytotoxicity of graphene oxide. ACS Nano 2011;5:3693–700.
[21] Vila M, Portolés MT, Marques PAAP, Feito MJ, Matesanz MC, Ramírez-Santillán C, et al. Cell uptake survey of pegylated nano graphene oxide. Nanotechnology 2012;23(465103):9.
[22] Gonçalves G, Marques PAAP, Granadeiro C, Nogueira HIS, Singh MK, Grácio J. Surface modification of graphene nanosheets with gold nanoparticles: the role of oxygen moieties at graphene surface on gold nucleation and growth. Chem Mater 2009;21:4796–802.
[23] Kalvacova M, Broz A, Kong J, Kalbac M. Graphene substrates promote adherence of human osteoblasts and mesenchymal stromal cells. Carbon 2010;48:4323–9.
[24] Chun YW, Wang W, Choi J, Nam TH, Lee YH, Cho KK, et al. Control of macrophage responses on hydrophobic and hydrophilic carbon nanostructures. Carbon 2011;49:2092–103.
[25] Nayak TR, Andersen H, Makam VS, Khaw C, Bae S, Xu X, et al. Graphene for controlled and accelerated osteogenic differentiation of human mesenchymal stem cells. ACS Nano 2011;5:4670–8.
[26] Fassina L, Visai L, Asti L, Benazzo F, Speziale P, Tanzi MC, et al. Calcified matrix production by Saos-2 cells inside a polyurethane porous scaffold, using a perfusion bioreactor. Tissue Eng 2005;11:685–700.
[27] Mayr-Wohlfart U, Fiedler J, Günther KP, Puhl W, Kessler S. Proliferation and differentiation rates of a human osteoblast-like cell line (Saos-2) in contact with different bone substitute materials. J Biomed Mater Res 2001;57:132–9.
[28] Rodan SB, Imai Y, Thiede MA, Wesolowski G, Thompson D, Bar-Shavit Z, et al. Characterization of a human osteosarcoma cell line (Saos-2) with osteoblastic properties. Cancer Res 1987;15:4961–6.
[29] Raschke WC, Baird S, Ralph P, Nakoinz I. Functional macrophage cell lines transformed by Abelson leukemia virus. Cell 1978;15:261–7.
[30] Li Y, Liu Y, Fu Y, Wei T, Guyader LL, Gao G, et al. The triggering of apoptosis in macrophages by pristine graphene through the MAPK and TGF-beta signalling pathways. Biomaterials 2012;33:402–11.
[31] Sun B, Geng S, Huang X, Zhu J, Liu S, Zhang Y, et al. Coleusin factor exerts cytotoxic activity by inducing G0/G1 cell cycle arrest and apoptosis in human gastric cancer BGC-823 cells. Cancer Lett 2011;301:95–105.
[32] Sanchez I, Dynlacht BD. New insights into cyclins, CDKs, and cell cycle control. Semin Cell Dev Biol 2005;16:311–21.
[33] Shah MA, Schwartz GK. Cyclin-dependent kinases as targets for cancer therapy. Cancer Chemother Biol Response Modif 2005;22:135–62.
[34] Fasshauer M, Iwig M, Glaesser D. Synthesis of proto-oncogene proteins and cyclins depends on intact microfilaments. Eur J Cell Biol 1998;77:188–95.
[35] Portugal M, Barak V, Ginsburg I, Kohen R. Interplay among oxidants, antioxidants, and cytokines in skin disorders: present status and future considerations. Biomed Pharmacother 2007;61:412–22.
[36] Nakajima A, Yamada K, Zou L-B, Yan Y, Mizuno M, Nabeshima T. Interleukin-6 protects PC12 cells from 4-hydroxynonenal-induced cytotoxicity by increasing intracellular glutathione levels. Free Radic Biol Med 2002;32:1324–32.

Una vez analizadas la cinética de incorporación de nano-GO y la respuesta de diferentes tipos celulares a este material, en la presente Tesis Doctoral se ha llevado a cabo la inducción *in vitro* de hipertermia sobre células de osteosarcoma humano Saos-2 cultivadas con nano-1-GO como modelo experimental. Para ello se ha utilizado un láser diodo de alta potencia (30W)(LASING S.A.) de emisión a 808nm que permite la irradiación de un área circular de 3 cm de diámetro (4 J/cm^2). En este estudio se han empleado diferentes condiciones de irradiación con el láser: potencia (1,5 w/cm^2 y 3 w/cm^2) y tiempo de exposición (1, 4, 7, 15 minutos), evaluando los efectos del aumento de temperatura en las células que contienen nano-GO y analizando los dos tipos principales de muerte celular, apoptosis y necrosis. Puesto que la muerte por necrosis normalmente va asociada a un proceso inflamatorio con secreción de citoquinas y activación de células de la respuesta inmune, los niveles de IL-6 fueron analizados en el medio de cultivo después de cada exposición.

Los resultados obtenidos se resumen a continuación y han dado lugar a la siguiente publicación:

- Vila M, Matesanz MC, Gonçalves G, Feito MJ, Linares J, Marques PAAP, Portolés MT, Vallet-Regí M. Triggering cell death by nanographene oxide mediated hyperthermia. Nanotechnology 25: 035101 (7pp); Global Medical Discovery, Key Nanotechnology Articles, June 27, 2014.

La irradiación del láser sobre los cultivos celulares indujo un incremento de temperatura en las células que habían incorporado nano-GO previamente. Sin embargo, las condiciones de exposición al láser no produjeron daño sobre cultivos control en ausencia del material. El incremento de temperatura fue dependiente en mayor medida de la potencia del láser que del tiempo de exposición, alcanzándose valores entre 44 y 57°C durante los ensayos. La irradiación con potencia baja (1,5 w/cm^2) no indujo muerte celular hasta los 7 minutos y la temperatura del cultivo se mantuvo por debajo de los 45°C. Sin embargo, alta potencia de láser (3 w/cm^2) dio lugar al aumento de la temperatura del cultivo por encima de los 50°C a los 4 minutos de irradiación, provocando la muerte celular principalmente por necrosis. Asimismo, se comprobó que la viabilidad celular tras la irradiación era inversamente proporcional a la incorporación de nano-GO. Cuando las células se sometieron a irradiación durante 15 minutos se observó mayor proporción de necrosis respecto a apoptosis con ambas potencias de láser y un pronunciado descenso de la proliferación celular (**Figura 37**). Dado que las células tumorales han desarrollado mecanismos para evadir la apoptosis, la necrosis parece el tipo de muerte celular más efectivo en éstas.

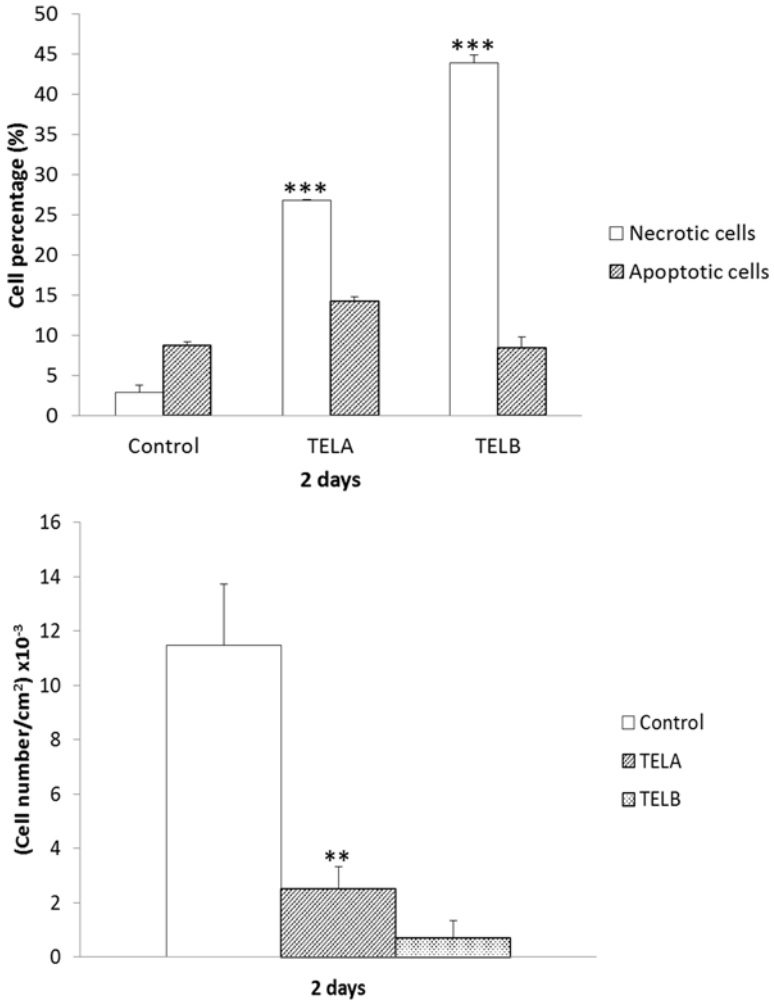

Figura 37. Porcentaje de poblaciones necróticas y apoptóticas (A) y proliferación celular (B) en cultivos de osteoblastos Saos-2 irradiados durante 15 minutos a 1,5 W/cm^2 (TELA) o 3 W/cm^2 (TELB). Gráficas procedentes de [*Vila M et al. 2014, Nanotechnology*].

Por otra parte, se observó una mayor secreción de IL-6 por las células sometidas a tiempos largos de irradiación (15 minutos) tanto con potencias bajas como altas de láser.

Los efectos adversos de la hipertermia se comprobaron mediante el estudio de la morfología celular después de cada tratamiento. Se observaron los filamentos de actina totalmente desorganizados y numerosas células en proceso de necrosis en los cultivos irradiados (**Figura 38**).

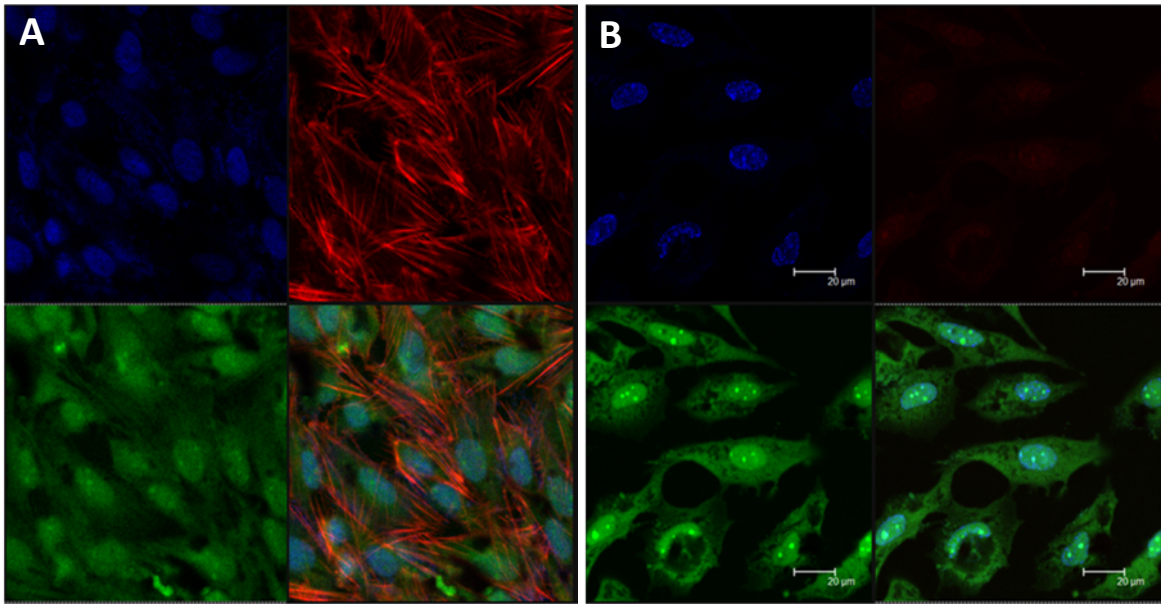

Figura 38. Osteoblastos Saos-2 cultivados en presencia de nano-GO antes (A) y después de la irradiación con el láser (B) observados por Microscopía Confocal. Imágenes procedentes de [*Vila M et al. 2014, Nanotechnology*].

El presente estudio sugiere la posibilidad de provocar la reducción de tumores por hipertermia seleccionando las condiciones de tiempo y potencia de exposición que permitan controlar el tipo de muerte celular, produciendo menores efectos secundarios en la zona afectada del organismo.

IOP Publishing Nanotechnology

Nanotechnology **25** (2014) 035101 (7pp) doi:10.1088/0957-4484/25/3/035101

Triggering cell death by nanographene oxide mediated hyperthermia

M Vila[1,2,5], M C Matesanz[3], G Gonçalves[4], M J Feito[3], J Linares[3], P A A P Marques[4], M T Portolés[3] and M Vallet-Regi[1,2]

[1] Department of Inorganic and Bioinorganic Chemistry, Faculty of Pharmacy, UCM, Instituto de Investigación Sanitaria Hospital 12 de Octubre i+12, E-28040-Madrid, Spain
[2] Networking Research Center on Bioengineering, Biomaterials and Nanomedicine, CIBER-BBN, Spain
[3] Department of Biochemistry and Molecular Biology I, Faculty of Chemistry, Universidad Complutense, E-28040-Madrid, Spain
[4] TEMA-NRD, Mechanical Engineering Department and Aveiro Institute of Nanotechnology (AIN), University of Aveiro, 3810-193 Aveiro, Portugal

E-mail: mvila@ucm.es

Received 5 September 2013, in final form 30 October 2013
Published 17 December 2013

Abstract

Graphene oxide (GO) has been proposed as an hyperthermia agent for anticancer therapies due to its near-infrared (NIR) optical absorption ability which, with its small two-dimensional size, could have a unique performance when compared to that of any other nanoparticle. Nevertheless, attention should be given to the hyperthermia route and the kind of GO–cell interactions induced in the process. The hyperthermia laser irradiation parameters, such as exposure time and laser power, were investigated to control the temperature rise and consequent damage in the GOs containing cell culture medium. The type of cell damage produced was evaluated as a function of these parameters. The results showed that cell culture temperature (after irradiating cells with internalized GO) increases preferentially with laser power rather than with exposure time. Moreover, when laser power is increased, necrosis is the preferential cell death leading to an increase of cytokine release to the medium.

Keywords: graphene oxide, cell death, cancer therapy, hyperthermia, photothermal therapy

S Online supplementary data available from stacks.iop.org/Nano/25/035101/mmedia

(Some figures may appear in colour only in the online journal)

1. Introduction

One of the most novel approaches of nanomedicine for targeting of tumours is the application of nanosystems as 'Trojan horses' to achieve tumour cell destruction while producing minimal side effects on healthy cells [1].

Nevertheless, an aggressive tumour microenvironment provokes drug resistance and tumour progression, whereas the extracellular matrix block penetration of drugs and nanoparticles leaves them concentrated in perivascular regions [2]. Although the initial burst of *in vivo* tests of these nanosystems has shown a potential efficiency, confirming that they could be the next generation of cancer treatments, their application will not be feasible without a previous understanding of vector–cell/tissue interactions, possible toxicity, and accumulation in organs [3–5]. This fact is slowing down the potential development of nanomedicine-based therapies for treating cancer.

Taking profit of the enhanced permeability and retention (EPR) effect, which allows preferential concentration of nanosystems on the tumour peripheric cells, hyperthermia mediated by these systems was suggested as an efficient therapy by triggering thermal heating on the tumoral area, thus producing preferential cell death after internalization of these nanoparticles [6, 7].

Although hyperthermia is a well-known concept [8], little is known about the type of damage, cell death, and secondary

[5] Address for correspondence: Facultad de Farmacia, Universidad Complutense, E-28040-Madrid, Spain.

Table 1. Laser irradiation time and laser irradiation powers.

	T short (TS) 1 min	T medium (TM) 4 min	T long (TL) 7 min	T extra-long (TEL) 15 min
Low power (A) 1.5 W cm^{-2}	TSA	TMA	TLA	TELA
High power (B) 3 W cm^{-2}	TSB	TMB	TLB	TELB

effects that these nanosystem-mediated therapies can provoke locally [9, 10], and attention should be given to the cell reactions that accompany the process.

Among hyperthermia potential agents, graphene represents the most thrilling discovery of the last decade [11]. Graphene and graphene oxide (GO), more orientated for this kind of application, have a strong near-infrared (NIR) (700–1100 nm range) optical absorption ability, and their unique and smaller two-dimensional shape and aspect ratio are incomparable to those of any other particle. Furthermore, it is mandatory to point out the low cost of production of GO in comparison with that of gold or magnetic responsive nanosystems. The use of NIR light for the induction of hyperthermia is particularly attractive, because biological systems mostly lack chromophores that absorb in the NIR region. Hence, tumours could be treated with an NIR laser emitting in the 'therapeutical window', where it is a non-invasive, harmless, and skin-penetrating irradiation. *In vitro* and *in vivo* experiments have already been successfully carried out by several authors [12–14].

Nevertheless, little is known about the interactions of these nanomaterials with cells for producing safe and efficient tumour cell destruction avoiding damage on untreated cells. We have recently published that, although is well known that cell-internalized pegylated graphene oxide nanosheets are efficient at producing cell death when activated by hyperthermia, high concentrations of this material cause a dose-dependent oxidative stress in different cell types and a slight loss of their viability [15]. Moreover, after internalization, nanosheets were localized on F-actin filaments inducing cell-cycle alterations and apoptosis [16].

In this work, we continued our previous study of cell internalization kinetics (specifically for targeting tumoral osteoblasts on a bone cancer model) by evaluating the type of toxicity and cell damage produced by this hyperthermia treatment in order to investigate the process and open the door to future understanding of the application and versatility of these nanovectors. Moreover, by controlling the type of cell damage provoked by the application of these nanosheets and its hyperthermia temperature, there is a chance of controlling the type of cell death (e.g., apoptosis or necrosis) [17], in order to tailor the possible immune response to the induced harm. This could alert the local antigen-presenting cells to stimulate the immune system, as any intracellular product will potentially be a danger signal when released [18]. As a proof of concept we have also assessed the release of pro-inflammatory cytokines.

2. Material and methods

2.1. GO nanosheets

GO nanosheets have been prepared following the method previously published by the authors [15]. Basically, GO nanosheets were functionalized by covalent bonding with non-toxic and non-immunogenic polymers poly(ethylene Glycol-amine), 1-arm PEG bis(3-aminopropyl) terminated (1.5 kDa), to avoid the intercession with cellular functions or target immunogenicities and to decrease aggregation. They were marked with the amine-reactive dye fluorescein isocyanate (FITC) covalently bonded to the PEG. Samples with these characteristics are called GO nanosheets for simplification. Transmission electron microscopy (TEM) was performed on a 200 kV JEOL JEM 2100. GO nanosheets were analysed by atomic force microscopy (AFM, VEECO multimode; USA). Dynamic light scattering (DLS) particle size analysis measurements were also performed in pH 5 solutions in a Zetasizer Nano Series instrument equipped with a 633 nm 'red' laser from Malvern Instruments, with reproducibility being verified by collection and comparison of sequential measurements.

2.2. Cell culture for GO nanosheet incorporation

Saos-2 osteoblasts were seeded at a density of 10^5 cells ml^{-1} in culture medium supplemented with 10% FBS, 1 mM L-glutamine, penicillin, and streptomycin, under a 5% CO_2 atmosphere and at 37 °C for 24 h in contact with 75 μg ml^{-1} GO material.

2.3. NIR laser irradiation

NIR radiation was provided by a high-power (30 W) diode laser (LASING S.A.) emitting in 808 nm, giving a circular irradiation area of diameter 3 cm (fluency: 4 J cm^{-2}). The module allows irradiation of culture plates in a sterile environment.

Irradiation was performed after GO–cell uptake which, based on previous results, was considered complete after 24 h of Saos-2 exposure to GO solution. Laser irradiations were performed at two different powers and four irradiation times; see the nomenclature of table 1. Afterwards, cells were harvested using 0.25% trypsin–EDTA and counted with a Neubauer hemocytometer. Three types of control have been taken into account in the work: cells without GO exposure and without laser irradiation (named CONTROL), cells exposed

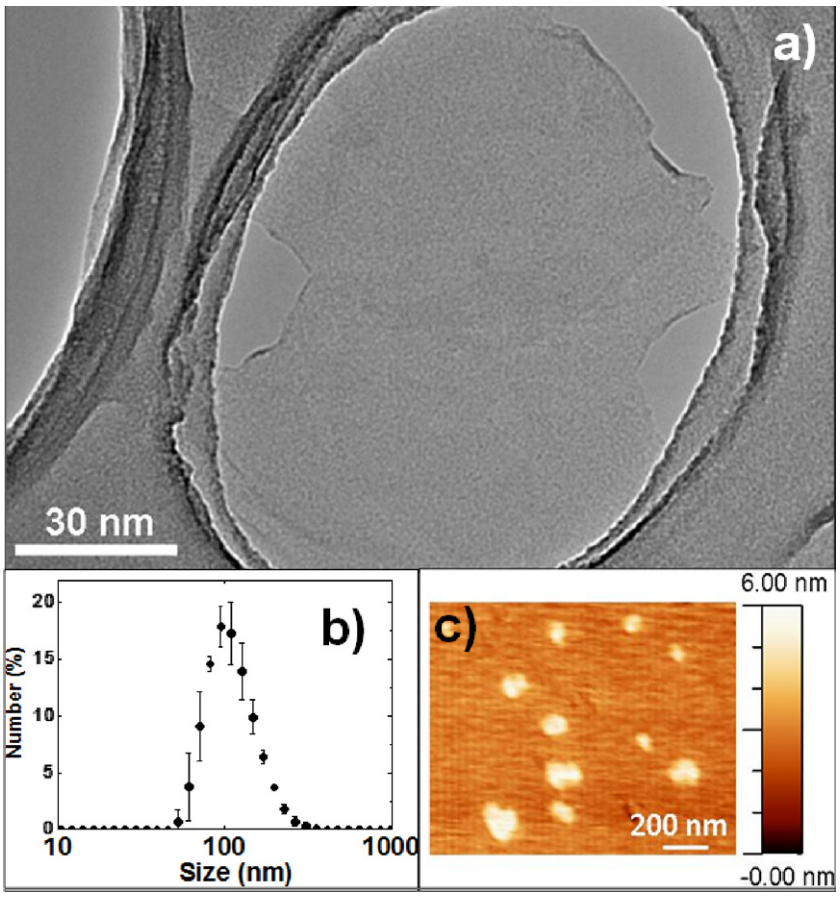

Figure 1. (a) Transmission electron micrograph of activated GOs. (b) GO particle size distribution obtained by DLS analysis. (c) AFM topographic image of dispersed GOs.

to GO but without laser irradiation (named CONTROL GO) and cells irradiated with the laser but without GO exposure (named CONTROL Laser).

A set of experiments was carried out to evaluate the cell morphology after the irradiation treatment. With this objective, the cultures were maintained under a 5% CO_2 atmosphere and at 37 °C for 24 h after GO treatment and laser exposure. These experiments were carried out for the two laser powers and a laser irradiation time of 7 min.

Changes of cell culture temperature during laser irradiation were measured with a PyroPen pyrometer (Calex Electron. Ltd).

2.4. Identification of viable, apoptotic, and necrotic cells. Evaluation of FITC–GO incorporation

After culture with GO material and laser treatment, cells were detached and incubated with propidium iodide (PI, 0.005% in PBS), and the PI fluorescence and cell light scattering properties (FSC) were simultaneously examined in a FACScan Becton Dickinson flow cytometer for identification of viable, apoptotic, and necrotic cells, as previously described [19]. To evaluate the FITC–GO incorporation by each cell fraction, the fluorescence of FITC was excited by a 15 mW laser tuned to 488 nm, and the emitted fluorescence was measured with a 530/30 band pass filter in a FACSCan Becton Dickinson flow cytometer.

2.5. Inflammatory cytokine detection

IL-6 cytokines released by cells to the culture medium were quantified by ELISA with a Gen-Probe Diaclone kit.

2.6. Confocal microscopy studies

Cells were seeded on glass coverslips and cultured in the presence of GO material for 24 h. Before and after laser irradiation, different samples were fixed with 3.7% paraformaldehyde in PBS, permeabilizated with 0.1% Triton X-100, and preincubated with PBS containing 1% BSA. Then, cells were incubated for 20 min with rhodamine–phalloidin (1:40), stained with 4′-6-diamidino-2′-phenylindole (DAPI, 3×10^{-6} M in PBS), and examined using a Leica SP-2 AOBS confocal laser scanning microscope. The rhodamine fluorescence was excited at 540 nm and measured at 565 nm. The DAPI fluorescence was excited at 405 nm and measured at 420–480 nm. The FITC–GO fluorescence was excited at 488 nm and measured at 491–586 nm.

2.7. Statistics

Data are expressed as means + standard deviations of a representative of three experiments carried out in triplicate. Statistical analysis was performed using the statistical

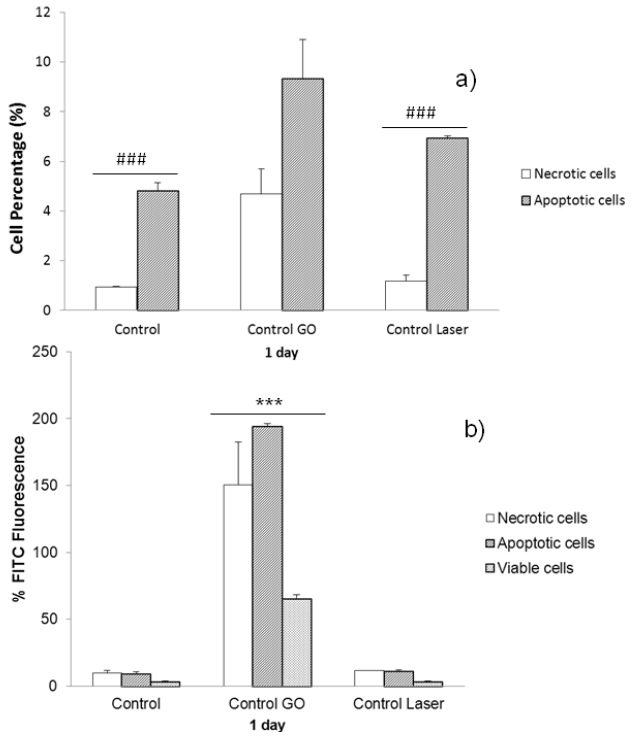

Figure 2. (a) Effects of either GOs or laser irradiation on the percentage of necrotic and apoptotic human Saos-2 osteoblasts. Statistical significance: $^{###}p < 0.005$ between necrotic and apoptotic cells. (b) FITC–GOs incorporated by necrotic, apoptotic, and viable cells. Control = cells without laser irradiation and without GOs. Control GO = cells without laser irradiation and with GOs. Control laser = cells without GOs and with laser irradiation. Statistical significance: $^{***}p < 0.005$; values are compared with the Control.

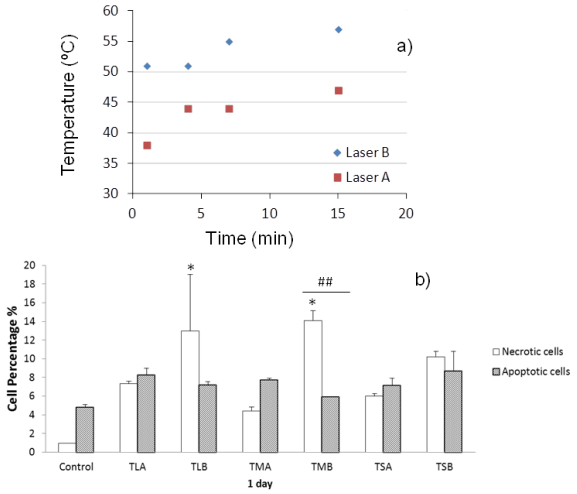

Figure 3. (a) Changes in temperature versus irradiation time at the two different laser powers. (b) Effects of GOs and two different laser powers (A, B) and three different times (L, M, S) on the percentage of necrotic and apoptotic human Saos-2 osteoblasts. Statistical significance: $^{*}p < 0.05$; values are compared with the Control; $^{##}p < 0.01$ between necrotic and apoptotic cells.

package for the social sciences (SPSS) version 19 software. Statistical comparisons were made by analysis of variance (ANOVA). The Scheffé test was used for *post hoc* evaluations of differences among groups. In all of the statistical evaluations, $p < 0.05$ was considered as statistically significant. There are two different statistical representations: (*) indicates significative differences with respect to the control, and ($^{\#}$) represents significative differences between necrotic/apoptotic cells.

3. Results and discussion

The exfoliation procedure of graphite gave rise to GO nanosheets of approx 3–4 layers, and after subsequent ultrasonic treatment and chemical functionalization resulted in sheets of pegylated GO labelled with fluorescent FITC with a hydrodynamic maximum size around 100 nm (see figure 1). A more detailed description of these material properties has been published previously [15].

Based on our previous studies of the GO internalization kinetics by osteoblast-like cells (Saos-2), the laser irradiation experiments were performed after culturing cells for 24 h in a GO-containing medium, as explained in section 2.3. At that time, the GO was considered to be fully taken up by cells [15].

First of all, in order to distinguish the cell damage produced only by simple cell exposure to GO from possible damage to untreated cells by the laser irradiation, different controls were considered and studied to be compared with the subsequent hyperthermia experiment results (figure 2(a)).

As was expected, laser irradiation of cells on the NIR wavelength 'therapeutical window', without any GO incorporation (control laser) resulted in no harmful effect when compared to the control. Nevertheless, confirming what we found out in our previous results, the simple internalization of GO (at a widely published used concentration and dose) by cells leads to an increase of cell death by apoptosis due to GOs being localized on F-actin filaments, which induces cell-cycle alterations, apoptosis, and oxidative stress [16], suggesting that a dose reduction is needed for achieving an optimal therapy performance. In this case, GO incorporation was detected by the increase of fluorescence due to FTIC labelling; see figure 2(b).

The first irradiation experiment was performed after 24 h culture of Saos-2 cells in the presence of GO solution. The increase of culture temperature induced by the laser irradiation is shown in figure 3(a). The different effects of laser exposure time and laser power are summarized in figure 3(b). It can be seen that, for low laser power (1.5 W cm^{-2}), there are not significant differences in cell death when the laser exposure time is increased from 1 to 7 min and the temperature is always maintained below 45 °C. Nevertheless, the dependence on the laser power is highly noticeable. For high laser power (3 W cm^{-2}), already the second exposure time (4 min) increases the temperature to above 50 °C, leading to significant differences in death provoked by necrosis. GO incorporation was monitored after the experiment (figure S1 supporting information available at stacks.iop.org/Nano/25/035101/mmedia) showing that the remaining viable cells were the ones that hardly take up any GO. Table 2 shows the percentage of cell residue and of necrotic, apoptotic, and viable cells after the laser irradiation

Table 2. Effect of GOs on cell viability of human Saos-2 osteoblasts, after laser irradiation treatment.

	Cell residue	Necrotic	Apoptotic	Viable cells
Control###	4.6 ± 0.7	0.9 ± 0.1	4.8 ± 0.3	88.1 ± 0.5
LB###	4.6 ± 0.4	1.2 ± 0.2	6.9 ± 0.1	86.2 ± 0.3
TLA	16.6 ± 1.03[a]	7.3 ± 0.3	8.3 ± 0.7	62.6 ± 1.8[b]
TLB	30.3 ± 1.4[c]	12.9 ± 6.1[a]	7.2 ± 0.4	37.8 ± 5.1[b]
TMA	14.8 ± 1.1[a]	4.4 ± 0.4	7.7 ± 0.2	68.2 ± 2.2[b]
TMB	21.8 ± 0.4[a]	14.1 ± 1.1[a]	5.9 ± 0.1	53.6 ± 1.4[b]
TSA	12.1 ± 1.3[a]	6.0 ± 0.2	7.1 ± 0.8	71.1 ± 2.0[a]
TSB	13.6 ± 1.4[a]	10.2 ± 0.6	8.7 ± 2.1	63.4 ± 3.1[b]

[a] Statistical significance at $p < 0.05$.
[b] Statistical significance at $p < 0.005$.
[c] Statistical significance at $p < 0.01$.

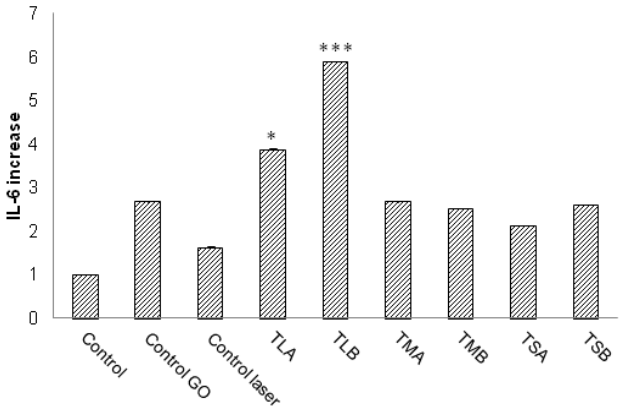

Figure 4. GOs effects on IL-6 release by cultured human Saos-2 osteoblasts after laser irradiation at different powers and exposure times.

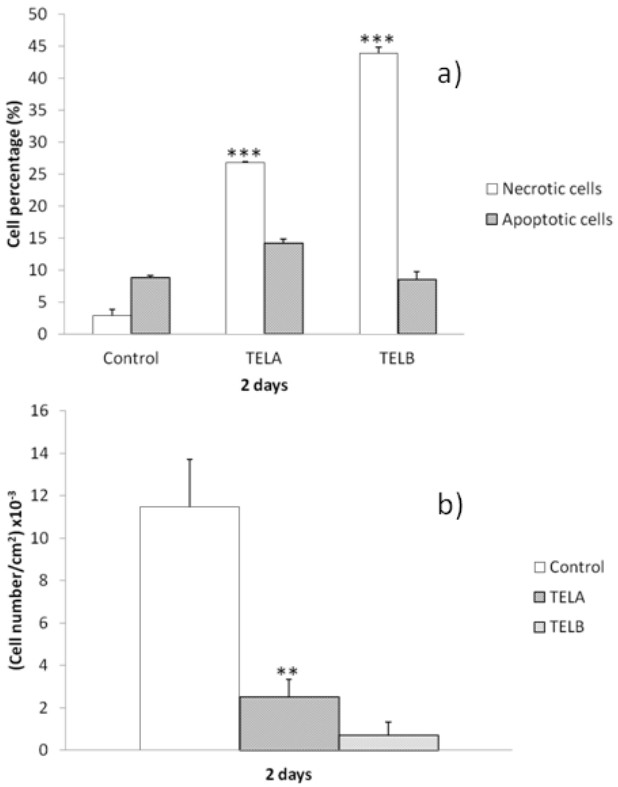

Figure 5. (a) Effects of GOs and two different laser powers (TELA, TELB) on the percentage of necrotic and apoptotic human Saos-2 osteoblasts. (b) Effects of GOs and two different laser powers (TELA, TELB) on cell proliferation. Control = cells without laser irradiation and without GOs. Statistical significance: $^{**}p < 0.01$, $^{***}p < 0.005$; values are compared with the Control.

experiments. The results show that for high power and long time (TLB) only ∼38% of viable cells are left, and necrosis (necrotic cells plus increased cell residue percentages) is the leading death process for this treatment. The same behaviour is shown for high power and medium time (TMB), where only ∼54% are viable, which is proportional, in this case, to the shorter irradiation time.

Due to the importance of controlling the type of cell death provoked and its consequences on the immune response, the effects on cytokine release after these treatments were assessed. Apoptotic cell death is often defined as programmed cell death in the absence of inflammation, suggesting that is an immunologically innocuous event that fails to activate immune responses unless under certain circumstances (some induction of apoptotic cell death *in vitro* resulted in T cell activation). On the other hand, necrotic cell death is normally associated with inflammation and induction of dendritic cell maturation causing strong immune responses [20]. Moreover, necrosis is capable of killing tumour cells that have developed strategies to evade apoptosis. Cells which die by this route initiate pro-inflammatory signalling cascades by actively releasing inflammatory cytokines and spilling their contents when they lyse.

Taking this into account, the secretion of interleukin-6 (IL-6) was assessed as a model of multifunctional cytokines which mediate various inflammation and cellular immune responses [21]. Figure 4 shows the IL-6 releases to the medium after each studied laser power and laser exposure time. As was expected from the results of cell death evaluation, effectively there is a significantly higher IL-6 release when both high laser power and high laser exposure time are applied (TLB). This result is of great importance as it could be the key for producing a localized body immune response if needed and could be part of the anticancer therapy. By controlling the type of cell death and damage, in agreement with the 'danger model' [22], nanovectors could eradicate a tumour by infecting it and/or causing it repeated damage in

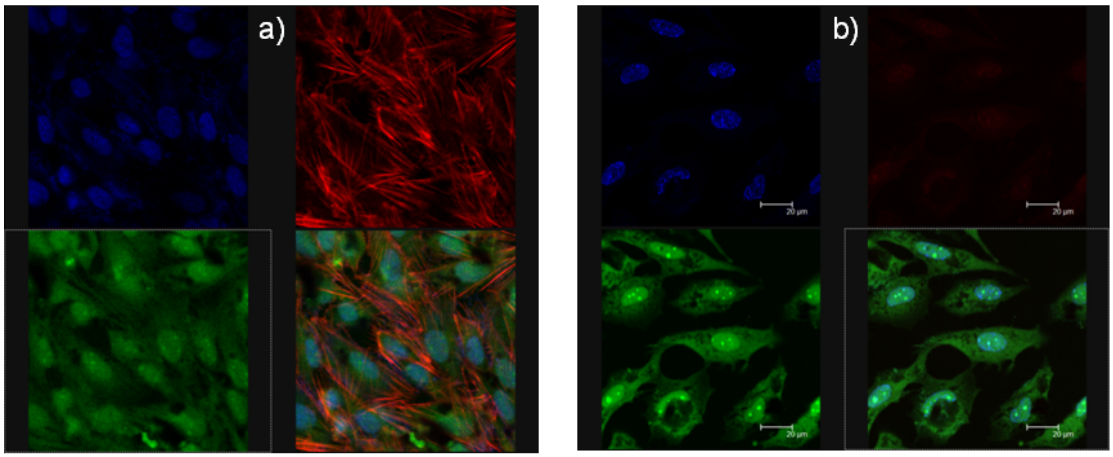

Figure 6. Morphology evaluation by confocal microscopy of cultured human Saos-2 osteoblasts in the presence of GOs after 7 min of 1.5 W cm^{-2} laser irradiation and 24 h of repose.

order to alert the local antigen-presenting cells to stimulate the immune system and work with the help of the best of weapons, the human body itself. Moreover, the fact that there is also a significant IL-6 release after low power irradiation at high exposure time (TLA) means that, even with lower necrotic damage, immune activation could be induced for softer treatment parameters.

When longer exposure times were used and left in repose for 24 h (figure 5(a)), as was expected, a higher necrosis occurred for both laser powers, with the high power treatment being more harmful, which was reflected also as a detrimental effect on cell proliferation; see figure 5(b). GO incorporation was also monitored by the FICT fluorescence (figure S2 supporting information available at stacks.iop.org/Nano/25/035101/mmedia), confirming these results.

The aggressive effects of the hyperthermia treatment are also corroborated by the confocal images of cell cultures before and after the treatments. Figure 6(a) shows the GO incorporated on the cultured osteoblast-like cell. Cells were stained with DAPI for the visualization of the cell nuclei in blue, rhodamine–phalloidin for the visualization of cytoplasmic F-actin filaments in red, and FITC–GOs for the visualization of GOs in green. As was previously published by the authors, figure 6(a) (right down corner), shows the whole composition with the three stainings, revealing that FITC–GO co-localizes with rhodamine–phalloidin, resulting in yellow/orange colouration. Figure 6(b) shows the cell culture after irradiation (low power, 7 min of laser exposure and 24 h of repose). It can be seen that necrosis is the leading process of cell death with the disorganized F-actin micro-filaments producing cell death.

4. Conclusions

Laser dosage and irradiation exposure time were investigated to control the temperature rise and consequent damage in the GOs containing cell culture medium. These results showed that cell culture temperature (after irradiating cells with internalized GO) increases preferentially with laser power rather than with exposure time. Moreover, when the laser power is increased, necrosis is the preferential cell death, leading to an increase of cytokine release to the medium.

The present study suggests that, by controlling the cell viability and tailoring cell death, the threshold for producing thermal ablation with soft or harmful damage could be specifically achieved. It has been also tested that irradiation over cells that have not been exposed to a GO nanovector medium does not alter their vital functions in any manner.

Acknowledgments

This study was supported by research grants from Spanish CICYT (Project MAT2008-00736) and CAM (Project S2009/MAT-1472). M Vila thanks the Spanish Ministry for an RyC grant and the FSE. M C Matesanz and J Linares are greatly indebted to MICINN and CIBER-BBN, respectively, for predoctoral fellowships. Gil Gonçalves thanks the Fundação para a Ciência e Tecnologia (FCT) for a PostDoc grant (SFRH/BDP/84419/2012) P Marques thanks QREN, programme Mais Centro-Programa Operacional Regional do Centro, and União Europeia/Fundo Europeu de Desenvolvimento Regional, project Biomaterials for Regenerative Medicine (CENTRO-07-ST24-FEDER-002030)'. P Marques thanks the Ciencia 2007 Program. The authors also wish to thank the staff of the Cytometry and Fluorescence Microscopy Center of the Universidad Complutense de Madrid (Spain) for assistance in the flow cytometry and confocal microscopy studies.

References

[1] Choi M R *et al* 2007 A cellular Trojan horse for delivery of therapeutic nanoparticles into tumors *Nano Lett.* **7** 3759–65
[2] Cuia J, Gongb Z and Shen H M 2013 The role of autophagy in liver cancer: molecular mechanisms and potential therapeutic targets *Biochim. Biophys. Acta (Rev. Cancer)* **1** 15–26
[3] Yang K, Wan J, Zhang S, Zhang Y, Lee S T and Liu Z 2011 *In vivo* pharmacokinetics, long-term biodistribution, and

toxicology of PEGylated graphene in mice *ACS Nano* **5** 516–22
[4] Bussy C, Ali-Boucetta H and Kostarelos K 2013 Safety considerations for graphene: lessons learnt from carbon nanotubes *Acc. Chem. Res.* **46** 692–701
[5] Soenen S J, Rivera-Gil P, Montenegro J M, Parak W K, De Smedt S C and Braeckmans K 2011 Cellular toxicity of inorganic nanoparticles: common aspects and guidelines for improved nanotoxicity evaluation *Nano Today* **6** 446–65
[6] Kennedy L C *et al* 2011 A new era for cancer treatment: gold-nanoparticle-mediated thermal therapies *Small* **7** 169–83
[7] Day E S, Morton J G and West J L 2009 Nanoparticles for thermal cancer therapy *J. Biomed. Eng.* **131** 074001
[8] Landry J, Samson S and Chretien P 1986 Hyperthermia-induced cell death, thermotolerance, and heat shock proteins in normal, respiration-deficient, and glycolysis-deficient Chinese hamster cells *Cancer Res.* **46** 324–7
[9] Prasad N K, Rathinasamy K, Panda D and Bahadur D 2007 Mechanism of cell death induced by magnetic hyperthermia with nanoparticles of γ-MnxFe$_2$–xO$_3$ synthesized by a single step process *J. Mater. Chem.* **17** 5042–51
[10] Krpetić Z, Nativo P, Sée V, Prior I A, Brust M and Volk M 2010 Inflicting controlled nonthermal damage to subcellular structures by laser-activated gold nanoparticles *Nano Lett.* **11** 4549–54
[11] Shen H, Zhang L, Liu M and Zhang Z 2012 Biomedical applications of graphene *Theranostics* **2** 283–94
[12] Yang K, Zhang S, Zhang G, Sun X, Lee S T and Liu Z 2010 Graphene in mice: ultrahigh *in vivo* tumor uptake and efficient photothermal therapy *Nano Lett.* **10** 3318
[13] Markovic Z M, Harhaji-Trajkovic L M, Todorovic-Markovic B M, Kepic D P, Arsikin K M and Jovanovi S P 2011 *In vitro* comparison of the photothermal anticancer activity of graphene nanoparticles and carbon nanotubes *Biomaterials* **32** 1121
[14] Robinson J T *et al* 2011 Ultrasmall reduced graphene oxide with high near-infrared absorbance for photothermal therapy *J. Am. Chem. Soc.* **133** 6825–31
[15] Vila M *et al* 2012 Cell uptake survey of pegylated nano graphene oxide *Nanotechnology* **23** 465103
[16] Matesanz M C *et al* 2013 The effects of graphene oxide nanosheets localized on *f*-actin filaments on cell cycle alterations *Biomaterials* **34** 1562–9
[17] Fiers W, Beyaert R, Declercq W and Vandenabeele P 1999 More than one way to die: apoptosis, necrosis and reactive oxygen damage *Oncogene* **18** 7719–30
[18] Gamrekelashvili J *et al* 2007 Necrotic tumor cell death *in vivo* impairs tumor-specific immune responses *J. Immunol.* **178** 1573–80
[19] Alcaide M, Serrano M C, Pagani R, Sanchéz-Salcedo S, Vallet-Regí M and Portolés M T 2009 Biocompatibility markers for the study of interactions between osteoblasts and composite biomaterials *Biomaterials* **30** 45–51
[20] Festjens N, Vanden Berghe T and Vandenabeele P 2006 Necrosis a well-orchestrated form of cell demise: signalling cascades, important mediators and concomitant immune response *Biochim. Biophys. Acta* **1757** 1371–87
[21] Confalone E, D'Alessio G and Furia A 2010 IL-6 induction by TNFα and IL-1β in an osteoblast-like cell line *Int. J. Biomed. Sci.* **6** 135–40
[22] Matzinger P 2002 The danger model: a renewed sense of self *Science* **296** 301–5

Supporting information

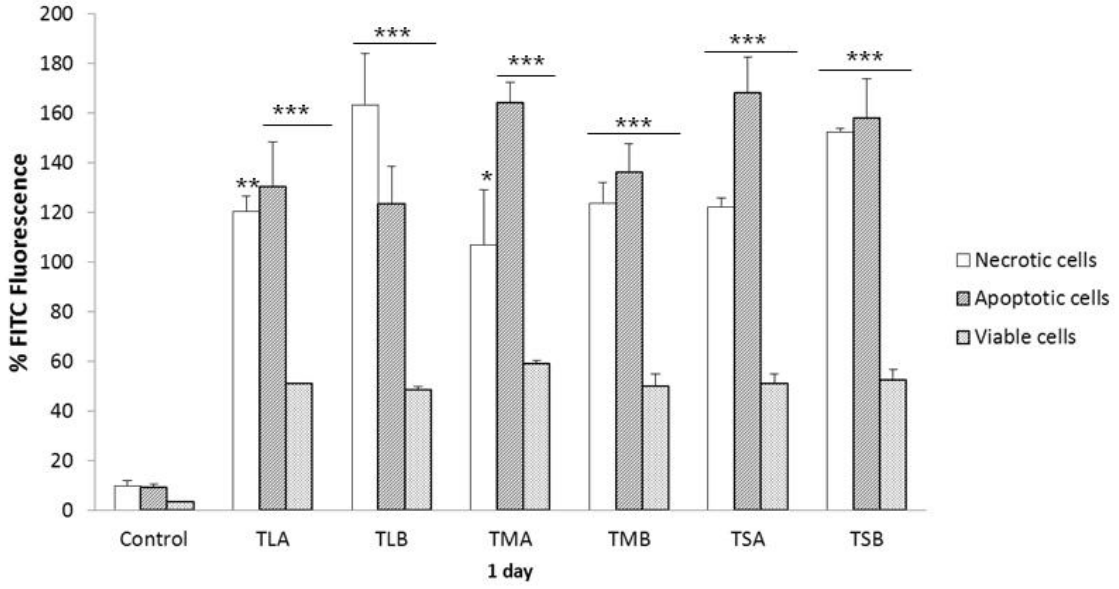

Figure S1. Incorporation of GOs labelled with FITC by human Saos-2 osteoblasts and its relationship with the percentage of viable, necrotic and apoptotic cell death provoked by the two different laser powers (A,B) and three different times (L,M,S).

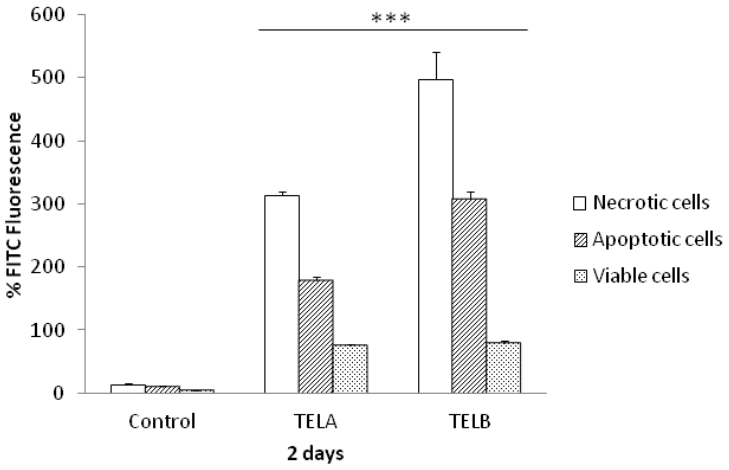

Figure S2. Incorporation of GOs labelled with FITC by human Saos-2 osteoblasts and its relation with the percentage of necrotic and apoptotic cell death provoked by the two different laser powers (A,B) and extra long exposure time after 24 h of repose. Statistical significance ***$p < 0.005$ values are compared with the Control.

REFERENCIAS DEL CAPÍTULO II

1. Akhavan O, Ghaderi E. Toxicity of graphene and graphene oxide nanowalls against bacteria. ACS Nano 4(10):5731-5736.

2. Bacci G, Briccoli A, Rocca M, Ferrari S, Donati D, Longhi A, Bertoni F, Bacchini P, Giacomini S, Forni C, Manfrini M, Galletti S. Neoadjuvant chemotherapy for osteosarcoma of the extremities with metastases at presentation: recent experience at the Rizzoli Institute in 57 patients treated with cisplatin, doxorubicin, and a high dose of methotrexate and ifosfamide. Annals of Oncology, 14(7):1126-34, 2003.

3. Bacon M, Bradley SJ, Nann T. Graphene Quantum Dots. Particle & Particle Systems Characterization, 31:415-428, 2014.

4. Bielack SS, Kempf-Bielack B, Delling G, Exner GU, Flege S, Helmke K, Kotz R, Salzer-Kuntschik M, Werner M, Winkelmann W, Zoubek A, Jürgens H, Winkler K. Prognostic factors in high-grade osteosarcoma of the extremities or trunk: an analysis of 1,702 patients treated on neoadjuvant cooperative osteosarcoma study group protocols. Journal of Clinic Oncology 20(3):776-790, 2002.

5. Bielack SS, Carrle D, Casali PG. ESMO Guidelines Working Group. Osteosarcoma: ESMO clinical recommendations for diagnosis, treatment and follow-up. Annals of Oncology, 20 Suppl 4:137-9, 2009.

6. Card JW, Zeldin DC, Bonner JC, Nestmann ER. Pulmonary applications and toxicity of engineered nanoparticles. Am J Physiol Lung Cell Mol Physiol. 295(3):L400-11, 2008.

7. Chang Y, Yang ST, Liu JH, Dong E, Wang Y, Cao A, Liu Y, Wang H. *In vitro* toxicity evaluation of graphene oxide on A549 cells. Toxicology Letters 200(3):201-10, 2011.

8. Chauhan VP, Stylianopoulos T, Boucher Y, Jain RK. Delivery of molecular and nanoscale medicine to tumors: transport barriers and strategies. Annu Rev Chem Biomol Eng. 2:281-98, 2011.

9. Chen B, Liu M, Zhang L, Huang J, Yao J, Zhang Z. Polyethylenimine-functionalized graphene oxide as an efficient gene delivery vector. Journal of Materials Chemistry, 21, 7736-7741, 2011.

10. Chien CT, Li SS, Lai WJ, Yeh YC, Chen HA, Chen IS, Chen LC, Chen KH, Nemoto T, Isoda S, Chen M, Fujita T, Eda G, Yamaguchi H, Chhowalla M, Chen CW. Tunable photoluminescence from graphene oxide. Angewante Chemie International Edition England. 51(27):6662-6666, 2012.

11. Cote LJ, Kim J, Tung VC, Luo J, Kim F, Huang J. Graphene oxide as surfactant sheets. Pure and Applied Chemistry, 83(1):95-110, 2011.

12. Day ES, Morton JG and West JL. Nanoparticles for thermal cancer therapy. J Biomed Eng 131(7):074001, 2009.

13. Depan D, Girase B, Shah JS, Misra RD. Structure-process-property relationship of the polar graphene oxide-mediated cellular response and stimulated growth of osteoblasts on hybrid chitosan network structure nanocomposite scaffolds. Acta Biomaterialia, 7(9):3432-45, 2011.

14. Entz-Werle N, Schneider A, Kalifa C, Voegeli AC, Tabone MD, Marec-Berard P, Marcellin L, Pacquement H, Terrier P, Boutard P, Meyer N, Gaub MP, Lutz P, Babin A, Oudet P. Genetic alterations in primary osteosarcoma from 54 children and adolescents by targeted allelotyping. British Journal of Cancer, 88(12):1925-1931, 2003.

15. Errani C, Longhi A, Rossi G, Rimondi E, Biazzo A, Toscano A, Alì N, Ruggieri P, Alberghini M, Picci P, Bacci G, Mercuri M. Palliative therapy for osteosarcoma. Expert Review of Anticancer Therapy, 11(2):217-227, 2011.

16. Feng L, Zhang S, Liu Z. Graphene based gene transfection. Nanoscale. 3(3):1252-1257, 2011.

17. Feng L, Wu L, Qu X. New Horizons for Diagnostic and Therapeutic Applications of Graphene and Graphene Oxide. Advanced Materials, 25:168-186, 2013.

18. Ferrari S, Palmerini E. Adjuvant and neoadjuvant combination chemotherapy for osteogenic sarcoma. Current Opinion in Oncology, 19(4):341-346,2007.

19. Gill J, Ahluwalia MK, Geller D, Gorlick R. New targets and approaches in osteosarcoma. Pharmacology & Therapeutics 137: 89-99, 2013.

20. Goncalves G, Marques PAAP, Granadeiro CM, Nogueira HIS, Singh MK, Grácio J. Surface Modification of Graphene Nanosheets with Gold Nanoparticles: The Role of Oxygen Moieties at Graphene Surface on Gold Nucleation and Growth. Chemical Materials, 21 20:4796–4802, 2009.

21. Gonçalves G, Vila M, Portolés MT, Vallet-Regí M, Gracio J, Marques PA. Nano-Graphene oxide: A potential multifunctional platfor for cancer therapy. Advanced Healthcare Materials 2(8):1072-90, 2013.

22. Gorlick R. Current concepts on the molecular biology of osteosarcoma. Cancer Treatment and Research, 152:467-478, 2009.

23. Hattinger CM, Pasello M, Ferrari S, Picci P, Serra M. Emerging drugs for high-grade osteosarcoma. Expert Opinion on Emerging Drugs, 15(4):615-634, 2010.

24. Hubbell JA, Chilkoti A. Chemistry. Nanomaterials for drug delivery. Science. 337(6092):303-5, 2012.

25. Kager L, Zoubek A, Dominkus M, Lang S, Bodmer N, Jundt G, Klingebiel T, Jürgens H, Gadner H, Bielack S; COSS Study Group. Osteosarcoma in very young children: experience of the Cooperative Osteosarcoma Study Group. Cancer, 116(22):5316-5324, 2010.

26. Kempf-Bielack B, Bielack SS, Jürgens H, Branscheid D, Berdel WE, Exner GU, Göbel U, Helmke K, Jundt G, Kabisch H, Kevric M, Klingebiel T, Kotz R, Maas R, Schwarz R, Semik M, Treuner J, Zoubek A, Winkler K. Osteosarcoma relapse after combined modality therapy: an analysis of unselected patients in the Cooperative Osteosarcoma Study Group (COSS). Journal of Clinical Oncology, 23(3):559-68, 2005.

27. Kotchey GP, Allen BL, Vedala H, Yanamala N, Kapralov AA, Tyurina YY, Klein-Seetharaman J, Kagan VE, Star A. The Enzymatic Oxidation of Graphene Oxide. American Chemical Society Nano, 5(3):2098–2108, 2011.

28. Kunkel SL, Lukacs NW, Strieter RM, Chensue SW. Animal models of granulomatous inflammation. Semin Respir Infect. 13(3):221-8, 1998.

29. Lee JH, Sahu A, Jang C, Tae G. The Effect of Ligand Density on *In Vivo* Tumor Targeting of Nano Graphene Oxide. Journal of Controlled Release. In Press, 2015.

30. Linares J, Matesanz MC, Vila M, Feito MJ, Gonçalves G, Vallet-Regí M, Marques PA, Portolés MT. Endocytic mechanisms of graphene oxide nanosheets in osteoblasts, hepatocytes and macrophages. ACS Applied Materials and Interfaces, 6(16):13697-13706, 2014.

31. Link MP, Goorin AM, Miser AW, Green AA, Pratt CB, Belasco JB, Pritchard J, Malpas JS, Baker AR, Kirkpatrick JA, et al. The effect of adjuvant chemotherapy on relapse-free survival in patients with osteosarcoma of the extremity. The New England Journal of Medicine, 314(25):1600-1606, 1986.

32. Liu X, Sen S, Liu J, Kulaots I, Geohegan D, Kane A, Puretzky AA, Rouleau CM, More KL, Palmore GT, Hurt RH. Antioxidant deactivation on graphenic nanocarbon surfaces. Small, 7(19):2775-2785, 2011.

33. Liu Z, Robinson JT, Sun X, Dai H. PEGylated nanographene oxide for delivery of water-insoluble cancer drugs. Journal of the American Chemical Society. 130(33):10876-10877, 2008.

34. Lu CH, Zhu CL, Li J, Liu JJ, Chen X, Yang HH. Using graphe ne to protect DNA from cleavage during cellular delivery. Chemical Communications (Cambridge), 46(18):3116-3118, 2010.

35. Luetke A, Meyers PA, Lewis I, Juergens H. Osteosarcoma treatment - where do we stand? A state of the art review. Cancer Treatment Reviews, 40(4):523-532, 2014.

36. Marcano DC, Kosynkin DV, Berlin JM, Sinitskii A, Sun Z, Slesarev A, Alemany LB, Lu W, Tour JM. Improved Synthesis of Graphene Oxide. American Chemical Society Nano, 4(8):4806–4814, 2010.

37. Marcove RC, Miké V, Hajek JV, Levin AG, Hutter RV. Osteogenic sarcoma under the age of twenty-one. A review of one hundred and forty-five operative cases. The Journal of Bone and Joint Surgery, 52(3):411-423, 1970.

38. Muñoz A, Alfaro J, Pardo N, García-Miguel P, Quintero V, Gros L, Melero C, Antuña MJ, Ocete G, de Las Heras J, Ruiz del Portal M, Huguet R, Maldonado MS. Long-term results of the Spanish Protocol SO-95 for the treatment of non-metastatic high-grade osteosarcoma of the extremities in children. Clinical and Translational Oncology, 11(6):387-92, 2009.

39. Nayak TR, Andersen H, Makam VS, Khaw C, Bae S, Xu X, Ee PL, Ahn JH, Hong BH, Pastorin G, Özyilmaz B. Graphene for controlled and accelerated osteogenic differentiation of human mesenchymal stem cells. ACS Nano 5(6):4670-4678, 2011. ARTÍCULO DE PAGO.

40. Nel AE, Mädler L, Velegol D, Xia T, Hoek EM, Somasundaran P, Klaessig F, Castranova V, Thompson M. Understanding biophysicochemical interactions at the nano-bio interface. Nature Materials, 8(7):543-557, 2009.

41. Ottaviani G, Jaffe N. The epidemiology of osteosarcoma. Cancer Treatment and Research, 152:3-13, 2009.

42. Ren H, Wang C, Zhang J, Zhou X, Xu D, Zheng J, Guo S, Zhang J. DNA cleavage system of nanosized graphene oxide sheets and copper ions. American Chemical Society Nano, 4(12):7169-7174, 2010.

43. Ryoo SR, Kim YK, Kim MH, Min DH. Behaviors of NIH-3T3 fibroblasts on graphene/carbon nanotubes: proliferation, focal adhesion, and gene transfection studies. ACS Nano. 4(11):6587-6598, 2010.

44. Sahu A, Choi WI, Lee JH, Tae G. Graphene oxide mediated delivery of methylene blue for combined photodynamic and photothermal therapy. Biomaterials, 34(26):6239-6248, 2013.

45. Shen H, Zhang L, Liu M, Zhang Z. Biomedical applications of graphene. Theranostics, 2(3):283-294, 2012.

46. Sun X, Liu Z, Welsher K, Robinson JT, Goodwin A, Zaric S, Dai H. Nano-Graphene Oxide for Cellular Imaging and Drug Delivery. Nano Research, 1(3):203-212, 2008.

47. Tung VC, Allen MJ, Yang Y, Kaner RB. High-throughput solution processing of large-scale graphene. Nature Nanotechnology, 4(1):25-29, 2009.

48. Yang K, Zhang S, Zhang G, Sun X, Lee ST, Liu Z. Graphene in mice: ultrahigh *in vivo* tumor uptake and efficient photothermal therapy. Nano Letters. 10(9):3318-23, 2010.

49. Yang K, Wan J, Zhang S, Zhang Y, Lee ST, Liu Z. *In Vivo* Pharmacokinetics, Long-Term Biodistribution, and Toxicology of PEGylated Graphene in Mice. ACS Nano. 5(1):516-522, 2011.

50. Yang ST, Chang Y, Wang H, Liu G, Chen S, Wang Y, Liu Y, Cao A. Folding/aggregation of graphene oxide and its application in Cu2+ removal. Journal of Colloid and Interface Science, 351(1):122-127, 2010.

51. Yang X, Wang Y, Huang X, Ma Y, Huang Y, Yang R, Duana H, Chen Y. Multi-functionalized graphene oxide based anticancer drug-carrier with dual-targeting function and pH-sensitivity. Journal of Materials Chemistry, 21, 3448-3454, 2011.

52. Wang K, Ruan J, Song H, Zhang J, Wo Y, Guo S, Cui D. Biocompatibility of graphene oxide. Nanoscale Research Letters 6, 8, 2011.

53. Wang Y, Li Z, Hu D, Lin CT, Li J, Lin Y. Aptamer/Graphene Oxide Nanocomplex for in Situ Molecular Probing in Living Cells. Journal of the American Chemical Society, 132(27):9274-9276, 2010.

54. Weissleder R. A clearer vision for *in vivo* imaging. Nature Biotechnology, 19(4):316-7, 2001.

55. Wu M, Kempaiah R, Huang PJ, Maheshwari V, Liu J. Adsorption and desorption of DNA on graphene oxide studied by fluorescently labeled oligonucleotides. Langmuir: the ACS Journal of Surfaces and Colloids, 27(6):2731-2738, 2011.

56. Xiong H, Guo Z, Zhang W, Zhong H, Liu S, Ji Y. Redox-responsive biodegradable PEGylated nanographene oxide for efficiently chemo-photothermal therapy: a comparative study with non-biodegradable PEGylated nanographene oxide. Journal of Photochemistry and Photobiology B, 138:191-201, 2014.

57. Zhang L, Lu Z, Zhao Q, Huang J, Shen H, Zhang Z. Enhanced chemotherapy efficacy by sequential delivery of siRNA and anticancer drugs using PEI-grafted graphene oxide. Small. 7(4):460-4, 2011.

58. Zhang L, Wang Z, Xu C, Li Y, Gao J, Wang W, Liu Y. High strength graphene oxide/polyvinyl alcohol composite hydrogels. Journal of Materials Chemistry, 21, 10399-10406, 2011.

59. Zhang M, Yin BC, Wang XF, Ye BC. Interaction of peptides with graphene oxide and its application for real-time monitoring of protease activity. Chemical Communications (Cambridge), 28;47(8):2399-2401, 2011.

60. Zhang Y, Ali SF, Dervishi E, Xu Y, Li Z, Casciano D, Biris AS. Cytotoxicity effects of graphene and single-wall carbon nanotubes in neural phaeochromocytoma-derived PC12 cells. ACS Nano. 4(6):3181-6, 2010.

Páginas web citadas en el Capítulo II

http://biospecimens.cancer.gov/meeting/brnsymposium/2011/Posters/Lana-508.pdf

http://www.illumina.com/documents/seminars/presentations/2009_06_mezazepeda_leonardo.pdf

Conclusiones / Conclusions

CONCLUSIONES

CAPÍTULO I

1- El estudio comparativo del comportamiento de fibroblastos, osteoblastos y preosteoblastos en contacto con los materiales HA y SiHA mediante diferentes parámetros celulares demuestra una mejor respuesta a SiHA, indicando el papel beneficioso del silicio para el crecimiento de las células óseas y la **excelente biocompatibilidad de SiHA**, que hace a este material idóneo para la reparación de defectos óseos.

2- El factor **FGF-2 unido al material SiHA representa una alternativa prometedora para regeneración ósea** ya que FGF-2 mantiene su actividad biológica estimulando en osteoblastos y preosteoblastos vías de señalización intracelular específicas como PLCγ y MAPK, implicadas en la proliferación y diferenciación de estas células óseas.

3- La **osteostatina potencia la actividad osteogénica y angiogénica del FGF unido a SiHA**, incrementando la expresión génica de Runx2, osteocalcina, VEGF y VEGFR1 y 2.

4- Las hidroxiapatitas nanocristalinas nano-HA y nano-SiHA disminuyen la proliferación de los macrófagos y su actividad fagocítica, induciendo la producción de citoquinas proinflamatorias (IL-6 y TNF-α) y la apoptosis de linfocitos T. Estos resultados indican que **tras la implantanción *in vivo* de estos materiales nanocristalinos podría producirse una activación temprana de la respuesta inmune innata.**

5- **Discos de nano-SiHA retrasan la diferenciación de los osteoclastos y disminuyen su actividad resorptiva** sobre su superficie en comparación con discos de nano-HA, sin afectar a la viabilidad celular. Este efecto de nano-SiHA, unido a su acción beneficiosa sobre osteoblastos, indica el potencial de este material para modular el proceso de remodelado óseo, previniendo la resorción y favoreciendo la formación de hueso en los lugares de implantación para tratamiento de osteoporosis y regeneración ósea.

CAPÍTULO II

1- El estudio de la **cinética de incorporación de nano-GO/PEG/FITC** en fibroblastos, macrófagos, osteoblastos y preosteoblastos revela que el proceso depende del tipo celular, siendo **más rápida y elevada en osteoblastos, sin verse alterada la membrana plasmática.** El número de brazos de PEG unidos a nano-GO afecta a la velocidad de incorporación y a la viabilidad celular.

2- Una vez internado, **nano-GO/PEG/FITC se asocia a los filamentos de F-actina en todos los tipos celulares estudiados, induciendo alteraciones del ciclo celular, apoptosis y estrés oxidativo.**

3- La **inducción *in vitro* de hipertermia sobre células de osteosarcoma humano Saos-2** cultivadas con nano-GO como modelo experimental demuestra que el incremento local de temperatura **depende de la potencia del láser durante la irradiación y del tiempo de exposición, siendo el primer factor más determinante.** El análisis simultáneo de apoptosis y necrosis demuestra que **el principal tipo de muerte celular tras la inducción de la hipertermia es la necrosis**, conduciendo a un incremento de la liberación de citoquinas proinflamatorias al medio. La selección de las condiciones de tiempo y potencia de exposición permitirán controlar el tipo de muerte celular, produciendo menores efectos secundarios en la zona afectada del organismo.

Las conclusiones de la presente Tesis Doctoral permiten conocer las respuestas celulares específicas a nano-SiHA y nano-GO, fundamentales para la posible aplicación biomédica de estos materiales en patologías óseas como osteoporosis y osteosarcoma, respectivamente.

CONCLUSIONS

CHAPTER I

1- The comparative study of fibroblast, osteoblast and preosteoblast behaviour in contact with HA and SiHA materials through different parameters evidences a better cell response to SiHA, showing the beneficial role of silicon for bone cell growth and the **excellent SiHA biocompatibility**, which makes this material suitable for the repair of bone defects.

2- **Fibroblast growth factor 2 (FGF-2) adsorbed on SiHA represents a promising alternative for bone regeneration** due to the maintenance of FGF-2 biological activity, stimulating specific intracellular signaling pathways in osteoblasts and preosteoblasts, like PLCγ y MAPK, involved in bone cell proliferation and differentiation.

3- **Osteostatin improves the osteogenic and angiogenic activity of FGF-2 adsorbed on SiHA**, increasing the gene expression of Runx2, osteocalcin, VEGF, VEGFR1 and VEGFR2.

4- Nanocrystalline hydroxyapatites, nano-HA and nano-SiHA, decrease macrophage proliferation and phagocitic activity, inducing proinflamatory cytokine synthesis (IL-6 y TNF-α) and T lymphocyte apoptosis. These results show that **these nanocrystalline materials could induce an early activation of the innate immune response after *in vivo* implantation**.

5- **Nano-SiHA disks delay osteoclast differentiation and decrease resorptive activity of these cells** on their surface, in comparison with nano-HA disks, without affecting cell viability. These results along with the beneficial effects on osteoblasts, suggest the potential of this material for modulating the fundamental process of bone remodelling, preventing resorption and enhancing bone formation at implantation sites in treatment of osteoporosis and bone regeneration.

CHAPTER II

1- The study of the **nano-GO/PEG/FITC incorporation kinetics** in fibroblasts, macrophages, osteoblasts and preosteoblasts reveals that this process depends on the cell type involved, being **faster and higher in osteoblasts, without plasma cell membrane damage**. The number of PEG branches bonded to GO affects cell viability and uptake kinetics.

2- After internalization, **nano-GO/PEG/FITC are localized on F-actin filaments inducing cell-cycle alterations, apoptosis and oxidative stress in all cell types studied.**

3- ***In vitro* hyperthermia induction on human osteosarcoma Saos-2** cells cultured with nano-GO as an experimental model shows that the cell culture temperature **increases preferentially with**

laser power rather than with the exposure time. The simultaneous analysis of apoptosis and necrosis reveals that **necrosis is the preferential cell death**, leading to an increase of proinflammatory cytokine release to the medium. By selecting the laser dosage and irradiation exposure time the cell death type can be controlled, producing less secondary effects in the affected area of the organism.

The results of the current PhD Thesis allow us to know the specific cell responses to nano-SiHA and nano-GO, which are fundamental for the possible biomedical application of these materials in bone diseases, such as osteoporosis and osteosarcoma, respectively.

Anexo

Otras publicaciones de la Doctoranda relacionadas con esta Tesis Doctoral

ANEXO. Otras publicaciones de la Doctoranda relacionadas con esta Tesis Doctoral

- González B, Ruiz-Hernández E, Feito MJ, López de Laorden C, Arcos D, Ramírez-Santillán C, **Matesanz C**, Portolés MT, Vallet-Regí M. Covalently bonded dendrimer-maghemite nanosystems: nonviral vectors for *in vitro* gene magnetofection. Journal of Materials Chemistry, 21: 4598-4604, 2011.

- Alcaide M, Ramírez-Santillán C, Feito MJ, **Matesanz MC**, Ruiz-Hernández E, Arcos D, Vallet-Regí M, Portoles MT. *In vitro* evaluation of glass-glass ceramic thermoseed induced hyperthermia on human osteosarcoma cell line Journal of Biomedical Materials Research, Part A, 100:64-71, 2012.

- Corrales T, Larraza I, Catalina F, Portolés MT, Ramírez-Santillán C, **Matesanz MC**, Abrusci C. *In vitro* biocompatibility and antimicrobial activity of Poly(ε-caprolactone)/montmorillonite nanocomposites. Biomacromolecules, 13: 4247-4256, 2012.

- Cabañas MV, Peña J, Román J, Ramírez-Santillán C, **Matesanz MC**, Feito MJ, Portolés MT, Vallet-Regí M. Design of tunable protein-releasing nanoapatite/hydrogel scaffolds for hard tissue engineering. Materials Chemistry and Physics 144: 409-417, 2014.

- Feito MJ, Vila M, **Matesanz MC**, Linares J, Gonçalves G, Marques PA, Vallet-Regí M, Rojo JM, Portolés MT. *In vitro* evaluation of graphene oxide nanosheets on immune function. Journal of Colloid and Interface Science, 432:221-228, 2014.

- Linares J, **Matesanz MC**, Vila M, Feito MJ, Gonçalves G, Vallet-Regí M, Marques PAAP, Portolés MT. Endocytic mechanisms of graphene oxide nanosheets in osteoblasts, hepatocytes and macrophages. ACS Applied Materials & Interfaces 6(16):13697-13706, 2014.

- **Matesanz MC**, Linares J, Oñaderra M, Feito MJ, Martínez-Vázquez FJ, Arcos D, Sánchez-Salcedo S,Portolés MT, Vallet-Regí M. Response of osteoblasts and preosteoblasts to calcium deficient and Si substituted hydroxyapatites treated at different temperaturas. Colloids and Surfaces B: Biointerfaces (Ref: COLSUB-D-15-00650, bajo revisión).

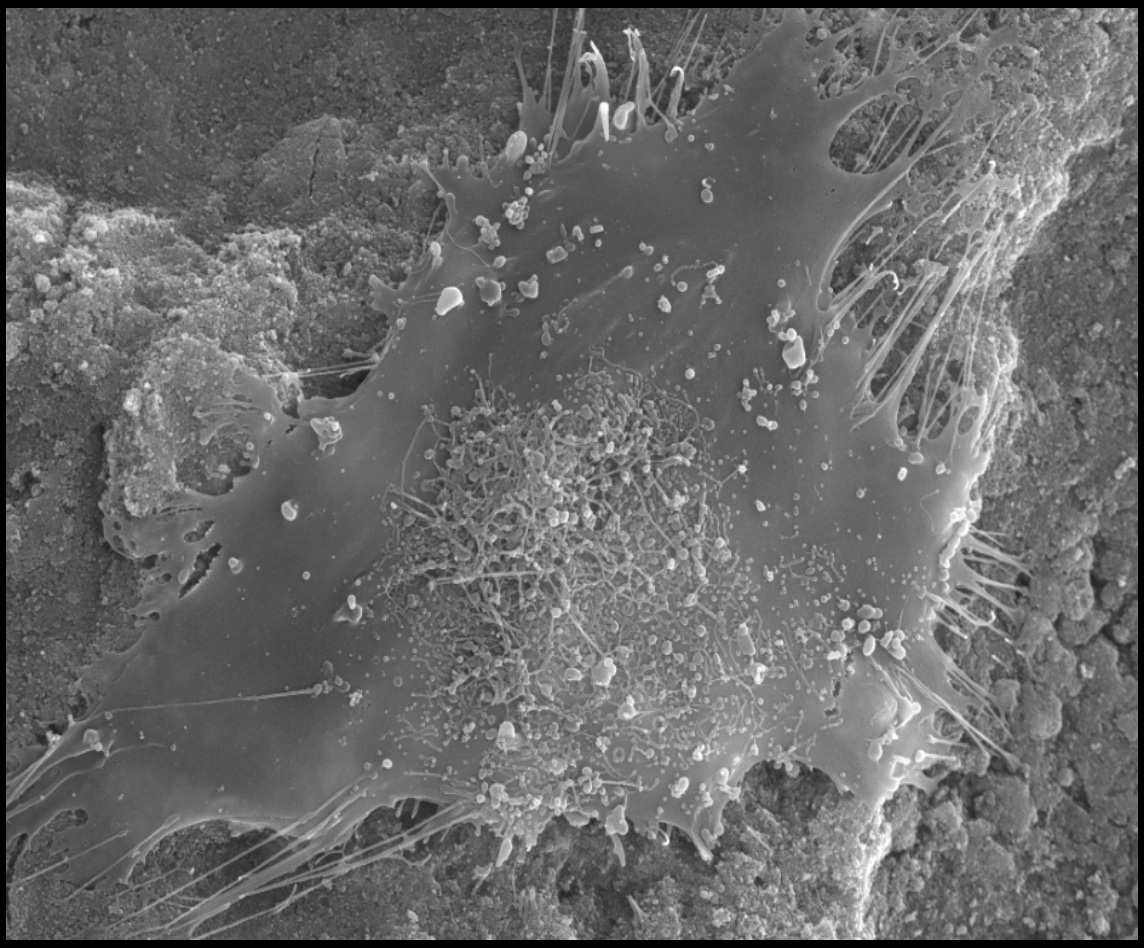

Los resultados obtenidos permiten conocer las respuestas celulares específicas a nano-SiHA y nano-GO, fundamentales para la posible aplicación biomédica de estos materiales en patologías óseas como osteoporosis y osteosarcoma, respectivamente.